Dissertation

submitted to the

Combined Faculty of Natural Sciences and Mathematics

of the Ruperto Carola University Heidelberg, Germany

for the degree of

Doctor of Natural Sciences

Presented by

Merve Keles, M.Sc.

born in: Istanbul, Turkey

Oral examination: 16 February 2023

Secreted long non-coding RNAs *Gadlor1* and *Gadlor2* act as mediators of cardiac remodelling during pressure overload

Referees: Prof. Dr. Thomas Wieland

Prof. Dr. Joerg Heineke

Declaration of Originality

I, Merve Keles, hereby confirm that the presented work in this thesis titled *'Secreted long non-coding RNAs Gadlor1 and Gadlor2 act as mediators of cardiac remodelling during pressure overload'* is the result of my own independent work, where the information has been derived from other sources, this was specifically indicated.

Signature: Merve Keles

Place/ Date:

1. Abstract

Background: Pathological cardiac overload triggers maladaptive myocardial remodelling that predisposes to the development of heart failure. The contribution of long non-coding RNAs (lncRNAs) to intercellular signalling during cardiac remodelling is largely unknown. In this study, two novel lncRNAs, *Gadlor1* and *Gadlor2*, which are enriched in endothelial-cell-derived extracellular vesicles (EVs) were described. The functional role of endogenous *Gadlor* lncRNAs was investigated in intra-cardiac communication during cardiac remodelling upon pressure overload.

Methods and Results: Analysis of the different cardiac cell types revealed that *Gadlor1* and *Gadlor2* expression were enriched in endothelial cells (EC) compared to fibroblast (FB) and cardiomyocytes (CM). Interestingly, the abundance of *Gadlor* lncRNAs was even more pronounced in EC-derived EVs, suggesting a potential role in paracrine signalling. The effect of *Gadlor* knock-out (*Gadlor*-KO) and *Gadlor* overexpression during cardiac pressure overload induced by transverse aortic constriction (TAC) was analysed by echocardiography, histological analyses and bulk RNA sequencing from isolated cardiac cells.

Gadlor1 and Gadlor*2* are upregulated in failing mouse hearts as well as in the myocardium and serum of hypertrophy patients. Interestingly, secreted *Gadlor* lncRNAs from ECs were mainly taken up by CM, and to a lesser extent by cardiac FBs. *Gadlor*-KO mice exhibited reduced cardiomyocyte hypertrophy, diminished myocardial fibrosis and improved cardiac function, but paradoxically, suffered from sudden death during prolonged pressure overload. *Gadlor* overexpression, in turn, triggered hypertrophy, fibrosis and cardiac dysfunction.

Mechanistically, *Gadlor1* and *Gadlor2* inhibited angiogenic gene expression in ECs, while promoting the expression of pro-fibrotic genes in cardiac FBs. In CMs, *Gadlor1 and Gadlor2* upregulate mitochondrial and pro-hypertrophic genes, but downregulate angiogenesis and inflammatory genes.

GLYR1 and CaMKII were identified as *Gadlor1/2* interaction partners by RNA antisense purification coupled with mass-spectrometry (RAP-MS). These binding partners could in part

explain the changes observed in gene expression of *Gadlor*-KO CMs, cardiomyocyte hypertrophy and perturbed calcium dynamics, respectively. Phosphorylation of phospholamban (p-PLN) by CaMKII at threonine-17 alters the activity of the SERCA pump and therefore calcium reuptake into the sarcoplasmic reticulum. A significant decrease in pThr17-PLN in *Gadlor*-KO heart tissue samples, and a considerable increase in pThr17-PLN in *Gadlor1/2* overexpressing heart tissue samples compared to WT after 2 weeks of TAC suggested that *Gadlor* lncRNAs promote CaMKII activity. Indeed, reduced or increased CaMKII activation could explain in large parts ameliorated or exaggerated maladaptive remodelling during Gadlor knock-out or overexpression, respectively.

Conclusions: *Gadlor1* and *Gadlor2* are novel lncRNAs, which are upregulated in cardiac pathological overload and are secreted from endothelial cells within EVs. *Gadlor1* and *Gadlor2* induce cardiac dysfunction, cardiomyocyte hypertrophy and myocardial fibrosis by acting on multiple cardiac cells, affecting cellular gene expression and by affecting calcium dynamics in cardiomyocytes, which take up the *Gadlor1/2* by EV-mediated transfer from endothelial cells. Targeted inhibition of *Gadlor* lncRNA*s* in endothelial cells or fibroblasts might serve as a therapeutic strategy in the future.

2. Zusammenfassung

Hintergrund: Eine pathologische Überlastung des Herzens löst einen maladaptiven Myokardumbau aus, der die Entwicklung einer Herzinsuffizienz begünstigt. Der Beitrag von langen nicht-kodierenden RNAs (lncRNAs) zur interzellulären Signalübertragung während des Herzumbaus ist weitgehend unbekannt. In dieser Studie wurden zwei neue lncRNAs, *Gadlor1* und *Gadlor2*, identifiziert, die in von Endothelzellen stammenden extrazellulären Vesikeln (EVs) angereichert sind. In dieser Arbeit wurde die funktionelle Rolle der endogenen Gadlor lncRNAs für das kardiale Remodelling bei Drucküberlastung untersucht.

Methoden und Ergebnisse: Die Analyse der verschiedenen Herzzelltypen ergab, dass die Expression von *Gadlor1* und *Gadlor2* in Endothelzellen (EC) im Vergleich zu Fibroblasten (FB) und Kardiomyozyten (CM) erhöht war. Interessanterweise waren die *Gadlor* lncRNAs insbesondere in aus EC stammenden extrazellulären Vesikeln (EVs) zu finden, was auf eine mögliche Rolle bei der parakrinen Signalübertragung schließen lässt. Die Wirkung von *Gadlor*-Knock-out (Gadlor-KO) und *Gadlor*-Überexpression wurde bei durch transversale Aortenkonstriktion (TAC) induzierter kardialer Drucküberlastung durch Echokardiographie, histologische Analysen und RNA-Sequenzierung aus isolierten Herzzellen analysiert.

Gadlor1 und *Gadlor2* sind in insuffizienten Mäuseherzen sowie im Myokard und Serum von Patienten mit kardialer Hypertrophie hochreguliert. Interessanterweise wurden die aus den ECs sezernierten Gadlor lncRNAs hauptsächlich von CM und in geringerem Maße von kardialen FBs aufgenommen. *Gadlor*-KO-Mäuse zeigten nach TAC eine reduzierte Kardiomyozytenhypertrophie, eine verringerte Myokardfibrose und eine verbesserte Herzfunktion, erlitten aber paradoxerweise bei längerer Drucküberlastung einen plötzlichen Tod. Die Überexpression von Gadlor wiederum verstärkte Hypertrophie, Fibrose und kardiale Dysfunktion nach TAC Operation.

Mechanistisch gesehen hemmten *Gadlor1* und *Gadlor2* die pro-angiogenes Genexpression in ECs, während sie die Expression von pro-fibrotischen Genen in kardialen FBs fördern. In CM regulieren

Gadlor1 und *Gadlor2* mitochondriale Gene hoch, während sie die Angiogenesegene herunterregulieren.

GLYR1 und CaMKII wurden als Interaktionspartner von *Gadlor1/2* durch RNA-Antisense-Reinigung in Verbindung mit Massenspektrometrie (RAP-MS) identifiziert, was die beobachteten Veränderungen in der Genexpression von Kardiomyozyten sowie die reduzierte Kardiomyozytenhypertrophie bzw. die gestörte Kalziumdynamik in den GADLOR KO Mäusen zum Teil erklären könnte. Die Phosphorylierung von Phospholamban (p-PLN) durch CaMKII an Threonin-17 verändert die Aktivität der SERCA-Pumpe und damit die Kalziumwiederaufnahme in das sarkoplasmatische Retikulum. Ein signifikanter Rückgang von pThr17-PLN in *Gadlor*-KO-Herzgewebeproben und ein beträchtlicher Anstieg von pThr17-PLN nach *Gadlor1/2*-überexprimierten Herzgewebeproben im Vergleich zu WT nach 2 Wochen TAC deuten darauf hin, dass *Gadlor* lncRNAs die CaMKII-Aktivität fördern. Eine reduzierte bzw. erhöhte CaMKII Aktivierung könnte einen wichtigen Beitrag zur Förderung bzw. Hemmung des maladaptiven Remodelings durch Gadlor knock-out, bzw. Überexpression sein.

Schlußfolgerungen: *Gadlor1* und *Gadlor2* sind neuartige lncRNAs, die bei pathologischer Überlastung des Herzens hochreguliert werden und von Endothelzellen in EVs sezerniert werden. *Gadlor1* und *Gadlor2* induzieren kardiale Dysfunktion, Kardiomyozytenhypertrophie und myokardiale Fibrose, indem sie auf mehrere Herzzellen einwirken und die zelluläre Genexpression sowie die Kalziumdynamik in Kardiomyozyten beeinflussen, welche *Gadlor1/2* durch EV-vermittelten Transfer aus Endothelzellen aufnehmen. Eine gezielte Hemmung von *Gadlor* lncRNAs in Endothelzellen oder Fibroblasten könnte in Zukunft als therapeutische Strategie dienen.

3. Acknowledgement

I would like to thank those who supported me throughout my doctoral study, especially my supervisor Professor Dr Joerg Heineke for his support, guidance and willingness to share his experience with me. I have been extremely lucky to have an opportunity to do my doctoral thesis project in his group.

A grateful appreciation to Professor Dr Thomas Wieland for his guidance throughout the doctoral programme as my faculty supervisor for the HBIGS, and for being part of the Thesis Advisory Committee meetings and the defence examination. A special thanks to PD Dr Philipp Reiners-Koch for his great support and suggestions during the Thesis Advisory Committee meetings. Additionally, I would like to thank the members of the Doctoral Defence Committee, Professor Dr Georg Stoecklin and Professor Dr Marc Freichel for being the examiners.

A big thanks to Felix Trogisch for his guidance, as well as for acting 'unofficially' as my mentor for the last three years. A special thanks to Shruthi for her friendship right from the start, and for being there for all rises and falls. I am very grateful for my lab mates, whom I have had a chance to develop my research skills and teach me how to be a good scientist. Thanks to Steve, Rhys, Rebecca, Aya and Nina for making my PhD time memorable, especially for not only being colleagues but for becoming friends. Also, a special thanks to all members of Heineke lab who have made coming to the lab each day enjoyable!

I am extremely grateful to be part of the Heidelberg Bioscience International Graduate School, and thanks the HBIGS team for their support and guidance from the beginning. Additionally, thanks to the Collaborative Research Center (CRC) 1366 "Vascular Control of Organ Function" for the funding and scientific support provided for this project.

I have been very fortunate to have the support from my best friends Segah and Nazlican, thanks for being just to phone-call away and cheering me up whenever I need it. And Mert, thank you for being there any time I need support on bioinformatics and listening to my PhD-based ideas even if you didn't quite understand.

Finally, my deepest appreciation to my family for their constant love and support, especially my mom and dad. They have carried me through the good times and the bad, for which I am extremely grateful. I would not be where I am and who I am without you. Thank you for everything, I love you!

4. Table of Contents

5. List of Figures

6. List of Tables

7. Abbreviations

ACE	Angiotensin-converting-enzyme
Actn2	Actinin Alpha 2
AHA	American Heart Association
ANG II	Angiotensin II
Angpt2	Angiopoietin 2
Angptl4	Angiopoietin-like 4
ANP	Atrial natriuretic peptide
AP1	Activator protein 1
AT1	Angiotensin II receptor type 1
ATP	Adenosine triphosphate
Aurkb	Aurora kinase b
BNP	B-type natriuretic peptide
BPM	Beats per minute
BSA	Bovine serum albumin
Ca^{2+}	Calcium
Cacna1c	L-type voltage dependent calcium channel, alpha 1C subunit
CAD	Coronary artery diseases
CaMKII	Calcium/ calmodulin dependent protein kinase II
CD	Cluster of Differentiation
Cdk1	Cyclin-dependent kinase 1
circRNA	Circular RNA
CM	Cardiomyocytes
Col1a1	Collagen type I
Col3a1	Collagen type III
Col4a1	Collagen type IV
Col6a1	Collagen type VI
CPAT	Coding Potential Assessment Tool

CVD	Cardiovascular diseases
Cxcl2	chemokine (C-X-C motif) ligand 2
DAD	Delayed afterdepolarizations
Dll1	Delta Like Canonical Notch Ligand 1
DMEM	Dulbecco's Modified Eagle Medium
EC	Endothelial cell
ECG	Electrocardiogram
ECM	Extracellular matrix
EF	Ejection fraction
Efna1	Ephrin A1
EndoMT	Endothelial to mesenchymal transition
ER	Endoplasmic reticulum
ESC	European Society of Cardiology
ESCRT	Endosomal Sorting Complex Required for Transport
ETC	Electron transport chain
ETC	Electron transport chain
EV	Extracellular vesicles
exRNA	Extracellular RNA
FA	Fatty acid
FACS	Fluorescent-activated cell sorting
FB	Fibroblast
FCS	Fetal Calf Serum
Fgfr1	Fibroblast growth factor receptor 1
GADLOR	GATA Downregulation Long-noncoding RNA
Gata4	GATA binding protein 4
GLS	Global Longitudinal strain
GLYR1	Glyoxylate Reductase 1 Homolog
GO	Gene ontology
GSK3	Glycogen synthase kinase-3

GWAS	Genome-wide association studies
HDAC4	Histone deacetylase 4
HF	Heart failure
IB4	Isolectin B4
Icam5	Intercellular Adhesion Molecule 5
IGF1	Insulin growth factor-1
IL-1β	Interleukin 1-beta
IL-6	Interleukin-6
ILV	Intralumenal vesicle
ISEV	International Society of Extracellular Vesicles
JAK-STAT	Janus kinase (JAK)-signal transducer and activator of transcription (STAT)
Klf15	Krüppel-like factor 15
KO	Knock-out
LCCA	Left common carotid artery
lncRNA	Long non-coding RNA
Lsamp	Limbic System Associated Membrane Protein
LTCC	L-type calcium channel
LV	Left ventricle
LVAD	Left Ventricular Assist Devices
LVID	Left ventricle internal diameter
LVPW	Left ventricle posterior wall
Lpm	Litres per minute
MAPK	Mitogen-activated protein kinases
MEF2	Myocyte enhancer factor 2
Mfn2	Mitofusin 2
MHC	Major histocompatibility complex
MI	Myocardial infarction
miRNA	Micro RNA
MMP	Matrix metallopeptidase

mtDNA	Mitochondrial DNA
MV	Microvesicles
MVB	Multivesicular bodies
MYDGF	Myeloid-derived growth factor
Myh6	Myosin heavy chain 6
Myh7	Myosin heavy chain 7
Myl3	Myosin light chain 3
Na^+	Sodium
NASH	Non-alcoholic steatohepatitis
NCBI	National Center for Biotechnology Information
NCX	Sodium-calcium exchanger
nDNA	Nuclear DNA
NF-KB	Nuclear factor 'kappa-light-chain-enhancer' of activated B-cells
NTA	Nanoparticle tracking analysis
PBS	Phosphate buffered saline
PCR	Polymerase chain reaction
PFA	Paraformaldehyde
PGC1	Peroxisome proliferator-activated receptor-gamma coactivator-1 alpha
PI3K	Phosphoinositide 3-kinase
PK/PD	Pharmacokinetics/ Pharmacodynamics
PKA	Protein kinase A
PLN	Phospholamban
PPARA	Peroxisome proliferator-activated receptor alpha
qRT-PCR	Quantitative Reverse Transcription Polymerase Chain Reaction
RAP-MS	RNA antisense purification coupled with mass spectroscopy
Rcan1.4	Regulator of Calcineurin 1 - Isoform 4
RCCA	Right common carotid artery
RIP	RNA Immunoprecipitation
ROS	Reactive oxygen species

RyR2	Ryanodine receptor type 2
SEM	Scanning electron microscopy
SERCA	Sarco/endoplasmic reticulum Ca^{2+}-ATPase
Sirt5	Sirtuin 1
SNARE	Soluble N-ethylmaleimide-sensitive fusion protein attachment protein receptors
SR	Sarcoplasmic reticulum
TAC	Transverse aortic constriction
TAVI	Transcatheter aortic valve implantation
TEM	Transmission electron microscopy
TG	Triglyceride
TGFB	Transforming growth factor beta
Tlr9	Toll-like receptor 9
TNFA	Tumour necrosis factor alpha
VEGF	Vascular endothelial growth factor
WGA	Wheat germ agglutinin
WT	Wild type

8. Chapter 1: Introduction

8.1. Cardiovascular Diseases (CVDs) and Heart Failure

8.1.1. Epidemiology of CVDs

Cardiovascular diseases (CVDs) include conditions affecting the heart, coronary arteries and peripheral vasculature.[1] Despite the recent developments in diagnostic and therapeutic options, cardiovascular diseases are still the leading cause of global mortality with approximately 18 million deaths worldwide, ahead of cancer.[2,3]

The reported incidence and prevalence of CVDs worldwide differ according to ethnicity, gender, urbanization, age and morbidity rates due to the effects of genetics, environmental triggers and the socioeconomic state of the country.[1,3,4] Even though the incidence rates are lower in women, they have higher mortality (Women (W): 45% vs Men (M): 39% mortality due to Ischemic heart disease) and poor prognosis following a cardiac event.[1] However, men have a higher mortality rate than women in age-adjusted analysis (W: 266 vs M:372 in 100.000 people) for the European region.[1] Even though they share common risk factors, the observed difference might be influenced by the lifestyle including diet, alcohol consumption, smoking and more involvement of men in industrial and hazardous occupations, which promotes the risk factors of blood pressure, cholesterol and stress, besides crucial differences between sexes in physiology and genetics.[4-6]

The prevalence of CVDs increases quite steeply with age, particularly after 60 years.[7] Early prediction of diagnosis and selection of proper treatment can reduce the hospitalization and economic burden of CVDs, of which the estimated cost is more than 200 billion Euros in Europe (European Society of Cardiology (ESC), 2021 Report).[8] Even though, in recent years the incidence rate and mortality of CVDs are quite stable and even slightly improving in high-income countries, the rates are much higher in countries with low to middle income due to limited access to sufficient diagnostic and therapeutic advancements.[1,3]

According to American Heart Association (AHA) guidelines, among all CVDs heart failure (HF) is one of the most prevalent following heart attack and stroke, and causing enormous medical and economic burdens.[4] In the US, currently more than 6 million people are diagnosed with HF and almost 40% die within the first year of diagnosis.[4,9]

8.1.2. Heart Failure

Heart failure (HF) is a clinical condition, which is defined by the insufficiency of the heart muscle to pump enough oxygenated blood that is required for systemic needs.[10] HF is usually associated with symptoms like fatigue and weakness, shortness of breath, and pulmonary and peripheral oedema, which are induced by abnormal changes in the structure and function of the ventricles.[10] In addition, HF is a progressive condition, in which cardiac function deteriorates gradually, and severity often increases over time, and eventually resulting in death.[10-12]

HF is generally triggered by different conditions including coronary artery diseases (CAD), myocardial infarction (MI), hypertension, cardiomyopathy, arrhythmias or congenital heart defects.[4] Diagnosis of HF is based on observations of the symptoms with clinical testing methods such as the electrocardiogram (ECG), echocardiography and evaluation of comorbidities (e.g. diabetes, anaemia, haemodynamic and renal dysfunctions).[10]

Treatment strategies for HF include pharmacological approaches, such as angiotensin-converting-enzyme (ACE) inhibitors, beta-receptor blockers and aldosterone antagonists, and changes in lifestyle with dietary recommendations (e.g. reduced salt intake), as well as the implantable devices (e.g. pacemakers, implantable defibrillators, LVAD).[13-15] Despite the improvements in the cardiovascular therapeutics, higher mortality and morbidity indicates the need for novel therapy options including nucleic-acid based methods.[16] The majority of current therapeutic options target protein-coding genes; however, recent studies revealed the significance of non-coding transcripts in cardiovascular development and disease conditions.[15,17,18]

8.1.2.1. Pathophysiology of Cardiac Hypertrophy and Heart Failure

Heart failure is typically induced by conditions like coronary artery diseases, ischemia or congenital disorders, but mostly these stress stimuli initially trigger cardiac hypertrophy to compensate for heart function.[11,12]

Cardiac hypertrophy is described as an enlargement of cardiomyocytes in both length and width for counteracting the increased stress on the ventricular walls,[11] and compensates for inadequate pumping function.[19] Since more than 80% of the heart is composed of cardiomyocytes, which are terminally differentiated cells with almost no capacity for proliferation, cardiac growth mainly occurs at the individual cardiomyocyte level via increased sarcomere assembly.[20] It is an initial adaptive response of the heart to stress conditions, such as pressure overload, which leads ultimately entails pathological remodelling.[17,21]

When induced by physiological demands like exercise or pregnancy, cardiac hypertrophy results in adaptive remodelling, which is not detrimental, and not accompanied by fibrosis, cell death or dysfunction.[20] For instance, hypertrophic growth in trained athletes results in an almost 60% increase in the left-ventricle mass compared to controls as an indication of plasticity of the heart.[22] The changes happening for the remodelling of the heart from normal to physiological hypertrophy are mostly reversible, however, pathological remodelling is only partially reversible, while advanced heart failure is irreversible.

Cardiac hypertrophy associated with physiological demand leads to changes in the heart structure which is a uniform increase in the chamber dimensions, and referred as eccentric remodelling.[11] In contrast, pathological hypertrophic growth is triggered by neurohormonal stimulation, hypertension or ischemic injury, and leads to maladaptive remodelling that is often followed by ventricular dysfunction, and electrophysiological problems causing arrhythmia, and consequently heart failure and death.[19] Pathological growth usually arises from concentric hypertrophy due to pressure overload (e.g. chronic hypertension or aortic valve stenosis), which is characterized by the increase in the wall thickness and septum without overall enlargement, and a decrease in the volume of ventricles.[11,20,23]

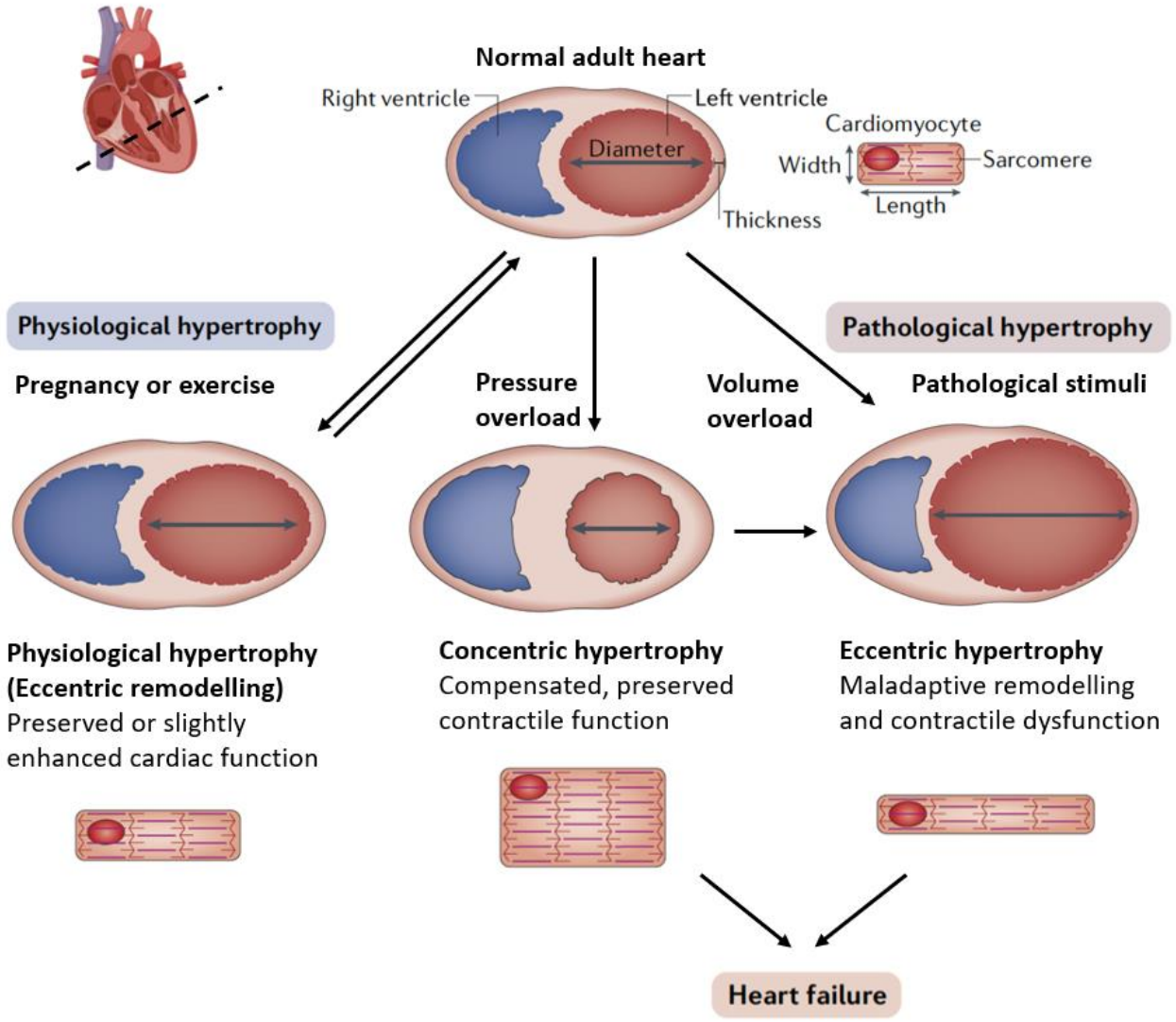

Figure 1: Process of cardiac remodelling associated with cardiac hypertrophy.

Scheme depicting the process of cardiac remodelling with different types of cardiac hypertrophy via physiological or pathological stimuli. The normal adult heart can adapt to stress conditions during pregnancy and endurance training with balanced eccentric remodelling in the process called physiological hypertrophy. In this case, the heart preserves, or even mildly improve cardiac function. In contrast, in response to pathological stimuli, such as aortic stenosis or hypertension, concentric hypertrophy usually forms with an increase in septal and wall thickness with reduced chamber dimension, which eventually can lead heart failure. In addition, pathological hypertrophic growth can be followed by eccentric hypertrophy resulting in dilated chambers, and cardiac contractile dysfunction, while some diseases directly result dilated cardiomyopathy. *Image is adapted from "Molecular basis of physiological heart growth: fundamental concepts and new players, Maillet et al. (2013)" and "Mechanisms of physiological and pathological cardiac hypertrophy, Nakamura and Sadoshima (2018)".*

In the later stages of heart failure, this maladaptive remodelling leads to the excessive dilation of the ventricle, without wall or septal increase, with eccentric hypertrophy[24] **(Figure 1).** In addition, cardiac dilation due to volume overload (e.g. MI or valve insufficiency) can also directly result in dilatory cardiac growth.[11]

8.1.2.2. Cellular and Molecular Changes in Cardiac Hypertrophy

During cardiac remodelling, the heart undergoes a series of structural changes in addition to hypertrophy, including extracellular matrix (ECM) deposition, altered vascularization, and changes in calcium handling, metabolism and gene expression.[12,20]

Fibrosis

Fibrosis is defined as the accumulation of ECM proteins including collagens, fibronectin, and matrix metalloproteinases (MMPs) during the pathological cardiac remodelling process, especially excessive deposition of collagen type I and III[12] **(Figure 2)**. Formation of balanced and organized ECM network for proper mechanical, chemical and electrical coordination of the heart is crucial for maintaining contractile function.[12,25] Under normal conditions, collagen production and degradation are strictly regulated and balanced, in which fibroblasts (FB) contribute to the process via secretion of regulatory cytokines and growth factors.[26]

Upon pathological stimulation, mainly FBs, but also endothelial cells (EC), macrophages and mast cells, and cardiomyocytes (CM) contribute to the formation of cardiac fibrosis via stimulating profibrotic pathways.[24] In recent years, the contribution of ECs to fibrotic remodelling by endothelial-to-mesenchymal transition (EndoMT) has been reported in many studies of disease hearts.[27-29] Additionally, both ECs and CMs activate profibrotic pathways via the secretion of proinflammatory signals.[12]

Angiotensin II (Ang II) is one of the major inducers of fibrosis[11] by binding to angiotensin II receptor type 1 (AT1) and stimulating the expression of transforming growth factor beta (TGFβ), which then contributes to the transdifferentiation of FBs to myofibroblast.[12] In response to

persistent pathological stimuli, myofibroblasts cause an excessive accumulation of collagens, leading to stiffness and contractile dysfunction.

In addition to TGFβ activation, Ang II can activate Janus kinase–Signal Transducers and Activators of Transcription (JAK-STAT) pathways including transcription factors nuclear factor kappa-light-chain-enhancer of activated B cell (NF-κB) and activator protein 1 (AP1). It has been shown that several MMPs have AP-1 and NF-κB binding sites in the promoter regions, such that Ang II stimulation on rat FBs triggered the collagen type I production via activation of these transcription factors.[30,31] Thus, fibrosis development can also be triggered by the inhibition of MMPs during pathological remodelling.

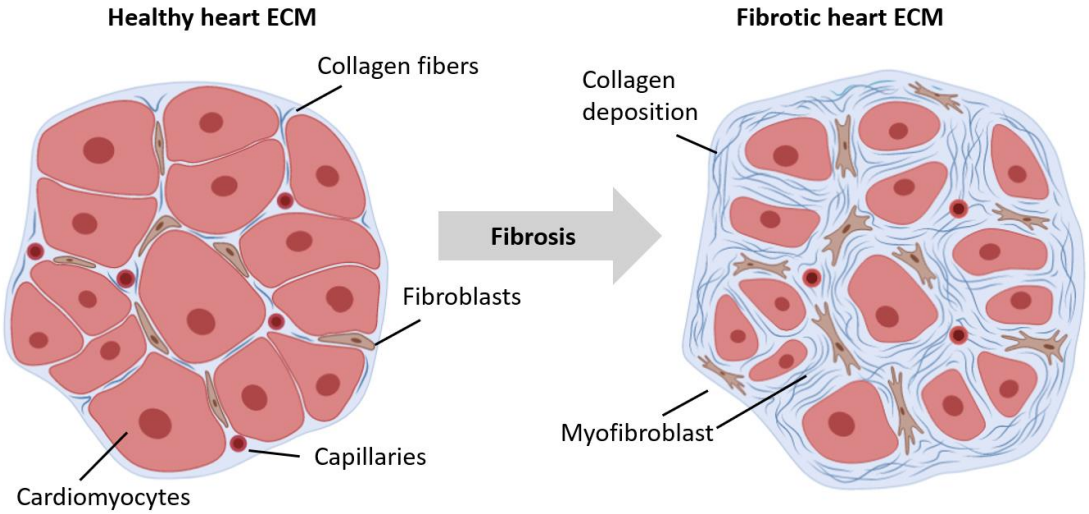

Figure 2: The overview of cardiac fibrosis development due to pathological remodelling.

The structure of ECM in the healthy and fibrotic heart after maladaptive remodelling due to pathological stimuli such as pressure overload. During fibrosis development, an excessive collagen network is deposited between cardiomyocytes and vasculature, which leads to the micro-scar formation, loss of capillaries and eventually loss of cardiomyocytes. *Illustration is adapted from "Cardiac Fibrosis in the Pressure Overloaded Left and Right Ventricle as a Therapeutic Target, Schimmel et al. (2022)" and created by using www.biorender.com.*

Angiogenesis

Angiogenesis is one of the key characteristics of the remodelling process in the heart upon both physiological and pathological stimuli. Since oxygen demand and nutrient supply are maintained by proper coronary perfusion, an increase in myocardial vascularization is an adaptive and protective mechanism during pathological remodelling.[32]

Shiojima and colleagues showed that conditional activation of *Akt1* expression in the heart exhibited physiological hypertrophy with preserved cardiac function for 2 weeks, in contrast, led to dilated cardiomyopathy and heart failure in the chronic phase after 6 weeks.[33]

Vascular endothelial growth factor (VEGF) is critical for vascularization, which is not only secreted by EC but also by CMs. Reduction of VEGF signalling in mice after pressure overload resulted in pathological remodelling with rarefaction of vascularization and contractile problems.[34] Heineke et al. initially showed a novel function of cardiomyocyte GATA4 in the regulation of angiogenesis, where GATA4 overexpression in myocytes facilitates angiogenesis through the secretion of VEGF-A.[35] In another key study of cardiac angiogenesis, Sano and colleagues demonstrated that accumulation of p53 due to pressure overload inhibits Hif-1 activation and consequent VEGF activation, thereby inducing maladaptive hypertrophy by inhibition of cardiac angiogenesis.[36] Additionally, Carmeliet and colleagues showed that cardiomyocyte-specific deletion of VEGF-A in mouse models led to decreased capillarization in the myocardium followed by contractile dysfunction, which indicates the importance of CM contribution in vascularization.[37]

Inflammation

During cardiac remodelling after a pathological trigger, increasing activity of the innate immune system stimulates the infiltration of proinflammatory cytokines such as TNF-α, IL-1β, and IL-6, which induces hypertrophy in CMs.[38] Inflammation contributes to the pathogenesis of HF, in which the acute response is suggested to be adaptive and beneficial for cardiac repair, and maintenance of the contractile function, however, chronic inflammation is considered to be detrimental and results in maladaptive changes.[12,39]

Studies have suggested a potential role of chronic inflammation in cardiac metabolism and contractility. Recently, Korf-Klingebiel and colleagues have identified cross-talk between CMs and inflammatory cells, in which myeloid-derived growth factor (MYDGF) affects calcium homeostasis and eventually contractility via sarcoplasmic reticulum Ca^{2+}-ATPase (SERCA2a), and protects the heart against pressure overload–induced HF.[40]

Calcium Homeostasis

Calcium (Ca^{2+}) handling is particularly important for cardiac muscle contraction in a process called excitation-contraction coupling (ECC).[41] In a healthy heart, an action potential triggers the depolarization of the cardiomyocyte membrane and Ca^{2+} influx into the cell via L-type Ca^{2+} channels (LTCC). LTCCs are located within the transverse tubules (T-tubules), which are the invaginations of the sarcolemma that extend towards the sarcoplasmic reticulum (SR) into the cell.[41] The influx of Ca^{2+} also triggers the release of more Ca^{2+} from the SR via ryanodine-receptor type-2 (RyR2) with a mechanism called calcium-induced calcium release. An increase in the intracellular calcium levels then triggers the binding of Ca^{2+} to troponin C, which shifts tropomyosin location, enables myosin/titin interaction and cross-bridge cycling[12,42] **(Figure 3)**.

The sarcoplasmic reticulum is a special organelle that stores, sequesters or releases Ca^{2+} via channels and pumps for balancing the intracellular calcium levels.[43] For relaxation to occur, Ca^{2+} need to be cleared from the cytosol, whereby the majority of the cytosolic Ca^{2+} return to SR by the SERCA2a pump while a smaller portion extruded from the cell with Na^{+}/Ca^{2+} exchanger (NCX) located on the sarcolemma.[41] Activity of SERCA2a is inhibited by phospholamban (PLN).[42] PLN phosphorylation can be mediated by protein kinase A (PKA) at serine-16 or Ca^{2+}/calmodulin-dependent protein kinase II (CaMKII) at threonine-17, and phosphorylated PLN (p-PLN) dissociates from SERCA2a and thus upregulates its activity.[44] Reduced phosphorylation of PLN results in impairment in the activity of SERCA to pump Ca^{2+} efficiently back to SR, thus accumulation of Ca^{2+} in the cytosol prevents proper relaxation.[41] Additionally, this results in less Ca^{2+} availability for the next systolic phase. Disruption in the calcium homeostasis can lead to arrhythmia, such that elevated levels of intracellular Ca^{2+} result in delayed after-depolarizations

(DAD) following the full repolarization[45], and moreover higher Ca^{2+} in the cytoplasm can activate other cation channels like NCX.[46]

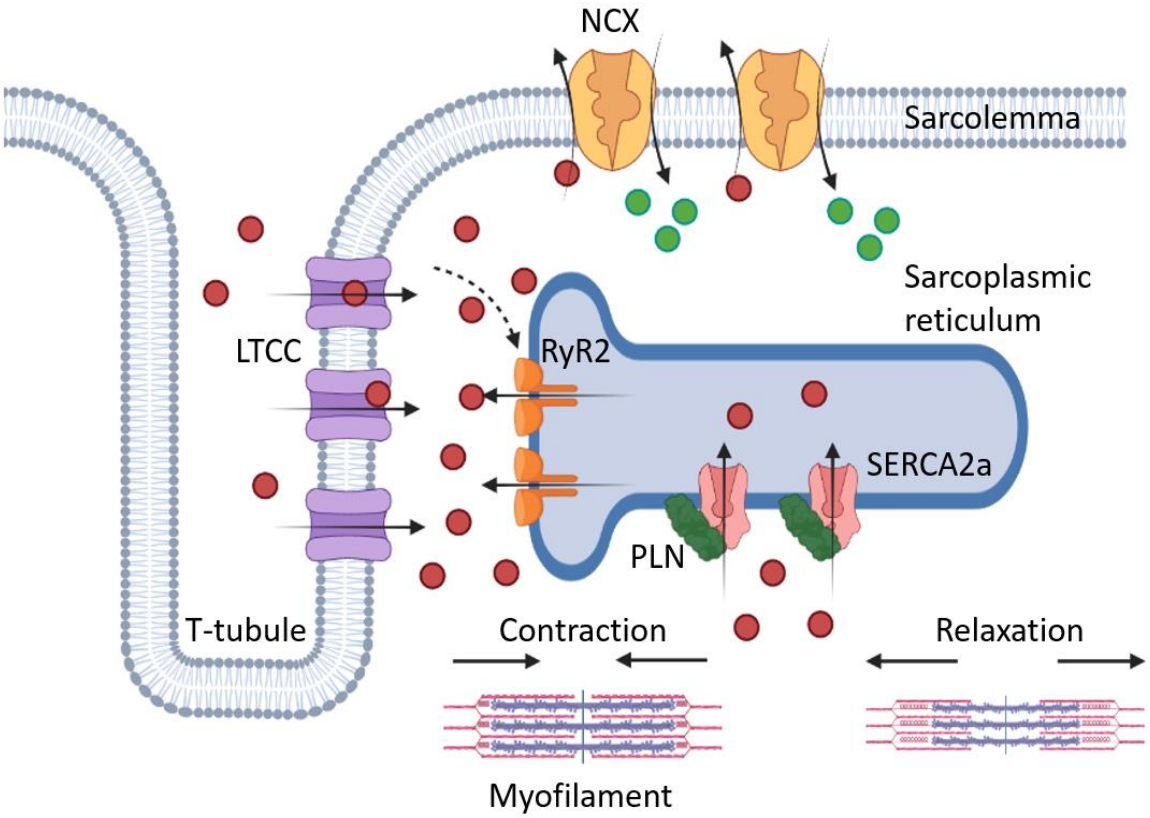

Figure 3: Regulation of calcium dynamics in cardiomyocytes during ECC.

Scheme depicting a simplified version of calcium dynamics during ECC. Following the action potential, calcium enters cardiomyocytes via L-type calcium channels, which are physically located nearby the ryanodine receptor type-2. Calcium current trigger the opening of RyR2, which further increases the intracellular calcium levels. The binding of calcium to myofilament proteins triggers the contraction. For relaxation to be initiated, calcium needs to be cleared from the cytosol by activation of SERCA2a, and a smaller amount is extruded from the cell by NCX. SERCA2a activity is controlled by the phosphorylation of PLN. *Illustration is adapted from "Mechanisms of Altered Ca^{2+} Handling in Heart Failure, Luo and Anderson (2013)" and created by using www.biorender.com.*

In heart failure, it has been demonstrated in multiple studies that SERCA2a levels are downregulated, or the activity of SERCA2a is reduced via PLN.[41,47-49] For instance, targeted knock-out of PLN has beneficial effects in contraction due to an increase in SERCA2a activity[50], however,

in another study, this increased mortality and altered mitochondrial calcium levels and led to cardiomyocyte death.[51] Inhibition of CaMKII has shown to have beneficial effects in cardiac remodelling by reducing hypertrophy and arrhythmias, however, inhibition usually results in dual effects in calcium dynamics in different disease models due to the lack of specificity of the inhibitors.[42,52]

Metabolism and Oxidative Stress

Mitochondria are the energy production machinery of the cells. Since the heart is the most metabolically active organ, it has the highest amount of mitochondria content compared to other organs taking almost 30% of its volume.[53] Adenosine triphosphate (ATP) generated in the mitochondria is actively used in the contraction and relaxation cycles of the heart, thus any disruption of this dynamic would lead to cardiac dysfunction.[54] However, the heart is an adaptable organ, and any change in the metabolic demands leads to a switch in the metabolic substrate used to maintain the constant energy supply.[12,55]

During embryonic and fetal development when cardiomyocytes are proliferative[20], glycolysis is the main energy source, which is then changed into fatty acids (FA) being the key substrate after birth.[56] Under normal conditions, almost 80% of the energy used is derived from FA oxidation and the rest from glucose and lactate.[56] When FAs entered CMs, they usually are directly utilized for beta-oxidation and some can undergo esterification to be stored as triglyceride (TG) lipid droplets[57] **(Figure 4)**. Upon pressure overload, FA oxidation genes, such as peroxisome proliferator-activated receptor-α (PPARα) and PPARγ co-activator-1α (PGC1-α) are downregulated.[58,59] This triggers the substrate switch to glucose/pyruvate and upregulates glycolytic genes.

In hypertrophic hearths, the energy demand is increasing due to the increasing amount of cardiac workload.[12,20] Thus, this substrate switch is considered to be an adaptive mechanism since glucose utilization requires less oxygen than FA utilization.[55] Moreover, it has been shown that TG lipid droplets can serve as an energy source, however, in cases like diabetic cardiomyopathy where substrate utilization is impaired, accumulation of lipid droplets can trigger autophagy and

cell death.[60,61] Overall, since HF has different types and it is a progressive disease, the metabolic changes are also complex, and there are still some studies with contradicting results indicating the importance of understanding cardiac metabolism.[54]

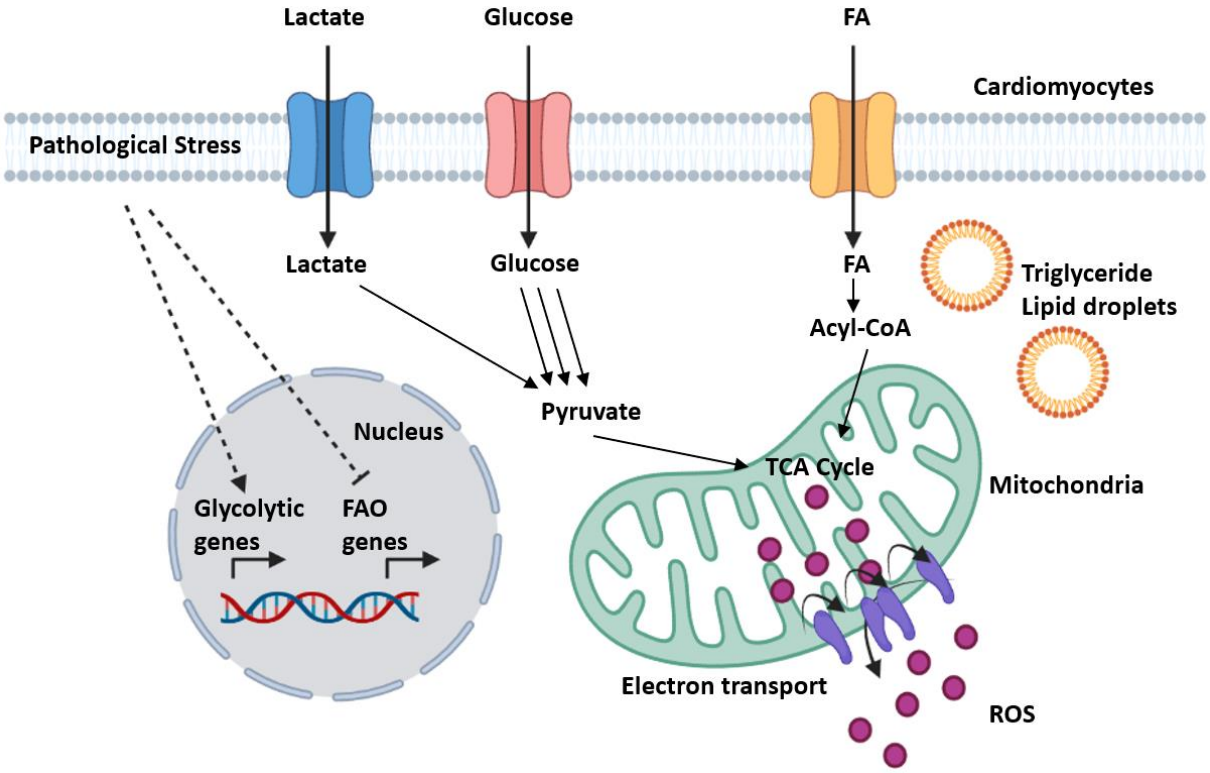

Figure 4: Overview of energy metabolism and substrate utilization in the heart.

Simplified illustration of energy metabolism in cardiomyocytes after pathological stress, which downregulates the transcription of FA oxidation genes, while glycolysis-associated genes are upregulated. The main substrate utilized for the energy demand is shifted to the glucose/pyruvate pathway and FA oxidation is downgraded. Mitochondrial dysfunction and ROS accumulation lead to mitochondrial autophagy and cell death. *Illustration is adapted from "Pathophysiology of cardiac hypertrophy and heart failure: signalling pathways and novel therapeutic targets, Tham et al. (2015)" and created by using www.biorender.com.*

Metabolic alterations during pathological remodelling result in unbalanced production and blunted detoxification of reactive oxygen species (ROS).[12,54] ROS accumulation can be a result of impaired coupling of the electron-transport chain (ETC) and electron leakage[54] **(Figure 4)**. Accumulation of ROS observed in HF patients, however, clinical trials with antioxidant therapies

provide unsatisfactory results,[62,63] thus the contribution of ROS in HF pathogenesis is not yet completely understood. Furthermore, Dai and colleagues have shown that pro-hypertrophic Ang II is also contributing to ROS production via MAPK-associated pathways, and eventually provokes damage in the mitochondria, hypertrophy and fibrosis.[64]

Mitochondria are an adaptable organelles, whereby in case of excessive ROS, mitochondrial autophagy will remove the damaged organelles.[12] However, during HF, increased impairment of mitochondria will result in apoptosis rather than autophagy.[65]

8.2. Non-coding Genome

The central dogma of molecular biology defined by Francis Crick explained the transfer of genomic information from DNA to messenger RNA (mRNA) via transcription, and mRNA to protein by translation.[66] Discovery of the non-coding genome challenged this definition to be revisited, since the majority of actively transcribed genome generate non-coding RNA transcripts, such as microRNAs (miRNA), long non-coding RNAs (lncRNA) and circular RNAs (circRNA).[17] The non-coding regions of the genome, which do not encode for a protein, were considered to be "junk DNA" until the completion of the Functional Annotation of the Mammalian Genome Project (FANTOM).[15] Only about 2-3% of the transcriptionally active region of the genome is protein-coding, and the rest corresponds to the non-coding genome.[67]

The advancements in next-generation sequencing technologies facilitate the studies for deciphering the importance of the non-coding genome. The non-coding genome is biologically and functionally heterogenous, and currently, at least three sub-classes of ncRNAs are being investigated.[15,67] MiRNAs are single-stranded, highly conserved, and short (21-23 nucleotides) non-coding RNAs, which are also quite stable and easily detectable.[68,69] MiRNAs are extensively studied in CVDs for their regulatory roles in post-transcriptional regulation of mRNAs, however, miRNA therapeutics have not been incorporated into the clinical practise yet.[68] LncRNAs are longer than 200 nucleotides, highly tissue and condition-specific, however, evolutionarily poorly conserved between species.[67] CircRNAs are the most recently defined class of non-coding RNAs, which form by back-splicing, and are more stable than linear RNAs due to covalent bond formation.[17]

8.2.1. Long non-coding RNAs: Characteristics, Classification and Function

The long non-coding RNAs (lncRNAs) are a diverse group of non-coding transcripts. LncRNAs are very similar to mRNAs as they are transcribed by RNA polymerase II, with subsequent modifications including 5'capping, splicing and polyadenylation.[69] Their open reading frame (ORF) is not translated, however, some contain cryptic ORFs. Hence, the majority of them do not code for any proteins, however, in recent studies, it has been shown that some can encode for micro-peptides. For instance, Anderson and colleagues identified a micro-peptide-based control of SERCA that affects muscle contractility via direct interaction.[70,71]

LncRNAs are classified based on their localization in the genome. If lncRNAs localized within a protein-coding gene and share the same promoter, they are called sense or antisense in the opposite strand.[67] They can also arise from the intronic region or the enhancer region of a protein-coding gene, or located between two protein-coding genes (intergenic region). Interestingly, the number of lncRNAs increases with the complexity of the organism, which might indicate a potential link to evolution.[72]

The role of lncRNAs is highly dependent on their structural properties, and because of their complex structure, elucidation of the mechanism of action is challenging.[67] Currently, known functions of the lncRNAs are: acting as chromatin modifiers or miRNA sponges, promoters of protein-protein interactions by scaffolding, and affecting mRNA stability by contributing to post-translational modifications.[17] LncRNAs can function in *cis* or *trans* action mechanisms, as they affect the neighbour genes on the same chromosome, or any gene distal to its location via different mechanisms, respectively[67] **(Figure 5)**. Cis-acting lncRNAs regulate the expression of the local genes by modifications in the chromatin via recruitment of chromatin-associated proteins, or direct interaction with the chromatin by generating loops[69,73] **(Figure 5A)**. Some examples of *cis*-regulatory lncRNAs include dosage compensation lncRNAs in such epigenetic silencing of one of the X chromosomes in females with the lncRNA *XIST*[74], and enhancer lncRNAs (eRNA) like *CCAT1-L,* which is located at 515 kilobases (kb) upstream of the *MYC* oncogene locus and provides chromosome looping in the gene promoter region.[75] *Trans*-acting lncRNAs mainly contribute to nuclear architecture at the epigenetic level by either changing the physical dynamics or acting on histone modifications[69,76] **(Figure 5B)**. For example, a well-studied lncRNA MALAT1 promotes the

alternative splicing of pre-mRNAs via interactions with various splicing factors and might involve direct DNA-RNA interactions.[77]

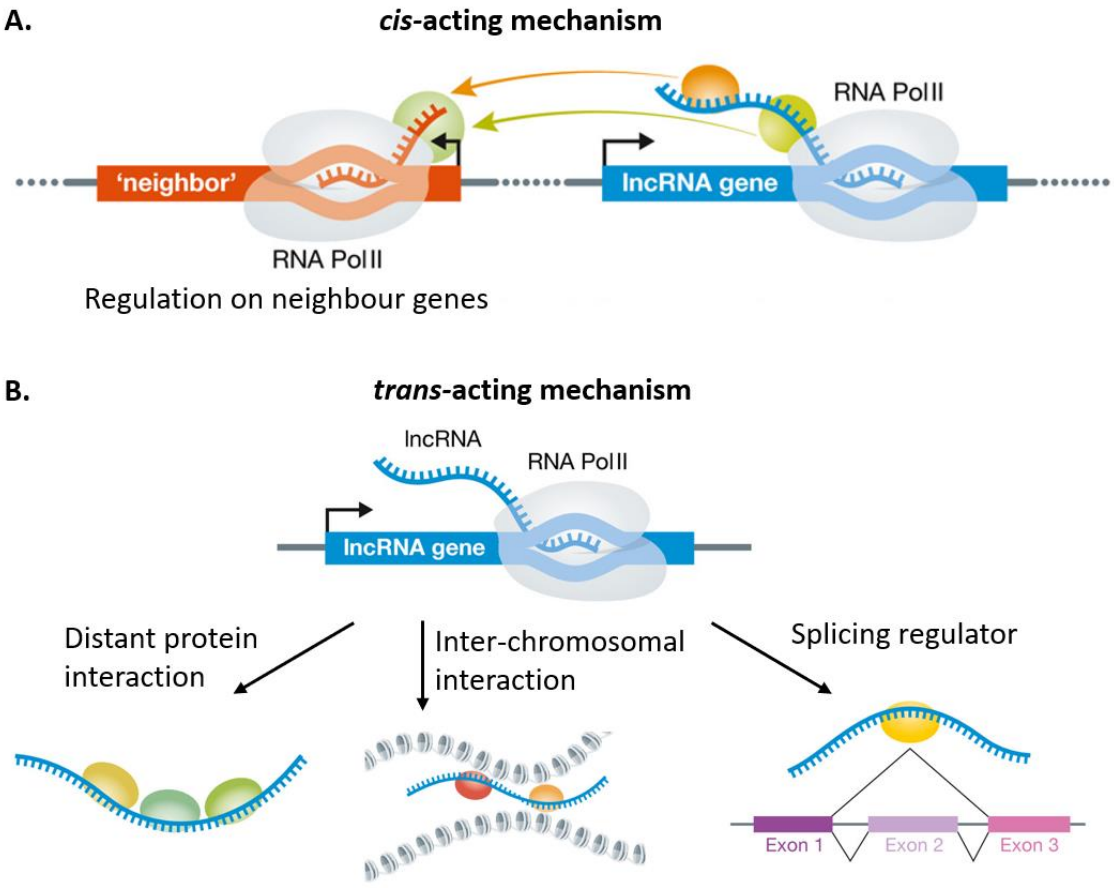

Figure 5: Function mechanism of long non-coding RNAs.

Illustration of defined acting mechanisms of lncRNAs. **A.** *Cis*-acting mechanism on local and neighbour genes. **B.** *Trans*-acting mechanism showing a distal interaction between lncRNA and proteins, miRNAs via acting as sponges or regulation of mRNA splicing. *Image is adapted from "Modulating the expression of long non-coding RNAs for functional studies, Liu and Lim (2018)".*

8.2.2. Role of lncRNAs in Cardiac Hypertrophy and Heart Failure

Recent studies have identified lncRNAs with a crucial role in regulating cardiac conditions, such as lncRNAs in cardiac development and regeneration, atherosclerosis and lipid metabolism, endothelial and vascular development, cardio-oncology, cardiac hypertrophy and heart failure via different mechanisms.[17,68,78,79] For instance, the lncRNA *Chast* (cardiac hypertrophy-associated

transcript) induces cardiac hypertrophy by disrupting the cardiomyocyte autophagy process via downregulation of *Plekhm1* (Pleckstrin homology domain-containing protein family M member 1), whereas *Mhrt* (myosin heavy-chain-associated RNA transcript) is a cardiac-specific anti-hypertrophic lncRNA that protects against heart failure by directly binding to Brg1 (Brahma-related gene 1) and preventing its chromatin remodelling function.[80,81]

Since lncRNAs are highly cell or tissue-specific, and in most cases condition-specific as well, their expression is altered based on disease progression, thus they could potentially be used as biomarkers or therapeutic targets.[15,79] Despite successful application in pre-clinical animal studies in the regulation of lncRNAs for CVDs, currently no lncRNA-based are established yet.[15,78] Only recently, the Swiss biotech company HAYA Therapeutics is working on the commercialization of ASO-mediated inhibition of super enhancer-associated lncRNA *Wisper*, which is a fibroblast enriched lncRNA, as antifibrotic approaches after MI.[82]

8.2.3. Circulating non-coding RNAs

Circulation of extracellular RNAs (exRNA) throughout the body via biofluids to act on distal targets has been recently described.[17] ExRNAs include various non-coding RNAs either encapsulated within the extracellular vesicles (EVs) or incorporated with lipoproteins to be protected from degradation.[78]

Non-coding transcripts can be detectable in human body fluids such as serum/plasma and urine, however, the origin of the RNA and how it is selectively transported into the EVs are still under debate. Circulating miRNAs and lncRNAs are currently being investigated as alternative clinical biomarkers, as well as for being paracrine mediators of cellular communication during stress conditions.[79,83,84] Intracardiac communication is a highly regulated process due to the complex physiology of the heart, where proper synchronicity is required between CM, EC and FB as being the major cardiac cell types.[85,86] Cellular communication during remodelling in response to stress signals can be mediated by the secretion and transfer of nanoscale EVs including microvesicles and exosomes carrying ncRNAs and alter the behaviour of the recipient cells.[67,87-89]

8.3. Extracellular Vesicles (EVs): Characteristics and Types

Extracellular vesicles (EVs) are a diverse group of nanoscale particles, which are phospholipid membrane-bound structures containing different proteins, lipids and nucleic acids including miRNAs, tRNA and lncRNAs.[90-92] EVs are heterogeneous in terms of biogenesis, RNA content, release and function. Due to their potential as biomarkers or therapeutic delivery vehicles, and role in intercellular cross-talk **(Figure 6A)**, understanding the origin of their bioactive cargo and how these are encapsulated within the vesicle is crucial, thus EVs are broadly studied in the field of cancer, immunology and as well as in CVDs.[78]

Defined surface markers including integrins, tetraspanins like CD9, CD63 and CD81, heat shock proteins, lipid rafts such as flotillins or ceramides, and major histocompatibility complex (MHC) on EVs have exhibited coexistence in different types[93] **(Figure 6B)**. Since EVs cannot be classified based on their surface markers, they are defined depending on their size, biogenesis and release mechanism. Traditionally, EV subtypes are based on their size defined as exosomes which are 50-120 nanometres (nm) in diameter, while microvesicles between 100-1000 nm and apoptotic bodies are larger than 1 micrometre (μm).[94,95] Given the fact that EV separation based on their size is challenging, the International Society of Extracellular Vesicles (ISEV) guidelines suggested classifying them as small EVs if sedimented at 100.000 xg, medium EVs, if sedimented at lower than 20.000 xg, and large EVs for the rest.[93]

Currently, there are various EV isolation methodologies used such as differential centrifugation, density gradient separation, affinity capture and size-exclusion chromatography.[96] All these methods have their advantages and limitations, however, isolation with ultracentrifugation is still the most widely used technique.[95] Visualization and size detection of EVs can be achieved with transmission electron microscopy (TEM), scanning electron microscopy (SEM) or cryo-electron microscopy, and nanoparticle tracking analysis (NTA).[97,98] In addition, the characterization of surface markers can be performed with flow cytometry, protein and lipid quantification, and omics technologies for deep understanding.[99] Since EVs are a heterogenous group of nanoparticles, standardization of the isolation protocols, characterization of the vesicles and deciphering the mechanism of RNA transport and delivery is still laborious.

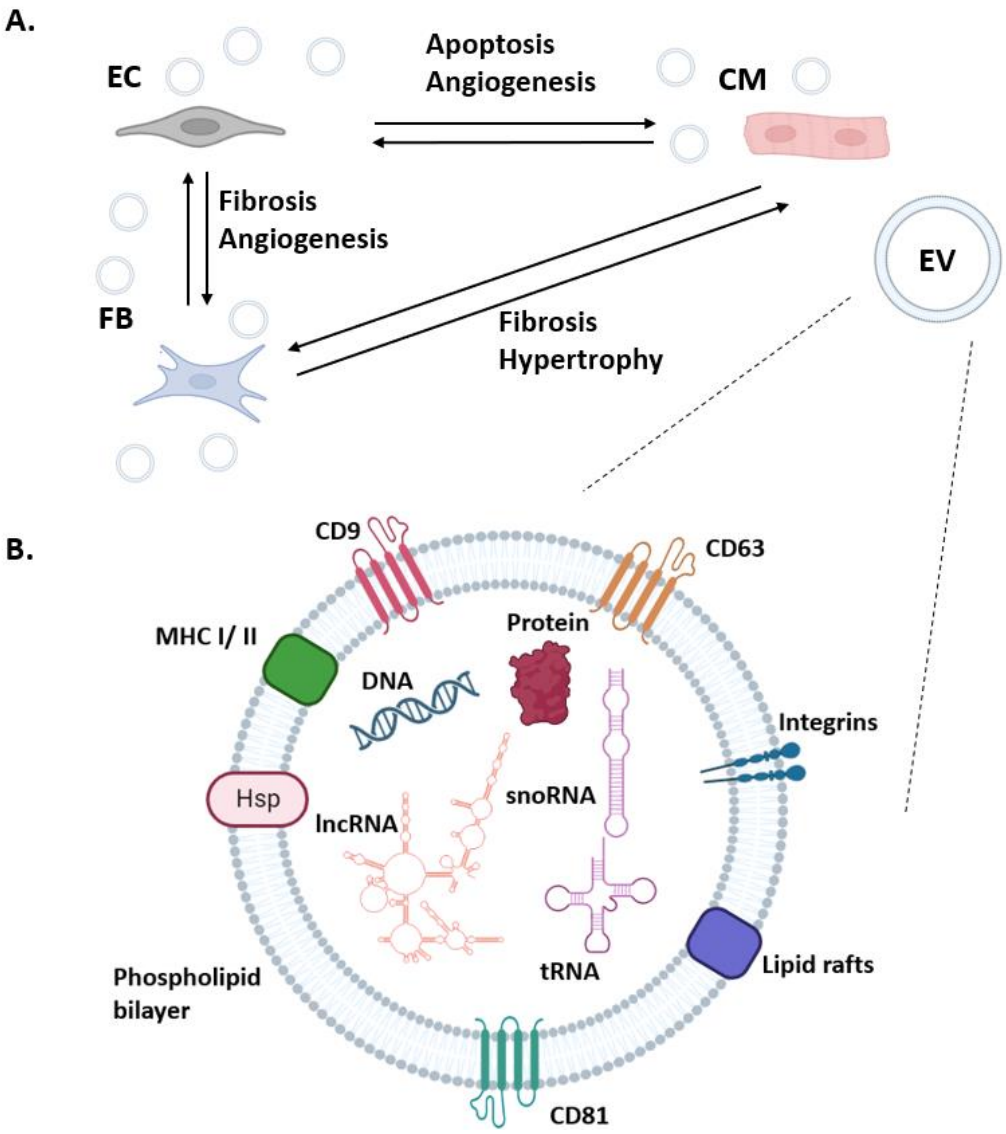

Figure 6: Intercellular communication between cardiac cells mediated by EV bioactive cargos.

Scheme demonstrating the role of EVs in the intercellular communication of cardiac cells**. A.** Simplified version of intracardiac communication between major cell types during cardiac remodelling. EVs mediating the cellular cross-talk via paracrine manner. Cells can release or uptake the EVs. **B.** EVs are the nanoscale membrane bound structures with bioactive cargos, including DNA, tRNA, snoRNA, mRNA or lncRNA, and proteins. Surface of the EVs exhibit common surface markers like tetraspanins, heat shock protein (Hsp), integrin and MHC I/II. *Illustration is adapted from "Extracellular Vesicles in Cardiac Regeneration: Potential Applications for Tissues-on-a-Chip, Wagner et al. (2021)" and created by using www.biorender.com.*

8.3.1. EV Biogenesis and Release

EV biogenesis and release mechanisms are extensively studied to define different subclasses, and understand their role in cellular communication since the EV release process can be cell-specific and modulated by physiological or pathological stress.[94] Exosomes and microvesicles (MVs) have different biogenesis mechanisms.

Exosome Biogenesis and Release

Exosomes are derived from the endosomal process including double-invagination of the plasma membrane, and the formation of several intraluminal vesicles (ILVs).[100] Initial invagination of the plasma membrane forms a pocket-shaped structure that can internalize the cargo and can fuse with early endosomes.[101] Golgi-network and endoplasmic reticulum (ER) contribute to the endosomal process, especially sorting bioactive cargos into the endosomes, which eventually form microvascular bodies (MVB) with several ILVs packed. If the cargo is for degradation, MVBs fuse to lysosomes to form autophagosomes, or if the cargo is for recycling or to be released then MVBs fuse to the plasma membrane. This double-invagination process releases the ILVs as exosomes[102] **(Figure 7A)**.

The endosomal process including the initiation of the first invagination to release exosomes requires initial membrane preparation, in which the endosomal membrane is enriched with tetraspanins and endosomal-sorting complexes required for transport (ESCRTs).[103,104] Even though the ESCRT-dependent pathway of endosomal biogenesis is considered to be the main mechanism, there are multiple ESCRT-independent pathways via the contribution of different proteins such as syndecan-1, sphingomyelinases and SNARE complexes.[105,106]

Overall, exosomes are generated by the endosomal process via different mechanisms, which might be related to the cell-type or physiological state of the organism.

Microvesicle Biogenesis and Release

Even though the biogenesis and mechanism of microvesicles are less broadly studied compared to exosomes, MVs generally form after the outward budding of the plasma membrane.[107] **(*Figure 7*B)**. MV biogenesis also requires some arrangements of the plasma membrane including alterations in the protein and lipid composition, and additional modifications including calcium-dependent enzymatic machinery and actin-myosin cytoskeletal machinery allowing contraction of the membrane leading to the budding and release.[108]

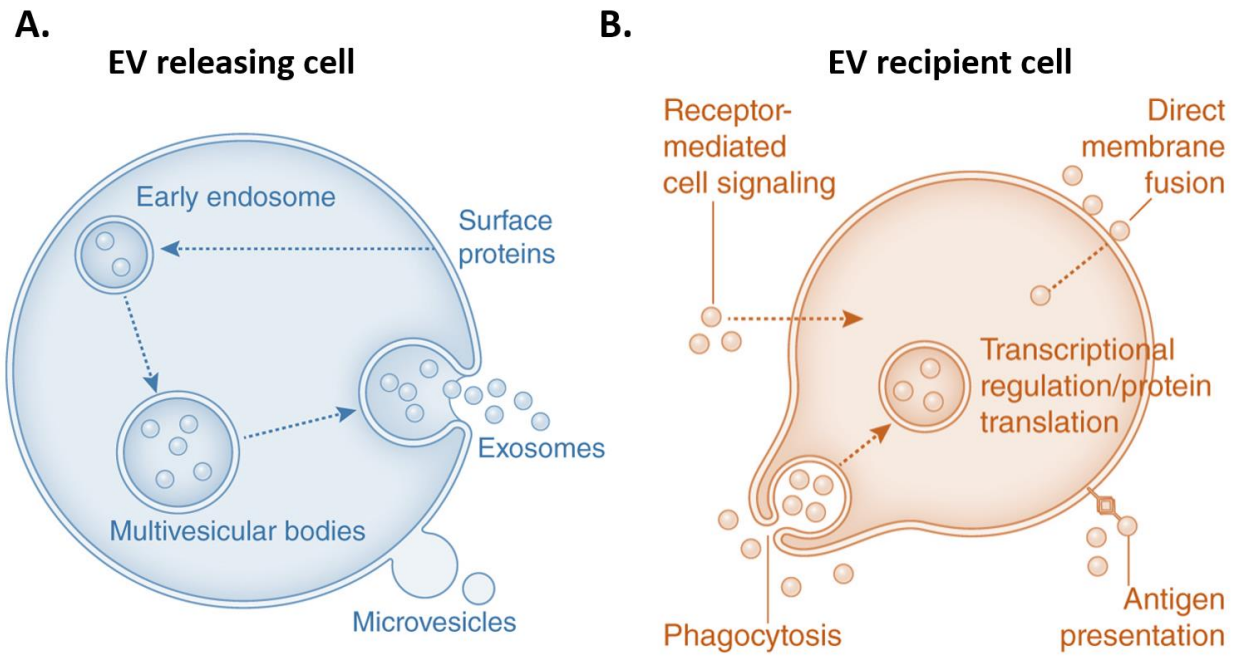

Figure 7: Exosome and microvesicle releasing and uptake mechanisms.

Exosome and microvesicle (MV) biogenesis and releasing mechanisms require proper adjustments in the cell architecture. **A.** Exosome biogenesis and release via endosomal pathways via formation of microvascular bodies (MVBs) released by fusion of vesicle to the plasma membrane after invagination. On the contrary, MVs are released after membrane shedding. **B.** Exosomes and MVs are taken by the recipient cell via phagocytosis, receptor-mediated transport or direct fusion to the plasma membrane. *Illustration is adapted from "Extracellular vesicles in kidney transplantation: a state-of-the-art review, Ashcroft et al. (2021)".*

8.3.2. EV Uptake

Once released from the producing cell, EVs can be taken up from the recipient cells via different mechanisms, which then can alter their gene expression or behaviour to certain pathophysiological conditions.[108] There is no clear consensus on why certain EVs are released from specific cells, and why they are targeted to the corresponding recipient cells.

The changes in the recipient cells triggered via EV uptake require initial binding of EVs, internalization by various mechanisms, and activation of signalling pathways that regulate gene expression. EVs can bind to the target cells via plasma membrane receptors, which then either remain bound to the surface to activate signalling pathways, or internalized via phagocytosis, clathrin-dependent transport mechanism, or endocytosis via lipid rafts or direct fusion to the plasma membrane[109,110] **(Figure 7B)**. Release of the bioactive cargos, such as mRNAs or ncRNAs, in the cell can affect the gene expression of the recipient cells upon stress stimuli.[87,89,111,112] In addition, EV fusion to the plasma membrane can change the lipid and protein composition of the target cell.[108] If the EVs are not providing a cargo that is required for the cell to maintain or adapt to different conditions, they are probably fused with lysosomes for clearance.[108]

8.3.3. Bioactive Cargos of EVs: RNA delivery

The content of EVs is suggested to differ based on cell type, and pathophysiological condition, in which lipids, proteins and nucleic acids can be packed.[113] The nucleic-acid content of EVs is particularly interesting, however, how nucleic-acids are selectively transported into the EVs is still unclear. Recent developments in omics technologies provide a useful tool to study the RNA content of the EVs[15], and indicated that mostly fragmented (approximately 200 nucleotide long) mRNAs and ncRNAs are compartmentalized into various vesicles.[114] The main reason for RNAs to be carried within EVs is considered to be protection from RNase degradation, and stabilization via binding to RNA-binding proteins (RBPs).[115,116] Moreover, some suggested mechanisms to control the transport of the ncRNAs, particularly miRNAs, into the EVs are associated with the existence of certain nucleotide motifs called ‘zipcode’[117], and interaction with specific RBPs.[118]

The therapeutic potential of EVs is being studied, not only as biomarkers but also as drug-delivery machinery.[15,119] It has been shown that exosomes can carry cargos to the targeted cell with minimal immune reaction, hence they are well-tolerated.[120] EVs can be packed with exogenous or endogenous loading methods to carry both natural or synthetic oligonucleotides[119], and efficient delivery to the target cell can be achieved with chemical modifications of the protein and lipid content.[15] The basics of RNA delivery with EVs also led to the idea for the recent COVID mRNA vaccines[121], which are previously studied mainly for mRNA delivery for dendritic cells to target tumours.[122] Despite the limitations in the field, using EVs in therapeutics has entered into several clinical trials, mostly for genetic diseases. For example, miR-124 carrying EVs isolated from pre-transfected mesenchymal stem cells is being tested for ischaemic stroke (NCT03384433).[123] Even though there are potential benefits for EVs used as delivery tools, possible adverse events on toxicity and a long-term immune response are under consideration.

8.3.4. EVs in cell-to-cell communication

Cell-to-cell communication is crucial for maintaining homeostasis during any alterations upon physiological or pathological stimuli. Since the heart is a complex organ with different cell types wired with a capillary and neural network, the proper contraction to be maintained is highly dependent on direct cell-to-cell contacts, cell-matrix interactions, electrical or chemical molecules, and extracellular signals including the ones carried by EVs.[85,124] EVs are known to carry the biological information via nucleic-acids or proteins that change the behaviour of the recipient cells. It has been shown that EV production usually increases upon stress stimuli, which indicates a potential role in the preservation of homeostasis via signalling to other cells, or organs.[125]

In the heart, most of the cell types including EC, FB, CM and immune cells can both release and receive the EVs as a part of strictly controlled intercellular communication between them, and the heart with other organs[124] **(Figure 6A)**. EVs can also be targeted to the producer cell itself, where endogenous EVs act on the cell as an autocrine mediator. Additionally, EVs can be also produced to be released and targeted to other cells as paracrine mediators. Furthermore, the same cell can be both producer and recipient cell depending on the physiological condition, in which the identification of endogenous and exogenous EVs is challenging.

In the recent past, the majority of studies in the circulating EVs were focusing on miRNAs. For example, it has been demonstrated that cardiac fibroblasts can release exosomes carrying miRNAs, which can be taken up by cardiomyocytes and regulates their response to stress conditions.[111] Recently in another study, Hosen and colleagues showed that shuttling of miR-122-5p via EVs altered viability and apoptosis in recipient cardiomyocytes[112]. Although, lncRNAs within EVs have not extensively been studied, the lncRNA *Neat1* is enriched in EVs during cardiac ischemia and contributes to the cellular communication between FB and CMs.[87] In another study, Huang and colleagues demonstrated the role of EVs collected from atorvastatin pre-treated mesenchymal stem cells (MSC) in cardio-protection after MI via upregulation of the lncRNA *H19.*[126] These studies indicate the importance of ncRNAs in cellular cross-talk both for homeostasis and in disease progression, as well as their potential as therapeutic targets.

8.4. Aim of the Study

GATA-**d**ownregulated **lo**ng-noncoding **R**NA1 and 2 (*Gadlor1* and *Gadlor2*) lncRNAs were identified as highly upregulated transcripts in a microarray study after endothelial-specific deletion of GATA2 as a previous unpublished observation by Joerg Heineke and colleagues (Froese N and Heineke J, unpublished).

Based on this previous observation, the overall purpose of this project can be listed as:

1. To study the changes in the endogenous expression levels of *Gadlor1* and *Gadlor2* lncRNAs during postnatal development, in different cells and organs of healthy and disease conditions, especially in response to cardiac pressure overload with transverse aortic constriction (TAC)
2. To assess the function of *Gadlor1* and *Gadlor2* during pressure overload-induced heart remodelling
3. To understand the detailed molecular mechanism of how *Gadlor* lncRNAs might exhibit their effect

9. Chapter 2: Material and Methods

The text of the following section summarizing the work that has been performed for this thesis was originally written by myself and has been published on the pre-print server *bioRxiv* with the title *"Secreted long non-coding RNAs Gadlor1 and Gadlor2 affect multiple cardiac cell types and aggravate cardiac remodeling during pressure overload"* (**Keles, M** and Grein, S *et al.,* 2022)[127], and the manuscript is currently in peer review process.

9.1. Human Samples

9.1.1. Human Tissue and Serum Samples

Studies with human heart tissue samples were approved by the Institutional Ethical Board of Massachusetts General Hospital, United States. Human failing heart tissue samples were collected from patients with end-stage heart failure undergoing cardiac transplantation. Control heart tissue samples were obtained from healthy organ volunteers when the organ was not eligible for transplantation, or from the victims of traffic accidents.

Human serum samples were obtained from healthy blood donors, or from aortic stenosis patients before the replacement of the aortic valve, where all donors provided a written informed consent for the collection and use of samples. Approval was granted from the Institutional Review Board of Christian-Albrechts-Universität Kiel (File number: A174/09).

9.1.2. Measurement of *GADLOR* lncRNAs in Human Serum Samples

Human serum samples were collected on the day before Transcatheter Aortic Valve Implantation (TAVI). Serum-RNA was extracted using miRNeasy serum/plasma kit (#217184; Qiagen) based on the manufacturer's instructions. LncRNA levels were normalized with 2 µl of TATAA universal RNA Spike (#RS10SII; Tataa Biocenter) prior to RNA isolation. RNA was transcribed to cDNA (#K1652; Maxima H Minus First Strand cDNA Synthesis Kit; Thermo Fisher) and analysed with TaqMan Non-coding RNA Technology (#4369016) using custom-specific TaqMan Gene Expression Assay (#43331348, ID: APPRKET und APRWEYP; Thermo Fisher). For quantitative RT-PCR Stratagene's MX4000 multiplex qPCR system was used.

This assay was designed and performed by Ricarda Haustein, MD in Hannover Medical School, Department of Cardiology and Angiology.

9.2. Animal Experiments

9.2.1. Animal Use and Welfare

All studies including the use and care of animals were performed ethically with the permission of the Regional Council Karlsruhe and the Lower Saxony State Office for Consumer Protection and Food Safety, Germany approved protocols 35-9185.81/G-144/18, I-22/03, 33.9-42502-12-10/0016, 33.19-42502-04-14/1403 and 33.8-42502-04-16/2356. All the experiments for the surgical interventions and the following physiological assessments were performed in accordance with The German Animal Welfare Act.

Wildtype ICR/CD1 mice were in-bred in-house and C57BL/6N mice were obtained from Janvier Labs (Le Genest-Saint-Isle, France). Animals were maintained in the temperature-humidity controlled (22± 2°C and 35-60% humidity), 12-h dark-light cycled room with unlimited access to water and standard food.

9.2.2. Generation of *Gadlor*-KO mouse model

Systemic *Gadlor* knock-out mice (*Gadlor*-KO) were generated by deletion of the whole region of mouse chromosome 16 using a CRISPR-Cas9-based strategy. Briefly, embryonic stem cells were transfected with gRNAs LNC1-01 (target sequence: 5'-TTGTACATGAGCGGTTGTAG) and LNC2-01 (target sequence 5'-AGTATACAGGGGGTTACCAT) as well as in vitro transcribed CAS9-GFP mRNA. GFP expressing cells were sorted and single-cell-derived clones were established. 5 out of 72 analysed clones showed extensive deletions between the gRNA target sites. Clones 1-37 comprised a deletion of 39995533 – 40004426 on one chromosome 16 allele. This clone was injected into C57BL/6 blastocysts to generate a transgenic mouse line which was then further crossed to achieve a homozygous deletion.

Generation of *Gadlor*-KO mice was designed and monitored by Professor Dr. Dagmar Wirth, Model Systems for Infection and Immunity, Helmholtz Centre for Infection Research.

9.2.3. Genotyping PCR

Genotyping of mice was performed with genomic DNA extracted with tissue after ear punch. Tissue samples were lysed in 200 µl of Solution A (1,25ml NaOH (1M) pH 5,0 + 48,75ml H2O) for 20 minutes at 95°C incubation. The lysate was then mixed with 200 µl of Solution B (2 ml Tris (1M pH5,0) + 20µl EDTA (0,5M)) and centrifuged for 15 minutes to collect supernatant for follow-up analysis. Genotyping was performed from all wild-type (WT) and *Gadlor* knock-out (*Gadlor*-KO) mice which WT animals produce a band of 670 bp and *Gadlor*-KO animals showed a band of 526 bp. The primers used for WT and *Gadlor*-KO genotyping were listed in **Table 1.**

Table 1: List of primers used for genotyping of Gadlor-KO mouse line

	Primer 1 (Forward)	**Primer 2 (Reverse)**
***Gadlor*-WT**	5'-CTTGAGCCGTCTCTCCAAAG-3'	5'-GGGTGGCATGCAAGATGATTGAGA-3'
***Gadlor*-KO**	5'-CTTGAGCCGTCTCTCCAAAG-3'	5'-TGTGGAGTGGACACATAGAGG-3'

The Gadlor-KO genotyping PCR reaction mix and thermocycler program is indicated below in **Table 2** and **Table 3**, respectively.

The amplified genomic DNA after the PCR was directly analysed with agarose gel electrophoresis for the separation of fragments. Agarose gel (2%) was prepared by dissolving 3 grams of agarose powder in 200 ml of TBE (1X) buffer by heating the solution without boiling. After cooling down 10 µl of Midori Green Xtra (MG10) was added to the solution which was then poured into a tray to solidify. Samples and Generuler 1 kb DNA ladder (Thermo Scientific) were loaded on the gel and run at 100 volts for 1 hour. The gel was visualized under UV light and band sizes were determined referenced to the DNA ladder.

Table 2: Gadlor-KO genotyping PCR reaction mix

Reagent	Per Reaction Sample
5x Green Buffer	5 µl
$MgCl_2$, 25 Mm	2.5 µl
dNTP, 10 Mm	0.5 µl
Primer Mix – Forward and Reverse	0.5 µl each (1:10 dilution each)
DMSO	0.15 µl
GoTaq-Polymerase	0.4 µl
Water	14.45 µl
DNA	1 µl
Total Volume	**25 µl**

Table 3: *Gadlor*-KO genotyping PCR program

Step	Temperature	Cycle	Time
1	98°C		5 min
2	98°C		30 sec
3	56°C	x 47	30 sec
4	72°C		2 min
5	72°C		5 min
6	Hold 4°C/RT		

9.3. Transverse Aortic Constriction (TAC)

Transverse aortic constriction (TAC) is a well-established experimental model of cardiac hypertrophy and failure induced by pressure-overload.[128]

TAC was induced in 8-10 weeks old mice and maintained for 1-2 weeks for short-term studies and 8-12 weeks for long-term studies. Briefly, mice were anaesthetized with 3% and then maintained with 2% of isoflurane in 1 Lpm oxygen via a mask during surgery and stabilized onto a heat-controlled surgery table to maintain the body temperature during the procedure. Analgesia (0.1

mg/kg buprenorphine) was provided by subcutaneous injection. Tracheal intubation was followed by upper thoracotomy to visualize the aortic arch, which was then tied with a 7-0 silk ligature around a 26-gauge needle that was removed immediately after secured constriction. The scheme describing the details of the constriction site is given in **Figure 8,** below. Mice were injected with 0.1 mg/kg atropine, and chest wall was closed with suture then followed by closure of the skin with surgical glue.

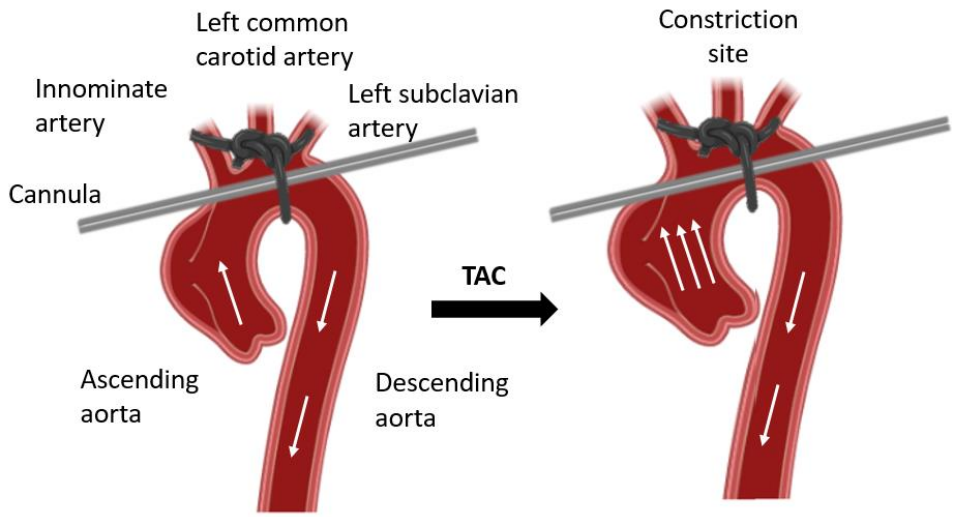

Figure 8: Scheme of transverse aortic constriction (TAC) procedure.

Scheme depicting the site of constriction in the aortic arch between the innominate artery and left common carotid artery with a 26-gauge needle. After the needle is removed from the constriction site, the increased flow can be measured in the right common carotid artery branch of the brachiocephalic trunk. *Illustration is created by using www.biorender.com.*

For postoperative care, additional analgesia was provided in drinking water for the following 5 days. To follow up mortality rate, mice were inspected daily after TAC for short-term and long-term study cohorts separately.

Sham-operated animals were treated with the same procedure and medications, however, no constriction was applied to the aortic arch.

All sham and TAC operations were performed by Steve Grein, Cardiovascular Physiology Department, Medical Faculty of Mannheim – Heidelberg University.

9.4. Transthoracic Echocardiography

Echocardiography was performed on sedated mice under mild isoflurane (initial application with 3% and stabilization with 1% isoflurane in 1 Lpm oxygen). Mice were dorsally placed on the heated table to maintain the body temperature during the procedure while ECG and respiration rate were recorded continuously. Echocardiography was recorded with a linear 30-40 MHz transducer (MX-550D) by using Vevo 3100 system (FUJIFILM VisualSonics, Toronto, Canada). Data were analysed with cardiac measurement packages of VevoLab 5.5.0 software (FUJIFILM).

9.4.1. Left Ventricle and Apical four Chamber View

Parameters were recorded in B-mode and M-mode in both parasternal long axis (PSLAX) and short-axis (SAX) view at the papillary muscle level. Left-ventricular posterior wall thickness and left-ventricular end-diastolic volume were used to characterize LV microanatomy (LVPW and LVEDV) and the change of LV diameter length from end-diastole (LVID) to end-systole was used to assess contractility and to calculate LV ejection fraction and fractional shortening (LV-EF and LV-FS) which were measured with PSLAX mode in the analysis. Visualization of the heart in the PSLAX position and measurement of required parameters by VevoLab software are shown in **Figure 9**, below.

B-mode tracing in the apical four-chamber view was recorded at the atrioventricular valve level with pulse wave-Doppler (PW-Doppler) and tissue-Doppler measurements.

9.4.2. Carotid flow measurement

To evaluate the strength of constriction of the aorta during TAC surgery, the peak velocity of flow in the right and left common carotid arteries (RCCA and LCCA) were measured 2-3 days after the operation with PW-Doppler at the level of carotid bifurcation to calculate the ratio of RCCA/LCCA.

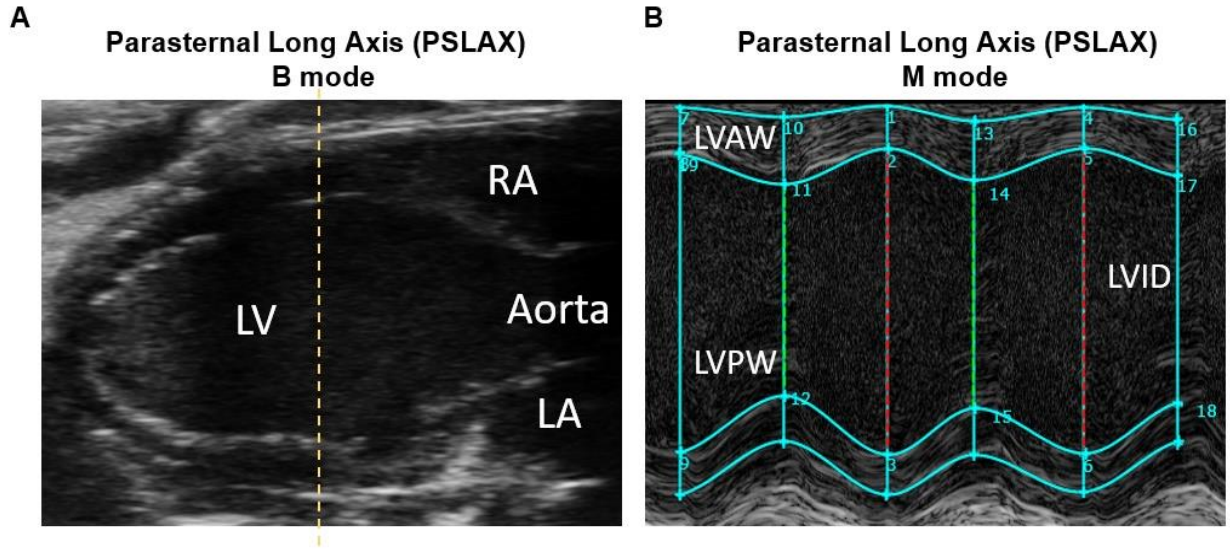

Figure 9: Parasternal long axis visualization modes for echocardiographic measurements.

Echocardiographic visualization of **A.** B-mode and **B.** M-mode in the parasternal long axis (PSLAX). Cardiac systolic function parameters (LV ejection fraction (%), LV posterior wall thickness (PW)) were measured in M-mode by detecting at least three consecutive contractions. *Yellow dash line indicating the plane of measurement. LV: Left ventricle, LA: left atrium, RA: Right atrium.*

9.5. Organ Harvest

At the end of the experiment, mice were weighed and euthanized to collect the heart, lungs, liver, spleen, kidney and brain. Organs were washed in cold PBS to remove the blood, and additionally, the heart was relaxed in 0.5% (w/v) KCl in PBS.

The heart was transversely cut into half, and the upper layer was immediately embedded into optimal cutting temperature (O.C.T.) embedding medium (Tissue-Tek O.C.T., 16-004004) in a cryomold and placed into a cooled n-pentane bath for slow freezing in liquid nitrogen for histological analysis. Other sections were dissected and snap-frozen for following RNA and protein analysis. Similarly, lungs were also cleaned from blood without rinsing in PBS, and O.C.T. embedding and tissue samples were collected similarly.

9.6. Histology

Tissues embedded in O.C.T. medium were sectioned with a rotary microtome (Thermo Fisher, HM355S) into slices of 7 µm and 12 µm for immunofluorescence and Picro-Sirius red staining, respectively. Tissue slides (Thermo Scientific - Menzel Glaser, 24 x 60 mm) were dried at room temperature (RT) for 30 minutes and then stored at -20°C until further use.

9.6.1. Immunofluorescence Staining Protocol

For immunofluorescence, tissue sections were fixed with 4% paraformaldehyde (PFA) for 20 minutes at RT and followed by three rounds of washing with 1x PBS for 5 minutes. Then, slides were permeabilized with 0.3% Triton-X in PBS for 20 minutes and washed again with 1x PBS as described before, and blocked with 3% BSA in PBS for 30 minutes at RT. Primary antibodies of the corresponding staining were incubated overnight at 4°C and washed with PBS on the next day. Corresponding secondary antibodies were then incubated for 1-2 hours at RT which the slides were mounted with mounting medium with DAPI (VECTASHIELD HardSet Antifade Mounting Medium With DAPI, Vector Lab, H-1500) and left to air dry at dark for 2 hours. Samples were visualized with Leica DMi8 Fluorescence microscope and images were analysed with Leica Application suite X (LAS X) 3.7. Further image analysis and quantification were performed with ImageJ.

Primary and secondary antibodies were listed with the applied dilutions in **Table 4**.

Table 4: List of antibodies and staining reagents used in immunofluorescence (IF) staining.

Target	Company, Catalogue No	Application
Isolectin B4 (IB4)	Vector Lab, FL-1201	1:50 (IF)
Rabbit Polyclonal Anti-Ki67	Abcam, ab15580	1:100 (IF)
VectaShield Hardset Antifade Mounting Medium with DAPI	Vector Lab, H-1500	
Wheat Germ Agglutinin (WGA)	Invitrogen, W21405	1:100 (IF)

9.6.2. Picro-sirius red Staining Protocol

Picro-sirius red staining was performed to detect the deposition of total collagen in the extracellular matrix. Briefly, tissue slides were fixed with 100% ice-cold acetone and air-dried for 2 minutes at RT. Slides were embedded into picric acid solution (150 ml saturated picric acid + 50 ml 37% formaldehyde solution) for 30 minutes and rinsed in 70% ethanol (EtOH) then transferred into picric acid with direct red dye (Direct Red 80, Sigma Aldrich 365548) for 60 minutes. Next, incubated for 10 minutes in hydrochloric acid (HCl, 10 mM) and washed with 70% and 100% EtOH for 5 minutes each. Finally, the tissue slides were washed in Roticlear (Roth Chemicals, A538.6) solution and mounted with RotiMount (Roth Chemicals, HP68.1).

Tissue sections were scanned with Zeiss Axio Scan.Z1 in bright-field with 20X, and images were analysed with ZEN 2.6 Blue Edition, Carl Zeiss and quantified with ImageJ.

9.7. Primary Cell Isolation and Cellular Assays

9.7.1. Isolation and Culture of Juvenile Mouse Endothelial Cells (mECs)

Hearts from 7-12 days old mice (CD1) were collected and washed in ice-cold Dulbecco's Modified Eagle Medium (DMEM) high-glucose to clean and remove the atria. The minced tissue was transferred into 5 ml of enzyme solution (for 3-4 hearts) and incubated with collagenase I (500 U/ml, Worthington - LS004176) and DNase I (150 U/ml, Worthington - LS002139) in HBSS (without Ca and Mg). After digestion, the lysate was washed with FCS and passed through a 70 µm cell strainer. The washed lysate was incubated with CD31 antibody (BD, 553370) with Dynabeads (Invitrogen, 11035) for the first step of isolation and then cells were plated on 0.5% gelatinized plates. For culturing, cells were maintained for 3-4 days until they reached 80-90% confluency. During the first passage, further purification of cells was achieved by incubation with CD102 antibody (BD, 553370) with Dynabeads. Primary endothelial cells maintained in DMEM with 20% FCS supplemented with non-essential amino acids and sodium pyruvate, and passaged up to P3 for corresponding experiments.

The details of the bead-coupled antibodies were listed in **Table 5,** below.

9.7.2. Isolation of Adult Mouse Endothelial Cells and Fibroblasts

Isolation of endothelial cells and fibroblasts from adult mice was performed with MACS-magnetic beads from Miltenyi Biotec. Briefly, heart tissue was washed in ice-cold PBS after immediate collection to gently pump the blood out, and minced into small pieces before incubating in an enzyme solution (collagenase I (500 U/ml, Worthington - LS004176) and DNase I (150 U/ml, Worthington - LS002139) in RPMI 1640 (Thermo Fischer Scientific: 31870025)). Digested tissue samples were passed through a 0.70 µm cell strainer and washed with FCS, and MACS buffer with BSA (Miltenyi Biotec, 130-091-222). After multiple washing steps, the tissue lysate was incubated with CD146 microbeads (Miltenyi Biotec, 130-092-007) which is then passed through magnetic columns (Miltenyi Biotec, MS columns 130-042-201) for positive selection of endothelial cells (EC). The flow-through was incubated with feeder removal microbeads (Miltenyi Biotech, 130-095-531) and eluted after multiple washing steps to collect fibroblasts (FB). Isolated cells were stored as a frozen cell pellet for later RNA or protein isolation for corresponding experiments.

The details of the microbeads and bead-coupled antibodies were listed in the **Table 5** below.

Table 5: List of antibodies, solutions and magnetic beads used in cell isolation methodologies.

Target	Company, Catalogue No
Anti-Mouse CD146 (LSEC) Microbeads	Miltenyi-Biotec, 130-092-007
Dynabeads	Invitrogen, 11035
Feeder Removal Microbeads, Mouse	Miltenyi-Biotec, 130-095-531
MACS BSA Stock Solution	Miltenyi-Biotec, Ref: 130-091-376
MACS MS-Columns	Miltenyi-Biotec, Ref: 130-042-201
MACS Rinsing Solution	Miltenyi-Biotec, Ref: 130-091-222
Octo-MACS Separator	Miltenyi-Biotec, Ref: 130-042-109
Purified Rat Anti-Mouse CD102	BD Pharmingen, 553326
Purified Rat Anti-Mouse CD31	BD Pharmingen, 553370

9.7.3. Isolation of Adult Mouse Cardiomyocytes

Isolation of adult cardiac myocytes was achieved by the Langendorff perfusion system as described before.[129] Briefly, immediately after excision, the heart was placed into ice-cold 1x perfusion buffer (Formulation of 10x stock solution is given in **Table 6**, below) to clean the tissue around the aorta under a microscope. Then aorta was placed onto a cannula (inner diameter 1mm) with forceps and tied with a silk suture to secure the proper hanging and perfusion through coronary arteries. The perfusion buffer was used to clean all the blood until the colour of the coronaries changed. Then the enzyme solution which contains Liberase DH (5 mg/ml, Roche, 5401089001), trypsin (1%, Gibco, 15090046) and $CaCl_2$ (100 mM) distributed uniformly to digest the tissue, while temperature was maintained at 37°C during the process.

Table 6: Reagent information and concentrations used in perfusion buffer.

Reagents (10x)	Concentration	Company	Catalogue No
NaCl	1130 mM	Sigma Aldrich	S9625
KCl	47 mM	Sigma Aldrich	P4504
KH_2PO_4	6 mM	Sigma Aldrich	P5379
Na_2HPO_4	6 mM	Sigma Aldrich	S0876
$MgSO_4.7H_2O$	12 mM	Sigma Aldrich	M1880
$NaHCO_3$	120 mM	Sigma Aldrich	S5761
$KHCO_3$	100 mM	Sigma Aldrich	60339
HEPES Buffer	100 mM	PAA	S11-001
Taurine	300 mM	Sigma Aldrich	T0625

Enzymatic digestion was finalized with Stop I and II solutions containing perfusion buffer with FCS and $CaCl_2$ (10 mM). Digested heart tissue samples were passed through a 100 µm cell strainer. Then, calcium concentration was gradually increased by manual administration into digested heart tissue with continuous gentle mixing. Then the cells were subjected to either IonOptix

analysis, or culturing for experiments. For culturing experiments, cardiomyocytes were plated with myocyte plating medium, which is then changed with myocyte culture medium within 2 hours.

The formulation of Stop I and II solutions, plating and culture media were listed in **Table 7**, below.

Table 7: Formulation of Stop I, Stop II and adult cardiomyocyte plating and culturing mediums.

Solution	Reagents	Volume or Dilution
STOP I (50 ML)	Perfusion buffer (1X)	45 ml
	FCS (10%)	5 ml
	$CaCl_2$ (10 mM)	62.5 µl
STOP II (50 ML)	Perfusion buffer (1X)	47.5 ml
	FCS (10%)	2.4 ml
	$CaCl_2$ (10 mM)	104.2 µl
Myocyte Plating Medium (120 ml)	MEM	109.2 ml
	FCS	6 ml
	Penicillin/ Streptomycin	1.2 ml
	L-Glutamine	1.2 ml
	BDM	2.4 ml
Myocyte Culture Medium (120 ml)	MEM	117.6 ml
	BSA	240 µl
	Penicillin/ Streptomycin	1.2 ml
	L-Glutamine	1.2 ml
	Blebbistatin	1:2000

Excision of the heart and perfusion via the Langendorff system was performed by Nina Weinzierl, at Cardiovascular Physiology Department, Medical Faculty of Mannheim of Heidelberg University.

9.7.4. Isolation of Neonatal Rat Cardiomyocytes (NRCM) and Fibroblasts (NRFB)

Hearts from 1-3 days old rats were collected and washed with ice-cold 1x ADS (pH 7.35) to clean the blood and remove the atria. The ventricular parts were minced in 1x ADS and digested in an enzyme solution containing collagenase Type II (Worthington: LS004176) and pancreatin (Sigma P3292). Digested tissue was loaded into a Percoll gradient to separate different cell types such as CM, ECs and FBs. NRCMs were plated (4.0×10^5 /well for 6 well-plate) on 0.5% gelatine-coated plates and cultured for cell-based assays. NRFB were plated (5.0×10^5 /well for 6 well-plate) on plates, and cells were washed and supplemented with fresh media after 2 hours.

9.8. Sarcomere Contractility and Calcium Transient Measurements

To measure the contractility and intracellular calcium concentration, adult cardiomyocytes were isolated by the Langendorff method after 1-week of TAC operation. Isolated adult CMs were plated on laminin-coated (10 µg/cm^2) 35 mm dishes (MatTek 10 mm Glass bottom dishes, P35G-1.5-10-C) with myocyte plating medium (formula given above **Table 7**). After 2 hours of incubation, cells were gently washed with Minimum Essential Medium (MEM) without serum and 2,3-Butanedione 2-monoxime (BDM). The plated cells were incubated with a final concentration of 1 µM fura-2, AM (Invitrogen, F1221) for 30 minutes at 37°C and 5% CO_2 for calcium measurements.

For measurements, the plate was then transferred into the Ion-Optix Multicell High-throughput System chamber (CytoCypher Perfusion System with Ion-Optix, USA), where the cells continuously perfused with culture MEM and simultaneously paced with 15 V, 3 Hz and 4 ms impulse duration. Cells were visualized with a camera in the chamber and randomly selected for measurement of parameters including sarcomere length and contraction, and single Ca^{2+} transients were simultaneously recorded with dual excitation fluorescence photomultiplier system (excitation at 360/380 nm and emission at 510 nm).

After the measurement of the transients, the recordings were analysed with IonWizard software. Parameters used for the measurements were summarised in **Table 8**, below.

Table 8: Parameters of contractility and calcium transient measurements.

IonWizard Parameter	Unit	Definition
Sarcomere shortening, %	Percentage (%)	Percentage of sarcomere shortening calculated with the peak and baseline values, indication of contraction
Time to 90% shortening	Seconds (s)	Time to reach a 90% percent of the peak during the deflection phase of the transient
Time to 90% relaxation	Seconds (s)	Time to reach a 90% percent of the peak during the recovery phase of the transient
Peak height	Arbitrary units (AU)	Peak transient amplitude of calcium, maximum value of the fluorescent ratio (Peak - Baseline)
Time to peak 90%	Seconds (s)	Time at which peak reaches 90% relative to the transient time
Tau	Seconds (s)	Exponential decay time constant, speed of recovery of calcium

9.9. Extracellular Vesicle Studies

9.9.1. Isolation of Extracellular Vesicles (EVs)

Isolation of EVs was performed with differential ultracentrifugation from the supernatant of C166 cells that were cultured with EV-depleted FCS. Initially, cell debris and large vesicles (apoptotic bodies) were removed by centrifugations at 300xg (10 minutes at 4°C) and 10.000xg (20 minutes at 4°C), respectively. Subsequently, small EVs (including microvesicles and exosomes) were collected with 100.000xg ultracentrifugation for 90 minutes, and washed with cold PBS before the second round of centrifugation, which EV pellets from a total of 280 ml of supernatant combined for one sample. The final EV pellet was re-suspended in PBS for NTA (ZetaView Nanoparticle Tracing Video microscope, PMX-120) measurements, or with QIAzol lysis buffer (Qiagen, 79306) for RNA isolation.

9.9.2. EV Characterization with FACS Staining

Characterization of common surface markers of EVs was performed with flow cytometry by staining EC-derived EVs with CD9-PerCP-Cy5.5 (Miltenyi Biotec, 130-102-278, Clone: MZ3), CD63-APC (Miltenyi Biotec, 130-108-894, Clone: REA563) and CD54-FITC (BD, 553252, Clone: 3E2) labelled antibodies for 1 hour at 4°C. Measurements were performed with BD FACSCanto ll.

Experiments were performed by Stefanie Uhlig at Core Facility Platform Mannheim (CFPM) FlowCore, Medical Faculty of Mannheim of Heidelberg University.

9.9.3. EV Visualization with Transmission Electron Microscopy (TEM)

Visualization of EVs was performed with TEM. Briefly, after centrifugation EV pellets were resuspended in the minimum possible volume of residual liquid and 25% aqueous glutaraldehyde was added to a final concentration of 1 %. After fixation overnight, samples were mixed 1:1 (v/v) with 4 % agar at 40 °C. After hardening, the agar blocks were cut into cubes of 1 mm in size.

Electron microscopy was performed with an FEI Morgagni 268 transmission electron microscope (FEI, Eindhoven, Netherlands) operated at 80 kV using a Veleta CCD camera (Olympus Soft Imaging Solutions).

The experiment was performed by Jan Hegermann at Core Unit Electron Microscopy, Institute of Functional and Applied Anatomy, Hannover Medical School.

9.9.4. EV-RNA isolation

RNA isolation from EVs was performed by RNA precipitation as described before.[130] EV pellet was resuspended with 1 ml of QIAzol and then mixed with 200 µl of chloroform for phase separation. Samples were mixed thoroughly and incubated for 5 minutes at RT, then centrifuged at 12.000xg at 4°C for 15 minutes. The aqueous upper layer was mixed with 10% (v/v) sodium acetate (3M, pH 5.5) and 4 µl of glycogen (5 mg/ml) in 1.5 ml absolute ethanol. Samples were mixed and incubated at -80°C overnight, then centrifuged at 16.000xg for 30 minutes to pellet the RNA. RNA

pellets were then washed with 70% ethanol by centrifuging for 10 minutes and dried at RT before being resuspended in nuclease-free water.

9.9.5. EV RNase and Proteinase-K Protection Assay

To test the transfer of *Gadlor* lncRNAs within EVs, RNase and proteinase K protection assays with and without prior application of Triton-X was performed. In brief, EVs were isolated as described earlier and treated with 100 ng/µl of RNase A, and 20 mg/µl of proteinase K for 30 minutes at 37°C. 5mM of PMSF was used to inactivate the proteinase K at RT.

As a control, selected EV pellets were incubated with 1% Triton-X for 1 hour to disrupt the lipid bilayer. After the treatment RNA isolation was performed as described above to measure the *Gadlor1* and *Gadlor2* expression with RT-qPCR.

As an additional negative control, RNA isolated from EVs were also treated with the same protocol.

9.9.6. EV-labelling with PKH67 cell linker

To visualize EVs for transfer and re-uptake experiments in vitro, they were labelled with PHK67 Green Fluorescent Cell Linker kit (Sigma MIDI67). Briefly, EV pellets were re-suspended with 1 ml of diluent C including 4 µl of PKH67 dye and incubated for 5 minutes at RT. Then, 1% BSA-PBS was added to the suspension to remove the unspecific binding of the dye. EVs were pelleted at 3000xg for 1 hour, which were then suspended with the cell culture medium and added to neonatal rat cardiomyocytes. Labelled EVs were visualized with the Leica Confocal Microscope TCS SP8 and obtained images were analysed by Leica Application Suite X (LAS X) 3.7.

9.9.7. EV-mediated *Gadlor1* and *Gadlor2* overexpression

As a gain-of-function approach, *Gadlor1* and *Gadlor2* were overexpressed in mouse hearts by *Gadlor1/2*-enriched EVs. To this end, C166 endothelial-cell line was infected with *Gadlor1* and *Gadlor2* adenovirus for 48 hours. EVs were collected with ExoQuick-TC solution (EXOTC50A-1,

SystemsBio) based on manufacturers' protocols with some adjustments. ExoQuick-TC provides polymer-based precipitation of exosomes and microvesicles in the tissue culture media, serum or urine samples.[95] Briefly, the supernatant of pre-treated C166 cells was centrifuged at 3000xg for 15 minutes at 4°C to remove the cell debris and apoptotic bodies. The supernatant was then transferred into a new tube and mixed with an appropriate amount of ExoQuick-TC solution and incubated at 4°C overnight. Then, the mixture was precipitated at 3000xg for 60 minutes and resuspended in 1xPBS for NTA analysis, or culture media for further experiments.

EV-mediated overexpression of *Gadlor1/2* was performed in both *in vivo* and *in vitro* experiments. *In vivo* overexpression of *Gadlor* lncRNAs was achieved by injecting EVs directly into mouse hearts before TAC surgery. Intra-ventricular injection was performed by simultaneous cross-clamping of the aorta and pulmonary artery distal of the origin of the coronary vessels. EV administration to mouse hearts, and following TAC operations were performed by Malgorzata Szaroszyk, PhD at Hannover Medical School, Department of Cardiology and Angiology.

9.10. Cell Manipulation and *In-vitro* Studies

9.10.1. Cell Culture and Maintenance

Cells were cultured and maintained at 37°C, 5% CO2 and 100% humidity. C166 (CRL-2581, ATCC) mouse embryonic endothelial cell line and NIH3T3 (CRL-1658, ATCC) mouse fibroblast cell line were cultured in Dulbecco's Modified Eagle's Medium (DMEM) with 10% FCS supplemented with L-glutamine (1%), penicillin/ streptomycin (1%) and HEPES.

MCEC (CLU510-P, Tebu-bio) immortalized mouse cardiac endothelial cells were cultured with DMEM with 5% FCS supplemented with L-glutamine (1%), penicillin/ streptomycin (1%) and HEPES.

HL-1 cardiac muscle cell line (SCC065, Merck) was cultured with Claycomb media (Sigma, 51800C) supplemented with 10% FCS, 0.1 mM norepinephrine, 2 mM L-glutamine and 1X penicillin-streptomycin (P/S). HL-1 cells were cultured on 0.1% gelatine-coated flasks, and cell culture media was refreshed daily. Cells were cultured up to 10 passages to maintain the cardiomyocyte characteristics.

9.10.2. Cryopreservation and Thawing the Cells

Cells were washed with PBS and collected with trypsin. After centrifugation at 200xg for 3 minutes, cells were resuspended in a cell-specific medium containing 10% DMSO and 20% FCS. For freezing HL1 cells, freezing medium containing 90% FCS and 10%DMSO was used. Then the cell suspension was transferred into cryovials (1 ml) and gradually frozen in an isopropanol-containing container at -80°C, which was then transferred into liquid nitrogen for long-term storage.

Cells were thawed slowly in the 37°C water bath and mixed with pre-warmed culture media. They were plated into corresponding plates after mixing gently to keep homogenous distribution.

9.10.3. Adenovirus-mediated Overexpression

For overexpression of *Gadlor* lncRNAs, recombinant adenoviruses were used. Mouse cDNAs of AK037972 (*Gadlor1*) and AK038629 (*Gadlor2*) were subcloned into the pShuttleCMV vector (Source Bioscience, UK) and adenoviruses were generated by the AdEasy Adenoviral Vector system (Agilent, 240009). An adenovirus overexpressing β-Galactosidase (Adβgal) was used as control.

After production of adenoviruses, the viral titer was calculated with AdEasy Viral Titer Kit (Agilent, 972500), and all the experiments were performed with 50 MOI (Multiplicity of Infection). Adenoviral infection on cultured cells was performed for 4 hours at 37°C, 5% CO_2 on cells with media containing heat-inactivated FCS. Cells were then washed twice with PBS and refreshed with culture media with 10%FCS.

9.10.4. Co-culture experiments

For co-culture experiments, adult mouse cardiomyocytes isolated with Langendorff perfusion from *Gadlor*-KO mice were seeded on laminin-coated (Santa Cruz, SC-29012) 6-well plates with myocyte plating medium. After 2 hours of incubation, cells were refreshed with myocyte culture

medium and cultured together with MCECs on 1 µm pore-sized inserts (Thincert, Greiner, 657610). Cells were collected separately after 48 hours for RNA isolation.

9.10.5. Endothelial-cell Sprouting Assay

To study the effect of *Gadlor* lncRNAs on angiogenesis, a sprouting assay was performed with C166 mouse ECs according to the well-established protocol described before.[131] Briefly, cells were infected with Ad.βgal or Ad.*Gadlor1/2* adenovirus for 24 hours. Then 50.000 cells were re-suspended with 4 mL DMEM + 10 % FCS and 1 mL methylcellulose solution (Sigma-Aldrich, M0512) and drops containing 25 µl of suspension were pipetted onto a 10 cm cell culture dish. These drops were then incubated upside-down in a cell culture incubator for 24 hours to allow spheroid formation.

On the following day, the cell spheroids were collected by gently washing off the hanging drops with PBS and collected by 200xg centrifugation for 5 minutes and re-suspended with methylcellulose solution containing 20 % FCS. Simultaneously, collagen matrix was prepared on ice with collagen stock solution (Corning, 11563550) and diluted in 10x M199 medium (Sigma-Aldrich, M0650) supplemented with sodium hydroxide to set the pH for polymerization. Then collagen medium was mixed with spheroids in the methylcellulose solution. 1 mL of the spheroid-collagen-methylcellulose solution were added per well in a 24-well plate and incubated in a cell culture incubator for 30 min to induce the polymerization of the collagen-methylcellulose matrix.

The endothelial-spheroids were stimulated with 100 µl of DMEM + 10 % FCS, 25 ng/mL FGF2 or 10 ng/mL TGF-β1 by adding it dropwise to the collagen matrix. After 24 hours incubation the sprouting assay was stopped by adding 1 mL of 4% paraformaldehyde to the wells.

Spheroids were visualized with 10X objective of the bright-field microscopy and quantified with ImageJ.

9.11. RNA and DNA Studies

9.11.1. RNA Isolation and qRT-PCR

RNA isolation from tissue samples was performed with QIAzol reagent (Qiagen, 79306), and from isolated cells with NucleoSpin RNA isolation kit (Macherey-Nagel, 740955.250) according to the manufacturers' protocols. cDNA was generated by using Maxima H minus First stand cDNA synthesis kit (Thermo Fisher Scientific, K1652). Quantitative PCR was performed with Maxima SYBR Green mix with ROX as reference dye (Thermo Scientific, K0253) on AriaMx Real-time PCR System (Agilent, G8830a). Gene expression was normalized to *Gapdh, 18S* or *U6* expression indicated within the experiment. All qPCR primer sequences are listed in the **Table 9**, below**.**

Table 9: List of primers used for qRT-PCR.

	Primer 1 (Forward)	**Primer 2 (Reverse)**
Gadlor1	5'-AGGTGAGCTCTGGTTGTGTT-3'	5'-CTGCTGCCTGTGAAAGATGG-3'
Gadlor2	TGAGACTCCACTTGCCACAT	TGTGGTTTCAGGCATGTTTCT
GADLOR1	AATTTCAGCCACAAGCATCC	TGCTTGGGGAAGAGGAAGTA
GADLOR2	TGGGATCTAAGCACTGACACC	GAGACAGACATTCGTTTGGTCA
18S	GTAACCCGTTGAACCCCATT	CCATCCAATCGGTAGTAGCG
U6	CTCGCTTCGGCAGCACA	AACGCTTCACGAATTTGCGT
Gapdh	CGTCCCGTAGACAAAATGGT	GAATTTGCCGTGAGTGGAGT
Acat1	GCAGGGAAGTTTGCCAGTGAGA	GAACACGGTCTTGAGCTTTGGC
Actn2	CACCTGGAGTTTGCCAAGAGAG	GCCTTGAACTGCTCATGTGCAG
Adam8	TGCCAACGTGACACTGGAGAAC	GCAGACACCTTAGCCAGTCCAA
Angpt2	AACTCGCTCCTTCAGAAGCAGC	TTCCGCACAGTCTCTGAAGGTG
Angptl4	CTGGACAGTGATTCAGAGACGC	GATGCTGTGCATCTTTTCCAGGC
Aurkb	CTTCTACGACCAGCAGAGGATC	GGCATCTGACAGTTCCTCCATG
Cacna1c	CGTTCTCATCCTGCTCAACACC	GAGCTTCAGGATCATCTCCACTG
Camk2d	GTGACACCTGAAGCCAAAGACC	CCTGTGCATCATGGAGGCAACA
Cdk1	CATGGACCTCAAGAAGTACCTGG	CAAGTCTCTGTGAAGAACTCGCC

Col15a1	ACACCCACAGTGACTCCCAAGA	TCCTCATTGCCCACGATGTCTC
Col1a1	CCGCTGGTCAAGATGGTC	CCTCGCTCTCCAGCCTTT
Col3a1	ATAAGCCCTGATGGTTCTCG	ATGCATGTTTCCCCAGTTTC
Col4a1	ATGGCTTGCCTGGAGAGATAGG	TGGTTGCCCTTTGAGTCCTGGA
Col6a1	GACACCTCTCAGTGTGCTCTGT	GCGATAAGCCTTGGCAGGAAATG
Comp	GTGCCCAACTTTGACCAGAGTG	ACAGGCATCACCCACAAAGTCG
Cox5a	GTCACACGAGACAGATGAGGAG	CCGTCTACATGCTCGCAATGCA
Cxcl2	CATCCAGAGCTTGAGTGTGACG	GGCTTCAGGGTCAAGGCAAACT
Dll1	GCTGGAAGTAGATGAGTGTGCTC	CACAGACCTTGCCATAGAAGCC
Efna1	GCTGAAGGTGACTGTCAATGGC	CGGCACTGTAACCAATGCTGTG
Fgfr2	GTCTCCGAGTATGAGTTGCCAG	CCACTGCTTCAGCCATGACTAC
Fh1	GAACTCACACGCAGGATGCTGT	GGCGGCTTTTATTCTCACCATCG
Fn1	TGTGACAACTGCCGTAGACC	TGGGGTGTGGATTGACCTTG
Gata4	GCCTCTATCACAAGATGAACGGC	TACAGGCTCACCCTCGGCATTA
Icam5	ACCGATGCACAGCAGTCAATGG	ATGTTCTGGGCAGCCTACACTG
Igf1	GTGGATGCTCTTCAGTTCGTGTG	TCCAGTCTCCTCAGATCACAGC
Il6	CGGCCTTCCCTACTTCACAA	TCCAGTTTGGTAGCATCCATCA
Klf15	ACACCAAGAGCAGCCACCTCAA	GCCTTGACAACTCATCTGAGCG
Lsamp	GGAGTCGAAGAGCAACGAAG	AATCTCAAGGCCATTTGCAC
Mfn2	GTGGAATACGCCAGTGAGAAGC	CAACTTGCTGGCACAGATGAGC
Myh6	GAGTGGGAGTTTATCGACTTCG	CCTTGACATTGCGAGGCTTC
Myh7	ACTGTCAACACTAAGAGGGTCA	TTGGATGATTTGATCTTCCAGGG
Nppa	TTCCTCGTCTTGGCCTTTTG	CCTCATCTTCTACCGGCATC
Nppb	GTCCAGCAGAGACCTCAAAA	AGGCAGAGTCAGAAACTGGA
Rcan1.4	CTTGTGTGGCAAACGATGATG	TGGTGTCCTTGTCATATGTTCTG
Sirt1	GGAGCAGATTAGTAAGCGGCTTG	GTTACTGCCACAGGAACTAGAGG
Sucla2	GGTGTCTCTGTTCCCAAAGGCT	TTTCCTCTGCCGCCAGCCAAAA
Tlr9	GCTGTCAATGGCTCTCAGTTCC	CCTGCAACTGTGGTAGCTCACT

9.11.2. DNA Isolation and qPCR

To analyse the mitochondrial DNA (mtDNA) to nuclear DNA (nDNA) ratio of *Gadlor*-KO and WT mouse hearts after 2-weeks of TAC, genomic DNA was isolated from mouse heart tissue samples obtained after TAC (2w) with a DNA isolation kit according to manufacturers' instructions (PureLink Genomic DNA Mini kit, Invitrogen, K182001). Briefly, heat tissue pieces were weighed and adjusted to 20 mg for each isolation. Tissue pieces were incubated at 55°C heating block with PureLink Genomic Digestion Buffer with Proteinase K for 2 hours. After addition of RNase A, samples were kept at RT for 5 minutes, and column-based separation was followed by washing steps and elution with nuclease-free water.

The mtDNA/ nDNA ratios were quantified by quantitative PCR using *ND1* and *16S* rRNA primers listed in the **Table 10**, below**.**

Table 10: List of primers used for qPCR.

	Primer 1 (Forward)	**Primer 2 (Reverse)**
ND1	5'-CTAGCAGAAACAAACCGGGC-3'	5'-CCGGCTGCGTATTCTACGTT-3'
16S	CCGCAAGGGAAAGATGAAAGAC	TCGTTTGGTTTCGGGGTTTC

9.11.3. RNA antisense purification coupled with mass spectrometry (RAP-MS)

To identify the protein interaction partners of *Gadlor* lncRNAs, RAP-MS was performed as described previously with minor modifications.[132] The 5' biotinylated antisense *Gadlor1* and *Gadlor2* probes were pooled in the experiment and the sequences are listed in **Table 11**, below**.** To this end, HL-1 cardiac muscle cells were used to overexpress *Gadlor1* and *Gadlor2* after infection with Ad.*Gadlor1* and Ad.*Gadlor2* for 48 hours. RNA antisense purification (RAP) was performed with cells collected from five 15 cm dishes per sample, where each experimental group contains three replicates (as a negative control to identify non-specific 'background' proteins) and four replicates with UV cross-linked conditions.

HL-1 cells were washed with cold PBS twice and cross-linked using 150 mJ/cm2 of 254 nm UV light. Cells were then lysed with lysis buffer, incubated 10 minutes on ice, homogenized by passing several times through a 21G needle and DNase digested with the addition of DNase salt solution and Turbo DNase for 10 minutes at 37^{o}C (ThermoFisher, AM2238). Hybridization conditions were adjusted by the addition of an equal amount of hybridization buffer. Lysates were precleared with streptavidin-coated magnetic beads. Biotin-labelled *Gadlor1* and *Gadlor2* probes were heated to 85^{o}C for 3 minutes and then incubated with the lysate for 2 hours at 67°C. Probe-RNA complexes were captured by pre-washed streptavidin coated magnetic beads and incubated at 37^{o}C for 30 minutes. Lysates were removed from beads by magnetic separation, and beads were washed four times in hybridization buffer at 67^{o}C. *Gadlor* RNA-bound proteins were then released by benzonase RNA digestion for two hours at 37^{o}C.

The captured protein samples were identified by TMT labelling followed by liquid chromatography-mass spectroscopy (LC-MS/MS) by the EMBL proteomics core facility.

Table 11: List of *Gadlor1* and *Gadlor2* probes used for RNA antisense purification (RAP).

	Probe Sequence
***Gadlor1* – Probe 1**	[Btn]AGGATTGTTAAATATGACTATGCTTGGTATAGTCACAAAACATGGGAGTAC
***Gadlor1* – Probe 2**	[Btn]TATCATAATCTTTCTGTAGGCCATTACTTGTTTCATATTTTAAAGGGACAG TCCACTCTAGGAATGTCAAGTGTCTGATCTCTGAAAACA
***Gadlor1* – Probe 3**	[Btn]TTTTCTGAATAGTTGAAAATTCTAACTAAACACAGGAAGAACAGAGNCAC AAGAATAAAGAAATTTAGATATATCCTAAATGTTTCCAGG
***Gadlor1* – Probe 4**	[Btn]ATAAAAGAAGGCGAGGGGTGGCATGCAAGATGATTGAGAAAGCCCAGT AGCCATTTTTGGGGTGGGGCAAAGGGAGTGGTCTGGGTAGGG
***Gadlor2* – Probe 1**	[Btn]GCTGCTATTTTATTATCTCTTTGGTTCTGTTTTTCATTTGTATTAAAAATG
***Gadlor2* – Probe 2**	[Btn]GTGATGGTGAAGATGAAATTGAGATGAATCATTTGAAGAACGATGTGCGTT TTAGAAGAATCACTTTGTC

9.11.4. RNA Immunoprecipitation (RIP)

We performed RIP with minor modifications to a previously described protocol[133] to confirm the interaction of *Gadlor1* and *Gadlor2* lncRNAs with CaMKII and GLYR1. HL-1 cardiomyocytes were used to overexpress *Gadlor* lncRNAs by adenovirus treatment, while Ad.βgal treated samples were used as control. Three 15 cm plates were combined for the preparation of each sample. Briefly, cells were washed with ice-cold PBS twice and lysed with polysome lysis buffer (100 mM KCl, 5 mM MgCl2, 10 mM HEPES pH 7, 0.5% IGEPAL CA-630, 0.1 mM DTT, 1 x protease inhibitor cocktail, 1 x RNasIN). Cell lysates were passed through a 26G needle multiple times for homogenization. Protein G magnetic beads (Bio-Rad SureBeads, 161-4221) were washed twice with NT-2 buffer (50 mM Tris-HCl pH 7.4, 150 mM NaCl, 5 mM MgCl2, 0.05 % IGEPAL CA-630) and coupled with anti-CaMKII antibody (Santa Cruz, sc-5306), anti-GLYR1 antibody (Proteintech, 14833-1-AP) or anti-IgG (mouse, Cell Signaling 7076, as control) overnight at 4°C. Antibody coupled beads were washed twice with NT-2 buffer and resuspended in NET-2 buffer (50 mM Tris-HCl pH 7.4, 150 mM NaCl, 5 mM MgCl2, 0.05 % IGEPAL CA-630, 20 mM EDTA pH 8, 1 mM DTT, 1 x RNaseIN). Cell lysates were added to beads and incubated at 4°C for 2 hours (10% lysate was removed as input and stored on ice prior to IP).

After the supernatant was removed from the beads, 1 ml of ice-cold NT-2 buffer was used to wash the beads five times in total. Then, beads were resuspended with Proteinase K buffer (1x NT-2 buffer and 1% SDS) and incubated at 55°C for 30 minutes with constant shaking while input sample conditions were adjusted accordingly and processed in parallel. The supernatant was transferred into fresh tubes and combined with NT-2 buffer and UltraPure phenol-chloroform (ThermoFisher, 15593031) for RNA purification. After centrifugation in heavy-lock tubes at 15.000 x g for 15 minutes, the clear aqueous phase was purified with RNA Clean and Concentrator kit (Zymo Research, R1017).

9.12. Protein Isolation and Western Blotting

Heart tissue protein lysates were prepared from frozen pulverized tissue with Kranias lysis buffer containing 30 mM Tris-pH 8.8, 5 mM EDTA-pH 8.0, 3% SDS (v/v), 10% glycerol (m/v), protease and phosphatase inhibitors. Protein quantification was performed with BCA assay (ThermoFisher,

Pierce BCA Protein Assay kit, 23225) to load an equal amount of protein lysates into gels. Samples were then boiled at 95°C for 5 minutes after the addition of Laemmli buffer (1X final concentration) and proteins were separated with SDS-PAGE electrophoresis.

Protein samples were run on 15% gel for phospholamban (PLN) and calsequestrin (CSQ) blots, Following the transfer of proteins into membranes, they were incubated with corresponding primary antibodies at 4°C overnight. Primary antibodies were detected with corresponding secondary antibodies after 1-hour incubation at room temperature, which are listed in **Table 12**. Western blot images were obtained with Amersham Imager 600 (GE Healthcare Life Sciences) and quantified with ImageJ.

Protein analysis were performed jointly with Santosh Lomada, PhD at Department of Experimental Pharmacology, Medical Faculty Mannheim of Heidelberg University.

Table 12: Primary and secondary antibodies used for protein analysis with western-blot

Antibody	Host	Company	Catalogue No
Calsequestrin	Rabbit	Thermo Scientific	PA1-913
Phospholamban	Mouse	Badrilla	A010-14
pThr17- Phospholamban	Rabbit	Badrilla	A010-13
Anti-mouse IgG (HRP-linked)	Rabbit	Cell Signalling	7076S
Anti-rabbit peroxidase (IgG)	Goat	Thermo Scientific	NA934V

9.13. RNA sequencing (RNAseq) and Bioinformatics

In order to perform RNA sequencing, RNA isolation was performed from isolated cells as described at indicated time points (2 weeks after TAC or sham surgery). Quality control of RNA samples (Agilent 2100 Fragment Analyser), and library preparation (DNBSEQ Eukaryotic Strand-specific mRNA library) were performed by BGI, Hong Kong. Bulk RNA sequencing from different cardiac cells was performed as single-ended with 50 base sequence read length by BGI with Illumina HiSeq 2500.

For RNAseq data analysis, the trimming of adapter sequences from *fastq* files was performed with R package *FastqCleaner*. Then the trimmed reads were aligned with R package *bowtie2* to the reference genome (mm10) after trimming. Gene annotation was performed with *bioMaRt* R package. Library size of the samples was normalized to counts per million (cpm) reads, and transformed into log2 values followed by calculation of differential gene expression with *edgeR* package of R. Significant change in gene expression between compared groups were filtered based on FDR < 0.05, and fold change (FC) > 1.5 and 0.75< (FC) for upregulated and downregulated genes in the corresponding conditions. Gene ontology (GO) analysis were performed with Metascape and DAVID online tools. Heatmaps that show the differentially regulated genes were generated by *heatmap.2* function in *ggplot2* library in R.

Raw files with processed data of RNAseq data sets were deposited in National Center for Biotechnology Information's Gene Expression Omnibus database with the accession number GSE213612.

9.14. Statistical Analysis

Data analysis and statistical analysis were performed with GraphPad Prism software, version 8. Data are shown as mean ± standard error of the mean (SEM). All the experiments were carried out in at least 3 biological replicates. The number of replicates for animal experiments and cell culture experiments were indicated in the figure legends.

The investigators were blinded for mouse genotype and treatment during surgeries, echocardiography, organ weight determination and all histological and immunofluorescence quantifications. Initially, all the datasets were analysed for normality to allow the application of a proper statistical test. An unpaired 2-tailed Student t-test was used for comparing 2 groups only. Comparing multiple groups for one condition was performed with one-way ANOVA and Fisher's LSD post-hoc test. Comparing multiple groups for multiple conditions was achieved with two-way ANOVA and followed with Fisher's LSD post-hoc test when applicable. For non-parametric data sets Mann-Whitney and Kruskal-Willis tests were used to compare two groups and multiple groups, respectively. Values of $p<0.05$ were considered statistically significant.

10. Chapter 3: Results

The text of the following section summarizing the work that has been performed for this thesis was originally written by myself and has been published on the pre-print server *bioRxiv* with the title *"Secreted long non-coding RNAs Gadlor1 and Gadlor2 affect multiple cardiac cell types and aggravate cardiac remodeling during pressure overload"* (**Keles, M** and Grein, S et al., 2022)[127], and the manuscript is currently peer-review.

10.1. Identification of novel lncRNAs: *Gadlor1* and *Gadlor2*

Based on previous observations of our group endothelial-specific deletion of GATA2 has led to the upregulation of two previously unknown lncRNAs named as GATA-downregulated long non-coding RNA1 and 2 (*Gadlor1* and *Gadlor2*) (Froese N and Heineke J, unpublished observation). *Gadlor1* (AK037972) and *Gadlor2* (AK038629) are located in close proximity to each other on mouse chromosome 16, and are embedded after exon1 of the *Lsamp* (limbic system-associated membrane protein) gene in its intronic region **(Figure 10A)**.

Gadlor1 and *Gadlor2* fragments are not matched with any known mouse peptides in The National Center for Biotechnology Information (NCBI) database when the BlastP algorithm is used. The low protein-coding probability of the transcripts was also verified by alignment-free method via using Coding-Potential Assessment tool (CPAT) algorithm by using the features of open reading frame (ORF) coverage, Fickett score and hexamer usage bias for prediction, which was additionally compared with well-known coding and non-coding transcripts as controls[134] **(Figure 10B)**.

In **Table 13** below, *Gata4, Acta1, Col1a1* and *Gapdh* were assessed for coding probability as selected protein-coding genes for confirmation, while known non-coding transcripts H19 and Malat1 were compared to *Gadlor1* and *Gadlor2*. Fickett-score and hexamer-score are the calculated computational parameters based on nucleotide composition and relative bias for hexamer usage, respectively. Hexamer score is one of the most reliable parameters defined by CPAT and negative values indicate non-coding parameters.[134] Overall, not only the alignment-based but also alignment-free structural parameters of *Gadlor1* and *Gadlor2* indicated that they are non-coding RNAs.

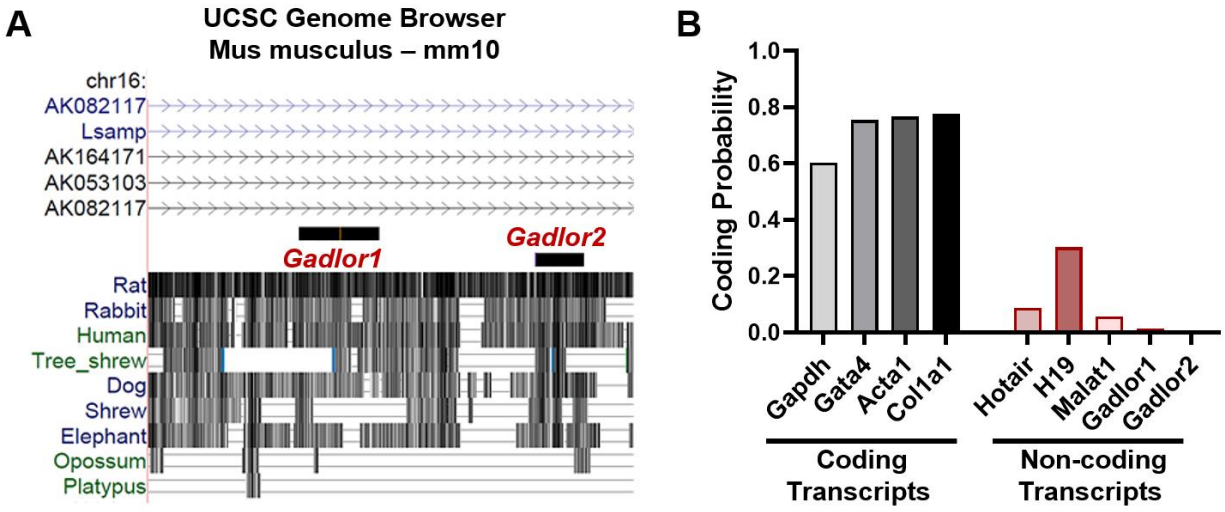

Figure 10: Genomic localization and coding probability of *Gadlor1* and *Gadlor2* lncRNAs.

A. UCSC Genome Browser visualization of AK037972 *(Gadlor1)* and AK038629 *(Gadlor2)* on mouse chromosome 16 and evolutionary conservation between different species. **B.** Coding probability of *Gadlor1* and *Gadlor2* was evaluated with online Coding Potential Assessment Tool (CPAT - http://lilab.research.bcm.edu/), and compared with coding transcripts and well-known lncRNAs for validation that revealed *Gadlor1* and *Gadlor2* are non-coding transcripts.

Table 13: Non-coding parameters of *Gadlor* lncRNAs using Coding-Potential Assessment Tool

	RNA Size	ORF Size	Fickett-Score	Hexamer Score	Coding Probability
Gata4	72799	627	0.9187	0.394172779	0.754159582
Acta1	3018	525	0.9135	0.274092501	0.765892884
Col1a1	16819	453	1.0984	0.403560104	0.776991212
Gapdh	4616	420	0.9703	0.251555407	0.602858755
H19	2617	399	0.7258	0.073194799	0.302321226
Malat1	6983	195	0.7228	-0.038862894	0.055998995
Gadlor1	**2296**	**234**	**0.4979**	**-0.400470043**	**0.014431338**
Gadlor2	**1393**	**87**	**0.9208**	**-0.47659889**	**0.008765529**

Gadlor lncRNAs are highly conserved between human, mouse and rat. The degree of conservation between different species were analysed with the EMBOSS-Water platform by assessing the local alignment of human and mouse sequences **(Figure 11)**.

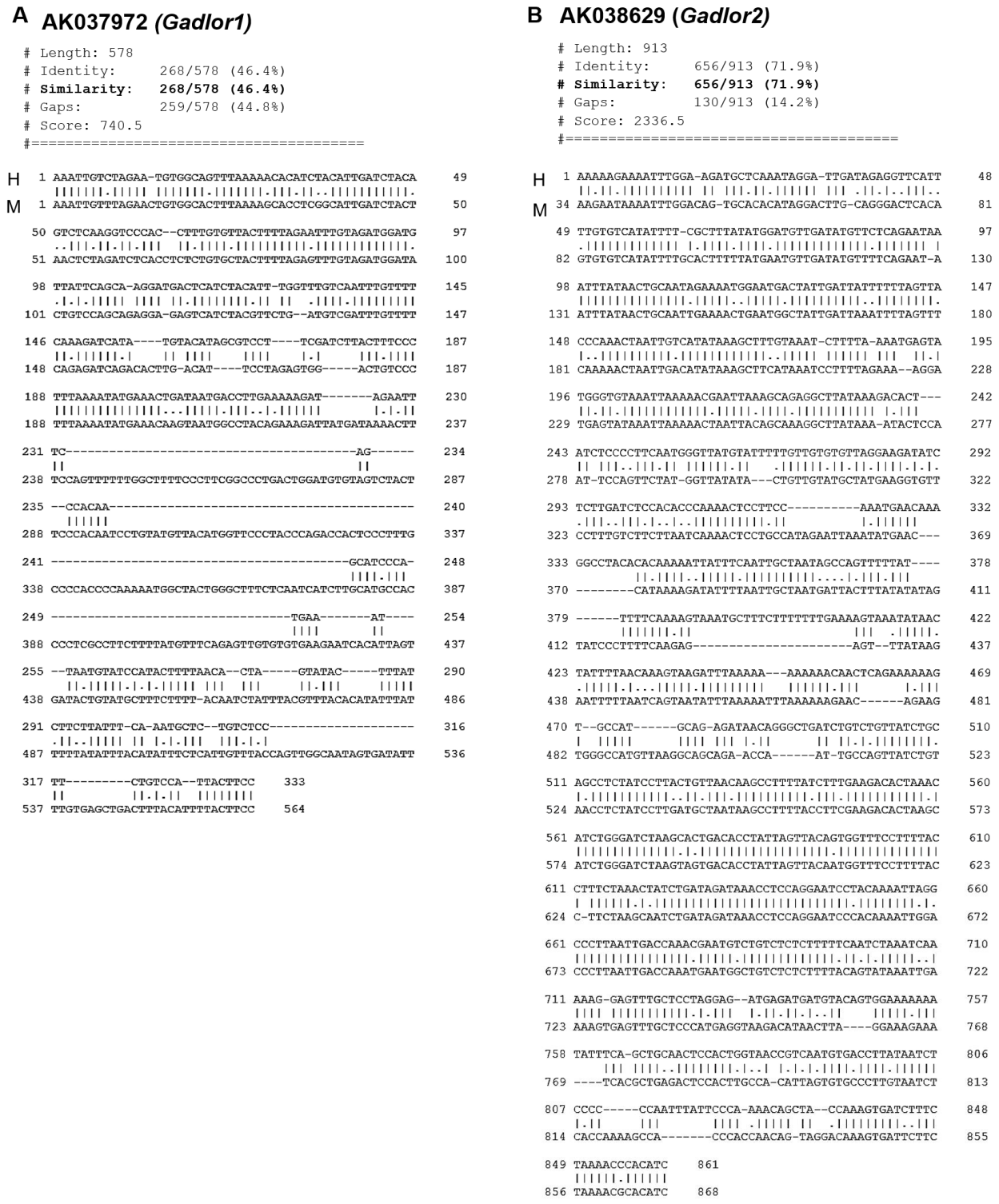

Figure 11: Alignment of *Gadlor1* and *Gadlor2* between mouse and human genome.

A-B. Assessment between human (H) and mouse (M) *Gadlor1/2* in sequence conservation level evaluated with EMBOSS-Water local alignment tool.
(https://www.ebi.ac.uk/Tools/psa/emboss_water/)

Human and mouse orthologs showed 46.6% similarity in AK037972 (*GADLOR1*) mainly due to gaps, however more than 70% (71.9%) similarity was found in AK038629 (*GADLOR2*) **(*Figure 12*)**.

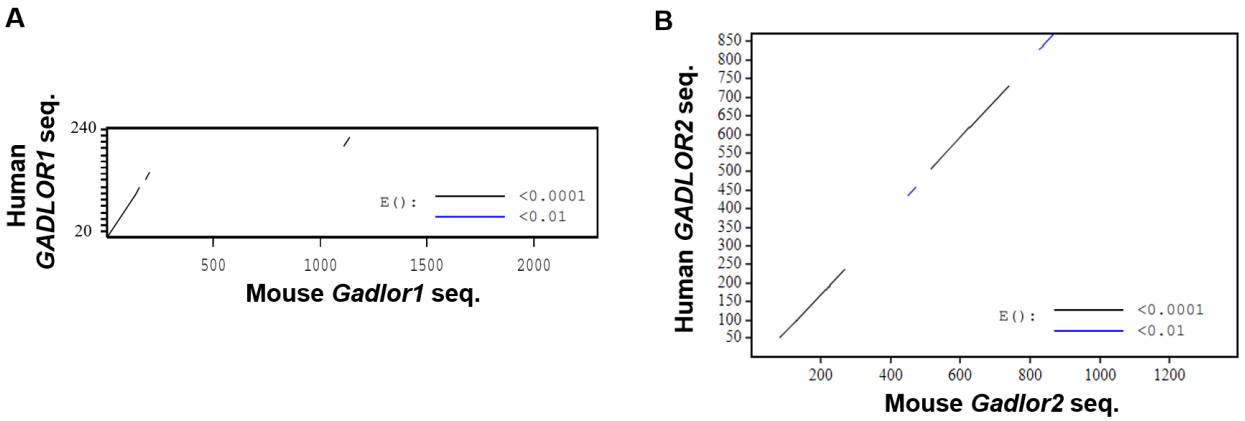

Figure 12: Conservation levels of *Gadlor1* and *Gadlor2* between mouse and human genome.

A-B. Visualization of pairwise local alignment with LALIGN DNA:DNA tool of University of Virginia (https://fastademo.bioch.virginia.edu/fasta_www2/fasta_www.cgi?rm=lplalign).
E-score, E(): Expectation value: The likelihood of the sequence appear only by chance.

10.2. Expression Profile of *Gadlor1* and *Gadlor2*

Gadlor1 and *Gadlor2* expression was assessed in heart tissue samples in different postnatal developmental stages including postnatal days 1 to 21 (P1, P5, P21) and adult (9 weeks old). *Gadlor1/2* expression was lower in the early postnatal period, but upregulated in the adult (2 months old) heart **(Figure 13A)**.

Cellular expression analysis among the main cell types in the heart revealed the highest *Gadlor1* and *Gadlor2* expression in EC, followed by fibroblasts (FB), while the lowest levels were detected in cardiomyocytes (CM). In addition, *Gadlor* lncRNA levels were also significantly enriched in ECs versus whole heart (WH) tissue **(Figure 13B).**

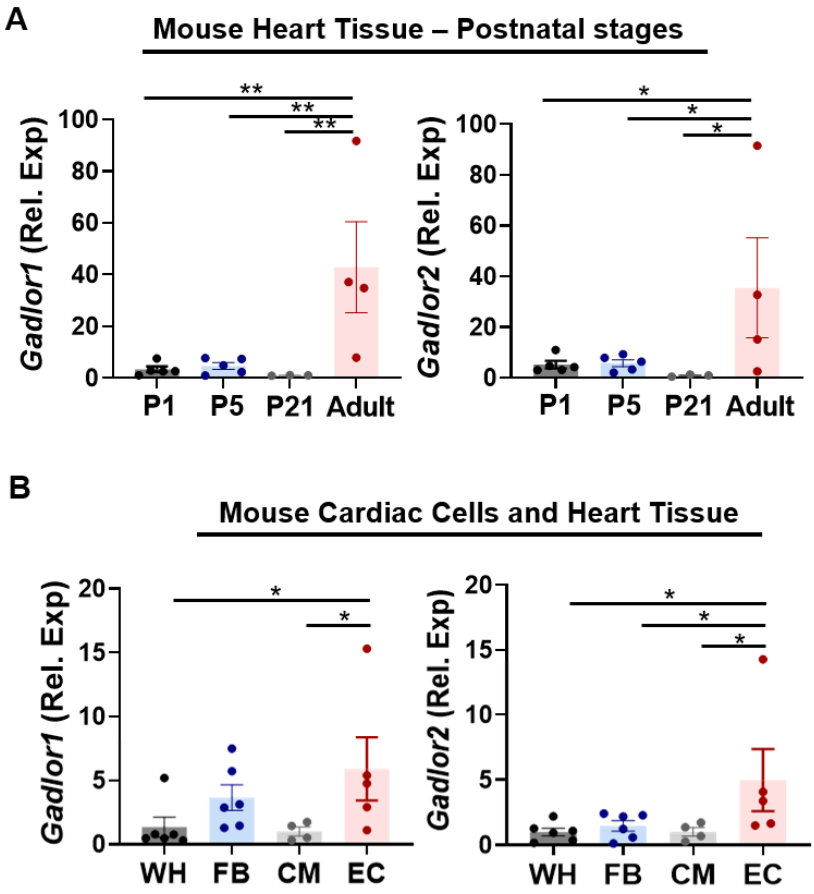

Figure 13: *Gadlor1* and *Gadlor2* expression in different developmental stages and different cardiac cell types.

A. *Gadlor1* and *Gadlor2* expression levels in mouse cardiac tissue from different post-natal developmental stages (P1 – n=5, P5 – n= 5, P21 – n=3 and adult (9-weeks old) – n=4), and in **B.** different cardiac cell-types (EC: endothelial cells – n=5, FB: fibroblast – n=6, CM: cardiomyocytes – n=4) and heart tissue (WH: whole heart – n=6). *Data are shown as mean±SEM. Data normality was evaluated with the Shapiro-Wilk test. P-values were calculated one-way ANOVA was applied for comparing multiple groups followed with Fisher's LSD post-hoc test. *p-value<0.05.*

Next, the expression levels of *Gadlor1/2* were evaluated during cardiac stress and disease state, which TAC was used as left-ventricle associated heart failure model. Myocardial expression levels of both *Gadlor1* and *Gadlor2* were strongly upregulated in the chronic phase of heart failure after TAC (12-weeks TAC) compared to sham hearts **(Figure 14A)**. Since *Gadlor1/2* are highly conserved in human, the expression levels were assessed in human heart tissue samples obtained from

patients suffering from advanced heart failure. Strongly elevated *GADLOR1* and *GADLOR2* levels were also confirmed in human failing heart samples **(Figure 14B)**.

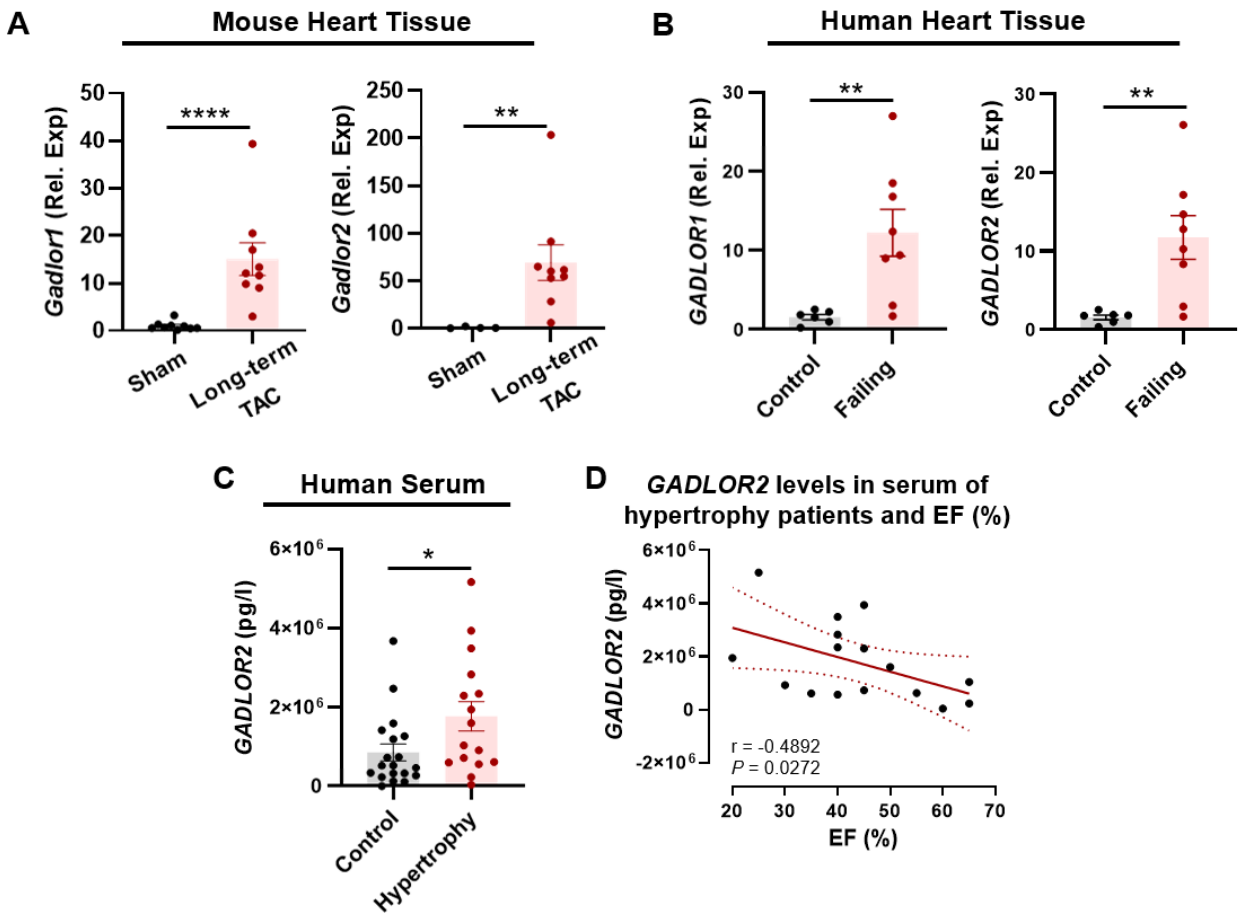

Figure 14: Expression of *Gadlor* lncRNAs in pre-clinical model of pressure overload in mice and in human failing heart samples.

A. *Gadlor* lncRNA levels in mouse cardiac tissue after long-term (12 weeks, n=9) TAC (transverse aortic constriction) compared to sham. **B.** *GADLOR1* and *2* expression in control (healthy, n=6) and human failing heart tissue (n=8) samples that were obtained from aortic stenosis patients. **C.** Detection of *GADLOR2* levels (pg/l: picogram/liter) in human serum of healthy volunteers (n=19) and patients with aortic stenosis (n=16). **D.** Correlation analysis of *GADLOR2* levels (pg/l) with ejection fraction (%) of hypertrophy patients (n=16), (Pearson correlation, Pearson r= -4892 and p-value = 0.0272). Experiments shown in C-D were performed by Dr. Ricarda Haustein and analysed by myself. *Data are shown as mean±SEM. Data normality was evaluated with the Shapiro-Wilk test. P-values were calculated with Student's t-test for parametric (or Mann-Whitney for non-parametric) for comparing two groups, *p-value<0.05, **p-value<0.01, ****p-value<0.0001.*

Interestingly, *GADLOR2* levels were significantly higher in serum of aortic stenosis patients with cardiac hypertrophy compared to healthy controls. In the same patient cohort, a negative correlation between *GADLOR2* levels and left-ventricular ejection fraction (LV-EF%) was observed **(Figure 14C-D).**

10.3. *Gadlor1* and *Gadlor2* are enriched in EC-derived extracellular vesicles (EVs)

As shown in recent studies, secreted EVs can carry lncRNAs in addition to their usual cargo molecules such as proteins or miRNAs.[87,126] Since *GADLOR2* was detectable in the human serum of heart failure patients **(Figure 14C)**, the hypothesis of whether *Gadlor1/*2 lncRNAs might be secreted was tested with EVs isolated from ECs. To this end, primary mouse cardiac ECs were cultured to collect secreted EVs with ultracentrifugation from the supernatant of those cells **(Figure 15)**.

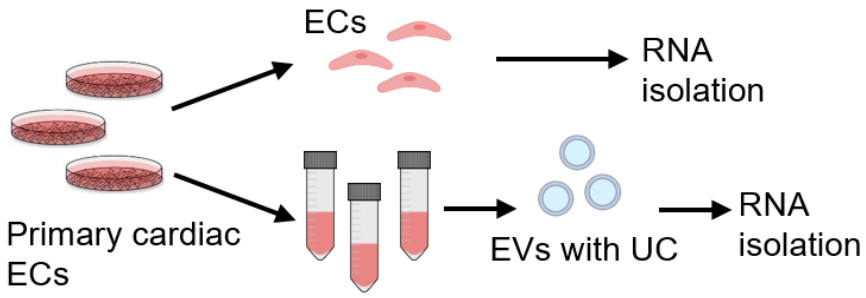

Figure 15: Experimental design for isolating extracellular vesicles (EV) from EC.

Scheme depicting the experimental design of EV isolation with ultracentrifugation (UC) from cultured primary cardiac ECs. *Illustration is created by using www.biorender.com.*

Initially, the isolation of EVs with ultracentrifugation was validated by the characterization of EVs according to the latest guidelines defined by the ISEV.[135] First, isolated vesicles were visualized with transmission electron microscopy (TEM) and particles were detected with Nanoparticle Tracking Analysis (NTA) as shown in **Figure 16A-B.** The average size of EVs was detected as slightly

larger than 100 nm in diameter, which indicated that the particles were in the range of microvesicles and exosomes. Moreover, flow cytometry assessment to check the common surface markers confirmed the presence of CD63, CD9 and CD54 **(Figure 16C)**.

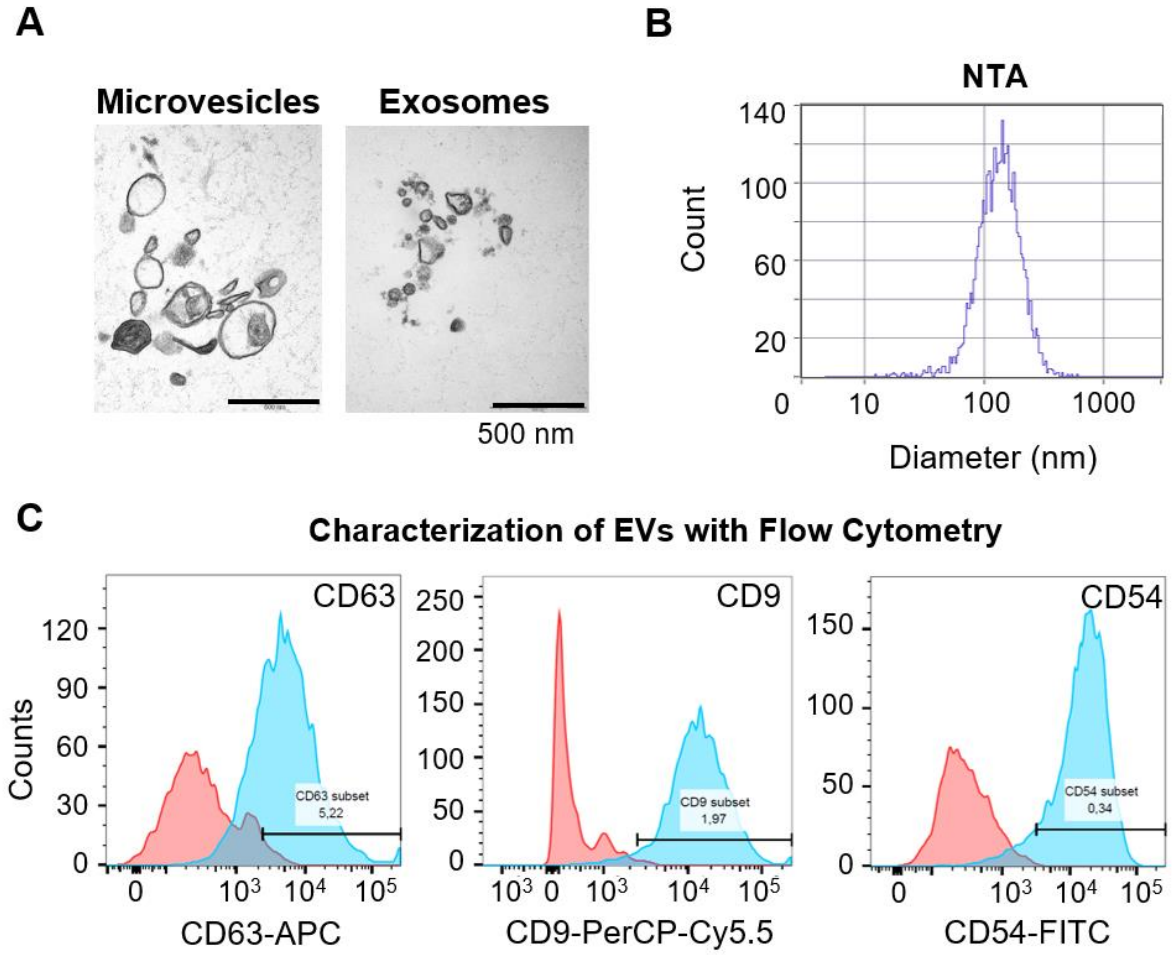

Figure 16: Characterization of extracellular vesicles with TEM, NTA and FACS.

A. Visualizing microvesicles and exosomes with transmission electron microscopy (TEM) (scale bar: 500 nm) and **B.** detecting the size in diameter (nm: nanometers) with Nanoparticle Tracking Analysis (NTA). **C.** Flow cytometry analysis of EV surface markers (CD63-APC, CD9-PerCP-Cy5.5 and CD54-FITC) on EC-derived EVs that were stained against markers (blue curve) and compared to isotype control (red curve). Experiments shown in figure A were performed by Jan Hegermann, PhD, and figure C were performed by Stefanie Uhlig, BSc and analysis performed by myself.

The absolute concentration of *Gadlor1* and *Gadlor2* was markedly higher in cardiac EC-derived EVs compared to cardiac ECs themselves **(Figure 17A)**. In addition to primary cardiac ECs, C166 mouse endothelial cell line also secreted *Gadlor* lncRNAs within EVs **(Figure 17B)**.

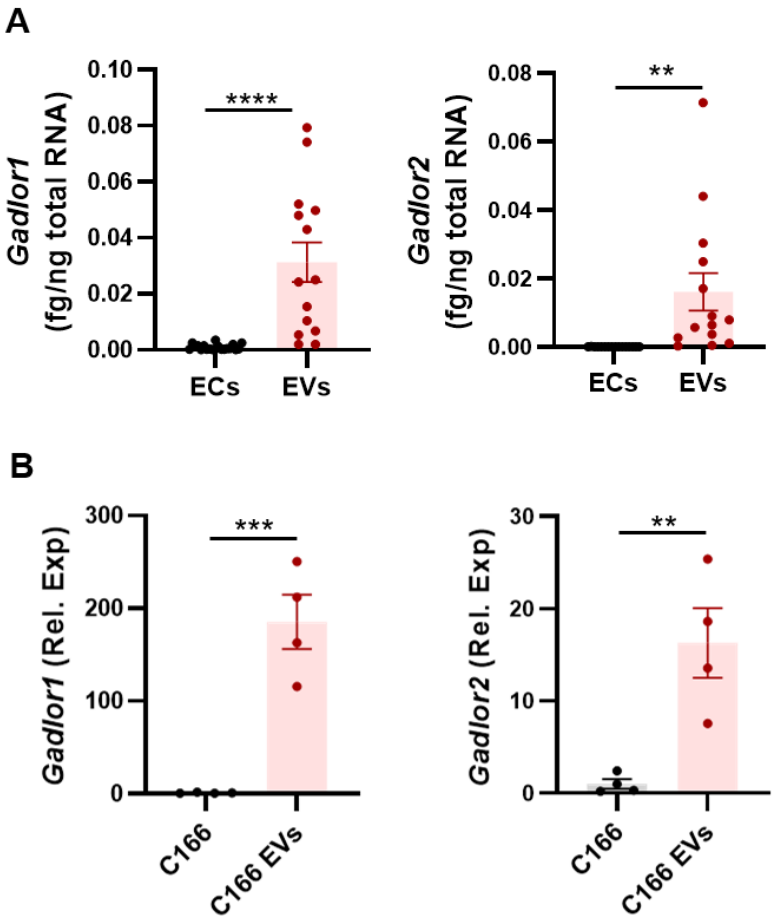

Figure 17: Enriched expression of *Gadlor1*/2 in extracellular vesicles compared to cells.

A. Absolute quantification of total RNA amount of *Gadlor1* and *Gadlor2* in ECs and EC-derived EVs (fg/ng: femtogram/ nanogram). **B.** Relative expression of *Gadlor1* and *Gadlor2* in C166 mouse endothelial cells and EVs derived from these cells. *Data are shown as mean±SEM. Data normality was evaluated with the Shapiro-Wilk test. P-values were calculated with Student's t-test for parametric (or Mann-Whitney for non-parametric) for comparing two groups. **p-value<0.01, ***p-value<0.001, ****p-value<0.0001.*

To explore whether secreted *Gadlor* lncRNAs were encapsulated within vesicles or bound to surface proteins, vesicle-RNA protection assay was performed. *Gadlor1* and *Gadlor2* levels were

not affected by proteinase K (PK) and RNase A treatment of EVs, which indicated that they are encapsulated within vesicles and protected from enzyme degradation **(Figure 18)**. In contrast, Triton-X treatment to disrupt the phospholipid membrane before RNase A addition, or direct treatment of RNase of EV RNA resulted in almost a complete degradation of *Gadlor* lncRNAs as expected.

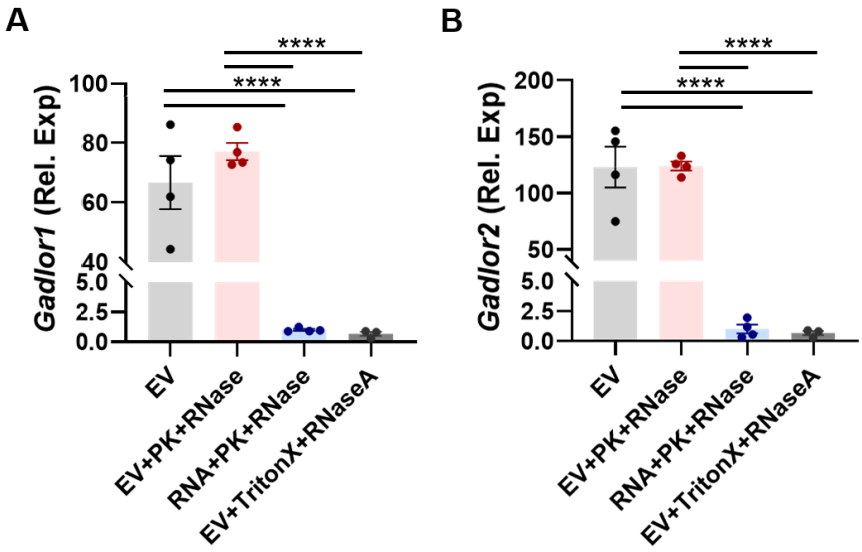

Figure 18: *Gadlor1* and *Gadlor2* are encapsulated into extracellular vesicles.

Detection of **A.** *Gadlor1* and **B.** *Gadlor2* lncRNAs in EC-derived EVs with proteinase K (PK), RNase or Triton-X as indicated. *Data are shown as mean±SEM. Data normality was evaluated with the Shapiro-Wilk test. P-values were calculated with Student's t-test for parametric (or Mann-Whitney for non-parametric) for comparing two groups, and one-way ANOVA was applied for comparing multiple groups followed with Fisher's LSD post-hoc test. ****p-value<0.0001.*

10.4. Systemic deletion of *Gadlor1* and *Gadlor2*: *Gadlor* knock-out (KO) mice

To investigate the role of *Gadlor1* and *Gadlor2* in healthy and disease conditions, systemic *Gadlor* knock-out mice (*Gadlor*-KO) were generated by deletion of the whole region of mouse chromosome 16 by using a CRISPR-Cas9 based strategy. The deletion sites for the designed model was shown in **Figure 19A**. There was no effect of *Gadlor1* and *Gadlor2* deletion on the expression

of the *Lsamp* gene, as no change in *Lsamp* expression in brain tissue between WT and *Gadlor*-KO was observed **(Figure 19B)**. *Lsamp* is mainly expressed in the brain compared to other organs.

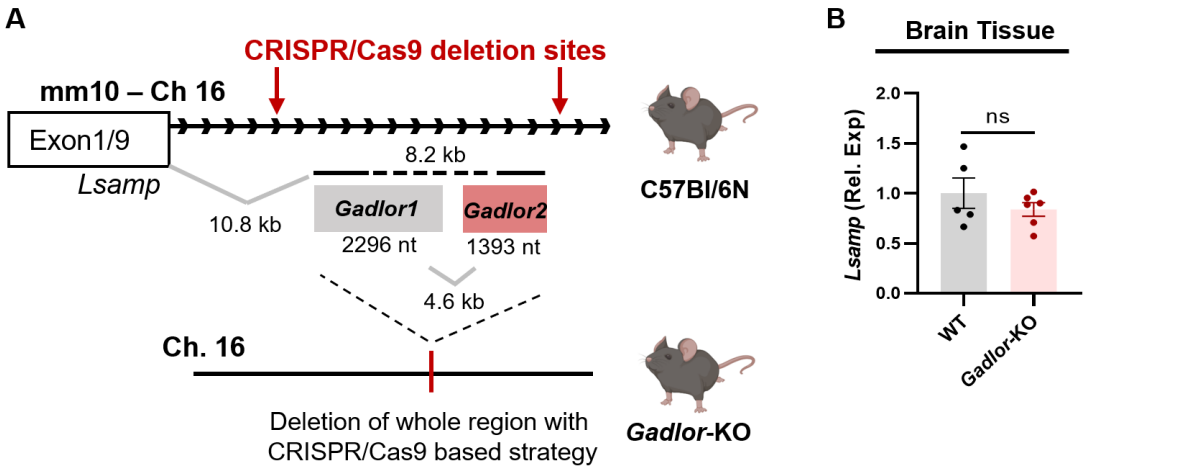

Figure 19: Generation of *Gadlor*-KO mouse model with CRISPR/ Cas9 based strategy.

A. Scheme of *Gadlor*-KO mouse line generation by systemic deletion of the region on chromosome 16 containing both *Gadlor1* and *Gadlor2* by a CRISPR/Cas9 approach. **B.** Systemic deletion of the whole region containing *Gadlor* lncRNAs did not affect the expression of neighbour gene *Lsamp*, which is mainly expressed in brain tissue. (Relative expression to *Gapdh*). *Data are shown as mean±SEM. Data normality was evaluated with Shapiro-Wilk test and p-values were calculated with Student's t-test for comparing two groups. Illustration is created by using www.biorender.com.*

The deletion of *Gadlor1* and *Gadlor2* was confirmed in different organs collected from *Gadlor*-KO animals by qRT-PCR **(Figure 20)**. The highest expression levels of *Gadlor1/2* were detected in the brain, liver, kidney and as well as in heart of WT mice. Indeed, the complete ablation of *Gadlor1/2* was validated in *Gadlor*-KO animals, since no *Gadlor1/2* expression was detectable.

Unchallenged *Gadlor*-KO mice were indistinguishable from their wild-type littermates (WT) based on appearance, body weight, heart weight, **(Figure 21)** and baseline echocardiographic analysis including left-ventricular (LV) ejection fraction (EF%), fractional shortening (FS%), LV posterior wall thickness and LV end-diastolic volume **(Figure 22A-B)**.

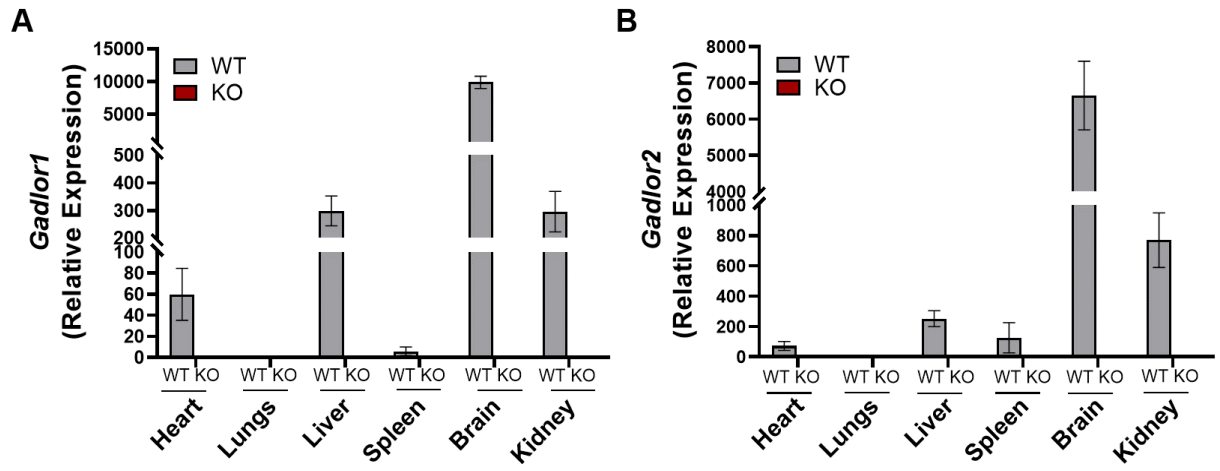

Figure 20: Validation of *Gadlor1* and *Gadlor2* ablation with qRT-PCR.

Validation of *Gadlor*-KO mouse line by assessing the relative expression of **A.** *Gadlor1* and **B.** *Gadlor2* in indicated organs in adult WT and *Gadlor*-KO mice (n≥8). The difference in *Gadlor1/2* expression levels between WT and *Gadlor*-KO animals were significant for all organs in which *Gadlor1* and *Gadlor2* were detected *Data are shown as mean±SEM. Heart: *p-value<0.05, Liver and Kidney: ***p-value<0.001, Brain: ****p-value<0.0001.*

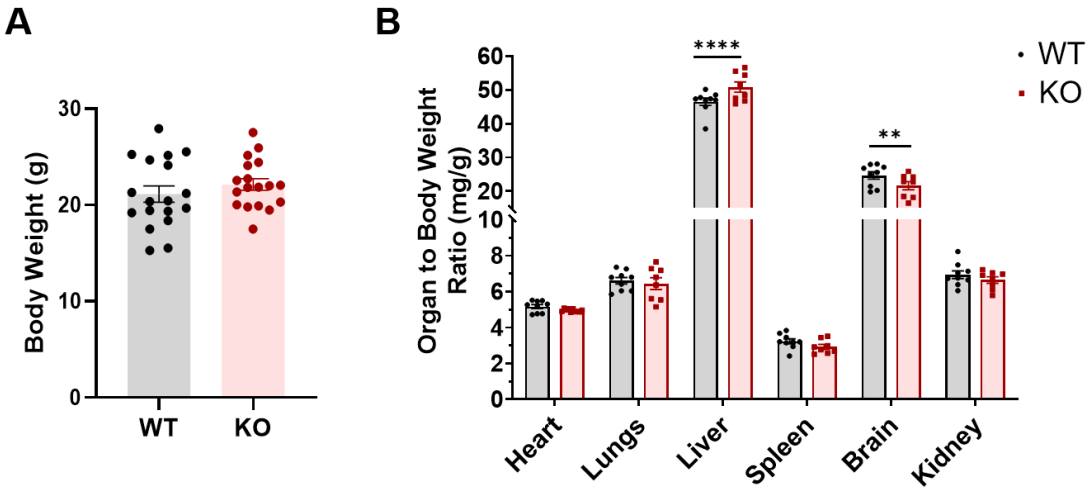

Figure 21: Baseline phenotypic characterization of *Gadlor*-KO mice compared to wild-type (WT) littermates.

A. Body weight (g) of adult (9 weeks old) WT and *Gadlor*-KO animals (n≥18), and **B.** organ to body weight ratio (mg/g) of isolated organs including heart, lungs, liver, spleen, brain and kidney (n≥8). *Data are shown as mean±SEM. Data normality was evaluated with the Shapiro-Wilk test. P-values were calculated with Student's t-test for parametric (or Mann-Whitney for non-parametric) for comparing two groups. **p-value<0.01, ****p-value<0.0001.*

Additional to systolic parameters, diastolic parameters including global longitudinal strain (GLS%) and MV E/E' ratio were also similar in both genotypes in the baseline. However, a mild increase in liver and decrease in brain weight was detected in KO animals compared to WT littermates **(Figure 21C)**.

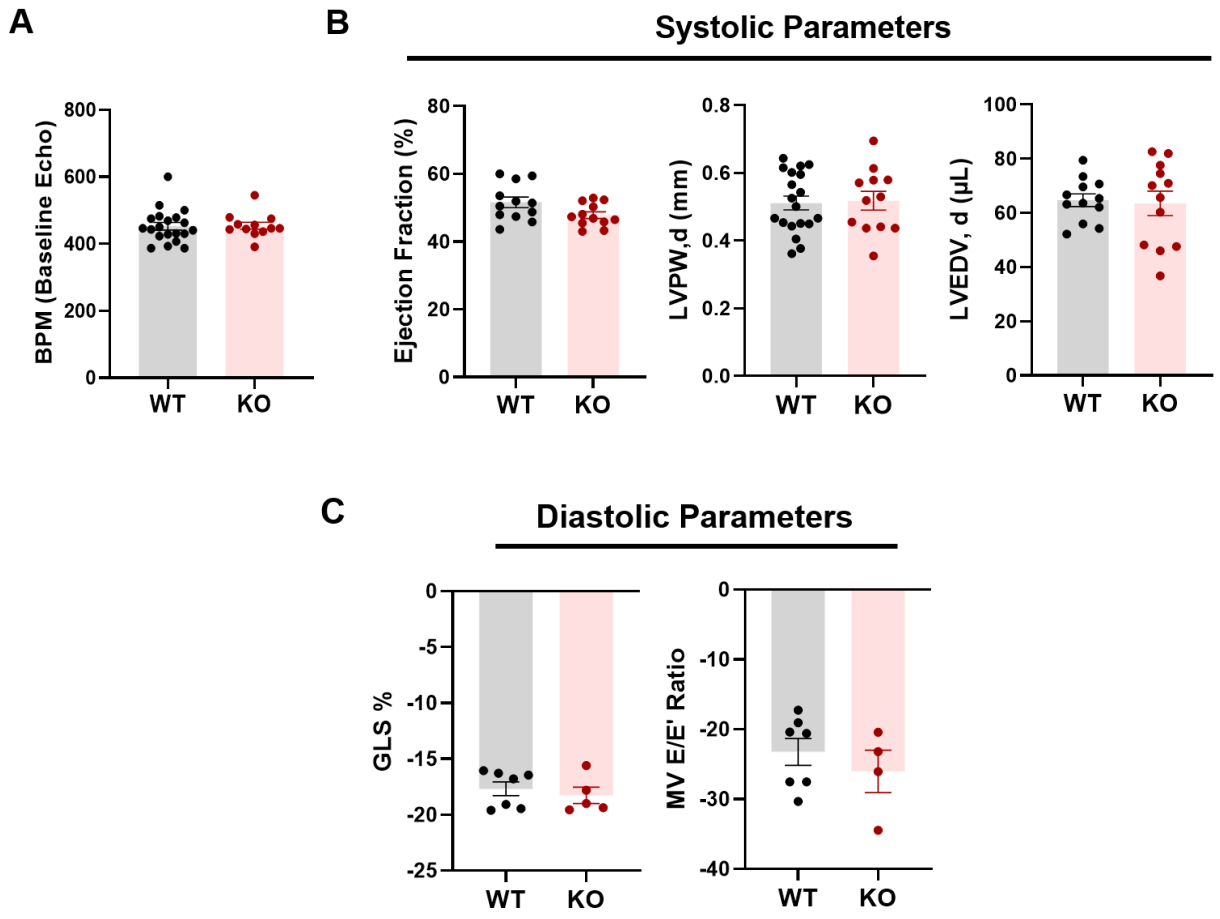

Figure 22: Baseline phenotypic characterization of *Gadlor*-KO mice with echocardiography.

A. Heart rate of WT and *Gadlor*-KO mice during echocardiography (BPM: beats per minute, n≥12). **B.** Analysis of systolic function parameters of left ventricle (LV) ejection fraction (%), fractional shortening (%), LV posterior wall thickness in diastole (mm) and LV end-diastolic volume (µl) (n≥12). **C.** Analysis of diastolic function parameters, global longitudinal strain (GLS, %) and mitral valve (MV) E to E' ratio (n≥4). *Data are shown as mean±SEM. Data normality was evaluated with the Shapiro-Wilk test. P-values were calculated with Student's t-test for parametric (or Mann-Whitney for non-parametric) for comparing two groups. *p-value<0.05, **p-value<0.01, ***p-value<0.001, ****p-value<0.0001.*

10.5. *Gadlor*-KO mice were protected from cardiac systolic dysfunction after TAC

To investigate the effect of *Gadlor1/2* during cardiac remodelling after pressure overload, both WT and *Gadlor*-KO mice were subjected to TAC and sham operation and monitored for 2 weeks with echocardiography **(Figure 23A)**.

To verify the strength of aortic constriction after TAC surgery on different cohorts, the carotid flow measurement in the right common carotid artery (RCCA) and left common carotid artery (LCCA) compared in both WT and *Gadlor*-KO mice after 2 days of TAC. The increase in the ratio of RCCA/ LCCA was the similar degree for both WT and *Gadlor*-KO animals **(Figure 23B-C)**.

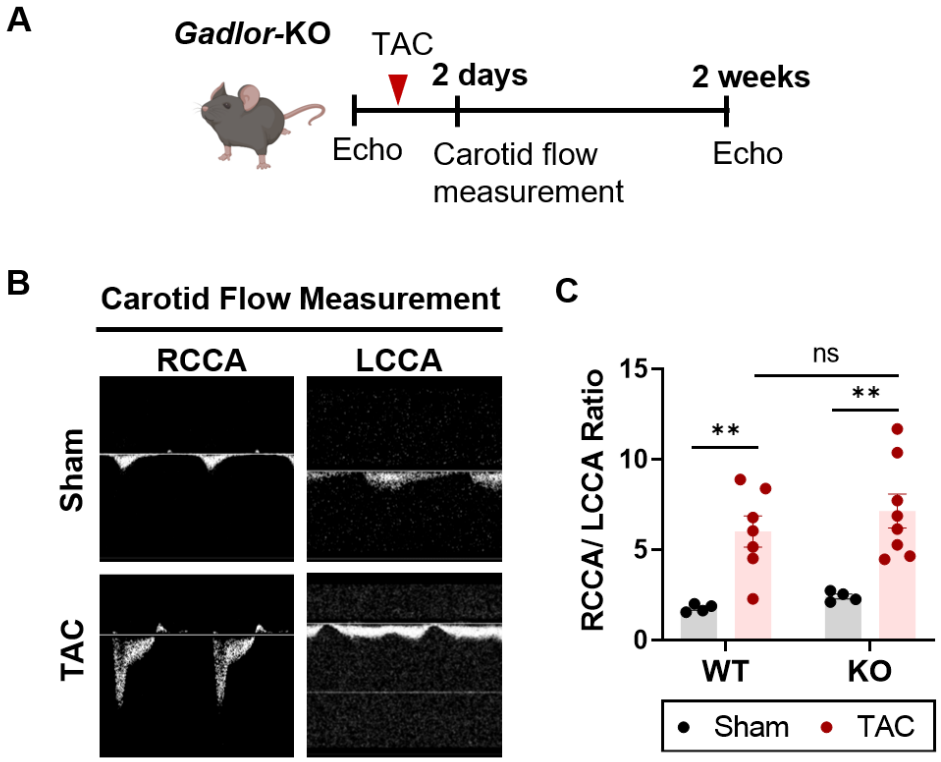

Figure 23: Experimental design for short term pressure overload with TAC.

A. Experimental design of TAC operation for *Gadlor*-KO and WT littermates. **B-C.** Representative images and quantification of flow measurement in the right and left common carotid arteries (RCCA and LCCA) after sham (n≥4) and TAC (n≥7) operation to measure the strength of TAC operation in WT and Gadlor-KO animals. *Data are shown as mean±SEM. Data normality was evaluated with Shapiro-Wilk test and p-values were calculated with two-way ANOVA for grouped analysis followed with Fisher's LSD post-hoc test. *p-value<0.05, **p-value<0.01.*

After 2 weeks of TAC, a significant increase in heart weight to body weight (HW/BW) ratio was detected in both WT and *Gadlor*-KO mice compared to sham-operated mice. However, less cardiac hypertrophy (i.e. reduced HW/BW ratio) was observed in *Gadlor*-KO mice compared to WT littermates after 2 weeks of TAC **(Figure 24A)**. Additionally, heart failure-induced pulmonary congestion detected as an increase in lung weight due to liquid accumulation, was only observed in WT animals while *Gadlor*-KO animals were protected **(Figure 24B).**

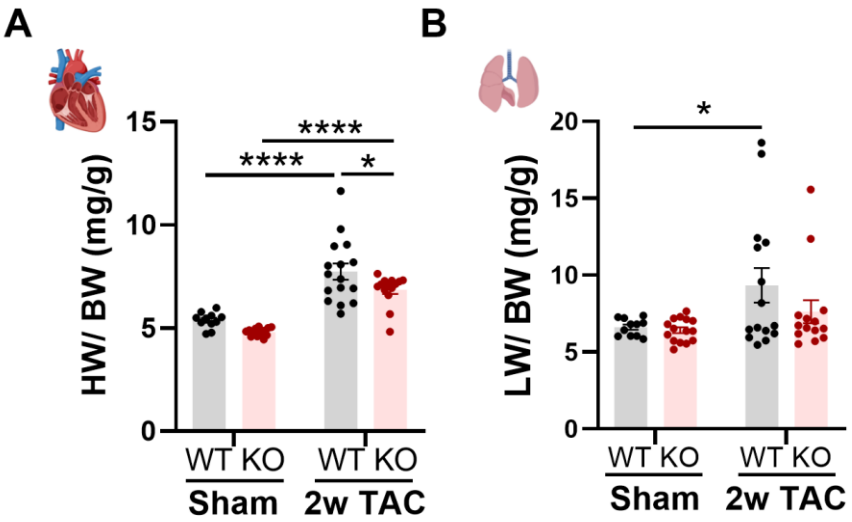

Figure 24: Deletion of Gadlor lncRNAs reduces cardiac hypertrophy and heart failure-induced pulmonary congestion.

A. Heart weight (milligrams) to body weight (grams) ratio (HW/BW) and **B.** lung weight (milligrams) to body weight (grams) ratio of *Gadlor*-KO and WT littermates in sham and after 2 weeks TAC (n≥11). *Data are shown as mean±SEM. Data normality was evaluated with Shapiro-Wilk test and p-values were calculated with two-way ANOVA for grouped analysis followed with Fisher's LSD post-hoc test. *p-value<0.05, ****p-value<0.0001.*

Cardiac function and dimensions before TAC (pre-TAC) and 2 weeks after the surgery (2w TAC) were recorded by echocardiography with a Vevo 3100 device (VisualSonics-Fujifilm). *Gadlor*-KO mice showed less TAC-induced cardiac systolic dysfunction as manifested by preserved ejection fraction (LV-EF%: 41.73 vs 30.66%, *Gadlor*-KO vs. WT, p<0.0001, n≤10) after 2 weeks of TAC **(Figure 25A-B)**. Furthermore, *Gadlor*-KO mice showed a reduced left ventricle wall thickness

(LVPW) and less chamber dilation measured as the left end-diastolic volume (LVEDV) compared to WT mice after 2 weeks of TAC **(Figure 25C-D)**.

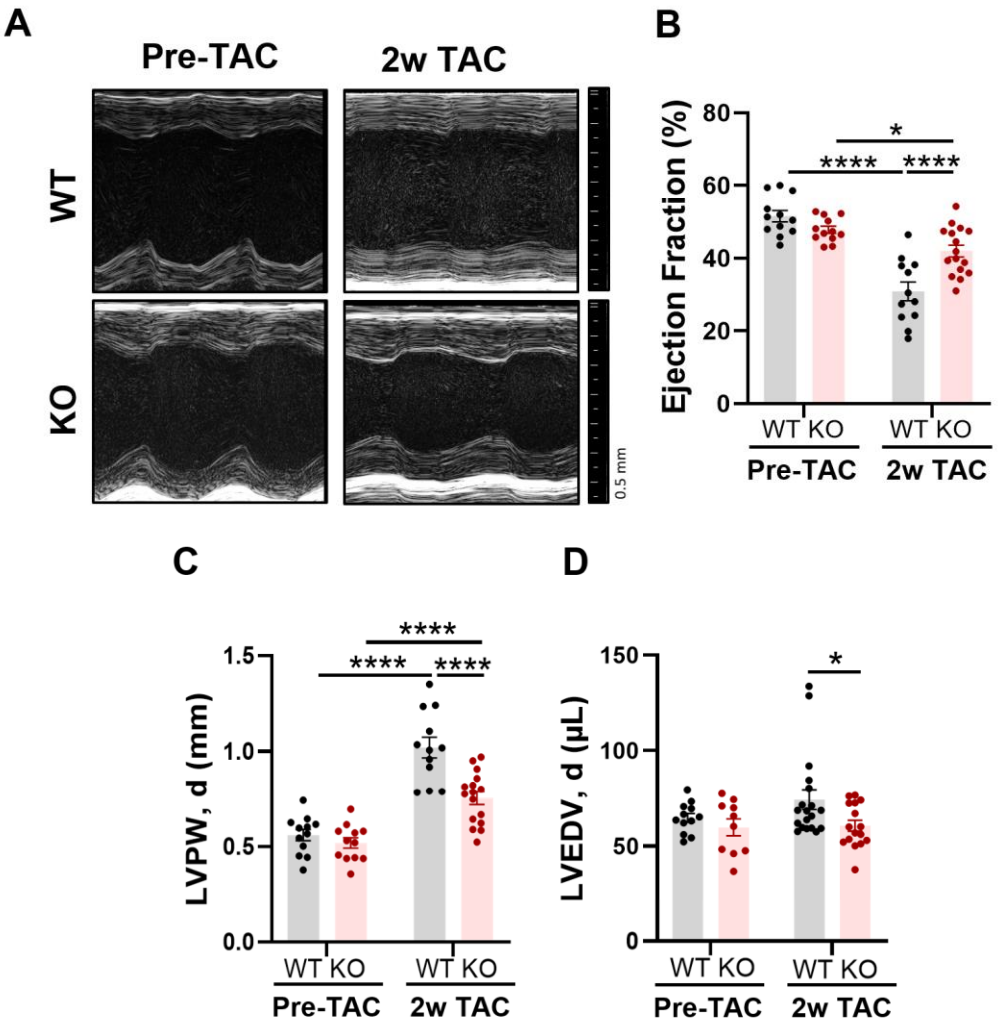

Figure 25: *Gadlor*-KO mice showed less cardiac systolic dysfunction after pressure overload.

A. Representative echocardiography images of *Gadlor*-KO and WT mice before (pre-TAC) and after 2 weeks of TAC (2w TAC) shown in parasternal long axis mode, and analysis of **B.** left ventricle (LV) ejection fraction (EF%), **C.** LV posterior wall thickness in diastole (mm) and **D.** LV end-diastolic volume (ul), (n≥12). *Data are shown as mean±SEM. Data normality was evaluated with Shapiro-Wilk test and p-values were calculated with two-way ANOVA for grouped analysis followed with Fisher's LSD post-hoc test. *p-value<0.05, **p-value<0.01, ***p-value<0.001, ****p-value<0.0001.*

Additional to analysis with WT and *Gadlor*-KO mice, *Gadlor*-WT/KO (heterozygous) mice were also analysed at the baseline, and after sham and 2 weeks of TAC to detect a potential dose-response effect of *Gadlor1/2* deletion **(Figure 26 and Figure 27)**.

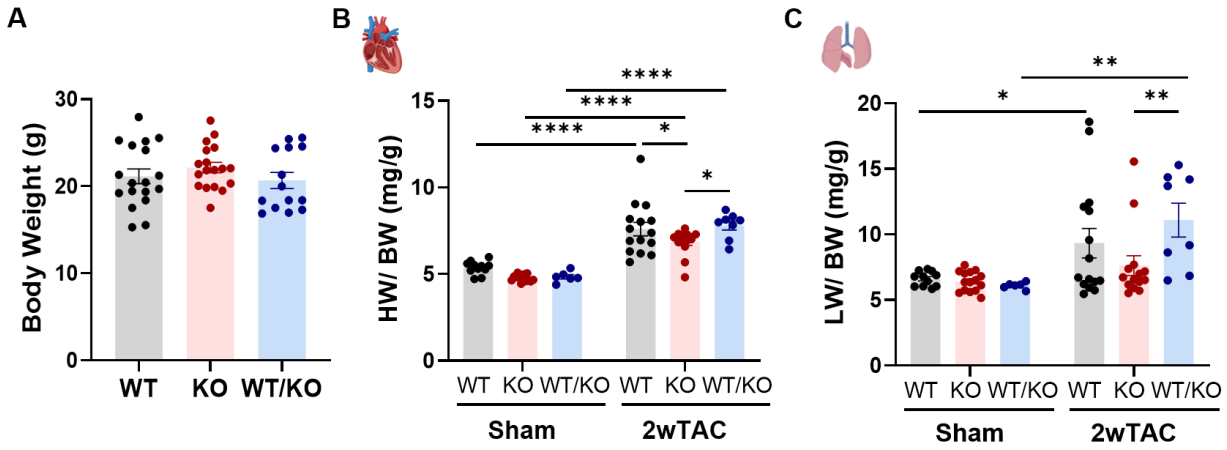

Figure 26: *Gadlor* heterozygous (WT/KO) mice showed similar phenotype to WT animals in baseline and after TAC.

A. Baseline body weight, **B.** heart weight (milligrams) to body weight (grams) ratio (HW/BW) and **C.** lung weight (milligrams) to body weight (grams) ratio of WT, *Gadlor*-KO and *Gadlor-WT/KO* (heterozygous) littermates in sham and after 2 weeks TAC (n≥8). *Data are shown as mean±SEM. Data normality was evaluated with Shapiro-Wilk test and p-values were calculated with two-way ANOVA for grouped analysis followed with Fisher's LSD post-hoc test. *p-value<0.05, **p-value<0.01, ***p-value<0.001, ****p-value<0.0001.*

There was no difference observed in either baseline organ parameters **(Figure 26)** and echocardiographic assessment **(Figure 27)**, nor in the analysis after 2 weeks of pressure overload in *Gadlor*-WT/KO mice and WT animals. Thus, the difference observed between *Gadlor*-KO and *Gadlor*-WT/KO animals were at a similar degree as the differences between *Gadlor*-KO and WT littermates. In accordance with these data, the follow-up studies were only conducted with Gadlor-KO and WT littermates.

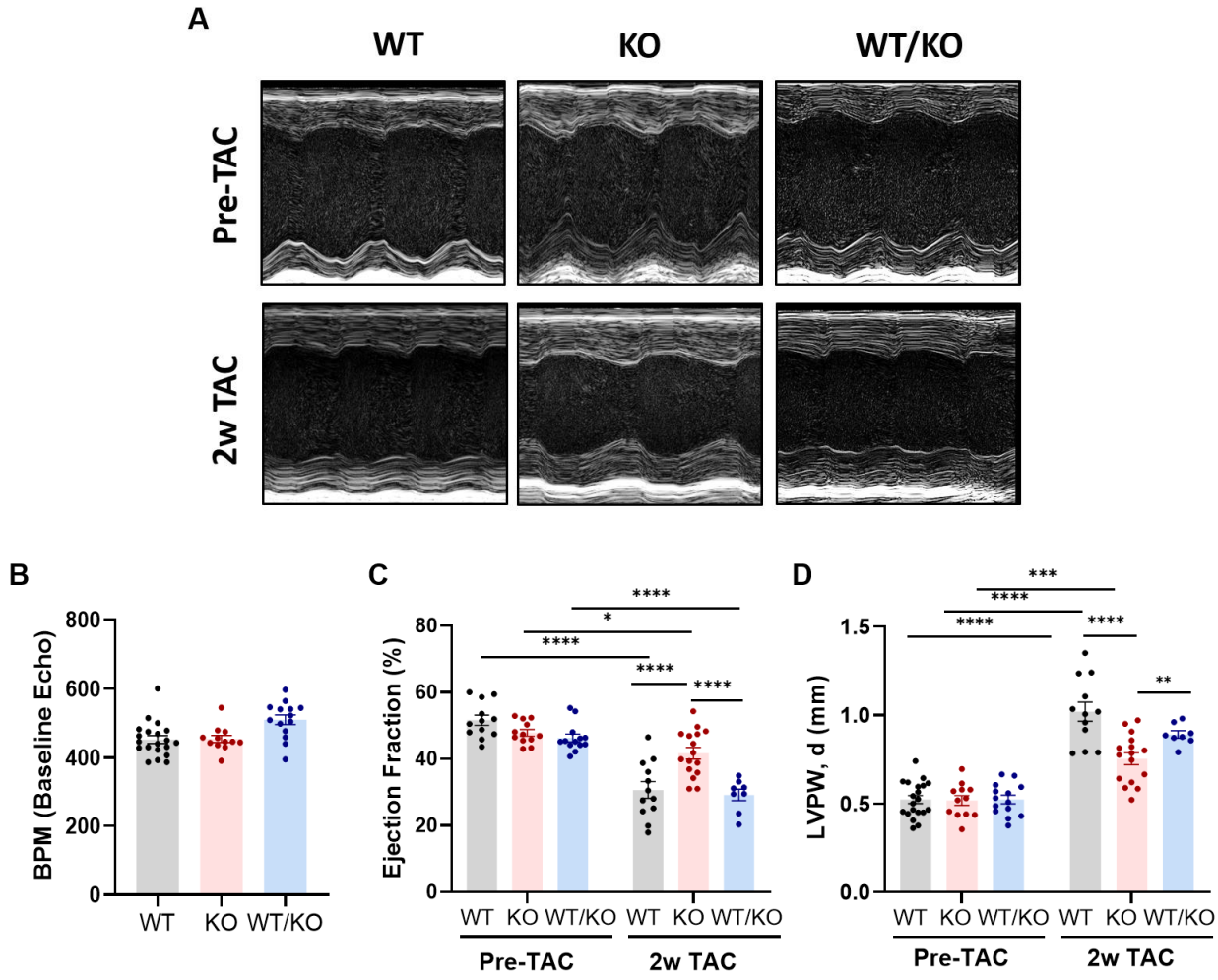

Figure 27: Cardiac function of *Gadlor*-WT/KO mice showed no difference from WT mice in the baseline and after 2 weeks of TAC.

A. Representative echocardiography images of WT, *Gadlor*-KO and *Gadlor*-WT/KO mice before (pre-TAC) and after 2 weeks of TAC (2w TAC) shown in parasternal long axis mode, and analysis of **B.** heart rate (BPM: beats per minute) during baseline echocardiography, **C.** left ventricle (LV) ejection fraction (EF%), **D.** LV posterior wall thickness in diastole (mm) (n≥10). *Data are shown as mean±SEM. Data normality was evaluated with Shapiro-Wilk test and p-values were calculated with two-way ANOVA for grouped analysis followed with Fisher's LSD post-hoc test. *p-value<0.05, **p-value<0.01, ***p-value<0.001, ****p-value<0.0001.*

10.6. Deletion of *Gadlor1* and *Gadlor2* alleviates cardiomyocyte hypertrophy and fibrosis *in vivo*

Structural and gene expression changes in the myocardium were analysed in heart sections of WT and *Gadlor*-KO mice after 2 weeks of TAC. Picro-sirius red staining revealed strongly diminished myocardial fibrosis in *Gadlor*-KO mice **(Figure 28)**, which was additionally supported by qRT-PCR analysis as detected in reduced cardiac *Col1a1* and *Col3a1* mRNA levels after TAC (approx. 2-fold vs. 6-fold increase in KO vs WT, $p<0.05$, n=5) shown in **Figure 29A.**

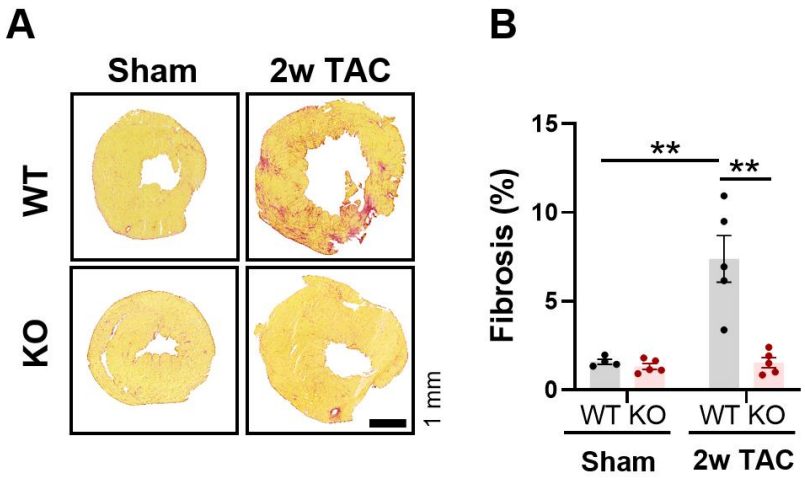

Figure 28: Deletion of Gadlor1 and Gadlor2 prevents fibrosis development after 2-week TAC.

A. Representative Sirius-red fibrosis staining in cardiac tissue sections of sham and 2w TAC animals (scale-bar: 1 mm) and **B.** quantification of fibrotic area (n≥4). *Data are shown as mean±SEM. Data normality was evaluated with Shapiro-Wilk test and p-values were calculated with two-way ANOVA for grouped analysis followed with Fisher's LSD post-hoc test. *p-value<0.05, **p-value<0.01, ***p-value<0.001, ****p-value<0.0001.*

Additionally, significantly reduced expression of hypertrophy-associated genes *Nppa*, *Nppb* and the ratio of *Myh7/Myh6* was in line with previous findings of reduced cardiac hypertrophy (i.e. less increase in HW/BW ration after TAC in *Gadlor*-KO mouse hearts) at the whole organ level which is shown in **Figure 24**.

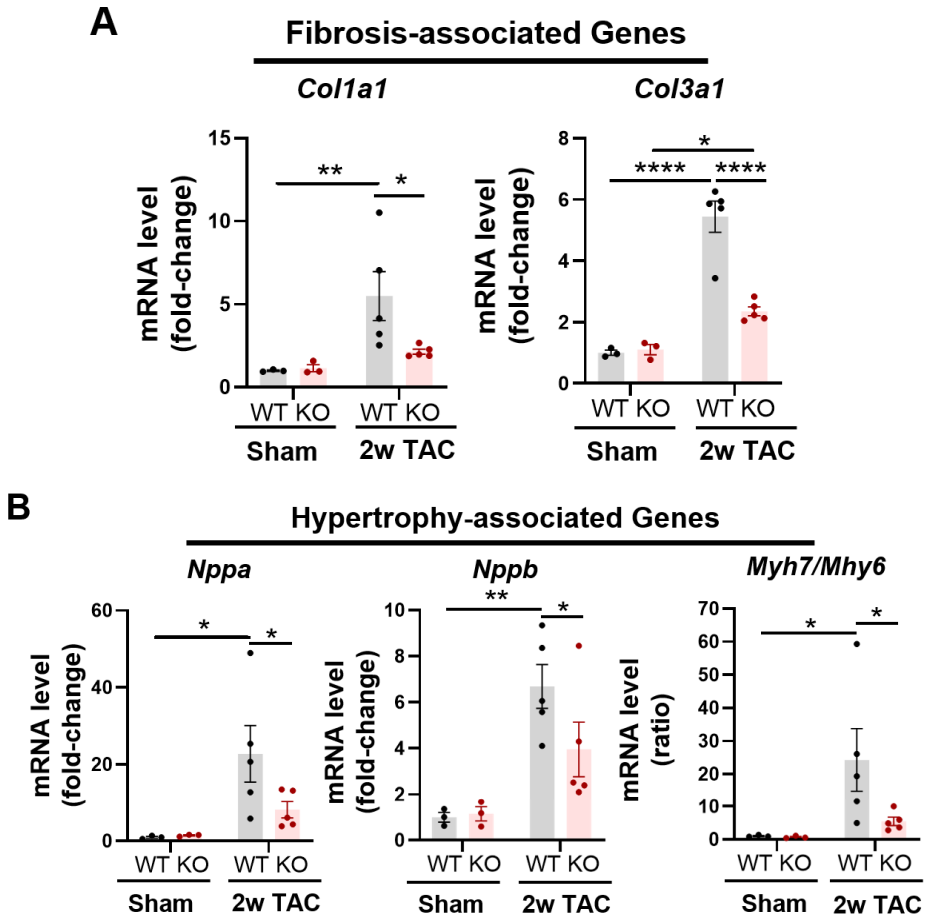

Figure 29: Changes in the expression of fibrosis and hypertrophy-associated genes after TAC in *Gadlor*-KO and WT mice.

A. Relative expression of fibrosis marker genes *Col1a1* and *Col3a1* and **B.** hypertrophy marker genes *Nppa, Nppb* and *Mhy7/6* ratio in mRNA levels in heart tissue samples of sham (n=3) and 2w TAC (n=5). *Data are shown as mean±SEM. Data normality was evaluated with Shapiro-Wilk test and p-values were calculated two-way ANOVA for grouped analysis followed with Fisher's LSD post-hoc test. *p-value<0.05, **p-value<0.01, ***p-value<0.001, ****p-value<0.0001.*

The structural changes in the myocardium were also assessed with wheat-germ agglutinin (WGA) and isolectin-B4 (IB4) staining which confirmed less cardiomyocyte hypertrophy at the cellular level as shown in representative pictures in **Figure 30A**, which was depicted by reduced increase in CM cross-sectional area after 2 weeks of TAC **(Figure 30B)**. Moreover, IB4 staining of capillaries revealed a substantial increase in capillary density in the myocardium of *Gadlor*-KO mice compared to WT animals after TAC **(Figure 30C)**.

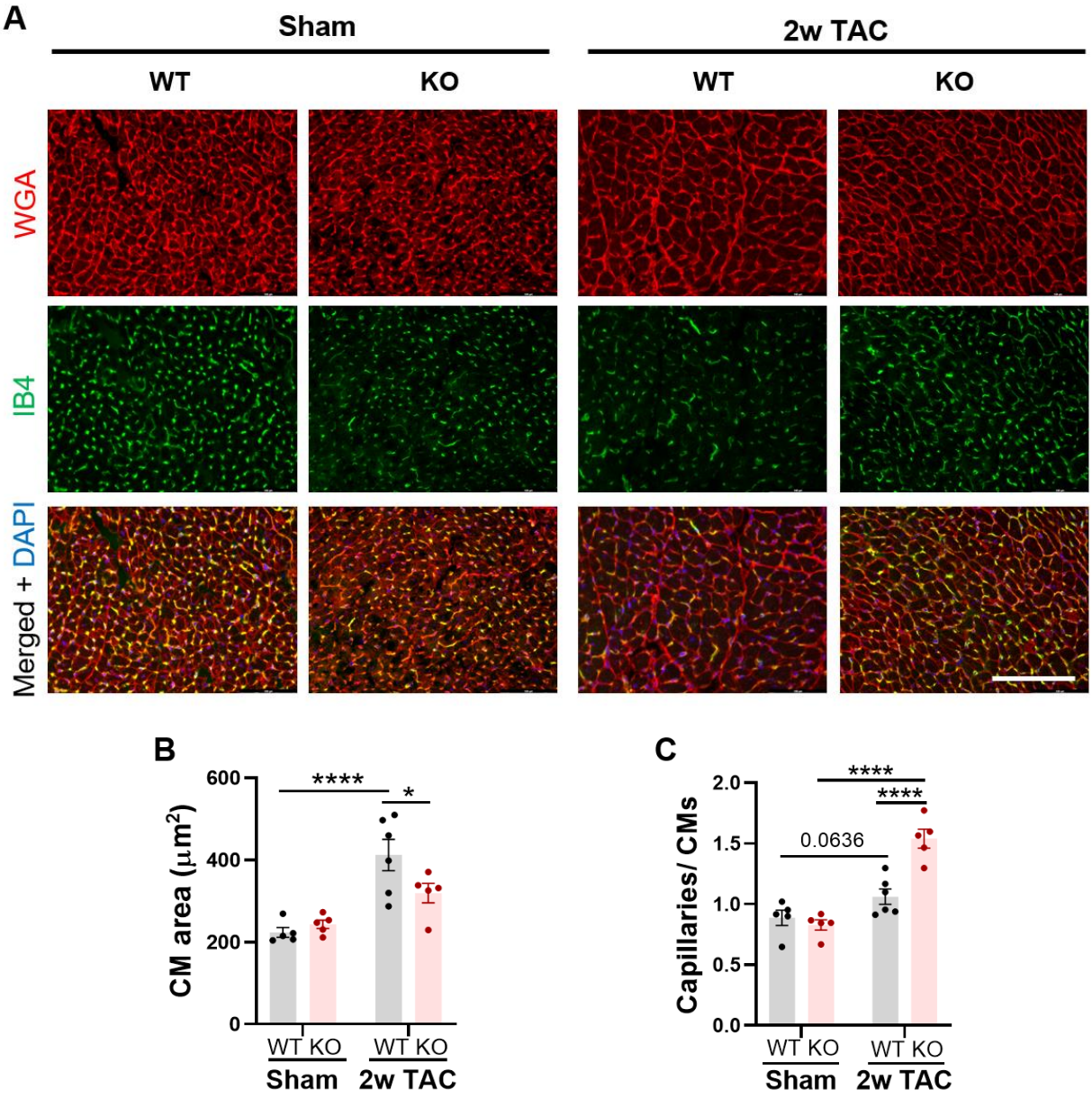

Figure 30: Deletion of *Gadlor* lncRNAs reduces cardiac hypertrophy at the cellular level and markedly increase capillarization.

A. Representative immunofluorescence images of cardiac tissue samples stained with WGA (wheat-germ agglutinin coupled with Alexa Fluor 555) and IB4 (Isolectin B4 coupled with Alexa Fluor 488) in sham and 2-weeks of TAC samples from *Gadlor*-KO and WT littermates, scale-bar: 100 µm. Quantification of **B.** cardiomyocyte cross-sectional area and **C.** myocardial capillary density per cardiomyocyte ratio. *Data are shown as mean±SEM. Data normality was evaluated with Shapiro-Wilk test and p-values were calculated with two-way ANOVA for grouped analysis followed with Fisher's LSD post-hoc test. *p-value<0.05, **p-value<0.01, ***p-value<0.001, ****p-value<0.0001.*

10.7. Overexpression of *Gadlor*1/2 via EVs triggers cardiac dysfunction and fibrosis

In order to decipher the functional effect of increased *Gadlor1* and *Gadlor2* levels during pressure overload, overexpression of *Gadlor1/2* was achieved with the administration of EC-derived EVs as depicted in the experimental scheme in **Figure 31A**. Control EVs were produced by purifying EC-derived EVs from the supernatant of control adenovirus (Ad.β*gal*) infected C166 mouse ECs, while *Gadlor1* and *Gadlor2* containing EVs were produced by purifying EVs from the supernatant of Ad.*Gadlor1* and Ad.*Gadlor2* infected C166 ECs. EC-derived control EVs and *Gadlor*-enriched EVs were administered to mouse hearts directly before TAC surgery by intra-ventricular injection while concomitant cross-clamping of the aorta and pulmonary artery distal of the origin of the coronary vessels. The overexpression of *Gadlor1* and *Gadlor2* was confirmed after 1-week of EV administration in heart tissue samples of *Gadlor*-EV injected animals as shown by 5-fold and 10-fold increase in *Gadlor1* and *Gadlor2* expression, respectively **(Figure 31B)**.

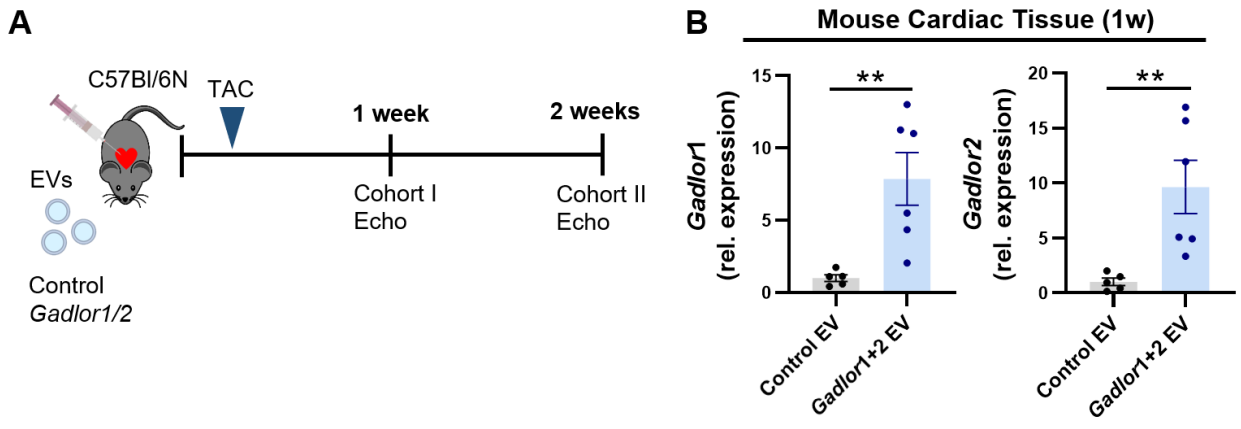

Figure 31: Gadlor1/2 overexpression via EV administration.

A. Scheme of the experimental design depicting the injection of *Gadlor1 and Gadlor2* containing extracellular vesicles for overexpression followed by TAC operation. **B.** Relative expression of *Gadlor1 and Gadlor2* in cardiac tissue samples after 1 week TAC (indicated as cohort I) to validate the overexpression after injection of control (Ad.βgal treated samples, n=5) and *Gadlor*-containing (Ad.*Gadlor1* and Ad.*Gadlor2* treated samples, n=6) EVs. *Data are shown as mean±SEM. Data normality was evaluated with Shapiro-Wilk test and p-values were calculated with Student's t-test. *p-value<0.05, **p-value<0.01.*

Gadlor-EV treated mice showed a marked reduction of cardiac systolic function after 1-week and 2-weeks of administration depicted in reduced LV-ejection fraction (LV-EF%: 58.74 vs. 38.66%, Control-EV vs. *Gadlor*-EV, p<0.001, n=10 after 2-weeks TAC) **(Figure 32A-B)**. Additionally, *Gadlor*-EV treated mice showed an increased wall thickness as an indication of enhanced hypertrophic remodelling, but unchanged left ventricular end-diastolic dimensions (LVEDA) compared to control-EV treated animals after 2 weeks of TAC **(Figure 32C-D)**.

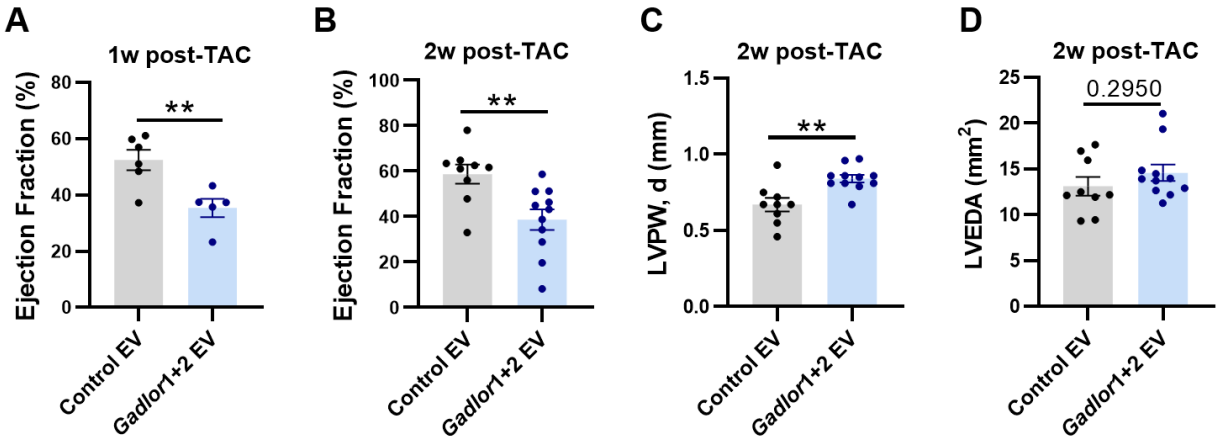

Figure 32: *Gadlor1* and *Gadlor2* overexpression via EVs triggered cardiac systolic dysfunction.

Echocardiographic analysis of **A.** left ventricle (LV) ejection fraction (EF%) after 1-week TAC, and **B.** LV-EF%, **C.** LV posterior wall thickness in diastole (mm), **D.** LV-end diastolic area (mm^2) after 2 weeks TAC in mice injected with control EVs and *Gadlor*1 and *Gadlor2* EVs. *Data are shown as mean±SEM. Data normality was evaluated with Shapiro-Wilk test and p-values were calculated with Student's t-test. **p-value<0.01.*

To analyse the structural changes in the myocardium, Picro-Sirius red staining was performed to detect collagen deposition. Significantly higher fibrosis development in *Gadlor1/2* overexpressing heart tissue samples after pressure overload compared to control samples **(Figure 33A-B)** revealed exaggerated myocardial fibrosis in *Gadlor*-EV treated mice. Analysis with qRT-PCR confirmed the considerable increase in *Col1a1* and *Col3a1* in mRNA levels in the myocardium of *Gadlor1/2*-EV treated samples after 2 weeks of TAC **(Figure 33C)**.

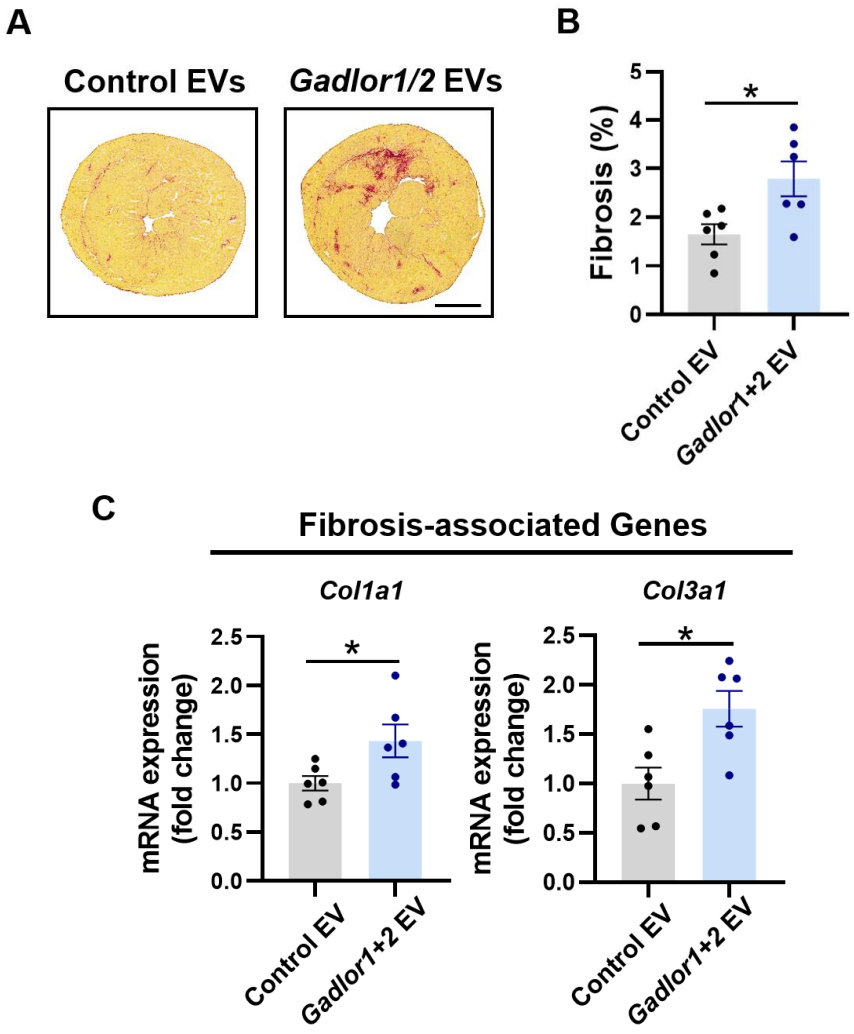

Figure 33: Overexpression of *Gadlor1* and *Gadlor2* triggers fibrosis after TAC.

A. Representative images of Sirius-red staining (scale bar: 1 mm) and **B.** quantification of fibrotic area after 2 weeks TAC in mice injected with control EVs and *Gadlor*1 and *2* EVs. **C.** Relative expression of fibrosis marker genes *Col1a1* and *Col3a1* in heart tissue samples of control-EV (n=6) and *Gadlor*-EVs (n=6) treated mice. *Data are shown as mean±SEM. Data normality was evaluated with Shapiro-Wilk test and p-values were calculated with Student's t-test. *p-value<0.05.*

Furthermore, an increased expression of *Nppa* and *Nppb*, as well as a trend towards larger cardiomyocyte cross-sectional area (CM area: 241.3 µm^2 vs. 290.0 µm^2, Control-EV vs. *Gadlor*-EV, p=0.0615, n=6) verified increased hypertrophic remodelling in *Gadlor*-EV treated mice **(Figure 34A-C)**. The myocardial capillary density, however, was not changed between experimental groups **(Figure 34B, D)**.

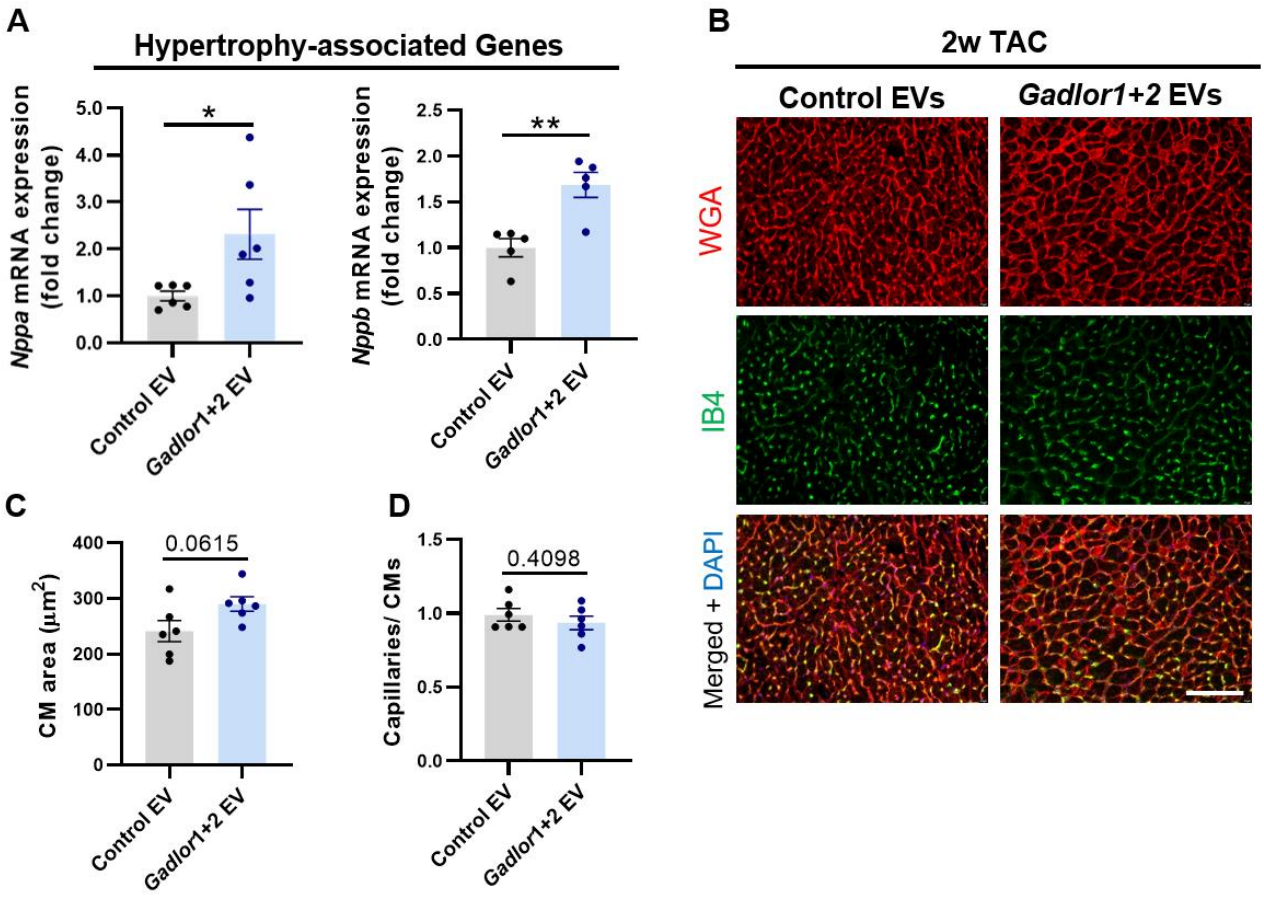

Figure 34: Overexpression of *Gadlor* lncRNAs aggravated cardiac hypertrophy.

A. Representative immunofluorescence images of cardiac tissue samples stained with WGA (wheat-germ agglutinin coupled with Alexa Fluor 555) and IB4 (Isolectin B4 coupled with Alexa Fluor 488) in samples from control EV and *Gadlor*-EV treated animals (scale-bar: 100 µm). Quantification of **B.** cardiomyocyte cross-sectional area and **C.** myocardial capillarization after EV treatment followed by 2 weeks of TAC. **D.** Relative expression of hypertrophy marker genes *Nppa* and *Nppb* in heart tissue samples of control-EV (n=6) and *Gadlor*-EVs (n=6) treated mice *Data are shown as mean±SEM. Data normality was evaluated with Shapiro-Wilk test and p-values were calculated with Student's t-test. *p-value<0.05, **p-value<0.01.*

10.8. *Gadlor*-KO mice showed higher mortality during chronic pressure-overload

To investigate whether the protective effects of *Gadlor1/2* ablation during cardiac remodelling were maintained during persisting long-term pressure overload, WT and *Gadlor*-KO animals were monitored with bi-weekly echocardiography up to 8 weeks of TAC **(Figure 35A)**. Similar to

previous findings, *Gadlor*-KO mice had a significantly reduced HW/BW ratio after 8-weeks of TAC compared to WT littermates **(Figure 35B)**.

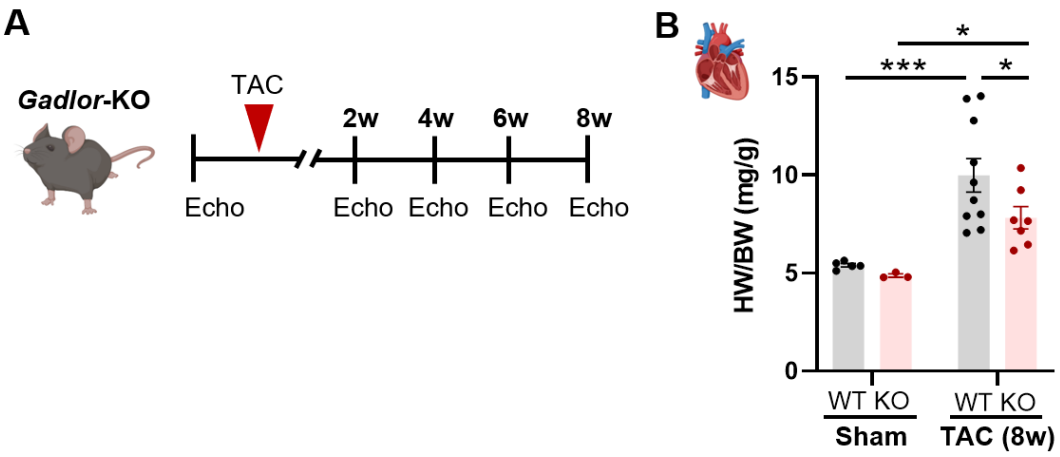

Figure 35: Effect of *Gadlor*-KO in persisting long-term pressure overload.

A. Experimental design of long-term TAC operation for *Gadlor*-KO and WT littermates up to 8-weeks after TAC. **B.** Heart weight (miligrams) to body weight (grams) ratio (HW/BW) of *Gadlor*-KO and WT mice in age comparable sham (n≥3) and after 8-weeks TAC (n≥7). *Data normality was evaluated with Shapiro-Wilk test and p-values were calculated with two-way ANOVA for grouped analysis followed with Fisher's LSD post-hoc test. *p-value<0.05, **p-value<0.01, ***p-value<0.001.*

Based on the echocardiographic assessment, *Gadlor*-KO mice showed better systolic left ventricular function depicted as higher ejection fraction in each time-point analysed, as well as at the end of the long-term study (8-week TAC: LV-EF%: 18.02 vs. 26.52, WT vs. *Gadlor*-KO, p<0.05, n≥6, unpaired-analysis) **(Figure 36A-B)**. As expected, an increase in posterior wall thickness after TAC was observed in both WT and *Gadlor*-KO mice, however, much less after deletion of *Gadlor1/2* as shown in **Figure 36B**. The difference in the LV-posterior wall thickness started to diminish after 6-weeks of TAC between experimental groups.

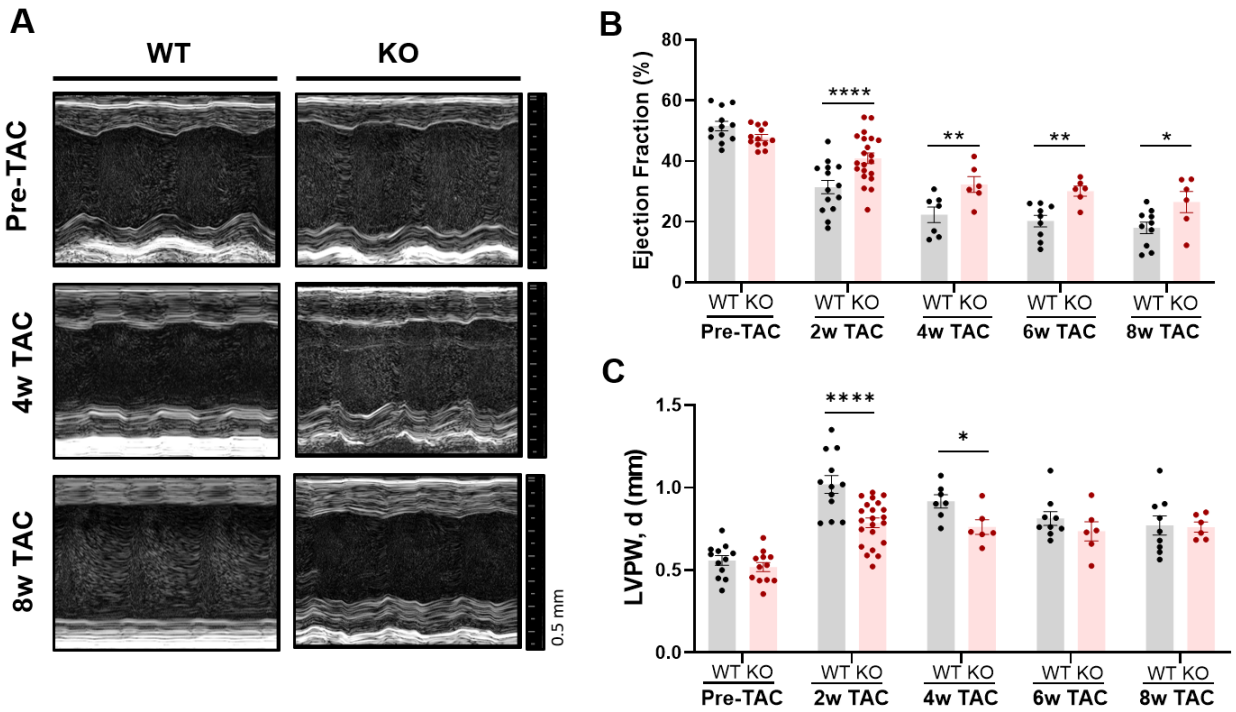

Figure 36: *Gadlor*-KO mice retain better systolic function after persisting long-term pressure overload.

A. Representative echocardiography images of *Gadlor*-KO and WT mice before (pre-TAC) and after 4-weeks and 8-weels TAC shown in parasternal long axis mode, and analysis of **B.** left ventricle (LV) ejection fraction (EF%) and **C.** left ventricle (LV) posterior wall thickness in diastole (mm), (unpaired analysis). Data are shown as mean±SEM. *Data normality was evaluated with Shapiro-Wilk test and p-values were calculated with Student's t-test for comparing two-groups. *p-value<0.05, **p-value<0.01, ***p-value<0.001, ****p-value<0.0001.*

The ultrastructural analysis of the myocardium was analysed with WGA and IB4 staining which confirmed less cardiac hypertrophy at the cellular level and significantly higher capillarization in *Gadlor*-KO mice after 8-weeks of TAC **(Figure 37)**.

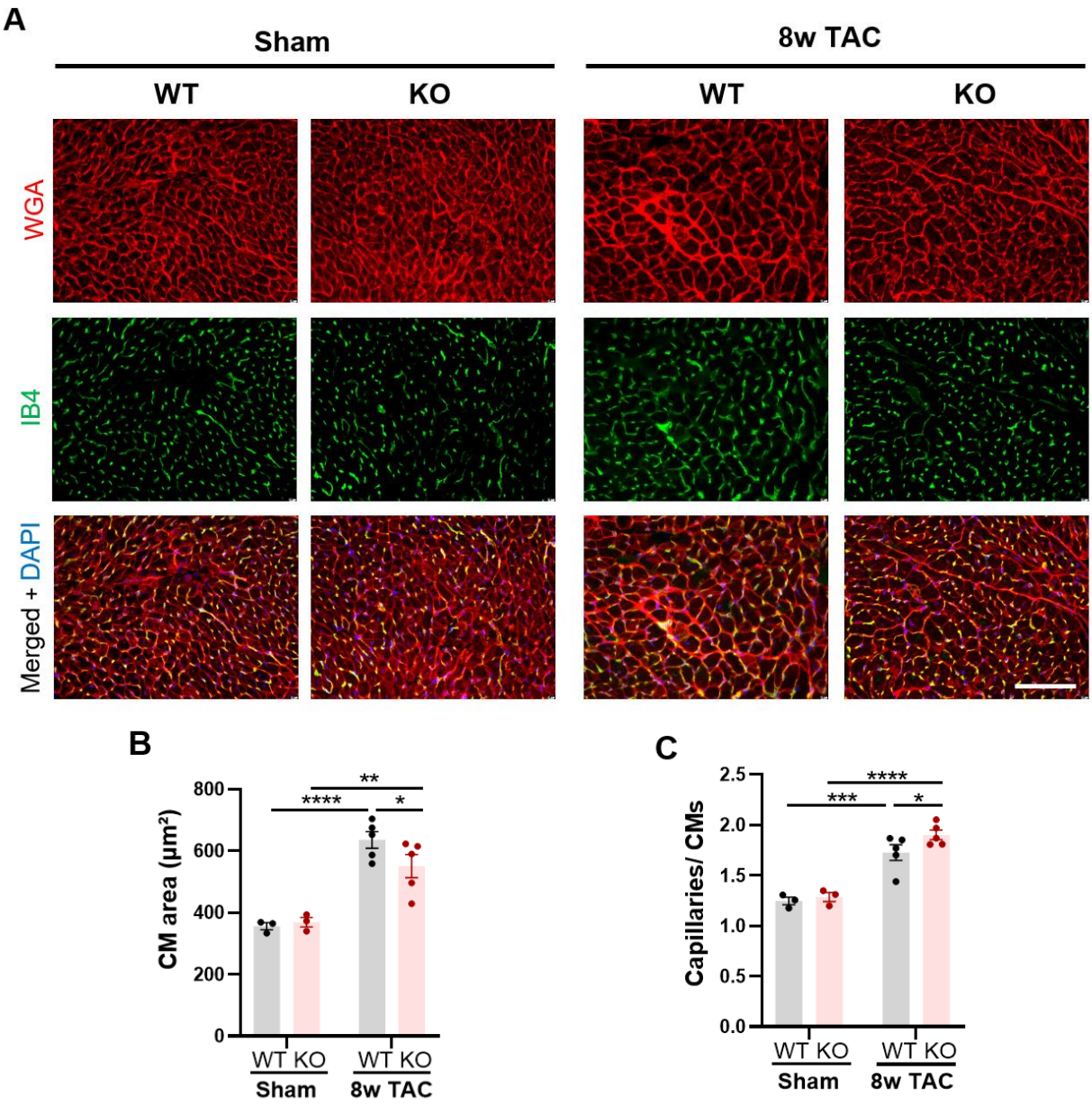

Figure 37: *Gadlor*-KO mice showed less cardiac hypertrophy and higher angiogenesis after persisting log-term pressure overload.

A. Representative immunofluorescence images of cardiac tissue samples stained with WGA (wheat-germ agglutinin coupled with Alexa Fluor 555) and IB4 (Isolectin B4 coupled with Alexa Fluor 488) in sham (n=3) and 8-week TAC (n=5) samples from *Gadlor*-KO and WT littermates, scale-bar: 100 µm. Quantification of **B.** cardiomyocyte cross-sectional area and **C.** myocardial capillary density per cardiomyocyte ratio. *Data are shown as mean±SEM. Data normality was evaluated with Shapiro-Wilk test and p-values were calculated with two-way ANOVA for grouped analysis followed with Fisher's LSD post-hoc test. *p-value<0.05, **p-value<0.01, ***p-value<0.001, ****p-value<0.0001.*

There was no difference observed between age-comparable sham groups from WT and *Gadlor*-KO mice. In addition, less fibrosis development was observed after persistent pressure overload in *Gadlor*-KO mice compared to WT littermates which was depicted by Picro-Sirius red staining (approx. 1.5-fold vs. 4-fold increase KO vs. WT, $p<0.05$, $n\geq6$) **(Figure 38)**.

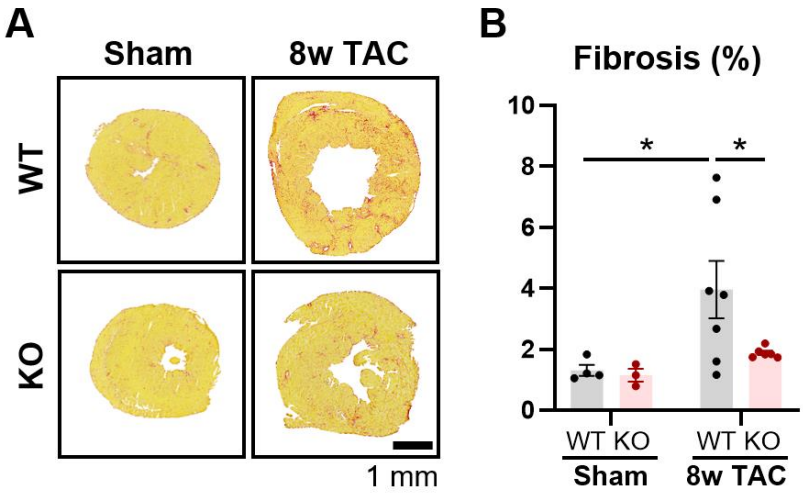

Figure 38: Deletion of *Gadlor* lncRNAs protected against fibrosis development after 8-week TAC.

Representative Sirius-red fibrosis staining in cardiac tissue sections of sham ($n\geq3$) and 8-week TAC ($n\geq6$) mice (scale-bar: 1 mm) and **B.** quantification of fibrotic area (%). *Data are shown as mean±SEM. Data normality was evaluated with Shapiro-Wilk test and p-values were calculated two-way ANOVA for grouped analysis followed with Fisher's LSD post-hoc test. *p-value<0.05.*

Despite retaining better systolic function and improved remodelling features, a considerably higher mortality rate was observed in *Gadlor*-KO mice starting around two and three weeks after TAC as shown in the probability of survival curves in **Figure 39**. Interestingly, WT and *Gadlor*-KO animals were indistinguishable in terms of appearance, behaviour and mobility after TAC operation, and death in *Gadlor*-KO mice was unexpected and sudden in nature, possibly due to cardiac arrhythmia.

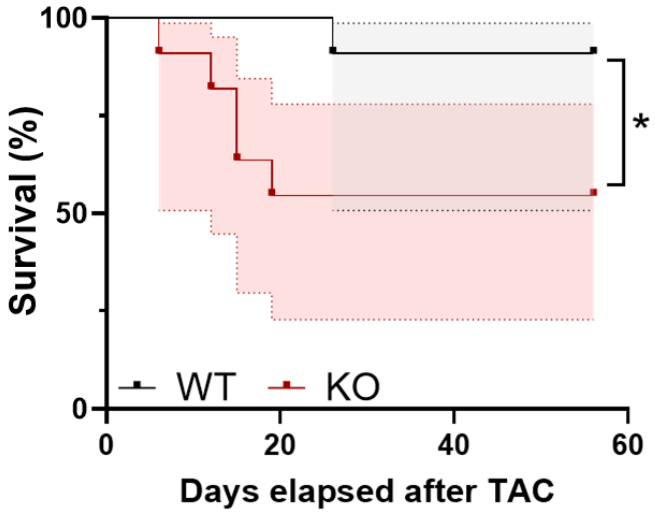

Figure 39: *Gadlor*-KO mice higher mortality despite retaining better cardiac function.

Survival curves of *Gadlor*-KO (red) and WT (black) mice after TAC (n=11) with error bars of 95% confidence interval (95% CI) indicated as filled area. *x-axis* showing the percentage of survival (%) and *y-axis* showing the days elapsed after TAC operation. Probability of survival compared with log-rank test (Mantel-Cox test), *p-value*=0.0467.

10.9. *Gadlor1* and *Gadlor2* affect gene-expression and angiogenic function in ECs

Since ECs are the main cardiac cell type expressing *Gadlor1* and *Gadlor2* and a substantial increase in myocardial capillarization after pressure overload was observed in *Gadlor*-KO mice, transcriptome analysis with bulk RNA sequencing (RNAseq) was performed with isolated cardiac ECs after 2 weeks of TAC. The purity of EC in MACS-based isolation procedure is >90% as shown in a previou publications by our group.[136]

Genome-wide transcriptome analysis identified a total of 3355 differentially expressed (DE) genes between WT and *Gadlor*-KO, which are shown in the heatmap in **Figure 40A**. Gene ontology (GO) analysis from DE genes, which are shown in the bar plots in **Figure 40B**, revealed an upregulation of angiogenesis, mitotic cell-cycle and respiratory electron transport-related genes and downregulation of inflammatory response genes in *Gadlor*-KO ECs after 2-weeks of TAC.

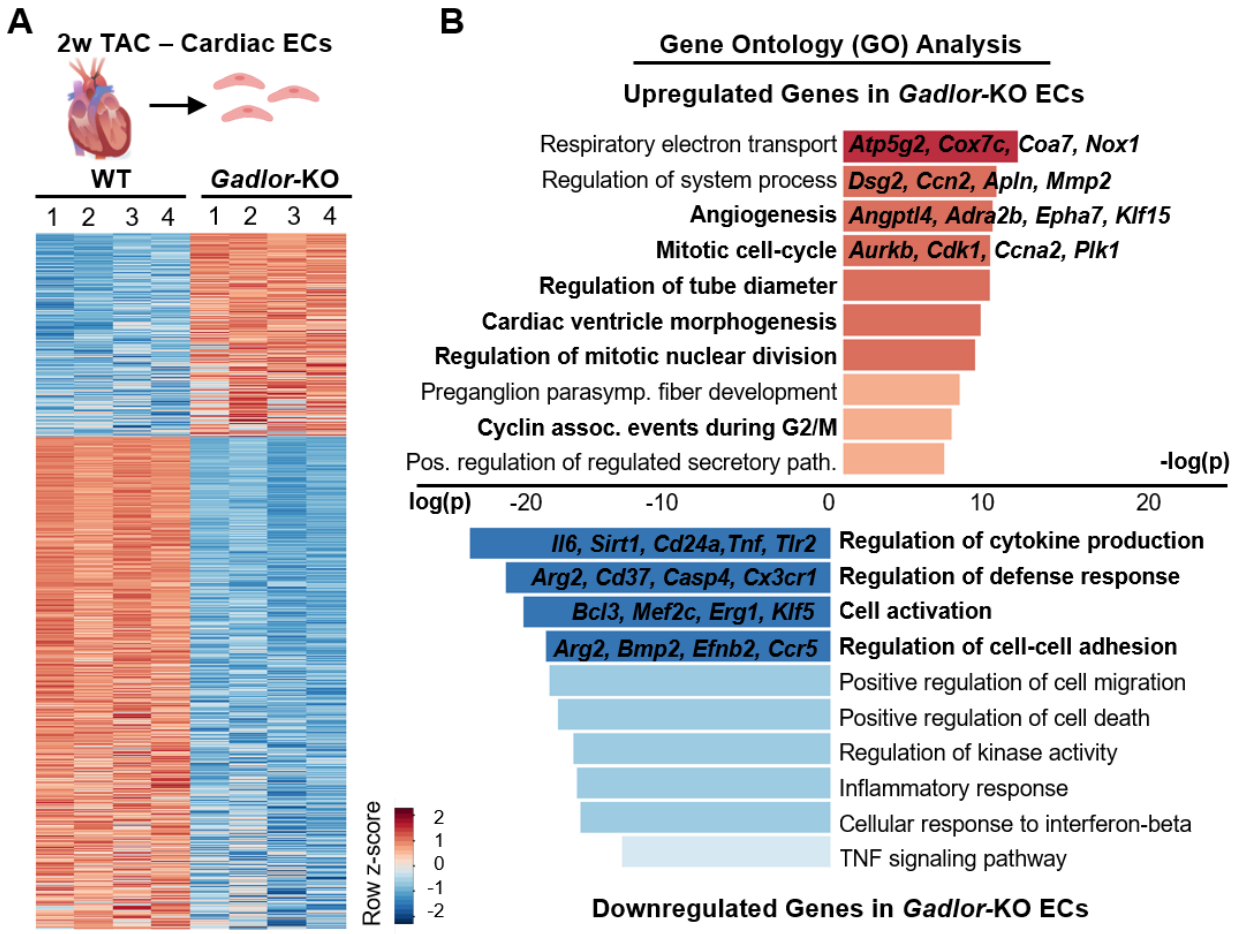

Figure 40: Genome-wide transcriptome analysis of bulk-RNA sequencing from *Gadlor*-KO cardiac endothelial cells after 2-week TAC.

A. Heatmap showing differentially regulated genes revealed by bulk RNAseq of cardiac endothelial-cells after 2-weeks TAC. **B.** Bar plots showing the gene-ontology (GO) analysis of upregulated and downregulated genes in *Gadlor*-KO ECs compared to WT ECs after 2-weeks TAC (Red: Upregulated in *Gadlor*-KO, Blue: Downregulated in *Gadlor*-KO). Some exemplary genes were listed for selected GO-terms. Genes were filtered with set thresholds of False Discovery Rate (FDR<0.05) and fold-change 0.75 ≤ FC and FC > 1.5.

The upregulation and downregulation of selected genes from RNAseq data such as *Angptl4, Klf15, Aurkb, Cdk1* and *Tlr9, Cxcl2, Icam5, Sirt1* RNAs were confirmed by qRT-PCR, respectively, in *Gadlor*-KO and WT ECs isolated after pressure overload **(Figure 41)**.

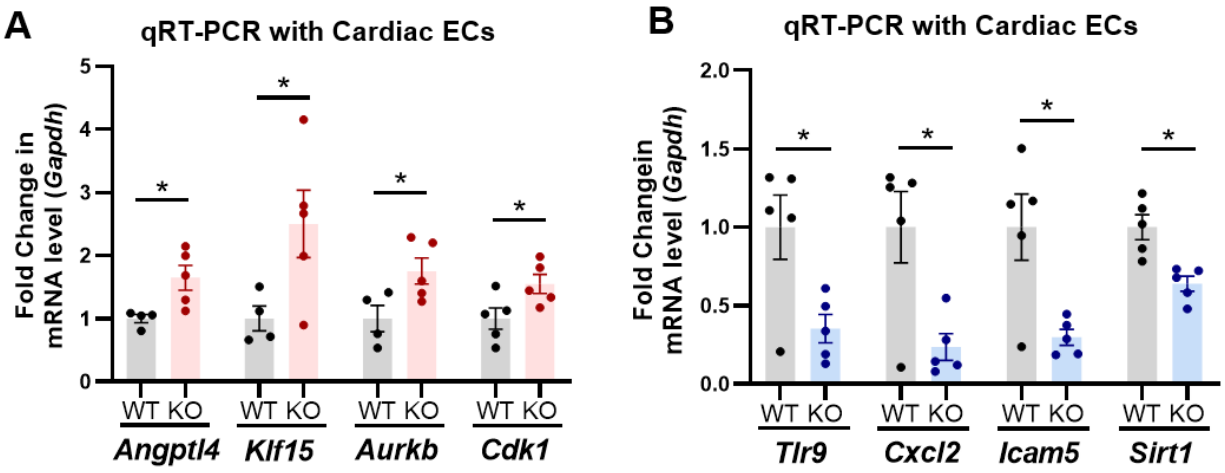

Figure 41: Validation of selected genes from RNAseq of cardiac ECs with qRT-PCR.

A-B. Validation of selected genes from RNAseq data with qRT-PCR in isolated cardiac ECs after 2 weeks of TAC (Red: Upregulated in Gadlor-KO, Blue: Downregulated in Gadlor-KO). *Data are shown as mean±SEM. Data normality was evaluated with Shapiro-Wilk test and p-values were calculated with Student's t-test for comparing two groups. *p-value<0.05.*

Based on the transcriptome analysis to investigate the effects of *Gadlor* lncRNAs in the mitotic cell cycle and proliferation, heart tissue samples were stained with IB4 for endothelial cells and Ki67 as a proliferation marker **(Figure 42A)**, which is expressed in all stages of cell cycle except G0 quiescent phase.[137] A significantly higher number of Ki67-positive ECs was observed in heart sections of *Gadlor*-KO mice after 2 weeks of TAC compared to WT littermates **(Figure 42B)**.

Additionally, the role of *Gadlor* lncRNAs in angiogenesis was assessed with an *in-vitro* sprouting assay performed with C166 mouse ECs **(Figure 43)**. Both *Gadlor1* and *Gadlor2* were overexpressed with adenovirus as a gain-of-function approach and compared with Ad.β*gal* treated samples as a control in basal and stimulated conditions. Collagen-embedded spheroids were used to determine formation of tubular structures.

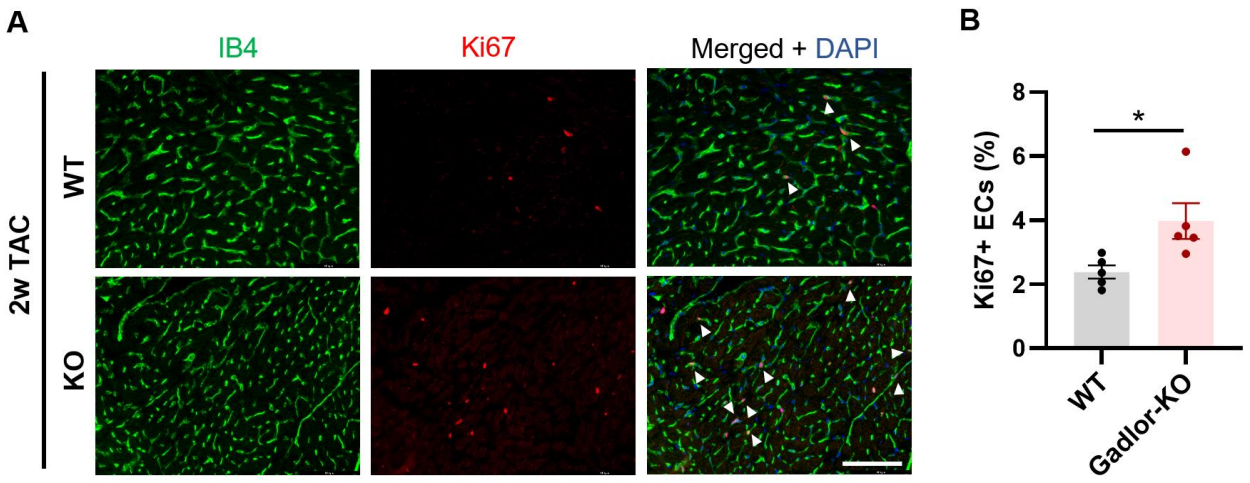

Figure 42: *Gadlor*-KO mice exhibited higher number of Ki67 positive endothelial-cells after TAC.

A. Representative immunofluorescence images of cardiac tissue samples stained with IB4 (Isolectin B4 coupled with Alexa Fluor 488) and Ki67 (coupled with Alexa Fluor 555) in 2-week TAC samples from *Gadlor*-KO and WT littermates, Scale bar: 100 µm. (Arrows showing Ki67+ ECs) **B.** Quantification of Ki67 positive endothelial-cells percentage (Ki67+ ECs%). *Data are shown as mean±SEM. Data normality was evaluated with Shapiro-Wilk test and p-values were calculated with Student's t-test for comparing two groups. *p-value<0.05.*

Spheroid outgrowth was investigated with or without the addition of FGF2 and TGFβ as stimulants **(Figure 43)**. There was no difference observed in basal endothelial cell sprouting length and the average number of sprouts in control and *Gadlor1/2* overexpressing ECs. All formed spheroids were continuous, but not disturbed (discontinuous). FGF2 increased angiogenic sprouting and the number of sprouts in Ad.β*gal* controls, but not in *Gadlor1/2* overexpressing cells, which was shown by almost no change in the average length of sprouts per spheroid, although the number of sprouts slightly increased **(Figure 43B)**. Furthermore, TGFβ decreased sprouting in control cells, and this response was more pronounced upon adenoviral *Gadlor1/2* overexpression. Overall, *Gadlor1* and *Gadlor2* lncRNAs exhibit anti-angiogenic properties in ECs.

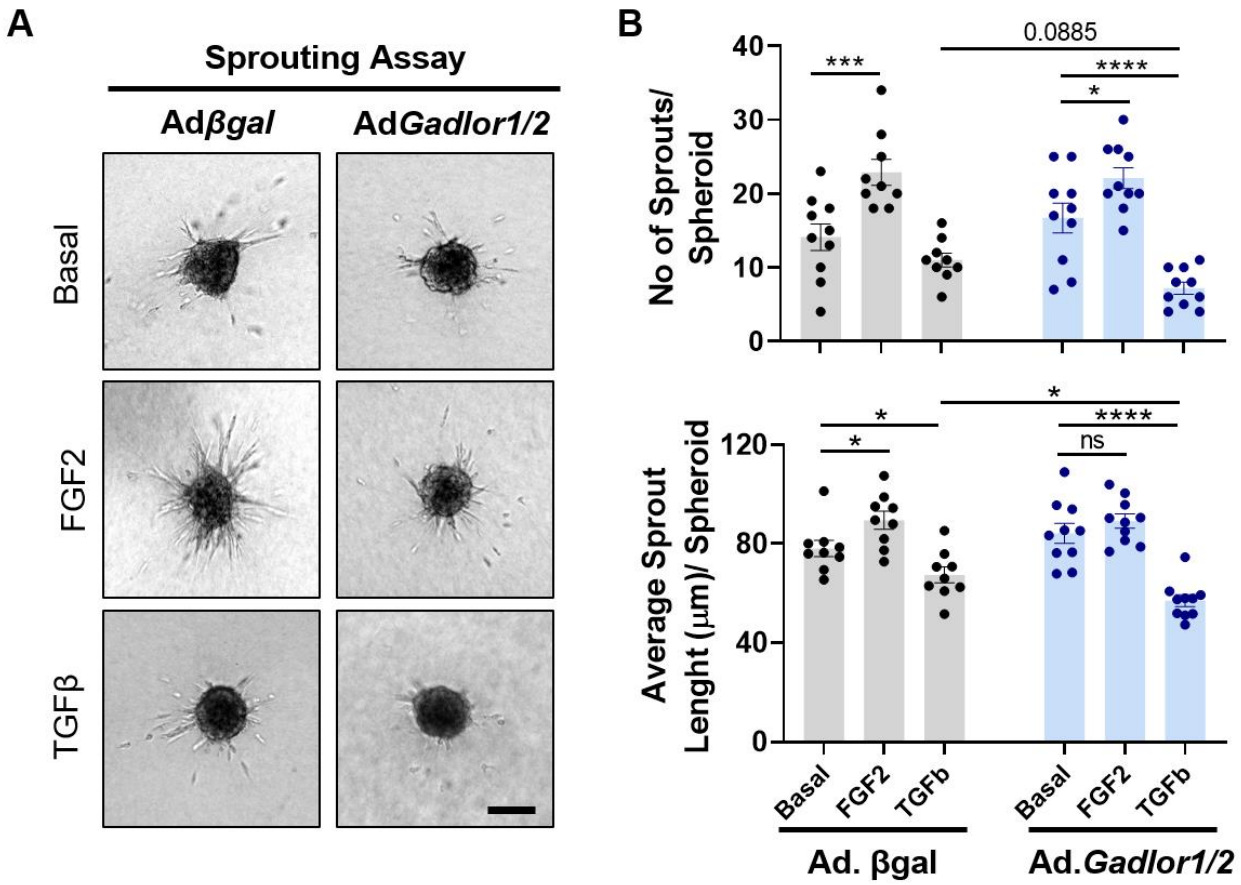

Figure 43: *Gadlor1* and *Gadlor2* overexpression affects the angiogenesis capacity of ECs.

A. Representative images of sprouting assay with C166 mouse ECs after adenovirus treatment (Ad*βgal* and Ad*Gadlor1/2*) followed by 24-hour FGF2 and TGFβ treatment. 3-dimentional (3D) collagen matrix embedded spheroids were allowed to form sprouts for 24 hours. Scale bar: 100 µm. **B.** Quantification of average number and length of sprouts per each spheroid. *Data are shown as mean±SEM. For grouped analysis, p-values were evaluated with two-way ANOVA followed with Fisher's LSD post-doc test. *p-value<0.05, **p-value<0.01, ***p-value<0.001, ****p-value<0.0001.*

According to gene ontology analysis, cytokine production, defence and inflammatory response-related genes were downregulated in *Gadlor*-KO cardiac ECs compared to WT ECs after TAC. To understand this further, staining with leukocyte common antigen (LCA, CD45) was performed with WGA on heart tissue sections collected after sham and 2 weeks of TAC **(Figure 44A).** The number of CD45 positive cells was quantified per high power field (HPF) and a significant increase was observed after TAC in both WT and *Gadlor*-KO hearts at a similar degree, thus no difference was detected after pressure overload **(Figure 44B).**

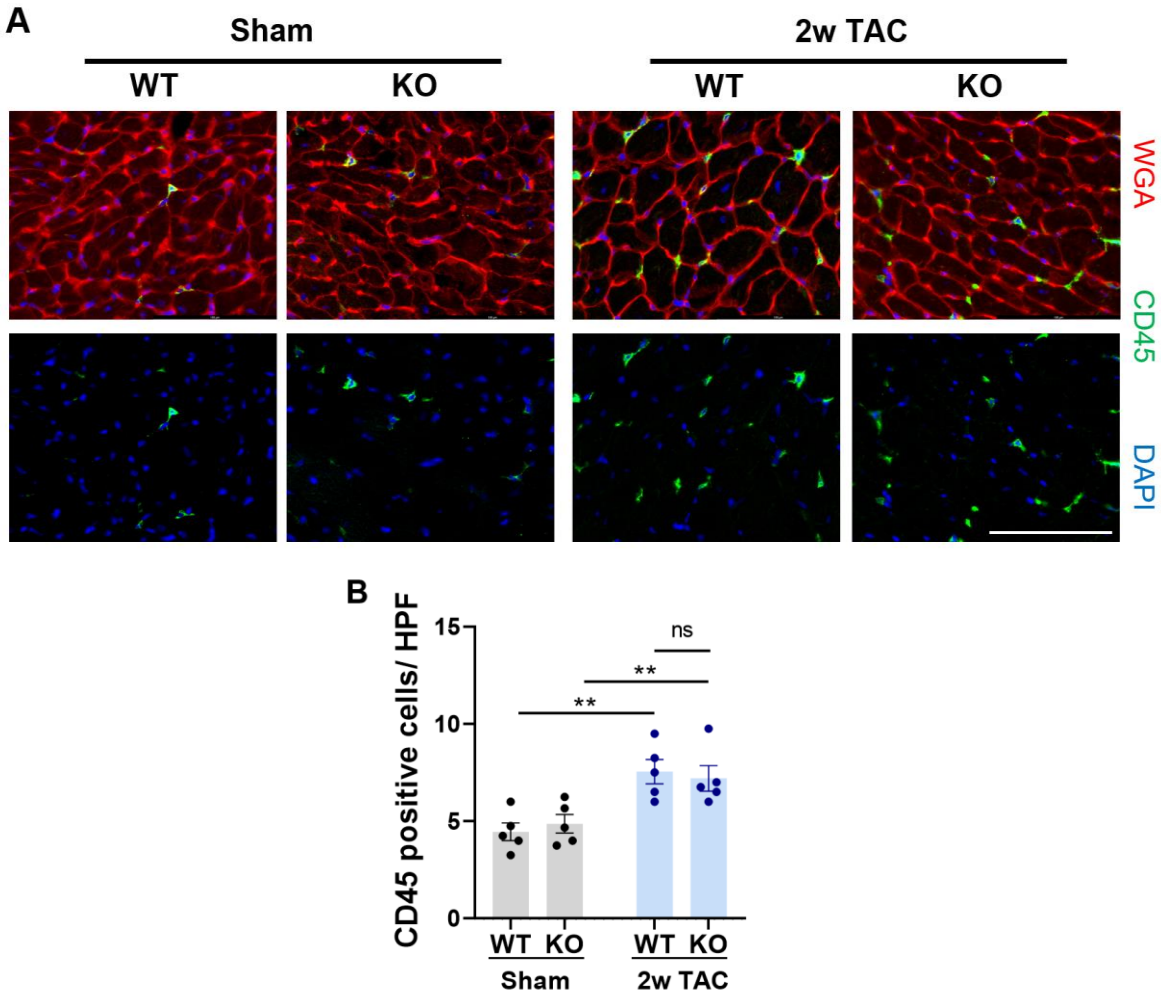

Figure 44: The effect of *Gadlor*-KO in inflammatory response assessed by common leukocyte marker CD45.

A. Representative immunofluorescence images of cardiac tissue samples stained with WGA (wheat-germ agglutinin coupled with Alexa Fluor 555) and leukocyte common antigen CD45 (coupled with Alexa Fluor 488) in sham and 2-weeks of TAC samples from *Gadlor*-KO and WT littermates, scale-bar: 100 µm. **B.** Quantification of CD45 positive cells per high power field (HPF) as images were taken by 40x objective. *Data are shown as mean±SEM. Data normality was evaluated with Shapiro-Wilk test and p-values were calculated with two-way ANOVA for grouped analysis followed with Fisher's LSD post-hoc test. **p-value<0.01*

10.10. *Gadlor*-KO cardiac FBs showed less induction of fibrosis-associated genes after TAC

Cellular expression analysis of *Gadlor1* and *Gadlor2* showed cardiac FBs have the second highest *Gadlor* lncRNA expression after cardiac ECs. To study the FB-specific changes in gene expression

upon *Gadlor1/2* deletion, bulk RNAseq from isolated cardiac FBs was performed after 2-weeks of TAC. The purity of cardiac FBs in MACS-based isolation procedure is >90% as shown in a previous study of our group.[136]

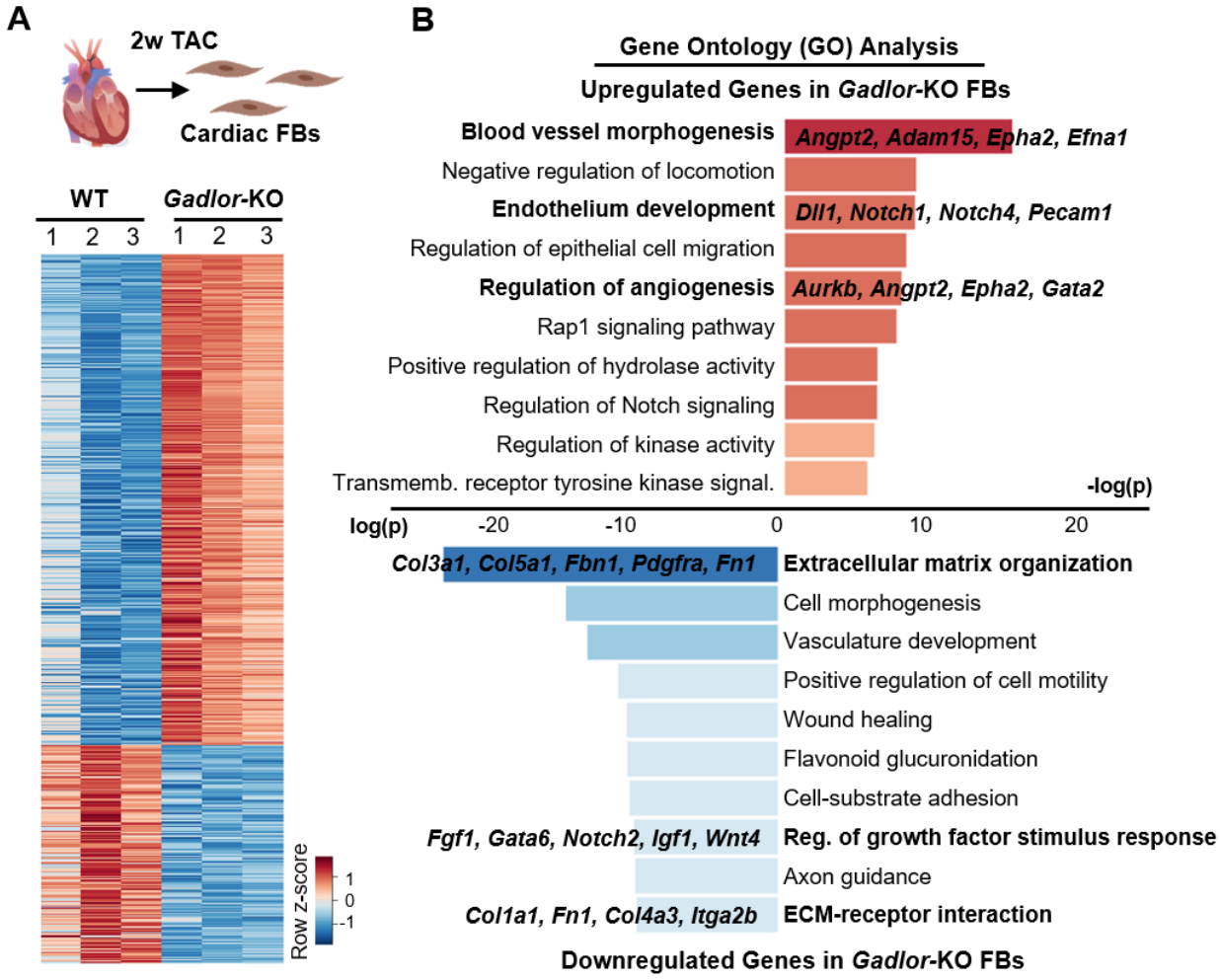

Figure 45: RNA sequencing of *Gadlor*-KO cardiac FBs showed less induction of fibrosis-associated genes after TAC.

A. Heatmap showing differentially regulated genes analysed after bulk RNAseq of isolated cardiac fibroblasts after 2-weeks TAC. **B.** Bar plots showing the gene-ontology (GO) analysis of upregulated and downregulated genes in *Gadlor*-KO FBs after 2-weeks TAC (Red: Upregulated in *Gadlor*-KO, Blue: Downregulated in *Gadlor*-KO). Some exemplary genes were listed for selected GO-terms. Genes were filtered with set thresholds of False Discovery Rate (FDR<0.05) and fold-change 0.75 ≤ FC and FC > 1.5.

Genome-wide analysis revealed a total of 915 downregulated and 998 upregulated genes in *Gadlor*-KO cardiac FBs compared to WT cardiac FBs after TAC, which are shown in a heatmap **(Figure 45A)**. Gene ontology analysis of differentially expressed genes revealed a strong downregulation of mainly extracellular matrix (ECM) organization and receptor interaction-associated genes **(Figure 45B)**. Amongst these, downregulation of *Fgfr1, Igf1, Col1a1, Col3a1* and *Col6a1* mRNA expression was confirmed with qRT-PCR **(Figure 46)**. Additionally, genes related to the regulation of angiogenesis, blood vessel and endothelium development were upregulated in *Gadlor*-KO FBs **(Figure 45B)**, which suggested a contribution of FBs for vessel development and angiogenesis previously observed in *Gadlor*-KO ECs upon overload **(Figure 40)**. The increased expression of *Angpt2, Efna1, Aurkb* and *Dll1* in cardiac FBs from *Gadlor*-KO mice was also confirmed by RT-qPCR **(Figure 46)**.

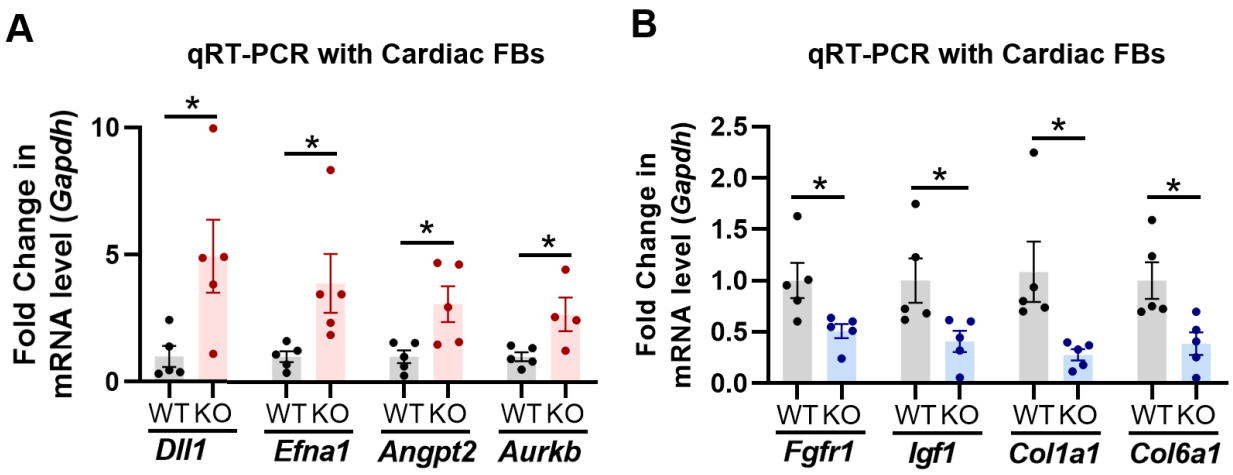

Figure 46: Validation of selected genes from RNAseq of cardiac FBs with qRT-PCR.

A-B. Validation of selected genes from RNAseq data with qRT-PCR in isolated cardiac FBs after 2 weeks of TAC (Red: Upregulated in *Gadlor*-KO, Blue: Downregulated in *Gadlor*-KO). *Data are shown as mean±SEM. Data normality was evaluated with Shapiro-Wilk test and p-values were calculated with Student's t-test for comparing two group. *p-value<0.05.*

Furthermore, as a gain-of-function approach upon adenoviral overexpression of *Gadlor1* and *Gadlor2* followed with phenylephrine (PE) stimulation, neonatal rat cardiac fibroblasts (NRFB)

showed a decreased expression of *Angpt2* and an increased expression of *Col1a1* and *Col3a1*, but no change in the expression of *Col4a1* or *Col6a1* was observed **(Figure 47)**. These results confirmed that *Gadlor* lncRNAs trigger pro-fibrotic gene expression in cardiac FBs upon stress.

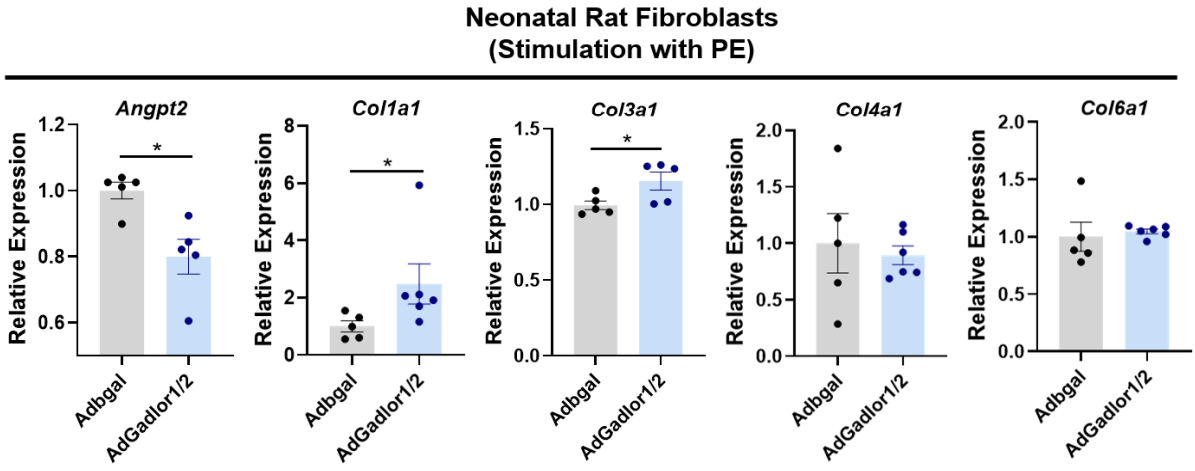

Figure 47: *Gadlor1* and *Gadlor2* overexpression triggered pro-fibrotic gene expression in FBs upon stress stimulus.

qRT-PCR of selected genes in neonatal rat fibroblasts (NRFB) overexpressing *Gadlor* lncRNAs after *Gadlor1/2* adenovirus treatment (βgal as control) followed by phenylephrine (PE) stimulation (100 µM, 24 hours). *Data are shown as mean±SEM. Data normality was evaluated with Shapiro-Wilk test and p-values were calculated with Student's t-test for parametric and Mann-Whitney test for non-parametric assessment. *p-value<0.05.*

10.11. *Gadlor* lncRNAs are transferred to cardiomyocytes via EC-derived EVs

Since *Gadlor1* and *Gadlor2* were mainly secreted from cardiac ECs, the possibility of a paracrine effect of *Gadlor* lncRNAs on different cardiac cells via EV-mediated transfer was investigated. To analyse whether *Gadlor* lncRNAs were transferred from cardiac ECs to CMs and/or FBs, EVs were collected from the supernatant of *Gadlor1* and *Gadlor2* overexpressing C166 mouse ECs with ultracentrifugation **(Figure 48A)**. The enhancement of *Gadlor1/2* expression in EVs after adenovirus treatment (*Gadlor*-EV) was confirmed compared to control (Adβgal) EVs (Control-EV) **(Figure 48B)**. The collected EVs were transferred to neonatal rat cardiomyocytes (NRCMs) or fibroblasts (NRFBs), separately.

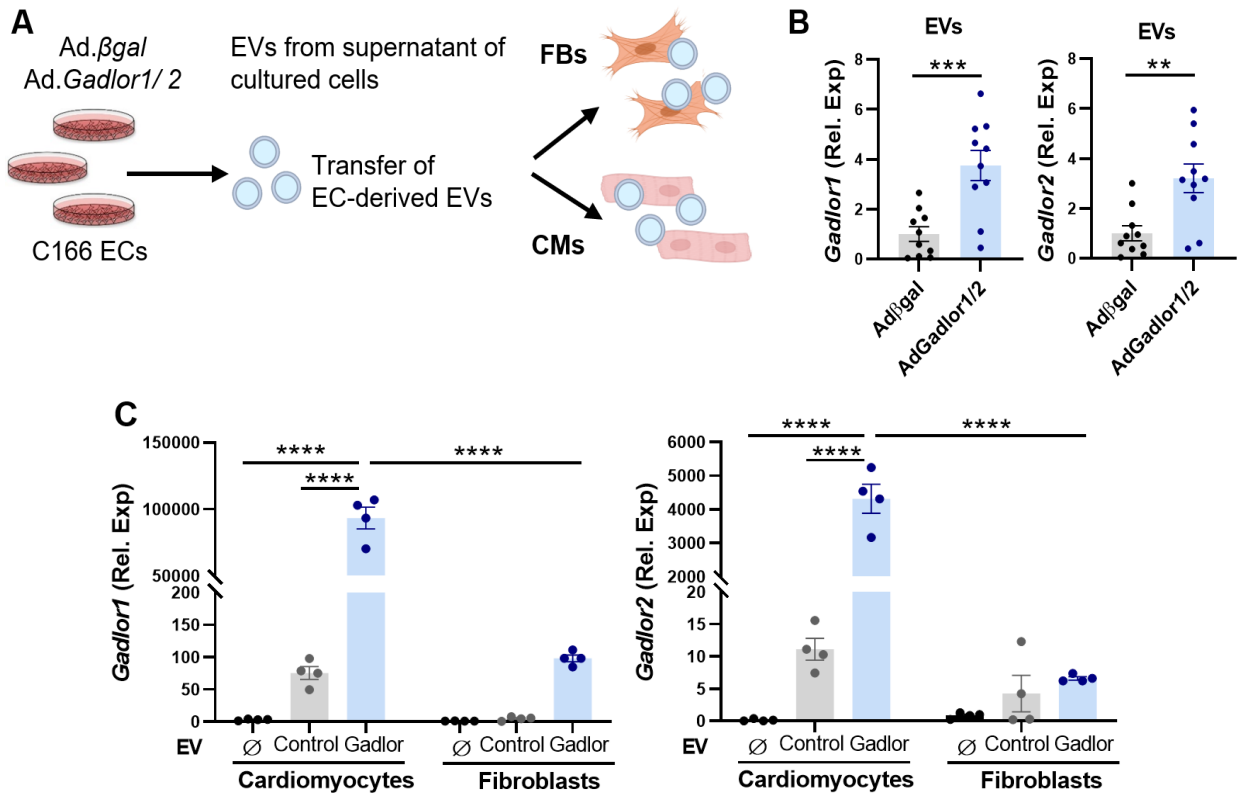

Figure 48: Transfer of *Gadlor1* and *Gadlor2* containing extracellular vesicles (EVs) to FB and CMs.

A. Schematic representation of experimental design which EVs isolated from C166 supernatant was transferred to NRCMs and NRFBs, separately. **B.** Validation of *Gadlor1* and *Gadlor2* overexpression in isolated EVs. **C.** RT-qPCR detection of *Gadlor1* and *Gadlor2* after transferring control EVs (Ad*βgal* treated) and *Gadlor*-EVs (Ad*Gadlor1/* 2 treated) isolated from C166 mouse ECs into neonatal rat cardiomyocytes (NRCMs) or into neonatal rat fibroblasts (NRFBs). The samples were collected after 6 hours of EV-containing media incubation. *Data are shown as mean±SEM. Data normality was evaluated with Shapiro-Wilk test and p-values were calculated with Student's t-*test. *Two-way ANOVA with Fisher's LSD post-hoc test was applied for grouped analysis when applicable. *p-value<0.05, **p-value<0.01, ***p-value<0.001, ****p-value<0.0001. Illustration is created by using www.biorender.com.*

RT-qPCR analysis showed a significantly higher abundance of *Gadlor1/2* in NRCMs incubated with *Gadlor*-EVs compared to samples incubated with control-EVs or cardiomyocytes without any EV treatment, which indicated that EVs were taken up by CMs **(Figure 48C)**. *Gadlor* lncRNAs were also transferred from ECs to cardiomyocytes by control-EVs, since higher cardiomyocyte *Gadlor1/2* levels were observed after control-EV compared to non-EV treatment NRCMs.

Additionally, a mild increase in both *Gadlor1* and *Gadlor2* abundance was also observed in NRFBs after incubation with *Gadlor*-EVs, however, at a much lower degree compared to NRCM **(Figure 48C)**. The uptake of EVs into the recipient cardiomyocytes was visualised by fluorescent labelling with PKH67 dye, which was analysed with confocal microscopy after EV-incubation of 6 hours and 24 hours with NRCMs **(Figure 49)**. Additionally, 3D imaging by confocal Z-stacks confirmed that EVs were internalized into the recipient cardiomyocytes rather than being attached to the surface **(Figure 49C).**

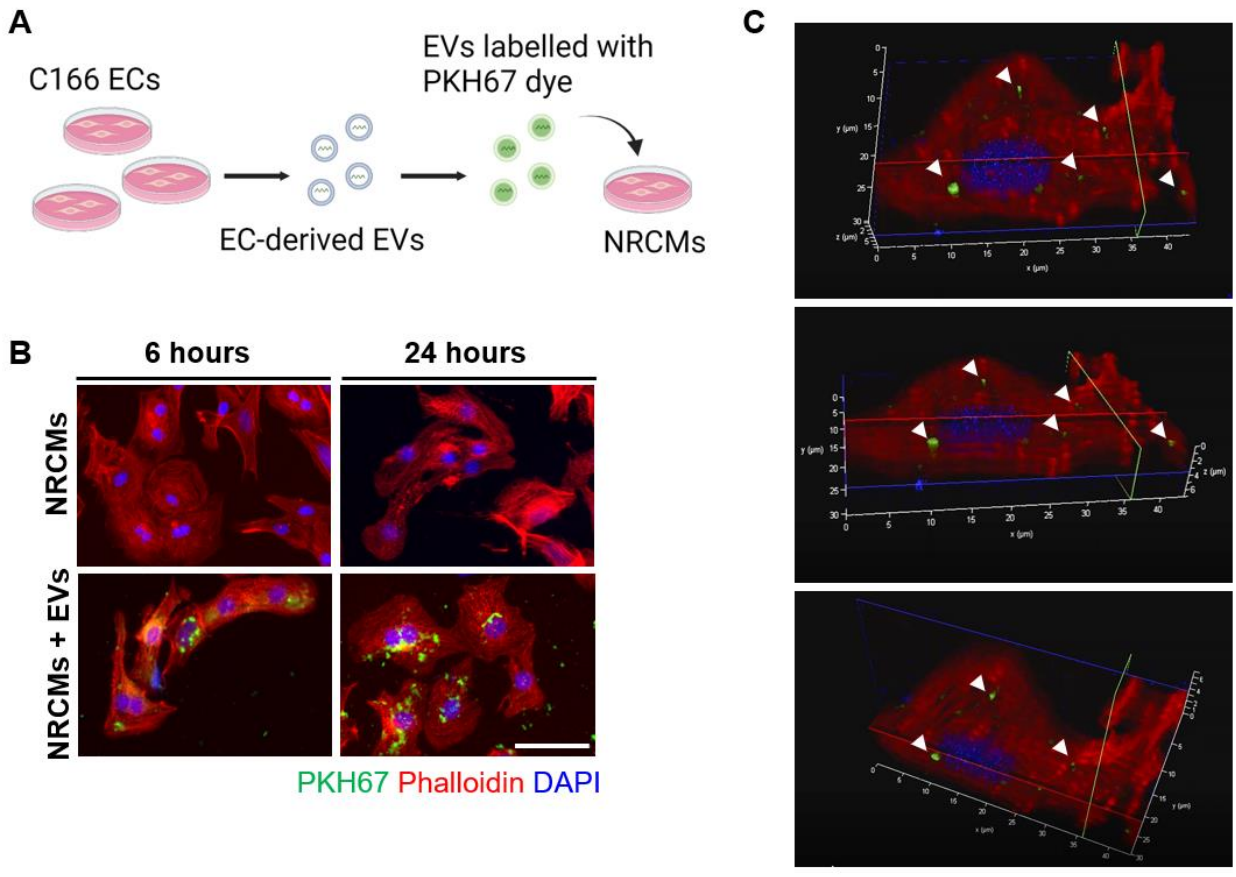

Figure 49: Transfer and visualization of fluorescently labelled EVs.

A. Schematic representation of experimental design for isolation of EVs from ECs and fluorescent labelling with PKH67 lipid dye. **B.** Visualization of NRCMs that were incubated with PKH67-labelled (green) EVs isolated from C166 ECs for 6 hours and 24 hours. **C.** Confocal frames of a NRCM showing internalized EVs at 0°, 90° and 270° recorded in the clockwise direction. Staining was performed with Phalloidin (red) and DAPI (blue). Scale bar: 50 µm. *Illustration is created by using www.biorender.com.*

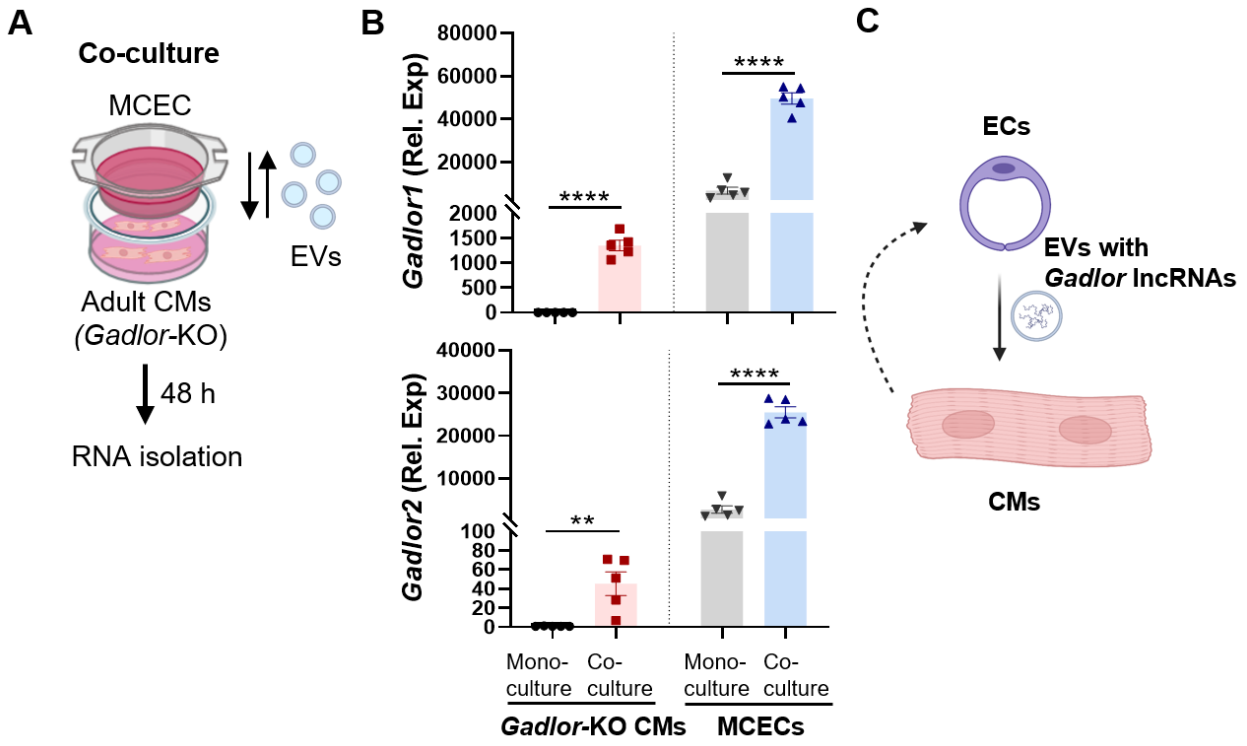

Figure 50: Secreted *Gadlor* lncRNAs are transferred to cardiomyocytes via endothelial-derived EVs.

A. Scheme of co-culture experiment with transwell (1 µm – allows EV transfer). MCEC on top cultured with *Gadlor*-KO CMs in the bottom well without direct cell contact. **B.** RT-qPCR detection of *Gadlor1* and *Gadlor2* in isolated *Gadlor*-KO CMs and MCEC mouse ECs after 48 hours of mono-culture and co-culture state. **C.** Proposed crosstalk between endothelial cells (ECs) and cardiomyocytes (CMs) via *Gadlor1/2* lncRNA containing EVs. *Data are shown as mean±SEM. Data normality was evaluated with Shapiro-Wilk test and p-values were calculated with Student's t-test or one-way ANOVA with Fisher's LSD post-hoc test were applied for comparing two or multiple groups, respectively. Two-way ANOVA with Fisher's LSD post-hoc test was applied for grouped analysis when applicable. **p-value<0.01, ****p-value<0.0001. Illustration is created by using www.biorender.com.*

To further confirm the transfer of EVs to CMs and study the possible effects in contraction, hypertrophy and arrhythmia, co-culture experiments with isolated *Gadlor*-KO CMs, which are lacking the endogenous *Gadlor1* and *Gadlor2* expression, and wild-type mouse cardiac endothelial cells (MCEC) was performed in transwell culture system without direct cell contact **(Figure 50A)**. *Gadlor*-KO cardiomyocytes were used to exclude confounding effects of

endogenous *Gadlor1/2* expression with exogenous *Gadlor1/2* uptake from EC-derived EVs. As expected, there was no *Gadlor1/2* expression in isolated *Gadlor*-KO CMs when they were kept in monoculture, whereas both *Gadlor1* and *Gadlor2* were detectable in *Gadlor*-KO CMs after co-culture with MCECs **(Figure 50B)**.

These results suggested that *Gadlor1/2* were transferred into *Gadlor*-KO CMs from MCECs via EV-mediated cell-to-cell transfer. Notably, MCECs that were co-cultured with *Gadlor*-KO CMs were also increasing their expression of *Gadlor*1/2, which might suggest a possible feedback mechanism between CMs and ECs **(Figure 50C)**.

Next, to determine the localization of *Gadlor* lncRNAs after they were taken up by the recipient cardiomyocytes (NRCMs), sub-cellular fractionation was performed **(Figure 51)**.

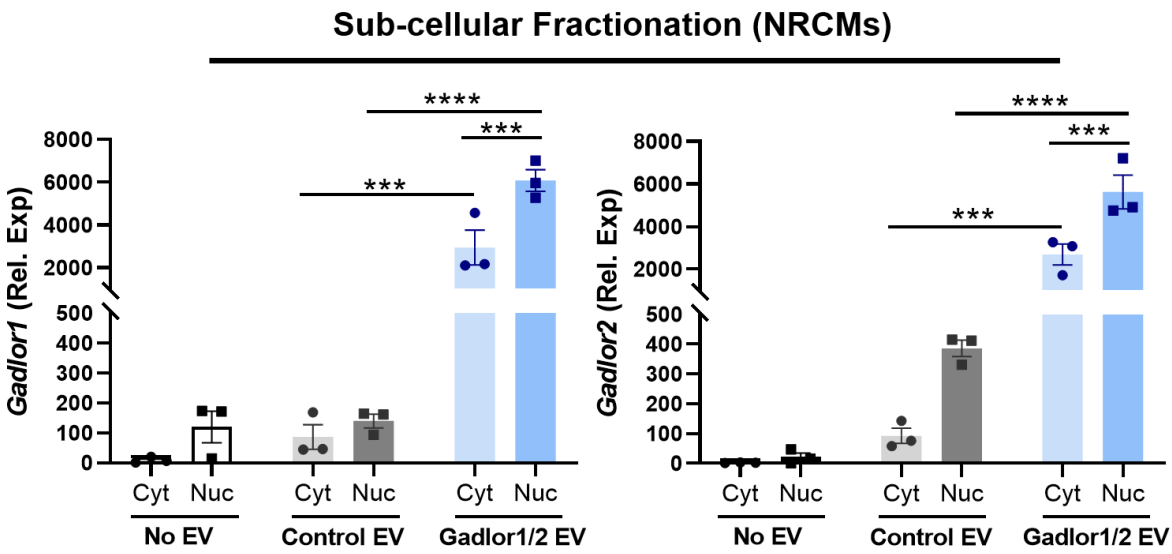

Figure 51: Sub-cellular localization of *Gadlor1* and *Gadlor2* in the recipient NRCMs.

Gadlor1 and *Gadlor2* expression in the cytosol and nucleus of the recipient neonatal rat cardiomyocytes (NRCMs) after they were taken up. Samples were treated with no EV, control EV (Adβgal) and *Gadlor* EV (Ad*Gadlor1* and Ad*Gadlor2* used for overexpression) and then fractionated to cytosol and nuclear associated fragments. *Data are shown as mean±SEM. Data normality was evaluated with Shapiro-Wilk test and p-values were calculated with one-way ANOVA with Fisher's LSD post-hoc test were applied for comparing multiple groups, respectively. ***p-value<0.001, ****p-value<0.0001.*

Gadlor1 and *Gadlor2* expression was compared with qRT-PCR in cytosol and nucleus fractions. *Gadlor* lncRNAs were detected both in the cytosol and even higher levels in the nucleus of the recipient cardiomyocytes, which might suggest a possible multi-functional effect of *Gadlor1* and *Gadlor2* based on where they are localized in the cell during different pathophysiological conditions.

10.12. *Gadlor* lncRNAs bind to calcium/calmodulin-dependent protein kinase type II - subunit delta in cardiomyocytes

As shown in recent studies lncRNAs can interact with proteins to affect their regulatory functions.[118] Even though CMs showed the least endogenous levels of *Gadlor* lncRNAs, still a strong effect was observed in CMs after *Gadlor1/2* deletion upon pressure overload. To decipher this further, the binding partners of *Gadlor1/2* in cardiomyocytes were identified by performing RNA antisense purification coupled with mass-spectrometry (RAP-MS) in HL1 cardiac muscle cells after overexpression of *Gadlor1/2* **(Figure 52)**.

The identified interaction partners were shown in the volcano plot in **Figure 53** as enriched in *Gadlor1/2* overexpressing and crossed-linked samples compared to controls (Adβgal treated) after elimination of unspecific binding, which was identified in the non-crosslinked condition of the samples. The potential interaction partners were filtered as at least 1.2-fold-enrichment in the *Gadlor1/2* crosslinked samples (shown as red dots in the volcano plot in **Figure 53**. Interestingly, calcium/calmodulin-dependent protein kinase type II, subunit delta (CaMKIIδ) as well as the gene-regulatory factor GLYR1 were identified as significant binding partners of *Gadlor1* and *Gadlor2* lncRNAs in cardiomyocytes.

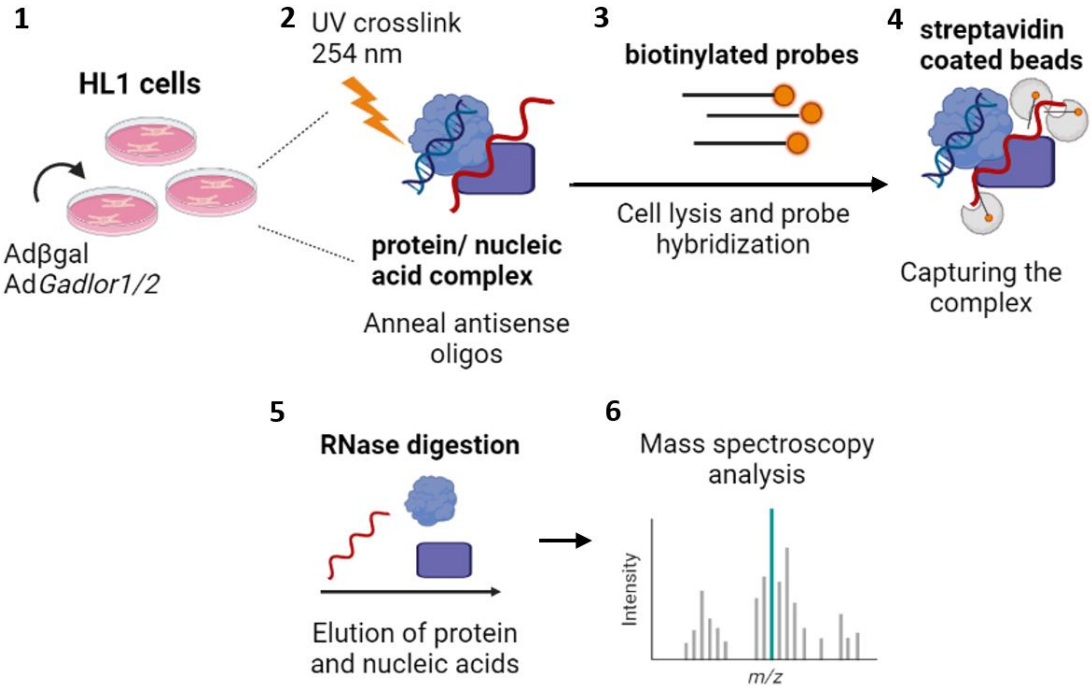

Figure 52: Scheme for RNA-antisense purification coupled with mass-spectrometry (RAP-MS).

Scheme of experimental procedure of RAP-MS in which *Gadlor1* and *Gadlor2* lncRNA-binding proteins were captured and identified in HL1 cardiac muscle cells. **1.** Adenovirus treated *Gadlor1/2* overexpressing HL1 cells were **2.** UV crosslinked to stabilize protein:nucleic acid complex. Next, **3.** hybridization with biotinylated probes were captured with **4.** Streptavidin-coated beads. After **5.** RNase digestion, eluted protein samples were analysed with **6.** mass spectroscopy. *Illustration is created by using www.biorender.com.*

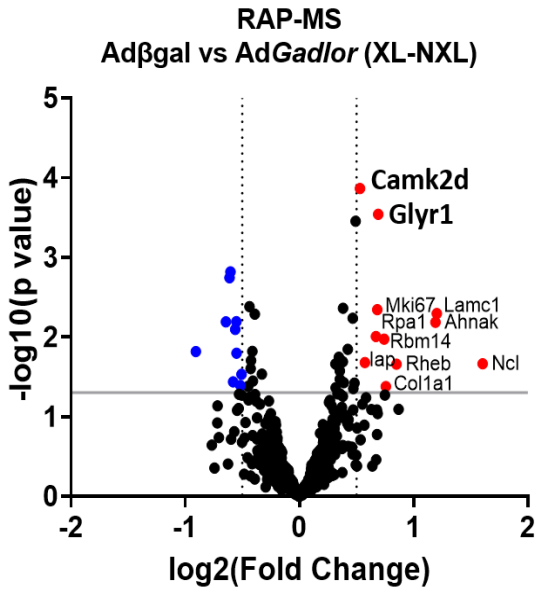

Figure 53: Volcano plot indicating the identified binding partners of *Gadlor1* and *Gadlor2* in cardiomyocytes by RAP-MS.

HL1 cardiomyocytes treated with β*gal* and *Gadlor1/2* adenovirus to identify interaction partners of *Gadlor* lncRNAs (Fold change (FC) threshold 1.2 and p-value < 0.05). UV crosslinking was used to stabilize protein:RNA interactions and non-crosslinked (N-XL) samples were used as background and removed from crosslinked (XL) samples for each indicated condition.

Next, the interaction of CaMKII and GLYR1 with *Gadlor1/2* was validated with native RNA immunoprecipitation (RIP) followed by qRT-PCR. After normalization to the input RNA, a significant enrichment of *Gadlor1* and *Gadlor2* was confirmed after CaMKII **(Figure 54A)** and GLYR1 **(Figure 54B)** IPs versus IP with IgG control.

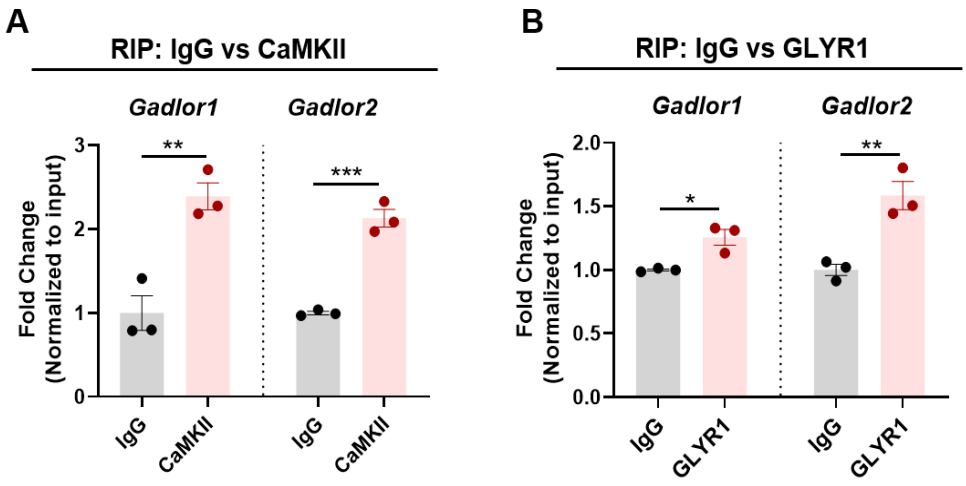

Figure 54: *Gadlor* lncRNAs bind to CaMKII and GLYR1 in cardiomyocytes.

A. RNA immunoprecipitation (RIP) performed with anti-IgG and anti-CaMKII antibodies incubated with HL-1 cardiac muscle cell lysate to validate the interaction of target RNAs. RT-qPCR analysis showing the enrichment of *Gadlor1* and *Gadlor2* compared to IgG controls. **B.** RNA immunoprecipitation (RIP) performed with anti-IgG and anti-GLYR1 antibodies with HL-1 cardiac muscle cell lysate to validate the interaction of target RNAs. RT-qPCR analysis showing the enrichment of Gadlor1 and Gadlor2 compared to IgG controls. *Data normalized to input RNA expression, n=3 for each condition.*

In addition, to decipher the functional impact of the interaction of *Gadlor1* and *Gadlor2* with CaMKII, the phosphorylation of phospholamban (PLN) at the Thr17 by CaMKII in *Gadlor*-KO mice was evaluated after TAC **(Figure 55)**. Phosphorylation of PLN (pThr17-PLN) reverses the inhibition of SERCA2a activity, thus increasing the calcium reuptake by sarcoplasmic reticulum.[44]

Based on western blot analysis, a significant decrease in pThr17-PLN was detected in *Gadlor*-KO heart tissue samples after pressure overload compared to WT littermates **(Figure 55A-B)**. On the

other hand, a substantial increase in pThr17-PLN was confirmed in *Gadlor*-EV-treated heart tissue samples after 2 weeks of TAC **(Figure 56C-D)**. This indicated that *Gadlor1* and *Gadlor2* might promote CaMKII activation in cardiomyocytes, and thus could contribute to cardiac contractility and relaxation via effecting PLN.

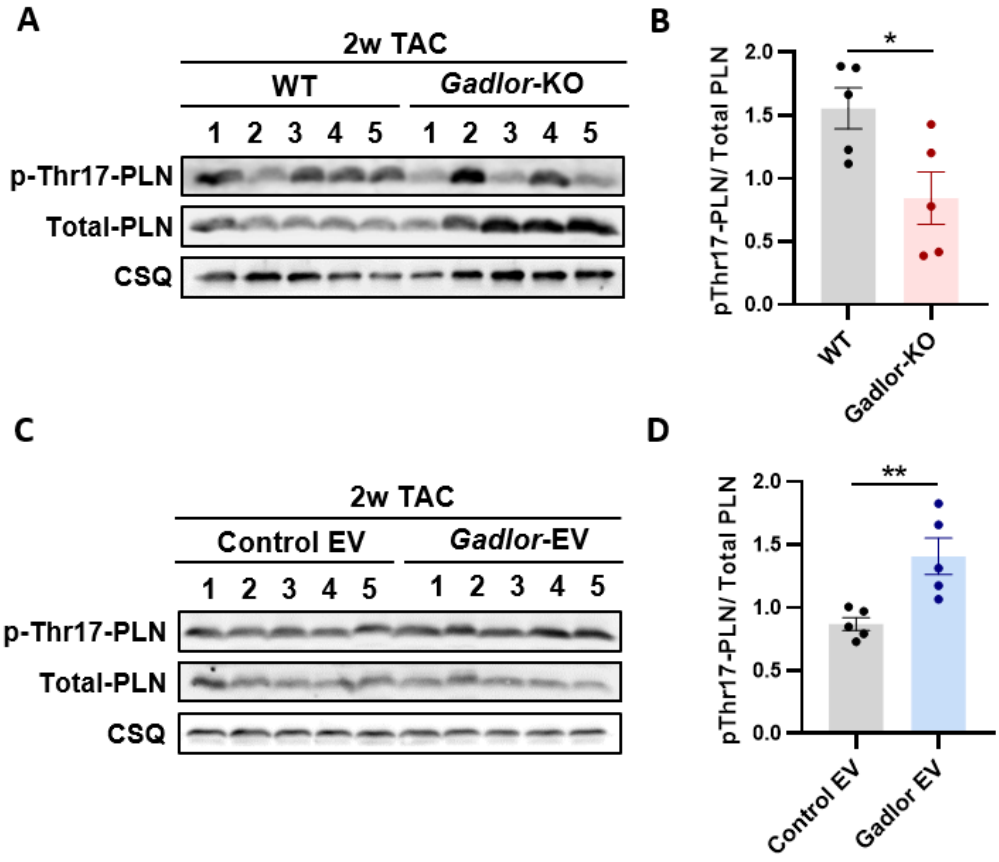

Figure 55: *Gadlor* lncRNAs promote CaMKII activation in cardiomyocytes via contributing pThr17-PLN.

A. Exemplary Western blots of phospho-Thr17-PLN and total PLN with CSQ as loading control in WT and *Gadlor*-KO heart tissue samples after 2 weeks TAC and **B.** quantification of western blots. **C.** Exemplary Western blots of phospho-Thr17-PLN and total PLN with CSQ as loading control in control-EV and *Gadlor*-EV treated mice heart tissue samples after 2 weeks TAC and **D.** quantification of western blots. Data were produced jointly Santosh Lomada, PhD and analysed by myself. *Data are shown as mean±SEM. Data normality was evaluated with Shapiro-Wilk test and p-values were calculated with Student's t-test) for comparing two groups. *p-value<0.05, **p-value<0.01.*

Since CaMKII was identified as a binding partner of *Gadlor* lncRNAs, which has a known role in excitation-contraction coupling, a further investigation of cardiomyocyte contractility and calcium dynamics was studied with the Multicell HT system (Ion-Optix) in isolated adult cardiomyocytes after 1-week of TAC **(Figure 56A)**. Interestingly, the analysis software detected a considerably high number of *Gadlor*-KO CMs with arrhythmic behaviour during the measurements compared to WT CMs **(Figure 56B)**.

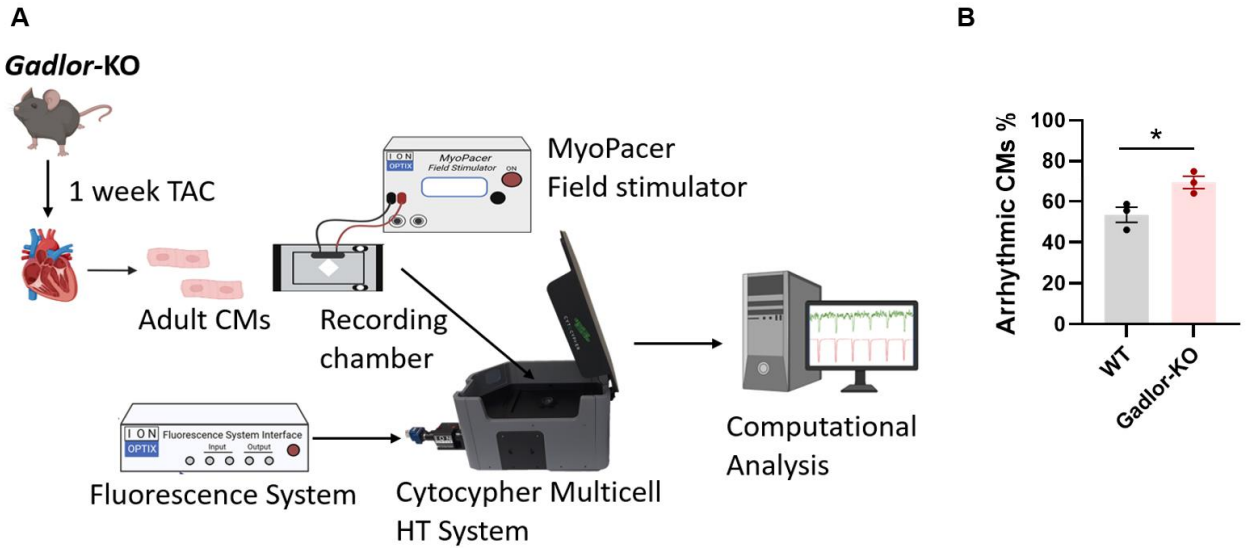

Figure 56: Experimental set-up for sarcomere contractility and calcium measurements.

A. Experimental set-up for ion-optix measurements with isolated adult cardiomyocytes after 1-week TAC in *Gadlor*-KO and WT animals. **B.** Percentage of arrhythmic cardiomyocytes (%) during measurements detected by analysis program. Each dot indicates at least 30 cardiomyocytes from different mice, n=3. *Data are shown as mean±SEM. Data normality was evaluated with Shapiro-Wilk test and p-values were calculated with Student's t-test for comparing two groups. *p-value<0.05. Illustration is created by using www.biorender.com.*

Based on sarcomere contractility measurements in isolated cardiomyocytes upon 1-week of pressure overload, sarcomere shortening and the timing of shortening were not affected while the timing of cardiomyocyte relaxation was delayed in *Gadlor*-KO CMs compared to WT CMs **(Figure 57A-B)**.

Moreover, *Gadlor*-KO CMs displayed a much slower calcium re-uptake into the sarcoplasmic reticulum (SR), which led to prolonged calcium transients and also an increased calcium peak height in *Gadlor*-KO CMs **(Figure 57C-D)**. The delay in the calcium reuptake was also depicted in a higher tau value, which tau represents the decay time constant indicating a much slower speed of recovery in *Gadlor*-KO cardiomyocytes compared to WT CMs after TAC.

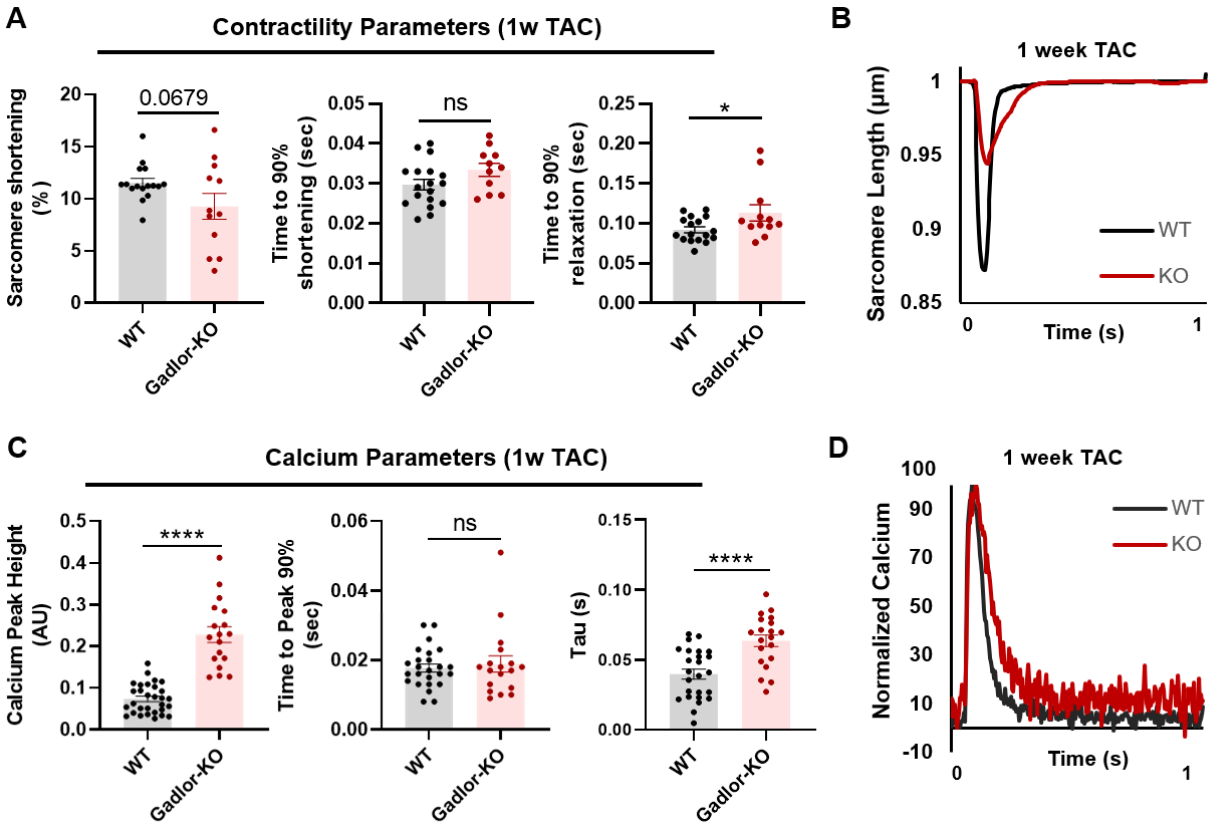

Figure 57: *Gadlor*-KO cardiomyocytes showed delayed calcium reuptake to the sarcoplasmic reticulum after TAC.

Contractility parameters including sarcomere shortening (%), time to 90% shortening (sec, systolic) and relaxation (sec, diastolic). **B.** Representative sarcomere contraction recordings of WT and *Gadlor*-KO CMs. **C.** Calcium parameters including calcium peak height (arbitrary units, AU), time to 90% peak of fura-2, AM ratio increase and decay time constant as an indication of the speed of recovery (tau, seconds). **D.** Representative calcium transient recordings of WT and *Gadlor*-KO mice shown as normalized levels of calcium (%). *Data are shown as mean±SEM. Data normality was evaluated with Shapiro-Wilk test and p-values were calculated with Student's t-test (Mann-Whitney for non-parametric) for comparing two groups. *p-value<0.05, ****p-value<0.0001.*

On the other hand, treatment of adult mouse cardiomyocytes with *Gadlor1/2*-enriched EVs compared to control-EVs led to augmented, but slower sarcomere shortening, and especially faster cardiomyocyte relaxation **(Figure 58A)**.

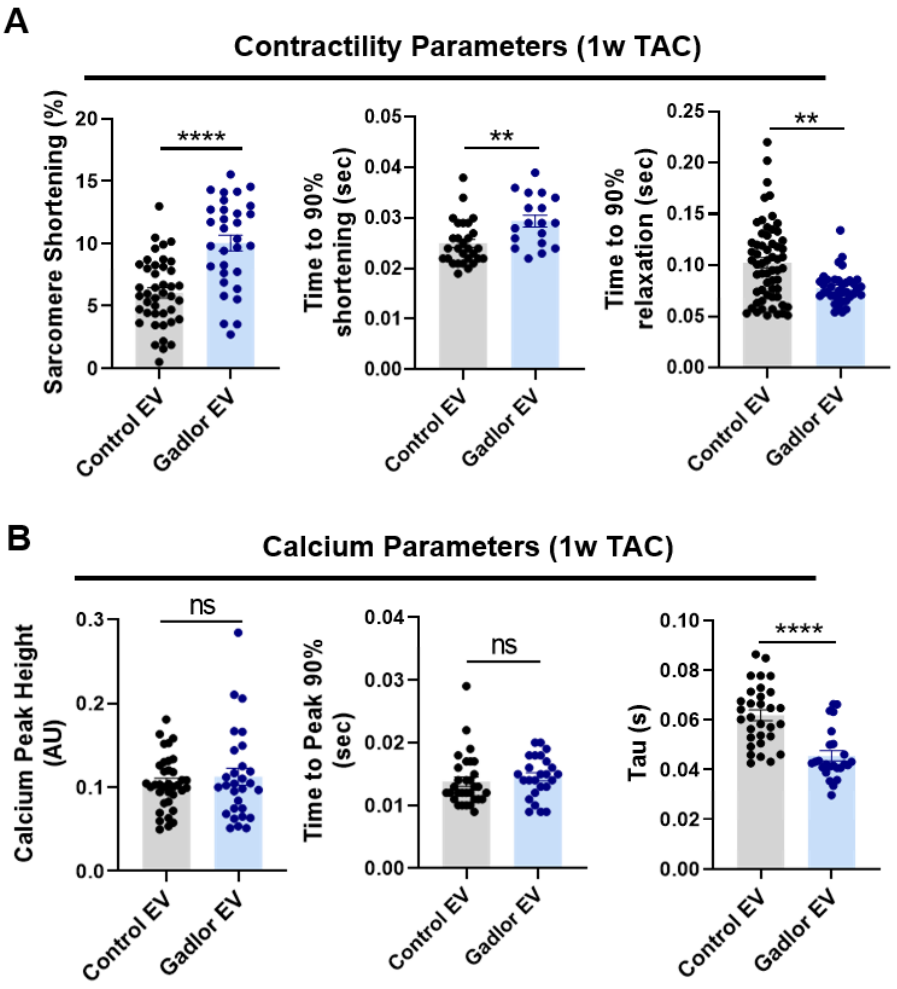

Figure 58: *Gadlor1* and *Gadlor2* overexpression via EVs leads faster cardiomyocyte relaxation.

Recordings were obtained in adult cardiomyocytes isolated from WT mice followed treated by incubation of control-EV (Ad.βgal) and *Gadlor1/2*-EVs (Ad.*Gadlor1* and Ad.*Gadlor2*) for 4 hours. **A.** Sarcomere function (sarcomere shortening (%), time to 90% shortening and relaxation (s)) and **B.** calcium transient (Calcium peak height, arbitrary units (AU), time to 90% peak of fura-2, AM ratio increase and decay time constant (tau, seconds). *Data are shown as mean±SEM. Data normality was evaluated with Shapiro-Wilk test and p-values were calculated with Student's t-test (Mann-Whitney for non-parametric) for comparing two groups. **p-value<0.01, ****p-value<0.0001.*

Additionally, calcium peak height and calcium release time were not changed, and a faster diastolic calcium re-uptake was detected by a decreased tau value **(Figure 58B)**.

Collectively*, Gadlor*-KO myocytes exhibited enhanced arrhythmic beating, slower diastolic relaxation and calcium re-uptake into SR which entailed as increased intercellular calcium levels. On the other hand, overexpression of *Gadlor1/2* led to a much faster cardiomyocyte relaxation and also faster re-uptake of calcium into the SR.

10.13. *Gadlor1* and *Gadlor2* affect gene expression in cardiomyocytes

In the studies to detect the localization of *Gadlor1* and *Gadlor2,* it has been shown that *Gadlor*1/2 were in part localized in the cardiomyocyte nucleus after the transfer **(Figure 51)**. Hence, the role of *Gadlor1* and *Gadlor2* in the regulation of cardiomyocyte gene expression was studied with bulk RNA sequencing from isolated adult cardiomyocytes of WT and *Gadlor*-KO after 2 weeks of TAC.

Comprehensive transcriptome analysis after TAC between WT and *Gadlor*-KO revealed that 2492 genes were upregulated, while 2956 genes were downregulated after ablation of *Gadlor1/2* as shown in the heatmap in **Figure 59A.**

The analysis of functional annotation of differentially expressed genes showed that genes related to vasculature development, ECM organization and regulation of cytokine production were upregulated while mitochondrial organization, TCA cycle and cardiac muscle contraction-associated genes were significantly downregulated in *Gadlor*-KO mice compared to WT after 2 weeks of TAC **(Figure 59B)**.

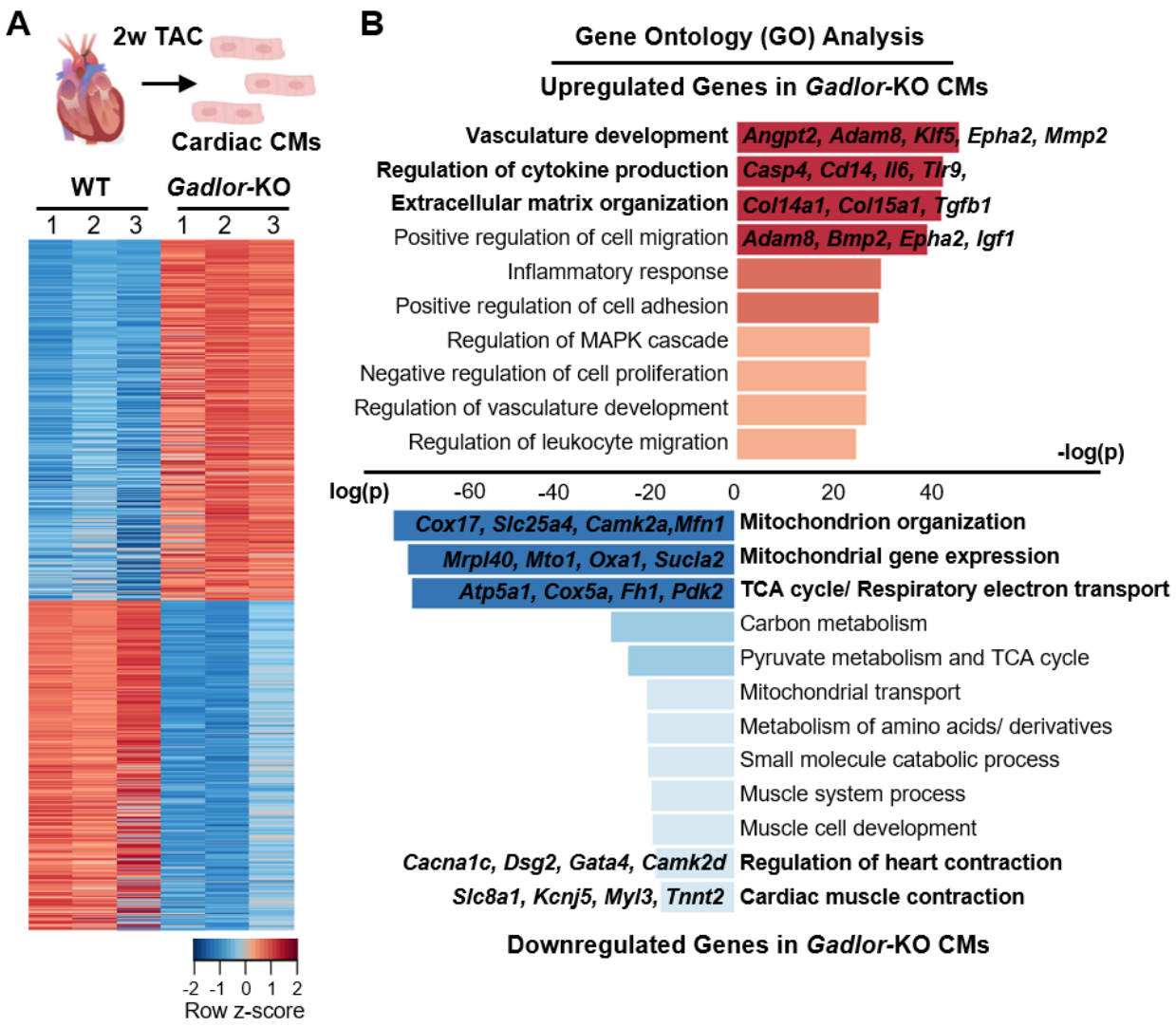

Figure 59: Deletion of Gadlor1 and Gadlor2 affects gene expression in cardiomyocytes.

A. Heatmap showing differentially regulated genes analysed after bulk RNAseq of isolated cardiomyocytes after 2-weeks TAC. **B.** Bar plots showing the gene-ontology (GO) analysis of upregulated and downregulated genes in *Gadlor*-KO CMs after 2-weeks TAC. (Red: Upregulated in *Gadlor*-KO, Blue: Downregulated in *Gadlor*-KO). Some exemplary genes were listed for selected GO-terms. Genes were filtered with set thresholds of False Discovery Rate (FDR<0.05) and fold-change 0.75 ≤ FC and FC > 1.5.

The upregulation and downregulation of the selected genes such as *Il6, Tlr9, Col15a1, Col14a1, Adam8* **(Figure 60A)** and *Camk2d, Gata4, Actn2, Mfn2* **(Figure 60B)** in mRNA level were verified in *Gadlor*-KO cardiomyocytes after TAC by RT-qPCR.

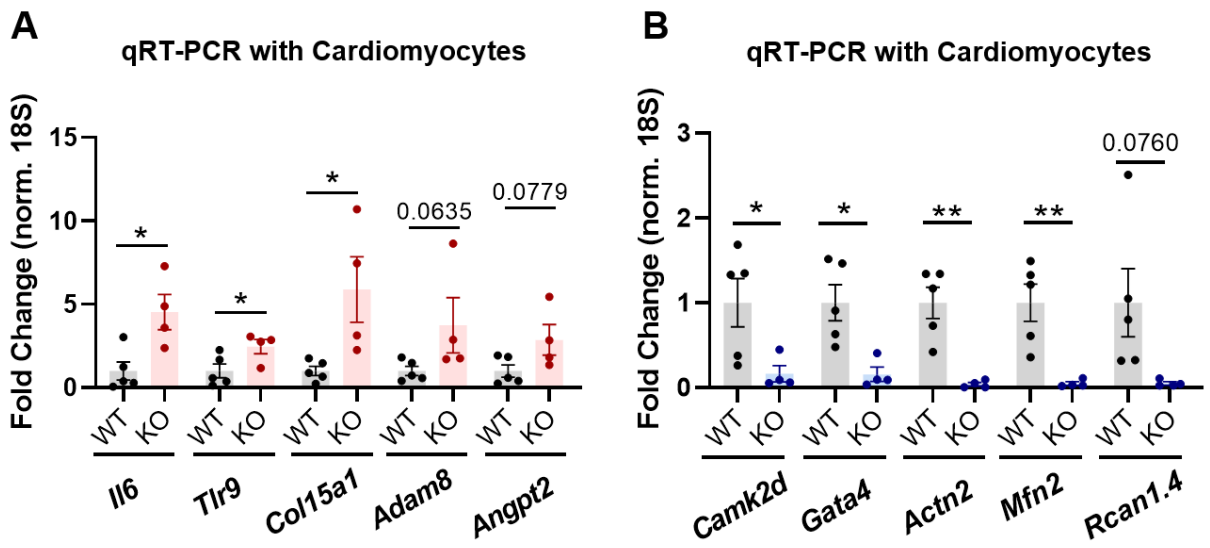

Figure 60: Validation of selected genes from RNAseq of cardiac CMs with qRT-PCR

A-B. Validation of selected genes from RNAseq data with qRT-PCR in isolated cardiac CMs after 2 weeks of TAC (Red: Upregulated in Gadlor-KO, Blue: Downregulated in *Gadlor*-KO). *Data are shown as mean±SEM. Data normality was evaluated with Shapiro-Wilk test. p-values were calculated with Student's t-test for parametric (or Mann-Whitney for non-parametric) for comparing two groups. *p-value<0.05, **p-value<0.01.*

Based on the gene-ontology analysis, mitochondrial gene expression and mitochondrion organization-associated genes were downregulated in *Gadlor*-KO cardiomyocytes after 1-week of TAC compared to WT cardiomyocytes **(Figure 59B)**. To understand whether this effect on mitochondrial gene expression was related to the number of mitochondria, the analysis of the mitochondrial to nuclear DNA ratio was evaluated with qPCR from whole heart tissue samples. There was no difference detected between *Gadlor*-KO and WT mice mitochondrial to nuclear DNA ratio upon pressure overload **(Figure 61)**. This finding confirmed the changes in the mitochondrial gene expression were not a result of a different number of mitochondria, thus actually reflecting the changes at the transcriptome level of *Gadlor*-KO mice.

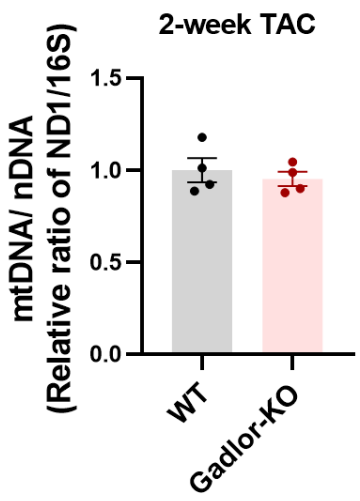

Figure 61: The effect of *Gadlor* lncRNAs in mitochondrial to nuclear DNA ratio.

Analysis of mitochondrial DNA (mtDNA) to nuclear DNA (nDNA) ratio determined via quantitative PCR by using WT and *Gadlor-KO* heart tissue DNA samples isolated 2-weeks after TAC. Measurement of ND1 and 16S rRNA DNA expression was used to determine the mtDNA/ nDNA ratio.

Data are shown as mean±SEM. Data normality was evaluated with Shapiro-Wilk test. p-values were calculated with Student's t-test for parametric for comparing two groups.

Next, the effect of *Gadlor1/2* overexpression in cardiomyocytes after PE stimulation was assessed in HL1 cardiac muscle cells **(Figure 62)**.

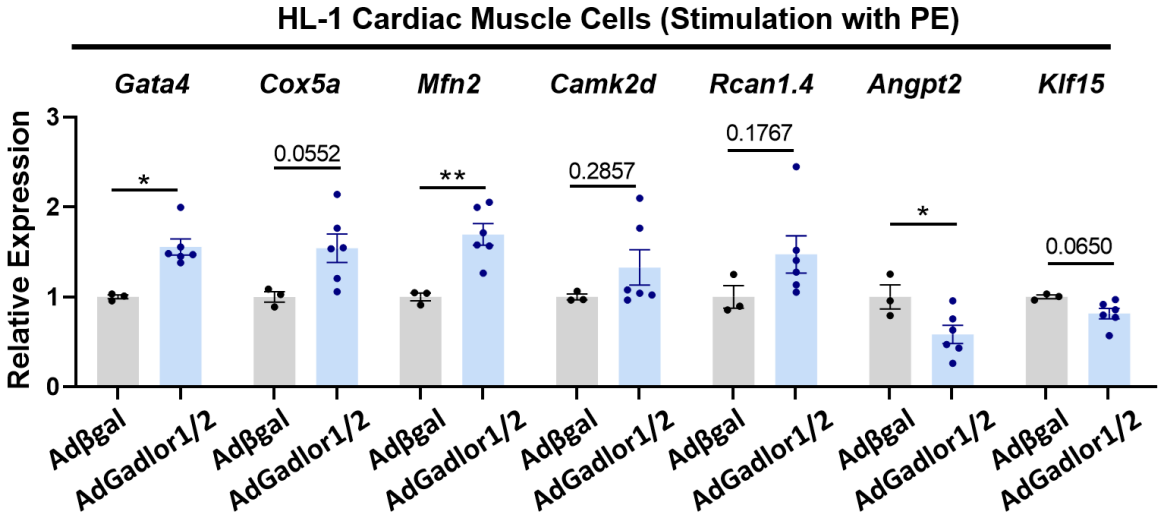

Figure 62: *Gadlor* overexpression affects the gene expression in HL1 cardiac muscle cells upon PE stimulation.

Quantitative RT-PCR of selected genes in HL-1 cardiac muscle cells overexpressing *Gadlor* lncRNAs after *Gadlor1/2* adenovirus treatment (β*gal* as control) followed by phenylephrine (PE) stimulation (100 µM, 24 hours). *Data are shown as mean±SEM. Data normality was evaluated with Shapiro-Wilk test. p-values were calculated with Student's t-test for parametric (or Mann-Whitney for non-parametric) for comparing two groups. *p-value<0.05, **p-value<0.01.*

An upregulation of *Gata4, Cox5a, Mfn2* and *Rcan1.4* RNAs and a downregulation for *Angpt2* and *Klf15* RNAs was confirmed upon *Gadlor1/2* overexpression with PE stimulation. This showed that *Gadlor1/2* overexpression in large parts revealed the opposite effects of what was found in *Gadlor*-KO cardiomyocytes **(Figure 62)**.

10.14. *Gadlor1* and *Gadlor2* has common but also unique gene targets in different cardiac cell types

To understand more about the common and differing effects of *Gadlor1* and *Gadlor2* knock-out in different cardiac cells upon pressure overload with TAC, bulk RNA sequencings from major cardiac cells types were studied in depth to analyse changes in the transcriptomic level. Data sets from *Gadlor*-KO cardiac ECs and FCs were combined with cardiomyocytes after 2-weeks of TAC in the conditions of upregulation *(fold-change ≥ 1.2)* or downregulation *(-1.2 ≤ fold-change)* in the gene expression compared to WT cardiac cells separately **(Figure 63)**.

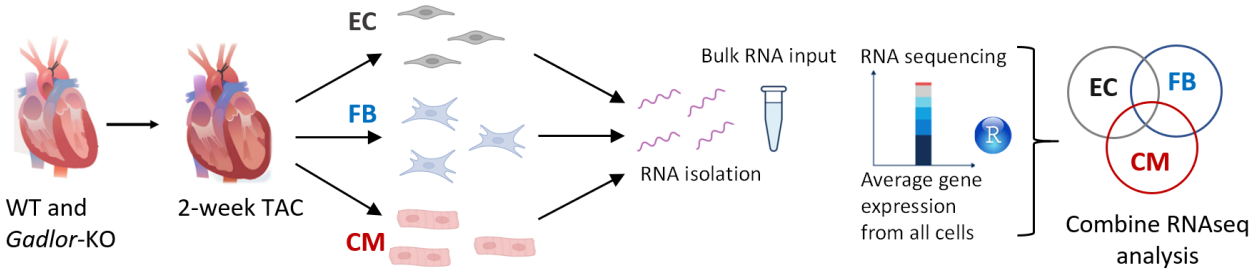

Figure 63: Identification of overlapping and unique differentially expressed genes in *Gadlor*-KO ECs, FBs and CMs after 2-weeks of TAC.

Scheme depicting the strategy of analysis in transcriptome level in isolated ECs, FB and CMs in *Gadlor*-KO mice compared to WT littermates after 2 weeks of TAC. Bulk RNA sequencings were performed from isolated major cardiac cell types following 2 weeks of pressure overload. Upregulated and downregulated genes in different cells were analysed for identification of common and unique regulatory roles of *Gadlor1* and *Gadlor2* lncRNAs.

Comparing the changes in the gene expression revealed a strong overlap among upregulated and downregulated genes in FBs, ECs and CMs, as well as unique gene targets which were depicted in Venn-diagrams in **Figure 64**. Overall, 333 genes were upregulated and 200 genes were downregulated in *Gadlor*-KO cardiac ECs, FBs and CMS in common compared to WT cells upon 2 weeks of pressure overload.

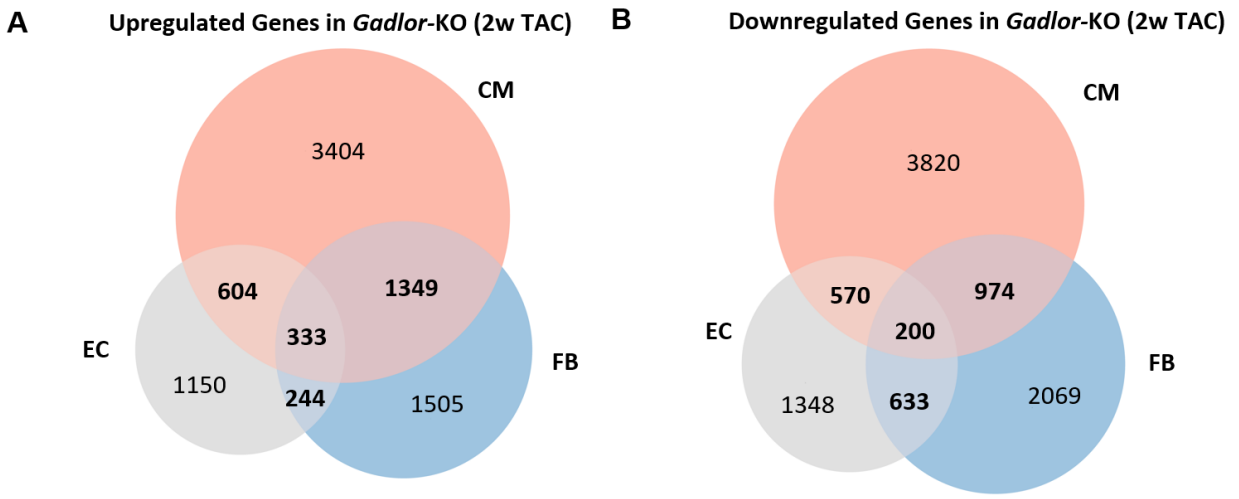

Figure 64: Venn diagrams of differentially expressed genes in different cardiac cell types of *Gadlor*-KO mice compared to WT littermates after 2 weeks of TAC.

Venn diagrams of **A.** upregulated and **B.** downregulated genes in different cardiac cell types (CM: red, EC: grey, FB: blue) of *Gadlor*-KO mice compared to WT after 2-weeks TAC. The numbers indicating the number of genes in corresponding cell types. Genes were filtered as fold-change greater or equals to 1.2 for each condition

According to the gene ontology enrichment analysis of upregulated genes in *Gadlor* knock-out cardiac ECs, FBs and CMs compared to WT cells **(Figure 65)**, genes related to energy-coupled proton transport through transmembrane, followed by cardiac muscle contraction and mitotic cell cycle related genes were common in all three major cell types**.** Mitotic cell cycle regulation with organization of spindle was common in ECs and CMs, while blood vessel morphogenesis was regulated in both CMs and FBs. Additionally, genes associated with mitotic spindle checkpoint

regulation, RNA processing and cardiac contraction were also regulated in both *Gadlor*-KO ECs and FBs.

On the other hand, genes related to the negative regulation of cell differentiation, cartilage development and the regulation of membrane potential were downregulated in all three cell types **(Figure 66).** Moreover, GO enrichment analysis indicated that genes related to cell migration, inflammatory response, extracellular matrix organization, heart contraction, calcineurin/NFAT signalling and mitochondrial organization were downregulated in at least two of the cell types in *Gadlor*-KO mice hearts**.** Therefore, *Gadlor1* and *Gadlor2* effects on gene-expression showed common, but also unique targets in different cardiac cell types.

Overall, the overlapping pathways affected from *Gadlor*-KO deletion in multiple cell types indicating a potential cross-talk between cardiac cells.

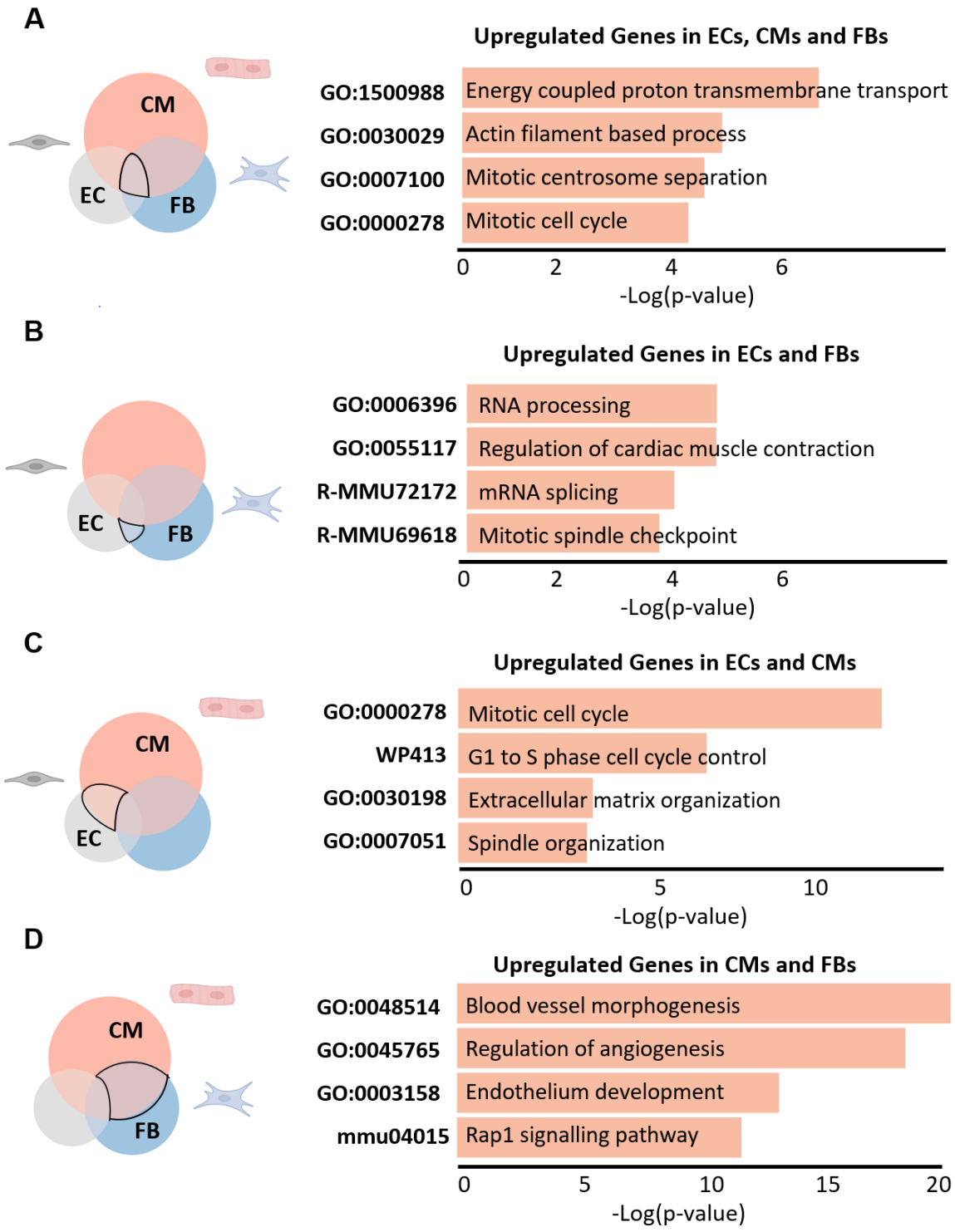

Figure 65: Gene ontology enrichment analysis of common upregulated genes in *Gadlor*-KO ECs, FB and CMs compared to WT after TAC.

A-D. Gene ontology (GO) analysis of indicated intersections representing the overlapping upregulated genes in shown cell types of *Gadlor*-KO compared to WT littermates after 2 weeks of pressure overload with TAC.

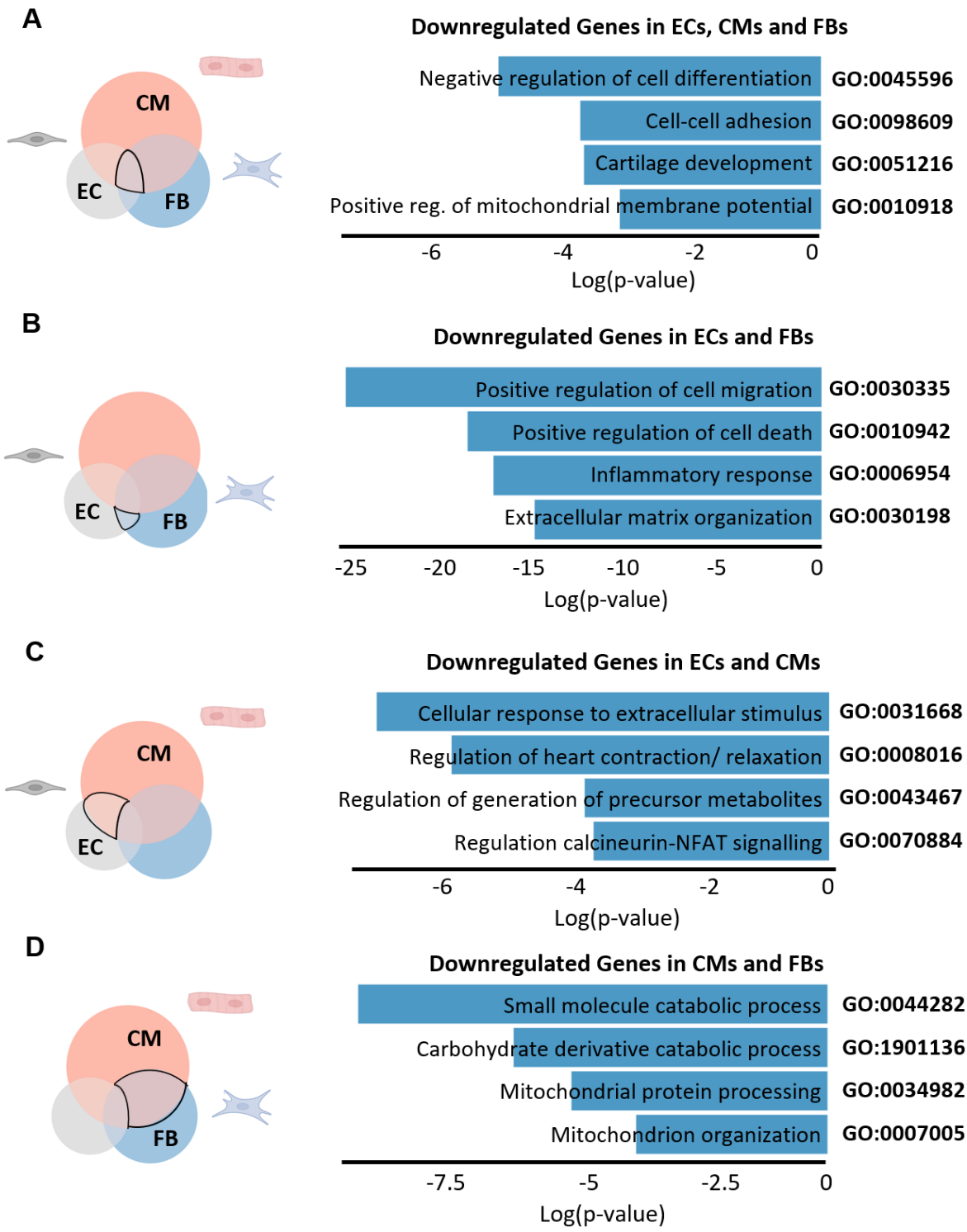

Figure 66: Gene ontology enrichment analysis of common downregulated genes in *Gadlor*-KO ECs, FB and CMs compared to WT after TAC.

A-D. Gene ontology (GO) analysis of indicated intersections representing the overlapping downregulated genes in shown cell types of *Gadlor*-KO compared to WT littermates after 2 weeks of pressure overload with TAC.

11. Chapter 4: Discussion

The discovery of active transcription and diverse functional roles of non-protein-coding genome including miRNAs, circRNAs and lncRNAs in physiological and pathological processes has triggered the investigation of non-coding RNAs as potential therapeutic targets for cardiovascular diseases.[17,78] Particularly, recent studies have shown lncRNAs that can affect gene expression with direct interaction with DNA, regulatory proteins, or transcription factors.

In this thesis, the detailed studies of deciphering the role and acting mechanism of two related and secreted novel lncRNAs named *Gadlor1* and *Gadlor2,* which are mainly expressed in EC-derived EVs and act as paracrine mediators in intracardiac cellular communication, were reported.

11.1. AK037972 (*Gadlor1*) and AK038629 (*Gadlor2*) are long non-coding transcripts and conserved in different species

Gadlor1 and Gadlor2 are novel non-coding transcripts, which are longer than 200 nucleotides and showed almost no sign of protein-coding probability, as confirmed with blastp database (NCBI) and alignment-free computational algorithm (CPAT) by calculating the size and structural properties of RNAs. LncRNAs are less abundant and poorly conserved compared to coding regions.[67,78] *Gadlor1* and *Gadlor2* are conserved between mice, rats and humans. Based on pairwise local alignment analysis *Gadlor1* is conserved more than 45% due to gaps, while *Gadlor2* is conserved over 70% in its human counterpart.

As reported in earlier studies, lncRNAs can have different roles based on their localization in the genome such as *trans*-acting or *cis*-acting mechanisms.[138] *Trans*-acting is affecting the protein-coding genes that are not localized nearby to the lncRNA, while *cis*-acting lncRNAs regulate the nearby protein-coding genes.[78,138] Since lncRNAs often act by *cis* gene regulatory mechanisms for the neighbour genes, the effect of *Gadlor1* and *Gadlor2* in the expression of *Lsamp* gene was assessed. *Gadlor1* and *Gadlor2* are located in the intronic region of the *Lsamp* gene, which did not show any regulation after deletion of the whole region containing *Gadlor* lncRNAs in chromosome 16, which excludes the *cis*-regulatory effect of *Gadlor* lncRNAs.

11.2. Expression of *Gadlor*1 and *Gadlor2* is highly increased in mice and human failing hearts

In the recent decade, the role of lncRNAs in cardiac remodelling during cardiac hypertrophy and heart failure has been extensively studied in both preclinical and clinical models to investigate the possible therapeutic role of the non-coding genome.[80,81,139] Inducing pressure overload to the left ventricle by TAC model increased the expression of both *Gadlor1* and *Gadlor2* lncRNAs in mouse heart tissue. Moreover, *GADLOR* lncRNAs were upregulated in human failing hearts as well as in the serum of patients with aortic stenosis. High *GADLOR2* levels were associated with low ejection fraction in the same patients, which suggested that *Gadlor* lncRNAs can be used as a potential biomarker or clinical target studies for the treatment of heart failure.

LncRNAs are mostly expressed less than protein-coding genes, however, they are highly tissue and condition-specific.[67,138] *Gadlor* lncRNAs exhibited the highest expression levels in the brain, liver, kidney and as well as in heart of the wild-type mice, which suggest that they can be studied within different organs in various physiological or disease conditions. *Gadlor1/2* were highly expressed in adulthood compared to earlier developmental stages. Among different cardiac cell types of adult mice, the highest expression levels were found in cardiac ECs, followed by FBs and CMs. Additional to these findings, the detection of *GADLOR2* in the serum of hypertrophy patients led to the idea of assessing *Gadlor1* and *Gadlor2* as secreted lncRNAs within vesicles.

11.3. *Gadlor* lncRNAs are secreted within EC-derived EVs

Studies in the past decade revealed extracellular vesicles can transfer bioactive cargos including DNA, RNA and proteins, and act as important nanoparticles that contribute to intercellular cross-talk between major cardiac cells.[85,87,111,140] Cardiac ECs, FBs and CMs are not only EV producer cells but also recipients responding to different pathophysiological conditions, as well as to maintain homeostasis.[85,140,141] Although the incorporation of miRNAs in EVs has been more extensively studied, lncRNAs within vesicles have not been well described. For instance, it has been demonstrated that cardiac fibroblasts can release exosomes carrying miRNAs, which can be taken up by cardiomyocytes and regulates their response to stress condition.[111] Recently in

another study, it is documented that EV-mediated shuttling of miR-122-5p regulates cardiomyocyte viability and apoptosis.[112] Based on the comparative analysis of *Gadlor* lncRNA levels in cardiac ECs and EC-derived extracellular vesicles, a significant enrichment of *Gadlor1* and *Gadlor2* in EC-derived EVs was detected. Additionally, *Gadlor* lncRNAs were protected from RNase-A and proteinase-K treatment, which confirmed that they are encapsulated into vesicles rather than being attached to the surface proteins. Overall, these results indicated that *Gadlor1* and *Gadlor2* are secreted lncRNAs, although this does not exclude their autocrine action.

Extracellular vesicles are membrane-bound nanoscale structures that carry nucleic acids, proteins, lipids or metabolites, which can be directed to distant recipient targets.[91,92,94,108] Due to their complex biogenesis and release mechanisms[90] and common characteristics (e.g overlap in size and surface markers), it is hard to classify EVs into subpopulations, thus there is not yet clearly defined separation.[93,108] To this end, it is crucial to standardize EV isolation and enrichment methods and characterize isolated EVs based on ISEV (International Society of Extracellular Vesicle) guidelines.[93,135] In accordance with the guidelines, EVs were isolated with ultracentrifugation, which is one of the most widely used standard methods[95] in this research area. Characterization of isolated EVs was performed with transmission electron microscopy (TEM), nanoparticle tracking analysis (NTA) for visualization of morphology, and size and concentration detection, respectively. Additional analysis with flow cytometry (FACS) further confirmed the existence of common surface markers such as CD9, CD54 and CD63, as shown also in previous studies. [112,142]

11.4. Deletion of *Gadlor1* and *Gadlor2* protects from cardiac dysfunction and fibrosis after TAC

Deletion of the whole region containing *Gadlor1* and *Gadlor2* on mouse chromosome 16 with CRISPR/Cas9-based methodology did not result in any change in baseline phenotype, which was confirmed with baseline organ level analysis and echocardiographic assessment. To study the effect of *Gadlor1* and *Gadlor2* in cardiac remodelling upon pressure overload, TAC model was used. TAC is a widely used model in mice that mimics pressure-overload and left-ventricle-associated cardiac hypertrophy followed by heart failure in later stages.[143] The experimental

model was initially described and validated by Rockman *et al.*[128], and since then widely used compared to other models due to its advantages such as: reproducibility and enabling to study of the compensatory and decompensatory phases of heart failure in a time-dependent manner.

Cardiac remodelling comprises global changes in the heart shape and function that are the consequence of cardiomyocyte hypertrophy, altered angiogenesis and myocardial fibrosis.[19,21,144] Accordingly, ablation of *Gadlor* lncRNAs attenuates maladaptive remodelling of pathological overload after short-term TAC (2-weeks). Pressure overload was confirmed with carotid flow measurements at the level of RCCA and LCCA[128], in which the increase in RCCA/ LCCA ratio was detected in both WT and *Gadlor*-KO mice in a similar degree indicating that the mice were subjected to a comparable degree of aortic constriction. Cardiac hypertrophy was evaluated with the HW/ BW ratio in the whole organ level, which was also confirmed at the cellular level with WGA staining that showed a smaller increase in the cross-sectional area for *Gadlor*-KO CMs after 2 weeks of TAC compared to WT CMs. Furthermore, these changes were validated with the expression of hypertrophy-associated genes (*Nppa, Nppb* and *Myh7/ Mhy6*), whereby less induction was observed after deletion of *Gadlor* lncRNAs. Morphological and structural changes in the heart tissue were additionally confirmed with echocardiographic observations, in which less increase in LVPW (mm) thickness and preserved LVEF (%) were observed in *Gadlor*-KO mice compared to WT mice upon pressure overload.

During cardiac remodelling, ECM-associated collagen network accumulation contributes to adverse remodelling due to myocardial fibrosis, which results in stiffness and loss of compliance of the heart.[23,145] Interestingly, *Gadlor*-KO animals were protected from ECM accumulation and showed a substantial increase in myocardial capillarization during the cardiac remodelling upon pressure overload. The oxygen demand of the myocardium is typically during cardiac hypertrophy, in which capillary density increases during the compensatory phase until rarefaction is observed in the later decompensatory stages.[23,32] The significant increase in angiogenesis levels after 2 weeks and even 8 weeks of TAC were observed after deletion of *Gadlor1/2*, in which a marked increase in capillarization with less fibrosis might contribute to better cardiomyocyte contractility in *Gadlor*-KO mice.

On the other hand, the gain-of-function model by perfusion of *Gadlor* containing EVs followed by TAC challenge showed that overexpression of *Gadlor1* and *Gadlor2* provoked systolic dysfunction, and enhanced fibrosis development while exhibiting larger cardiomyocytes. These findings were confirmed at the mRNA level with the much higher increase in hypertrophy and fibrosis-associated genes (*Nppa, Nppb, Col1a1, Col3a1*) compared to controls.

Overall, *Gadlor*-KO mice exhibit better adaptive cardiac remodelling with less fibrosis, more myocardial capillarization and preserved systolic function after pressure overload, while enhanced *Gadlor1/2* expression triggers aggravated heart failure, myocardial hypertrophy and fibrosis.

11.5. Deletion of *Gadlor1/2* induces angiogenesis in ECs and suppresses fibrosis-associated genes in FBs after TAC

Among the different cell types in the myocardium, the highest *Gadlor1/2* expression was detected in ECs, followed by FBs. Since lncRNAs can exert their functional effects by modifying gene expression[17,67], the observed effects of *Gadlor1/2* deletion upon pressure overload were analysed in depth with RNA sequencing from cardiac ECs and FBs after 2 weeks of TAC. The previous observations with WT and *Gadlor*-KO mice at the whole organ level were consistent with the findings of extensive bulk RNA sequencing, which less fibrosis and more angiogenesis were confirmed in genome-wide analysis.

Gene ontology enrichment analysis in *Gadlor*-KO ECs after TAC revealed strong upregulation of angiogenesis and cell cycle-associated genes, which can explain the substantial increase observed in the capillarization of the myocardium. Moreover, downregulation of pro-inflammatory genes after TAC in *Gadlor*-KO ECs was confirmed in mRNA level, however, the difference did not result in increased abundance of CD45 positive leukocytes in the myocardium. It has been reported that the cardiac remodelling process after pressure overload with TAC triggers inflammation, fibrosis development and alterations in vascular integrity.[146,147] Local infiltration of inflammatory cells and anti-inflammatory and pro-inflammatory cytokines contribute to the cardiac remodelling process by easing or promoting the adverse progression, respectively.[146,148] Accordingly, the case that the

difference in inflammatory response was not detectable with CD45 staining between WT and *Gadlor*-KO mice can be explained by the existence of multiple subgroups of $CD45^+$ immune cells in the myocardium after pressure overload[147], which detection of a specific subpopulation might show the difference in the inflammatory reaction to TAC. Thus, further experiments targeting pro-inflammatory and anti-inflammatory subpopulations could be performed for detailed understanding.

In addition, increased proliferation in ECs (Ki67 positive ECs) in *Gadlor*-KO heart tissue sections confirmed the effect of *Gadlor1/2* in cell-cycle regulation, which *Gadlor1* and *Gadlor2* knock-out entailed an increased capillary density and increased endothelial cell proliferation. On the other hand, *in vitro* sprouting assays further showed a less angiogenic capacity of *Gadlor1/2* overexpressing ECs indicating that *Gadlor1/2* lncRNAs inhibit angiogenic activity in ECs. The fact that the reducing effect of *Gadlor1/2* overexpression in capillary density was not observed in *ex vivo* analysis after TAC could be the result of insufficient overexpression of *Gadlor1/2* via *Gadlor*-containing EVs. Overall, these findings imply that *Gadlor1* and *Gadlor2* might act both in an autocrine and paracrine manner via EVs, and the angiogenic effects on ECs could be explained with a cell-autonomous response while increasing expression of pro-angiogenic genes in CMs and FBs could indicate their role as paracrine mediators.

Fibrosis is another crucial process in cardiac remodelling, which occurs in response to ageing or myocardial injury and includes mainly the changes in the composition of ECM components that lead to scarring, stiffness, cardiac dysfunction and conductance problems.[149-151] During ECM remodelling collagen types I and III are the main contributors to fibrosis development.[150] *Gadlor*-KO mice were protected from ECM deposition shown in Picro-Sirius red staining in the whole organ level, and less induction of *Col1a1* and *Col3a1* levels after TAC compared to WT hearts. These findings were also confirmed in RNA sequencing from isolated FBs after pressure overload, in which ECM organization genes were downregulated in *Gadlor*-KO mice. Additionally, overexpression of *Gadlor* lncRNAs upon phenylephrine (PE) stimulation resulted in a significant increase in collagen type I and III, but not in collagen type IV and VI. There is no well-defined role of collagen type IV and VI like collagen type I and III in the pathogenesis of cardiac fibrosis, which are less abundant components of ECM.[151] However, some studies indicated that non-fibrillar

collagen type VI might play a role in fibroblast activation and trans-differentiation, but has no significant effect on overall cardiac function.[152,153]

FBs exhibit the second highest *Gadlor1/2* expression among the major cardiac cells, however, the data showing the transfer of EC-derived *Gadlor1/2* overexpressing EVs into the NRFBs suggested both autocrine and paracrine effects of *Gadlor* lncRNAs on FBs. Based on RNA sequencing from isolated FBs after TAC, the development of fibrosis was mainly regulated by FBs at the transcriptome level, since deletion of *Gadlor1/2* downregulates ECM organizational genes. The main acting mechanism of *Gadlor1/2* on FBs, in which whether they mainly rely on their endogenous *Gadlor1/2* expression, or external *Gadlor1/2* that is transferred via EC-derived EVs, is still unknown. To understand the contribution of autocrine or paracrine effects of *Gadlor1* and *Gadlor2* on FBs regarding fibrosis development should be investigated with further studies.

11.6. *Gadlor*-KO mice showed higher mortality despite retaining better cardiac function

Paradoxically, despite retaining better heart function and an adaptive remodelling process after pressure overload, the complete lack of *Gadlor* lncRNAs during chronic pressure overload (up to 8 weeks after TAC) entailed sudden and unexpected death. Typical mortality reported within the first four weeks of TAC operation is less than 20% in wild-type mice.[154] In addition, the death of animals directly related to complications during the first 24-hours after the operation were excluded from the analysis. Since the animals had not demonstrated any gradual indication of sickness or problems of mobility that might affect them to reach food or water, this sudden death of *Gadlor*-KO mice was most likely to be explained by an arrhythmia-related cause. It is particularly interesting that the mortality started approximately after two or three weeks after TAC, which is still the compensatory phase during pressure overload.

11.7. *Gadlor1* and *Gadlor2* act as paracrine mediators in intracardiac cross-talk

Considering the fact that *Gadlor1* and *Gadlor2* are mainly secreted within EVs from EC, which was validated by a highly enriched expression in endothelial-derived EVs compared to cells by qRT-

PCR analysis, a potential role of *Gadlor* lncRNAs as paracrine mediators was investigated in the heart. Indeed, EVs were reported to contain mainly miRNAs, but also lncRNAs and mRNAs, whereby these RNAs are protected from extracellular RNases while being trafficked to the desired destination.[155] EVs might thereby play a role in intercellular communication, especially during stress stimulation or disease condition, when their production is typically increased.[156] In this study with cell culture experiments, an effective uptake of *Gadlor1* and *Gadlor2* into the neonatal and adult cardiomyocytes via endothelial-derived EVs was shown with qRT-PCR analysis and tracking of EVs with fluorescently labelled dye. Analysis with confocal microscopy revealed that PKH67 labelled EVs were taken up by the cells rather than being attached to the surface. Additionally, qRT-PCR analysis confirmed that cardiomyocytes are the main cell type taking up these *Gadlor1* and *Gadlor2* containing EVs, even though they express the least endogenous levels.

Furthermore, when adult cardiomyocytes isolated from *Gadlor*-KO mice, which naturally cannot upregulate intrinsic *Gadlor1* and *Gadlor2* expression, were co-cultured in the bottom well of a two-chamber system with wild-type EC in the upper well, these effectively restored *Gadlor1/2* levels in the knock-out cardiomyocytes. In addition, the co-cultured ECs markedly upregulated their *Gadlor1/2* expression compared to when they were cultured alone.

Overall these results suggest a reciprocal intercellular signalling circuit between EC and cardiomyocytes, whereby EC provide *Gadlor* lncRNAs within EVs to cardiomyocytes, which signal back to EC by currently unknown mechanisms to indicate insufficient *Gadlor1/2* levels, when necessary. Indeed, signal responsive EV release had been previously described.[156]

11.8. *Gadlor* lncRNAs bind to CaMKII and GLYR1 in cardiomyocytes

LncRNAs have various different action mechanisms to regulate gene expression depending on which tissue and condition they are expressed in and their subcellular localization.[67,138] Gene expression regulation can be mediated by lncRNAs via direct interaction with DNA, RNA and/or proteins, which then affect chromatin dynamics, transcription of the neighbour or distant genes, and stability or translation of RNAs.[157-160] Cellular fractionation analysis showed that *Gadlor1/2*

are localized in both cytoplasm and nucleus of recipient cardiomyocytes, which might indicate different roles of *Gadlor* lncRNAs in different pathophysiological conditions.

Identification of CaMKII and GLYR1 as unique interaction partners of *Gadlor1* and *Gadlor2* in cardiomyocytes with RAP-MS was then additionally confirmed by native RIP. Accordingly, identified *Gadlor1* and *Gadlor2* interaction partner CaMKII is present in the cytosol and in the nucleus, while GLYR1 has a predominant nuclear localization.[161]

CaMKII activity is regulated by the state of the holoenzyme complex which is mainly regulated by calcium/calmodulin, autophosphorylation, glycosylation, oxidation or nitrosylation.[162] Activity of CaMKII is known to be increased in human failing hearts and many pre-clinical models of heart failure in the mouse.[42,163] CaMKII has a dual activity including acute modulatory effects on ion channels, and a slower response to stress signals at the transcription level.[162] CaMKII promotes maladaptive features in cardiomyocytes such as hypertrophy and fibrosis by phosphorylating class II histone deacetylase 4 (HDAC4), which then leads to the activation of hypertrophic transcription factors like myocyte enhancer factor 2 (MEF2) and activates pathological remodelling.[164-168] Additionally, CaMKII contributes to the maintenance of intercellular calcium homeostasis and instability of the membrane potential which may result in arrhythmia.[42]

Since CaMKII is multifunctional, it also contributes to the adaptive features in cardiac remodelling in the early stages.[42] For instance, it promotes calcium re-uptake into the SR by phosphorylating phospholamban (PLN) at the Threonine-17 (Thr17) site which is important for the β-adrenergic response and maintaining the recovery of contractility.[169,170] Because *Gadlor1* and *Gadlor2* bind to CaMKII in cardiomyocytes, and phosphorylation of PLN at Thr17 is reduced in *Gadlor*-KO mice after pressure overload while overexpression of *Gadlor1/2* led to enhancement of pThr17-PLN suggesting that *Gadlor* lncRNAs might promote CaMKII activation via a feed-forward loop.

11.9. *Gadlor*-KO cardiomyocytes showed delayed calcium re-uptake to sarcoplasmic reticulum after TAC

Since *Gadlor*-KO mice showed a higher mortality rate, which the death of the animals was sudden by nature compared to WT mice after pressure overload, and CaMKII was identified as an

interaction partner of *Gadlor* lncRNAs, the effect of *Gadlor*1/2 in cardiomyocyte contractility and calcium homeostasis was evaluated using Ionoptix MultiCell High Throughput System (IonOptix corp. Milton, MA, USA). Altered calcium dynamics are a crucial regulatory mechanism for cardiac contractility, which can be altered during disease state, such as heart failure.[42,170] Even though the percentage of sarcomere shortening and time of shortening were not different, the timing of cardiomyocyte relaxation was delayed in *Gadlor*-KO CMs. In addition, the decay time constant (tau) for calcium replenishment in SR was significantly higher in *Gadlor*-KO cardiomyocytes after TAC, which was also depicted in the shift in the change of intercellular calcium levels. Slower re-uptake of calcium ions into SR resulted in a significant increase in calcium peak height due to the accumulation of Ca^{2+} ions in the cytoplasm of the *Gadlor*-KO cardiomyocytes. Higher cytoplasmic Ca^{2+} levels can lead to arrhythmia by delayed after-depolarization (DAD) following the full repolarization[45], in which higher calcium levels in the cytoplasm can activate other cation channels and calcium-sensitive pathways.[46] Indeed, decreased CaMKII activity could account for the improved cardiac remodelling features that were detected in *Gadlor* knock-out mice, while at the same time slowing down calcium re-uptake into the SR and leading to increased cytosolic calcium levels with pro-arrhythmic activity.

On the other hand, overexpression of *Gadlor1* and *Gadlor2* in isolated WT CMs after the transfer of *Gadlor1/2* containing EVs alters the sarcomere shortening and time for shortening, which the effect was not observed in the corresponding calcium parameters. However, treatment of *Gadlor1/2* EVs triggered faster relaxation and faster recovery of Ca^{2+} back into SR. Even though isolated adult CMs and overexpression of *Gadlor* lncRNAs via EVs were created in this artificial model, the results were in line with the results from *Gadlor*-KO cardiomyocytes. Overall, these data indicated that *Gadlor1/2* contributes to diastolic Ca^{2+} homeostasis during pressure overload via interacting with CaMKII.

11.10. *Gadlor* lncRNAs affect cardiomyocyte gene expression in response to TAC

Although cardiomyocytes exhibit the least endogenous *Gadlor1* and *Gadlor2* expression compared to other cardiac cells, they are the main recipient cell type which takes up EV-encapsulated *Gadlor* lncRNAs. Since *Gadlor1/2* was detectable both in the cytoplasm and nucleus

of the recipient cardiomyocytes, the changes in the transcriptome level of cardiomyocytes were assessed with bulk RNA sequencing after 2 weeks of TAC. In addition, the identification of GLYR1 as one of the interaction partners of *Gadlor* lncRNAs also supported the idea that *Gadlor1/2* might contribute CM gene expression.

GLYR1 was identified as a nucleosome-destabilizing factor that is recruited to gene bodies to facilitate the transcription of many genes.[161] In a recent study, it has been shown that GATA4 and GLYR1 are physically interacting and co-activating cardiac developmental genes, whereby *GLYR1* missense mutation affecting this interaction results in dysfunction in mice.[171] In addition, *Gata4* expression is significantly downregulated in *Gadlor*-KO CMs after TAC. Thus, *Gadlor1* and *Gadlor2* might act on gene expression in part by binding to GLYR1 and promoting the changes in the chromatin regulation in cardiomyocytes, however, more work is needed to decipher this interaction.

Based on gene ontology analysis, upregulation of blood vessel morphogenesis, inflammatory response and ECM organization-related genes was observed in *Gadlor*-KO cardiomyocytes compared to WT CMs after TAC. The changes in the vasculature during cardiac remodelling upon pressure overload are triggered by different cardiac cells including ECs, FBs and CMs, which is observed as well in *Gadlor*-KO CMs as upregulation of pro-angiogenic genes. This additionally supports the considerable increase observed in the capillarization of myocardium after deletion of *Gadlor1/2,* which ECs might act as the main contributor to the upregulation of cell cycle and angiogenesis regulation genes, however, the effect of FBs and CMs might additionally pronounce the vascularization via paracrine signalling, which might contribute to the observed better cardiac function at the whole organ level. Upregulation of collagen production in cardiomyocytes due to stress conditions, including after pressure overload by TAC, was detected in previous studies, nevertheless, the contribution of cardiomyocyte collagens to the remodelling process is still unclear.[28,136,172,173]

The contractile function is directly related to the alterations in cardiac metabolism during heart failure.[9,174] Under normal conditions, more than 95% of ATP used in cardiac contractility is generated by oxidative phosphorylation, while only a small fraction is generated with glycolysis.[174] Moreover, the majority of the cardiac ATP (approximately 80%) is the consequence

of fatty acid (FA) oxidation[175] which can change during different pathophysiological conditions due to the alterations in the energy demand of the heart.[174] For instance, since glucose metabolism required less oxygen to produce energy compared to FA-dependent pathways, a shift to using more glucose compared to normoxic conditions was observed in many studies of heart failure.[54] It has been shown that FA oxidation was reduced even in the early stages of HF with reduced left-ventricle EF.[176] Moreover, Zhabyeyev and colleagues have shown also glucose/pyruvate oxidation was reduced while FA/palmitate oxidation was preserved after TAC until systolic dysfunction is manifested.[177] Considering the fact that HF is a progressive and complex condition, the changes in the selection of substrate would be influenced by the cardiac remodelling process (e.g compensatory or decompensatory phase).[54] Despite the increasing number of work on cardiac metabolism, it is still controversial and open for further investigations.

Gene ontology analysis from isolated CMs after 2-weeks of TAC revealed that genes involved in the mitochondrial organization, TCA cycle and pyruvate metabolism were downregulated in addition to ion channels and cardiac muscle contraction-associated genes in *Gadlor*-KO CMs compared to WT CMs. The changes in mitochondrial genes were not the consequence of a reduced number of mitochondria, which was confirmed by no change in the mtDNA/nDNA ratio in *Gadlor*-KO and WT hearts after 2 weeks of TAC. These results might suggest that the effect of *Gadlor1/2* deletion can alter the functional properties or trigger transcriptome level changes, rather than causing mitochondrial loss such as autophagy due to the accumulation of reactive oxygen species (ROS).[54,178] It has been demonstrated in previous studies that mainly electron transport chain (ETC) proteins are downregulated during the progression of heart failure, which affects mitochondrial energetics and substrate selection directly.[64,179] Downregulation of mitochondrial electron transport and carbohydrate catabolic process genes were in common in both *Gadlor*-KO FBs and CMs after 2 weeks of TAC, which might contribute to cardiomyocyte dysfunction at the cellular level.

In addition, downregulation of contractility and ion channel-associated genes, such as *Camk2d, Cacna1c* and *Myl3,* was observed in *Gadlor*-KO CMs compared to WT CMs. These changes in the heart contraction-associated gene expression, considering the effect of *Gadlor1/2* ablation in CMs detected in the experiments of contractility and calcium dynamics, could explain the susceptibility

to arrhythmias in knock-out mice. Moreover, the opposite effect in the gene expression or at least a trend of change was observed with HL1 cells overexpressing *Gadlor1/2* lncRNAs, which a decrease in angiogenesis genes and increase in mitochondrial and contractility-related genes were confirmed with qRT-PCR.

11.11. Gene expression patterns were both in common, but mostly unique in ECs, FBs and CMs after *Gadlor1* and *Gadlor2* deletion upon pressure overload

Interestingly, systemic ablation of *Gadlor1* and *Gadlor2* had some common, but mostly different effects in the major cardiac cell types. Gene expression patterns of EC, FB and CM were analysed with bulk RNA sequencing and then compared for identification of common and unique pathways affected by deletion of *Gadlor1/2* after pressure overload-induced by TAC.

Commonly affected pathways within different cell types can imply a potential cross-talk between cells to maintain homeostasis.[85] For instance, an increase in myocardial capillarization is one of the strongest phenotypes observed after *Gadlor1* and *Gadlor2* deletion, in both compensatory (2 weeks) and decompensatory phases (8 weeks) of TAC. ECs are considered as the main contributor, however upregulation of blood vessel morphogenesis and angiogenesis regulatory genes in both *Gadlor*-KO FBs and CMs indicates a strong contribution from those cells. Additionally, the downregulation of cartilage development-associated genes in all *Gadlor*-KO cardiac cells, and ECM-organization genes in mainly ECs and FBs might also suggest a cross-talk between cells and resulted in less fibrosis in *Gadlor*-KO mice after short-term and long-term TAC.

Overall, deletion of *Gadlor1* and *Gadlor2* has beneficial effects in cardiac ECs and FBs, in which these features of adaptive remodelling during pathological cardiac overload including an increase in vascularization and decrease in fibrosis development might mask the potential maladaptive effects of *Gadlor1/2* ablation in CMs, such as perturbed calcium handling. These beneficial effects of *Gadlor1/2* deletion in ECs and FBs after TAC might also explain why the mortality of the animals was not a continuous process, but rather sudden and irregular.

11.12. Clinical Relevance: Targeted deletion of *Gadlor1* and *Gadlor2*

CVDs are still one of the main medical and economic burdens with high mortality rates and decreasing quality of life for the patients.[4] Even though the pharmacological agents and devices developed widely improved the situation in European countries[1], there is still an unmet medical need for effective therapeutics.

Improvements in RNA sequencing methods and nucleic-acid-based technologies provide fast progress for the discovery and translation of novel non-coding transcripts in the cardiovascular area.[78] Current studies mainly focus on miRNAs as biomarkers, and potential targets for therapeutics, however, lncRNAs and circRNAs have been providing promising results in preclinical studies with animal disease models.[17,78,79]

Following the studies that have been described here, *Gadlor1* and *Gadlor2* are novel lncRNAs that are secreted, and *GADLOR2* is also detectable in the serum of hypertrophy patients. Additionally, the observed negative correlation between the *GADLOR2* levels and EF% of the hypertrophy patient cohort indicates the specificity of the lncRNAs in pathological overload.

Inhibition of *Gadlor1* and *Gadlor2* in cardiomyocytes might not be a suitable therapeutic strategy during cardiac overload due to the dichotomous role of *Gadlor1/2* in CMs, in which the ablation of *Gadlor1/2* would lead to inhibition of hypertrophy, but there might be the danger of arrhythmia or sudden death. On the contrary, inhibition of *Gadlor1/2* lncRNAs in EC and FB could be beneficial, as it would entail increased angiogenesis and reduce FB-mediated fibrosis, which according to the data presented in this study, is likely to be the main underlying reasons for *Gadlor1/2* triggered cardiac dysfunction. Although more work is needed, inhibition of *Gadlor1* and *Gadlor2* lncRNAs in cardiac non-myocytes is suggested to be a promising strategy to treat heart failure in the future.

Even though lncRNAs can be very promising targets for CVD therapeutics, there are some obstacles to overcome for translational use in clinics.[82] Besides common difficulties with any treatment method such as pharmacokinetics and pharmacodynamic (PK/PD) properties of the machinery molecules for efficiency, the stability of RNA and off-target effects are also being considered.[78] Additionally, targeting specific tissues, especially delivery to the heart might be

challenging. However, the advancements in novel drug delivery molecules, such as extracellular vesicles might be useful for applications of nucleic-acid therapies.[113,120] Modifications to increase the stability and specificity of lncRNA delivery might be a very promising tool to overcome CVDs in the distant future.

11.13. Limitations and Future Prospects

Even though extracellular vesicles are getting attention for various purposes such as working as drug delivery molecules and biomarkers or in the context of intercellular cross-talk, the standardization of the isolation and characterization methods is needed.[93,124,135]

Studies to identify novel non-coding RNAs has been triggered by the progress of next-generation sequencing, and the accessibility of open-source data platforms[15], however, often the mechanism of action and molecular interaction partners still remain elusive. In this study, the effects of *Gadlor1* and *Gadlor2* during cardiac remodelling upon pathological overload were assessed with systemic deletion of the whole region containing *Gadlor1* and *Gadlor2.* Cell type-specific, inducible knock-out of *Gadlor* lncRNAs might provide a more specific and detailed understanding of the effects of *Gadlor* lncRNAs during cardiac remodelling. To overcome this limitation, genome-wide analysis of isolated endothelial cells, cardiac fibroblasts and cardiomyocytes from *Gadlor*-KO mice after 2 weeks of TAC were compared with WT. Deep analysis of each cell type provided a broad understanding of the function of *Gadlor* lncRNAs upon pathological stimuli.

Another limitation faced during the studies due to knocking-out *Gadlor1* and *Gadlor2* globally was the restriction to analyse the individual effects of these lncRNAs. Even though, *Gadlor1* and *Gadlor2* are mostly co-expressed lncRNAs based on the data presented in this work, individual deletion of *Gadlor1* and *Gadlor2* might have provided a deeper understanding of specific functions, which can be applied to future studies.

In addition, as a gain-of-function model, *Gadlor1* and *Gadlor2* were overexpressed by adenovirus pre-treated *Gadlor*-enriched EVs, which were intraventricularly injected into the heart before TAC operation. The idea was to perfuse *Gadlor*-EVs through coronaries thus they can initially be taken up by the endothelium, however, the delivery is not targeted to a specific cell type. Thus, the main

cell type receiving the *Gadlor*-EVs was assessed with *in vitro* co-culture models. Additionally, the upregulation of *Gadlor1* and *Gadlor2* after injection of EVs was assessed and confirmed with qRT-PCR analysis after 1-week and 2-weeks of post-injection in the whole heart tissue. However, the dose-response or the stability of EV-mediated transfer was not assessed exclusively. Moreover, some studies suggested that direct injection to the heart, but not vascular infusion, is more efficient for therapeutic approaches, which might be applied to future studies.[180,181]

Overall, observed strong vascularization and prevention of fibrosis in the *Gadlor*-KO mice can be assessed in different preclinical disease models in the future, such as in liver fibrosis models like non-alcoholic steatohepatitis (NASH) since *Gadlor1* and *Gadlor2* are highly expressed in the liver tissue.

12. Conclusion

In this study, two novel and secreted lncRNAs named *Gadlor1* and *Gadlor2* (GATA-downregulated long non-coding RNA), which are markedly upregulated after endothelial deletion of GATA2 were assessed for their function during cardiac remodelling upon pressure overload. The expression of *Gadlor* lncRNAs is significantly increased in mice after transverse aortic constriction (TAC), but also in the myocardium and the serum of patients suffering from chronic heart failure.

Based on the studies performed here, *Gadlor1* and *Gadlor2* are secreted within EVs predominantly derived by cardiac EC, which then are mainly taken up by cardiomyocytes, although they also have autocrine/intracrine effects on ECs and potentially on FBs since they have endogenous *Gadlor1/2* expression. Analysis of bulk RNA sequencing from isolated adult ECs, FBs and CMs after 2 weeks of TAC indicated that in cardiomyocytes, *Gadlor1/2* impacts calcium handling and gene expression, while they trigger pro-fibrotic gene expression in FBs and anti-angiogenic effects in ECs.

Systemic genetic deletion of *Gadlor1* and *Gadlor2*, in turn, led to improved cardiac function, reduced hypertrophy and strongly diminished fibrosis, although increased mortality emerged in *Gadlor* knock-out (KO) mice upon prolonged pressure overload. On the other hand, as a gain-of-function approach, administration of *Gadlor1/2* enriched-EVs after TAC exaggerated cardiac dysfunction, augmented fibrosis and cardiomyocyte hypertrophy.

This study reveals that secreted *Gadlor1* and *Gadlor2* lncRNAs are involved in intracardiac communication via trafficking between cells by EVs, and deletion of *Gadlor* lncRNAs has beneficial effects on ECs and FBs while disrupting calcium handling in CMs **(Figure 67)**. Thus, targeted inhibition of *Gadlor1* and *Gadlor2* in non-myocytes might serve as a novel therapeutic strategy in heart failure.

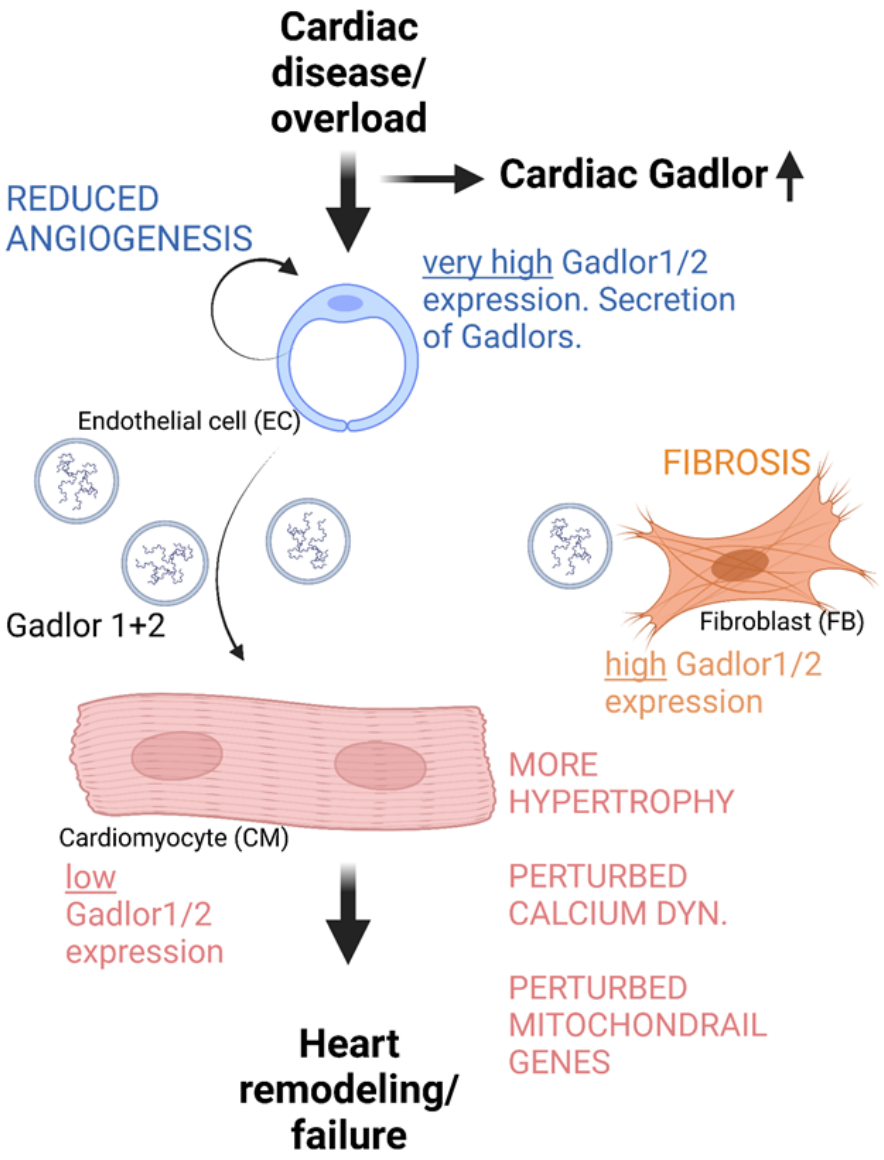

Figure 67: Proposed mechanism of action of *Gadlor1* and *Gadlor2* lncRNAs in cardiac remodelling.

Scheme depicting the proposed mechanism of action of *Gadlor1* and *Gadlor2* during cardiac remodelling upon pressure overload. *Gadlor1* and *Gadlor2* expression is increasing after pathological stimuli. *Gadlor* lncRNAs are mainly expressed in cardiac ECs, which are even more enriched in EC-derived EVs (exosome and microvesicles). EC-derived EVs are mainly taken up by CMs and a lesser extent by cardiac FBs. *Gadlor* lncRNAs affecting ECs and reducing angiogenesis capacity, while in CMs promoted cardiac hypertrophy, altered calcium dynamics and perturbed mitochondrial genes. On the other hand, cardiac FBs express endogenous *Gadlor1/2*. *Gadlor1/2* deletion downregulated ECM-associated gene in cardiac FB after TAC. *Illustration is created by using www.biorender.com.*

References

1. Timmis A, Vardas P, Townsend N, Torbica A, Katus H, De Smedt D, Gale CP, Maggioni AP, Petersen SE, Huculeci R, et al. European Society of Cardiology: cardiovascular disease statistics 2021. *Eur Heart J*. 2022;43:716-799. doi: 10.1093/eurheartj/ehab892
2. Tabassum R, Ripatti S. Integrating lipidomics and genomics: emerging tools to understand cardiovascular diseases. *Cell Mol Life Sci*. 2021;78:2565-2584. doi: 10.1007/s00018-020-03715-4
3. Cardiovascular diseases (CVDs). World Health Organization (WHO). https://www.who.int/news-room/fact-sheets/detail/cardiovascular-diseases-(cvds).
4. Tsao CW, Aday AW, Almarzooq ZI, Alonso A, Beaton AZ, Bittencourt MS, Boehme AK, Buxton AE, Carson AP, Commodore-Mensah Y, et al. Heart Disease and Stroke Statistics-2022 Update: A Report From the American Heart Association. *Circulation*. 2022;145:e153-e639. doi: 10.1161/CIR.0000000000001052
5. Mosca L, Barrett-Connor E, Wenger NK. Sex/gender differences in cardiovascular disease prevention: what a difference a decade makes. *Circulation*. 2011;124:2145-2154. doi: 10.1161/CIRCULATIONAHA.110.968792
6. Gao Z, Chen Z, Sun A, Deng X. Gender differences in cardiovascular disease. *Medicine in Novel Technology and Devices*. 2019;4:100025. doi: https://doi.org/10.1016/j.medntd.2019.100025
7. Townsend N, Kazakiewicz D, Lucy Wright F, Timmis A, Huculeci R, Torbica A, Gale CP, Achenbach S, Weidinger F, Vardas P. Epidemiology of cardiovascular disease in Europe. *Nat Rev Cardiol*. 2022;19:133-143. doi: 10.1038/s41569-021-00607-3
8. Timmis A, Townsend N, Gale CP, Torbica A, Lettino M, Petersen SE, Mossialos EA, Maggioni AP, Kazakiewicz D, May HT, et al. European Society of Cardiology: Cardiovascular Disease Statistics 2019. *Eur Heart J*. 2020;41:12-85. doi: 10.1093/eurheartj/ehz859
9. Neubauer S. The failing heart--an engine out of fuel. *N Engl J Med*. 2007;356:1140-1151. doi: 10.1056/NEJMra063052
10. Henry Krum WTA. Heart failure. *Lancet* 2009; VOLUME 373:P941-955. doi: https://doi.org/10.1016/S0140-6736(09)60236-1
11. Heineke J, Molkentin JD. Regulation of cardiac hypertrophy by intracellular signalling pathways. *Nat Rev Mol Cell Biol*. 2006;7:589-600. doi: 10.1038/nrm1983
12. Tham YK, Bernardo BC, Ooi JY, Weeks KL, McMullen JR. Pathophysiology of cardiac hypertrophy and heart failure: signaling pathways and novel therapeutic targets. *Arch Toxicol*. 2015;89:1401-1438. doi: 10.1007/s00204-015-1477-x
13. Sweitzer NK. What is an angiotensin converting enzyme inhibitor? *Circulation*. 2003;108:E16-E18. doi: 10.1161/01.Cir.0000075957.16003.07
14. Frishman WH. Beta-adrenergic blockers. *Circulation*. 2003;107:E117-E119. doi: 10.1161/01.Cir.0000070983.15903.A2
15. Robinson EL, Port JD. Utilization and Potential of RNA-Based Therapies in Cardiovascular Disease. *JACC: Basic to Translational Science*. 2022;7:956-969. doi: doi.org/10.1016/j.jacbts.2022.02.003
16. Lu D, Thum T. RNA-based diagnostic and therapeutic strategies for cardiovascular disease. *Nat Rev Cardiol*. 2019;16:661-674. doi: 10.1038/s41569-019-0218-x
17. Bar C, Chatterjee S, Falcao Pires I, Rodrigues P, Sluijter JPG, Boon RA, Nevado RM, Andres V, Sansonetti M, de Windt L, et al. Non-coding RNAs: update on mechanisms and therapeutic targets from the ESC Working Groups of Myocardial Function and Cellular Biology of the Heart. *Cardiovasc Res*. 2020;116:1805-1819. doi: 10.1093/cvr/cvaa195
18. Huang CK, Kafert-Kasting S, Thum T. Preclinical and Clinical Development of Noncoding RNA Therapeutics for Cardiovascular Disease. *Circ Res*. 2020;126:663-678. doi: 10.1161/CIRCRESAHA.119.315856

19. Hill JA, Olson EN. Cardiac plasticity. *N Engl J Med*. 2008;358:1370-1380. doi: 10.1056/NEJMra072139
20. Maillet M, van Berlo JH, Molkentin JD. Molecular basis of physiological heart growth: fundamental concepts and new players. *Nat Rev Mol Cell Biol*. 2013;14:38-48. doi: 10.1038/nrm3495
21. Frey N, Katus HA, Olson EN, Hill JA. Hypertrophy of the heart: a new therapeutic target? *Circulation*. 2004;109:1580-1589. doi: 10.1161/01.CIR.0000120390.68287.BB
22. Fagard R. Athlete's heart. *Heart*. 2003;89:1455-1461. doi: DOI 10.1136/heart.89.12.1455
23. Kehat I, Molkentin JD. Molecular pathways underlying cardiac remodeling during pathophysiological stimulation. *Circulation*. 2010;122:2727-2735. doi: 10.1161/CIRCULATIONAHA.110.942268
24. van Berlo JH, Maillet M, Molkentin JD. Signaling effectors underlying pathologic growth and remodeling of the heart. *J Clin Invest*. 2013;123:37-45. doi: 10.1172/JCI62839
25. Schirone L, Forte M, Palmerio S, Yee D, Nocella C, Angelini F, Pagano F, Schiavon S, Bordin A, Carrizzo A, et al. A Review of the Molecular Mechanisms Underlying the Development and Progression of Cardiac Remodeling. *Oxid Med Cell Longev*. 2017;2017:3920195. doi: 10.1155/2017/3920195
26. Schimmel K, Ichimura K, Reddy S, Haddad F, Spiekerkoetter E. Cardiac Fibrosis in the Pressure Overloaded Left and Right Ventricle as a Therapeutic Target. *Front Cardiovasc Med*. 2022;9:886553. doi: 10.3389/fcvm.2022.886553
27. Kovacic JC, Dimmeler S, Harvey RP, Finkel T, Aikawa E, Krenning G, Baker AH. Endothelial to Mesenchymal Transition in Cardiovascular Disease: JACC State-of-the-Art Review. *J Am Coll Cardiol*. 2019;73:190-209. doi: 10.1016/j.jacc.2018.09.089
28. Kanisicak O, Khalil H, Ivey MJ, Karch J, Maliken BD, Correll RN, Brody MJ, SC JL, Aronow BJ, Tallquist MD, et al. Genetic lineage tracing defines myofibroblast origin and function in the injured heart. *Nat Commun*. 2016;7:12260. doi: 10.1038/ncomms12260
29. Zeisberg EM, Tarnavski O, Zeisberg M, Dorfman AL, McMullen JR, Gustafsson E, Chandraker A, Yuan X, Pu WT, Roberts AB, et al. Endothelial-to-mesenchymal transition contributes to cardiac fibrosis. *Nat Med*. 2007;13:952-961. doi: 10.1038/nm1613
30. Chen K, Chen J, Li D, Zhang X, Mehta JL. Angiotensin II regulation of collagen type I expression in cardiac fibroblasts: modulation by PPAR-gamma ligand pioglitazone. *Hypertension*. 2004;44:655-661. doi: 10.1161/01.HYP.0000144400.49062.6b
31. Deschamps AM, Spinale FG. Pathways of matrix metalloproteinase induction in heart failure: bioactive molecules and transcriptional regulation. *Cardiovasc Res*. 2006;69:666-676. doi: 10.1016/j.cardiores.2005.10.004
32. Hudlicka O, Brown M, Egginton S. Angiogenesis in skeletal and cardiac muscle. *Physiol Rev*. 1992;72:369-417. doi: 10.1152/physrev.1992.72.2.369
33. Shiojima I, Sato K, Izumiya Y, Schiekofer S, Ito M, Liao R, Colucci WS, Walsh K. Disruption of coordinated cardiac hypertrophy and angiogenesis contributes to the transition to heart failure. *J Clin Invest*. 2005;115:2108-2118. doi: 10.1172/JCI24682
34. Izumiya Y, Shiojima I, Sato K, Sawyer DB, Colucci WS, Walsh K. Vascular endothelial growth factor blockade promotes the transition from compensatory cardiac hypertrophy to failure in response to pressure overload. *Hypertension*. 2006;47:887-893. doi: 10.1161/01.HYP.0000215207.54689.31
35. Heineke J, Auger-Messier M, Xu J, Oka T, Sargent MA, York A, Klevitsky R, Vaikunth S, Duncan SA, Aronow BJ, et al. Cardiomyocyte GATA4 functions as a stress-responsive regulator of angiogenesis in the murine heart. *J Clin Invest*. 2007;117:3198-3210. doi: 10.1172/JCI32573

36. Sano M, Minamino T, Toko H, Miyauchi H, Orimo M, Qin Y, Akazawa H, Tateno K, Kayama Y, Harada M, et al. p53-induced inhibition of Hif-1 causes cardiac dysfunction during pressure overload. *Nature*. 2007;446:444-448. doi: 10.1038/nature05602
37. Carmeliet P, Ng YS, Nuyens D, Theilmeier G, Brusselmans K, Cornelissen I, Ehler E, Kakkar VV, Stalmans I, Mattot V, et al. Impaired myocardial angiogenesis and ischemic cardiomyopathy in mice lacking the vascular endothelial growth factor isoforms VEGF164 and VEGF188. *Nat Med*. 1999;5:495-502. doi: 10.1038/8379
38. Palmer JN, Hartogensis WE, Patten M, Fortuin FD, Long CS. Interleukin-1 beta induces cardiac myocyte growth but inhibits cardiac fibroblast proliferation in culture. *J Clin Invest*. 1995;95:2555-2564. doi: 10.1172/JCI117956
39. Mann DL. Inflammatory mediators and the failing heart: past, present, and the foreseeable future. *Circ Res*. 2002;91:988-998. doi: 10.1161/01.res.0000043825.01705.1b
40. Korf-Klingebiel M, Reboll MR, Polten F, Weber N, Jackle F, Wu X, Kallikourdis M, Kunderfranco P, Condorelli G, Giannitsis E, et al. Myeloid-Derived Growth Factor Protects Against Pressure Overload-Induced Heart Failure by Preserving Sarco/Endoplasmic Reticulum Ca(2+)-ATPase Expression in Cardiomyocytes. *Circulation*. 2021;144:1227-1240. doi: 10.1161/CIRCULATIONAHA.120.053365
41. Luo M, Anderson ME. Mechanisms of altered Ca(2)(+) handling in heart failure. *Circ Res*. 2013;113:690-708. doi: 10.1161/CIRCRESAHA.113.301651
42. Anderson ME. CaMKII and a failing strategy for growth in heart. *J Clin Invest*. 2009;119:1082-1085. doi: 10.1172/jci39262
43. Bers DM. Altered cardiac myocyte Ca regulation in heart failure. *Physiology (Bethesda)*. 2006;21:380-387. doi: 10.1152/physiol.00019.2006
44. Kranias EG, Hajjar RJ. Modulation of cardiac contractility by the phospholamban/SERCA2a regulatome. *Circ Res*. 2012;110:1646-1660. doi: 10.1161/CIRCRESAHA.111.259754
45. Landstrom AP, Dobrev D, Wehrens XHT. Calcium Signaling and Cardiac Arrhythmias. *Circ Res*. 2017;120:1969-1993. doi: 10.1161/CIRCRESAHA.117.310083
46. Asakura K, Cha CY, Yamaoka H, Horikawa Y, Memida H, Powell T, Amano A, Noma A. EAD and DAD mechanisms analyzed by developing a new human ventricular cell model. *Prog Biophys Mol Biol*. 2014;116:11-24. doi: 10.1016/j.pbiomolbio.2014.08.008
47. Gwathmey JK, Copelas L, MacKinnon R, Schoen FJ, Feldman MD, Grossman W, Morgan JP. Abnormal intracellular calcium handling in myocardium from patients with end-stage heart failure. *Circ Res*. 1987;61:70-76. doi: 10.1161/01.res.61.1.70
48. Lindner M, Brandt MC, Sauer H, Hescheler J, Bohle T, Beuckelmann DJ. Calcium sparks in human ventricular cardiomyocytes from patients with terminal heart failure. *Cell Calcium*. 2002;31:175-182. doi: 10.1054/ceca.2002.0272
49. Schwinger RH, Bohm M, Schmidt U, Karczewski P, Bavendiek U, Flesch M, Krause EG, Erdmann E. Unchanged protein levels of SERCA II and phospholamban but reduced Ca2+ uptake and Ca(2+)-ATPase activity of cardiac sarcoplasmic reticulum from dilated cardiomyopathy patients compared with patients with nonfailing hearts. *Circulation*. 1995;92:3220-3228. doi: 10.1161/01.cir.92.11.3220
50. Luo W, Grupp IL, Harrer J, Ponniah S, Grupp G, Duffy JJ, Doetschman T, Kranias EG. Targeted ablation of the phospholamban gene is associated with markedly enhanced myocardial contractility and loss of beta-agonist stimulation. *Circ Res*. 1994;75:401-409. doi: 10.1161/01.res.75.3.401
51. Zhang T, Guo T, Mishra S, Dalton ND, Kranias EG, Peterson KL, Bers DM, Brown JH. Phospholamban ablation rescues sarcoplasmic reticulum Ca(2+) handling but exacerbates cardiac dysfunction in CaMKIIdelta(C) transgenic mice. *Circ Res*. 2010;106:354-362. doi: 10.1161/CIRCRESAHA.109.207423

52. Sadredini M, Hansen MH, Frisk M, Louch WE, Lehnart SE, Sjaastad I, Stokke MK. CaMKII inhibition has dual effects on spontaneous Ca2+ release and Ca2+ alternans in ventricular cardiomyocytes from mice with a gain-of-function RyR2 mutation. *Am J Physiol-Heart C*. 2021;321:H446-H460. doi: 10.1152/ajpheart.00011.2021
53. Schaper J. Ultrastructural changes of the myocardium in regional ischaemia and infarction. *Eur Heart J*. 1986;7 Suppl B:3-9. doi: 10.1093/eurheartj/7.suppl_b.3
54. Doenst T, Nguyen TD, Abel ED. Cardiac metabolism in heart failure: implications beyond ATP production. *Circ Res*. 2013;113:709-724. doi: 10.1161/CIRCRESAHA.113.300376
55. Stanley WC, Chandler MP. Energy metabolism in the normal and failing heart: potential for therapeutic interventions. *Heart Fail Rev*. 2002;7:115-130. doi: 10.1023/a:1015320423577
56. Kato T, Niizuma S, Inuzuka Y, Kawashima T, Okuda J, Tamaki Y, Iwanaga Y, Narazaki M, Matsuda T, Soga T, et al. Analysis of metabolic remodeling in compensated left ventricular hypertrophy and heart failure. *Circ Heart Fail*. 2010;3:420-430. doi: 10.1161/CIRCHEARTFAILURE.109.888479
57. Kienesberger PC, Pulinilkunnil T, Nagendran J, Dyck JR. Myocardial triacylglycerol metabolism. *J Mol Cell Cardiol*. 2013;55:101-110. doi: 10.1016/j.yjmcc.2012.06.018
58. Morissette MR, Howes AL, Zhang T, Heller Brown J. Upregulation of GLUT1 expression is necessary for hypertrophy and survival of neonatal rat cardiomyocytes. *J Mol Cell Cardiol*. 2003;35:1217-1227. doi: 10.1016/s0022-2828(03)00212-8
59. Allard MF, Schonekess BO, Henning SL, English DR, Lopaschuk GD. Contribution of oxidative metabolism and glycolysis to ATP production in hypertrophied hearts. *Am J Physiol*. 1994;267:H742-750. doi: 10.1152/ajpheart.1994.267.2.H742
60. Battiprolu PK, Lopez-Crisosto C, Wang ZV, Nemchenko A, Lavandero S, Hill JA. Diabetic cardiomyopathy and metabolic remodeling of the heart. *Life Sci*. 2013;92:609-615. doi: 10.1016/j.lfs.2012.10.011
61. Cepeda-Valery B, Pressman GS, Figueredo VM, Romero-Corral A. Impact of obesity on total and cardiovascular mortality--fat or fiction? *Nat Rev Cardiol*. 2011;8:233-237. doi: 10.1038/nrcardio.2010.209
62. Heart Outcomes Prevention Evaluation Study I, Yusuf S, Dagenais G, Pogue J, Bosch J, Sleight P. Vitamin E supplementation and cardiovascular events in high-risk patients. *N Engl J Med*. 2000;342:154-160. doi: 10.1056/NEJM200001203420302
63. Lonn E, Bosch J, Yusuf S, Sheridan P, Pogue J, Arnold JM, Ross C, Arnold A, Sleight P, Probstfield J, et al. Effects of long-term vitamin E supplementation on cardiovascular events and cancer: a randomized controlled trial. *JAMA*. 2005;293:1338-1347. doi: 10.1001/jama.293.11.1338
64. Dai DF, Hsieh EJ, Liu Y, Chen T, Beyer RP, Chin MT, MacCoss MJ, Rabinovitch PS. Mitochondrial proteome remodelling in pressure overload-induced heart failure: the role of mitochondrial oxidative stress. *Cardiovasc Res*. 2012;93:79-88. doi: 10.1093/cvr/cvr274
65. Dorn GW, 2nd, Kitsis RN. The mitochondrial dynamism-mitophagy-cell death interactome: multiple roles performed by members of a mitochondrial molecular ensemble. *Circ Res*. 2015;116:167-182. doi: 10.1161/CIRCRESAHA.116.303554
66. Crick FH. On protein synthesis. *Symp Soc Exp Biol*. 1958;12:138-163.
67. Uchida S, Dimmeler S. Long noncoding RNAs in cardiovascular diseases. *Circ Res*. 2015;116:737-750. doi: 10.1161/CIRCRESAHA.116.302521
68. Prestes PR, Maier MC, Woods BA, Charchar FJ. A Guide to the Short, Long and Circular RNAs in Hypertension and Cardiovascular Disease. *Int J Mol Sci*. 2020;21. doi: 10.3390/ijms21103666
69. Quinn JJ, Chang HY. Unique features of long non-coding RNA biogenesis and function. *Nat Rev Genet*. 2016;17:47-62. doi: 10.1038/nrg.2015.10
70. Anderson DM, Anderson KM, Chang CL, Makarewich CA, Nelson BR, McAnally JR, Kasaragod P, Shelton JM, Liou J, Bassel-Duby R, et al. A micropeptide encoded by a putative long noncoding RNA regulates muscle performance. *Cell*. 2015;160:595-606. doi: 10.1016/j.cell.2015.01.009

71. Nelson BR, Makarewich CA, Anderson DM, Winders BR, Troupes CD, Wu F, Reese AL, McAnally JR, Chen X, Kavalali ET, et al. A peptide encoded by a transcript annotated as long noncoding RNA enhances SERCA activity in muscle. *Science*. 2016;351:271-275. doi: 10.1126/science.aad4076
72. Kapusta A, Feschotte C. Volatile evolution of long noncoding RNA repertoires: mechanisms and biological implications. *Trends Genet*. 2014;30:439-452. doi: 10.1016/j.tig.2014.08.004
73. Guil S, Esteller M. Cis-acting noncoding RNAs: friends and foes. *Nat Struct Mol Biol*. 2012;19:1068-1075. doi: 10.1038/nsmb.2428
74. Lee JT, Jaenisch R. Long-range cis effects of ectopic X-inactivation centres on a mouse autosome. *Nature*. 1997;386:275-279. doi: 10.1038/386275a0
75. Xiang JF, Yin QF, Chen T, Zhang Y, Zhang XO, Wu Z, Zhang S, Wang HB, Ge J, Lu X, et al. Human colorectal cancer-specific CCAT1-L lncRNA regulates long-range chromatin interactions at the MYC locus. *Cell Res*. 2014;24:513-531. doi: 10.1038/cr.2014.35
76. Geisler S, Coller J. RNA in unexpected places: long non-coding RNA functions in diverse cellular contexts. *Nat Rev Mol Cell Biol*. 2013;14:699-712. doi: 10.1038/nrm3679
77. West JA, Davis CP, Sunwoo H, Simon MD, Sadreyev RI, Wang PI, Tolstorukov MY, Kingston RE. The long noncoding RNAs NEAT1 and MALAT1 bind active chromatin sites. *Mol Cell*. 2014;55:791-802. doi: 10.1016/j.molcel.2014.07.012
78. Das S, Shah R, Dimmeler S, Freedman JE, Holley C, Lee JM, Moore K, Musunuru K, Wang DZ, Xiao J, et al. Noncoding RNAs in Cardiovascular Disease: Current Knowledge, Tools and Technologies for Investigation, and Future Directions: A Scientific Statement From the American Heart Association. *Circ Genom Precis Med*. 2020;13:e000062. doi: 10.1161/HCG.0000000000000062
79. Schulte C, Barwari T, Joshi A, Zeller T, Mayr M. Noncoding RNAs versus Protein Biomarkers in Cardiovascular Disease. *Trends Mol Med*. 2020;26:583-596. doi: 10.1016/j.molmed.2020.02.001
80. Viereck J, Kumarswamy R, Foinquinos A, Xiao K, Avramopoulos P, Kunz M, Dittrich M, Maetzig T, Zimmer K, Remke J, et al. Long noncoding RNA Chast promotes cardiac remodeling. *Sci Transl Med*. 2016;8:326ra322. doi: 10.1126/scitranslmed.aaf1475
81. Han P, Li W, Lin CH, Yang J, Shang C, Nuernberg ST, Jin KK, Xu W, Lin CY, Lin CJ, et al. A long noncoding RNA protects the heart from pathological hypertrophy. *Nature*. 2014;514:102-106. doi: 10.1038/nature13596
82. Micheletti R, Plaisance I, Abraham BJ, Sarre A, Ting CC, Alexanian M, Maric D, Maison D, Nemir M, Young RA, et al. The long noncoding RNA Wisper controls cardiac fibrosis and remodeling. *Sci Transl Med*. 2017;9. doi: 10.1126/scitranslmed.aai9118
83. Cheng Y, Wang X, Yang J, Duan X, Yao Y, Shi X, Chen Z, Fan Z, Liu X, Qin S, et al. A translational study of urine miRNAs in acute myocardial infarction. *J Mol Cell Cardiol*. 2012;53:668-676. doi: 10.1016/j.yjmcc.2012.08.010
84. Kuwabara Y, Ono K, Horie T, Nishi H, Nagao K, Kinoshita M, Watanabe S, Baba O, Kojima Y, Shizuta S, et al. Increased microRNA-1 and microRNA-133a levels in serum of patients with cardiovascular disease indicate myocardial damage. *Circ Cardiovasc Genet*. 2011;4:446-454. doi: 10.1161/CIRCGENETICS.110.958975
85. Sluijter JP, Verhage V, Deddens JC, van den Akker F, Doevendans PA. Microvesicles and exosomes for intracardiac communication. *Cardiovasc Res*. 2014;102:302-311. doi: 10.1093/cvr/cvu022
86. Pinto AR, Ilinykh A, Ivey MJ, Kuwabara JT, D'Antoni ML, Debuque R, Chandran A, Wang L, Arora K, Rosenthal NA, et al. Revisiting Cardiac Cellular Composition. *Circ Res*. 2016;118:400-409. doi: 10.1161/CIRCRESAHA.115.307778
87. Kenneweg F, Bang C, Xiao K, Boulanger CM, Loyer X, Mazlan S, Schroen B, Hermans-Beijnsberger S, Foinquinos A, Hirt MN, et al. Long Noncoding RNA-Enriched Vesicles Secreted by Hypoxic Cardiomyocytes Drive Cardiac Fibrosis. *Mol Ther Nucleic Acids*. 2019;18:363-374. doi: 10.1016/j.omtn.2019.09.003

88. Piccoli MT, Gupta SK, Viereck J, Foinquinos A, Samolovac S, Kramer FL, Garg A, Remke J, Zimmer K, Batkai S, et al. Inhibition of the Cardiac Fibroblast-Enriched lncRNA Meg3 Prevents Cardiac Fibrosis and Diastolic Dysfunction. *Circ Res*. 2017;121:575-583. doi: 10.1161/CIRCRESAHA.117.310624
89. Hosen MR, Li Q, Liu Y, Zietzer A, Maus K, Goody P, Uchida S, Latz E, Werner N, Nickenig G, et al. CAD increases the long noncoding RNA PUNISHER in small extracellular vesicles and regulates endothelial cell function via vesicular shuttling. *Mol Ther Nucleic Acids*. 2021;25:388-405. doi: 10.1016/j.omtn.2021.05.023
90. Mathieu M, Martin-Jaular L, Lavieu G, Thery C. Specificities of secretion and uptake of exosomes and other extracellular vesicles for cell-to-cell communication. *Nat Cell Biol*. 2019;21:9-17. doi: 10.1038/s41556-018-0250-9
91. Kalluri R, LeBleu VS. The biology, function, and biomedical applications of exosomes. *Science*. 2020;367. doi: 10.1126/science.aau6977
92. O'Brien K, Breyne K, Ughetto S, Laurent LC, Breakefield XO. RNA delivery by extracellular vesicles in mammalian cells and its applications. *Nat Rev Mol Cell Biol*. 2020;21:585-606. doi: 10.1038/s41580-020-0251-y
93. Mateescu B, Kowal EJ, van Balkom BW, Bartel S, Bhattacharyya SN, Buzas EI, Buck AH, de Candia P, Chow FW, Das S, et al. Obstacles and opportunities in the functional analysis of extracellular vesicle RNA - an ISEV position paper. *J Extracell Vesicles*. 2017;6:1286095. doi: 10.1080/20013078.2017.1286095
94. van Niel G, D'Angelo G, Raposo G. Shedding light on the cell biology of extracellular vesicles. *Nat Rev Mol Cell Biol*. 2018;19:213-228. doi: 10.1038/nrm.2017.125
95. Osteikoetxea X, Nemeth A, Sodar BW, Vukman KV, Buzas EI. Extracellular vesicles in cardiovascular disease: are they Jedi or Sith? *J Physiol*. 2016;594:2881-2894. doi: 10.1113/JP271336
96. Thery C, Amigorena S, Raposo G, Clayton A. Isolation and characterization of exosomes from cell culture supernatants and biological fluids. *Curr Protoc Cell Biol*. 2006;Chapter 3:Unit 3 22. doi: 10.1002/0471143030.cb0322s30
97. Pan BT, Teng K, Wu C, Adam M, Johnstone RM. Electron microscopic evidence for externalization of the transferrin receptor in vesicular form in sheep reticulocytes. *J Cell Biol*. 1985;101:942-948. doi: 10.1083/jcb.101.3.942
98. van der Pol E, Coumans FA, Grootemaat AE, Gardiner C, Sargent IL, Harrison P, Sturk A, van Leeuwen TG, Nieuwland R. Particle size distribution of exosomes and microvesicles determined by transmission electron microscopy, flow cytometry, nanoparticle tracking analysis, and resistive pulse sensing. *J Thromb Haemost*. 2014;12:1182-1192. doi: 10.1111/jth.12602
99. Kim HK, Song KS, Lee ES, Lee YJ, Park YS, Lee KR, Lee SN. Optimized flow cytometric assay for the measurement of platelet microparticles in plasma: pre-analytic and analytic considerations. *Blood Coagul Fibrinolysis*. 2002;13:393-397. doi: 10.1097/00001721-200207000-00003
100. Grant BD, Donaldson JG. Pathways and mechanisms of endocytic recycling. *Nat Rev Mol Cell Biol*. 2009;10:597-608. doi: 10.1038/nrm2755
101. Stoorvogel W, Strous GJ, Geuze HJ, Oorschot V, Schwartz AL. Late endosomes derive from early endosomes by maturation. *Cell*. 1991;65:417-427. doi: 10.1016/0092-8674(91)90459-c
102. Settembre C, Fraldi A, Medina DL, Ballabio A. Signals from the lysosome: a control centre for cellular clearance and energy metabolism. *Nat Rev Mol Cell Biol*. 2013;14:283-296. doi: 10.1038/nrm3565
103. Henne WM, Stenmark H, Emr SD. Molecular mechanisms of the membrane sculpting ESCRT pathway. *Cold Spring Harb Perspect Biol*. 2013;5. doi: 10.1101/cshperspect.a016766
104. Raiborg C, Stenmark H. The ESCRT machinery in endosomal sorting of ubiquitylated membrane proteins. *Nature*. 2009;458:445-452. doi: 10.1038/nature07961

105. Stuffers S, Sem Wegner C, Stenmark H, Brech A. Multivesicular endosome biogenesis in the absence of ESCRTs. *Traffic*. 2009;10:925-937. doi: 10.1111/j.1600-0854.2009.00920.x
106. Puri N, Roche PA. Mast cells possess distinct secretory granule subsets whose exocytosis is regulated by different SNARE isoforms. *Proc Natl Acad Sci U S A*. 2008;105:2580-2585. doi: 10.1073/pnas.0707854105
107. Muralidharan-Chari V, Clancy J, Plou C, Romao M, Chavrier P, Raposo G, D'Souza-Schorey C. ARF6-regulated shedding of tumor cell-derived plasma membrane microvesicles. *Curr Biol*. 2009;19:1875-1885. doi: 10.1016/j.cub.2009.09.059
108. Abels ER, Breakefield XO. Introduction to Extracellular Vesicles: Biogenesis, RNA Cargo Selection, Content, Release, and Uptake. *Cell Mol Neurobiol*. 2016;36:301-312. doi: 10.1007/s10571-016-0366-z
109. Mulcahy LA, Pink RC, Carter DR. Routes and mechanisms of extracellular vesicle uptake. *J Extracell Vesicles*. 2014;3. doi: 10.3402/jev.v3.24641
110. Morelli AE, Larregina AT, Shufesky WJ, Sullivan ML, Stolz DB, Papworth GD, Zahorchak AF, Logar AJ, Wang Z, Watkins SC, et al. Endocytosis, intracellular sorting, and processing of exosomes by dendritic cells. *Blood*. 2004;104:3257-3266. doi: 10.1182/blood-2004-03-0824
111. Bang C, Batkai S, Dangwal S, Gupta SK, Foinquinos A, Holzmann A, Just A, Remke J, Zimmer K, Zeug A, et al. Cardiac fibroblast-derived microRNA passenger strand-enriched exosomes mediate cardiomyocyte hypertrophy. *J Clin Invest*. 2014;124:2136-2146. doi: 10.1172/JCI70577
112. Hosen MR, Goody PR, Zietzer A, Xiang X, Niepmann ST, Sedaghat A, Tiyerili V, Chennupati R, Moore JBt, Boon RA, et al. Circulating MicroRNA-122-5p Is Associated With a Lack of Improvement in Left Ventricular Function After Transcatheter Aortic Valve Replacement and Regulates Viability of Cardiomyocytes Through Extracellular Vesicles. *Circulation*. 2022:101161CIRCULATIONAHA122060258. doi: 10.1161/CIRCULATIONAHA.122.060258
113. Saheera S, Jani VP, Witwer KW, Kutty S. Extracellular vesicle interplay in cardiovascular pathophysiology. *Am J Physiol Heart Circ Physiol*. 2021;320:H1749-H1761. doi: 10.1152/ajpheart.00925.2020
114. Batagov AO, Kurochkin IV. Exosomes secreted by human cells transport largely mRNA fragments that are enriched in the 3'-untranslated regions. *Biol Direct*. 2013;8:12. doi: 10.1186/1745-6150-8-12
115. Henderson MC, Azorsa DO. The genomic and proteomic content of cancer cell-derived exosomes. *Front Oncol*. 2012;2:38. doi: 10.3389/fonc.2012.00038
116. Thery C, Zitvogel L, Amigorena S. Exosomes: composition, biogenesis and function. *Nat Rev Immunol*. 2002;2:569-579. doi: 10.1038/nri855
117. Bolukbasi MF, Mizrak A, Ozdener GB, Madlener S, Strobel T, Erkan EP, Fan JB, Breakefield XO, Saydam O. miR-1289 and "Zipcode"-like Sequence Enrich mRNAs in Microvesicles. *Mol Ther Nucleic Acids*. 2012;1:e10. doi: 10.1038/mtna.2011.2
118. Villarroya-Beltri C, Gutierrez-Vazquez C, Sanchez-Cabo F, Perez-Hernandez D, Vazquez J, Martin-Cofreces N, Martinez-Herrera DJ, Pascual-Montano A, Mittelbrunn M, Sanchez-Madrid F. Sumoylated hnRNPA2B1 controls the sorting of miRNAs into exosomes through binding to specific motifs. *Nature Communications*. 2013;4. doi: ARTN 298010.1038/ncomms3980
119. Murphy DE, de Jong OG, Brouwer M, Wood MJ, Lavieu G, Schiffelers RM, Vader P. Extracellular vesicle-based therapeutics: natural versus engineered targeting and trafficking. *Exp Mol Med*. 2019;51:1-12. doi: 10.1038/s12276-019-0223-5
120. Elsharkasy OM, Nordin JZ, Hagey DW, de Jong OG, Schiffelers RM, El Andaloussi S, Vader P. Extracellular vesicles as drug delivery systems: Why and how? *Adv Drug Deliver Rev*. 2020;159:332-343. doi: 10.1016/j.addr.2020.04.004

121. Chaudhary N, Weissman D, Whitehead KA. mRNA vaccines for infectious diseases: principles, delivery and clinical translation. *Nat Rev Drug Discov*. 2021;20:817-838. doi: 10.1038/s41573-021-00283-5
122. Andre F, Schartz NE, Chaput N, Flament C, Raposo G, Amigorena S, Angevin E, Zitvogel L. Tumor-derived exosomes: a new source of tumor rejection antigens. *Vaccine*. 2002;20 Suppl 4:A28-31. doi: 10.1016/s0264-410x(02)00384-5
123. Bang OY, Kim EH. Mesenchymal Stem Cell-Derived Extracellular Vesicle Therapy for Stroke: Challenges and Progress. *Front Neurol*. 2019;10:211. doi: 10.3389/fneur.2019.00211
124. Gabisonia K, Khan M, Recchia FA. Extracellular vesicle-mediated bidirectional communication between heart and other organs. *Am J Physiol Heart Circ Physiol*. 2022;322:H769-H784. doi: 10.1152/ajpheart.00659.2021
125. Perbellini F, Watson SA, Bardi I, Terracciano CM. Heterocellularity and Cellular Cross-Talk in the Cardiovascular System. *Front Cardiovasc Med*. 2018;5:143. doi: 10.3389/fcvm.2018.00143
126. Huang P, Wang L, Li Q, Tian X, Xu J, Xu J, Xiong Y, Chen G, Qian H, Jin C, et al. Atorvastatin enhances the therapeutic efficacy of mesenchymal stem cells-derived exosomes in acute myocardial infarction via up-regulating long non-coding RNA H19. *Cardiovasc Res*. 2020;116:353-367. doi: 10.1093/cvr/cvz139
127. Keles M, Grein S, Froese N, Wirth D, Trogisch FA, Wardman R, Hemanna S, Weinzierl N, Uhlig S, Lomada S, et al. Secreted long non-coding RNAs Gadlor1 and Gadlor2 affect multiple cardiac cell types and aggravate cardiac remodeling during pressure overload. *bioRxiv*. 2022:2022.2009.2019.508486. doi: 10.1101/2022.09.19.508486
128. Rockman HA, Ross RS, Harris AN, Knowlton KU, Steinhelper ME, Field LJ, Ross J, Jr., Chien KR. Segregation of atrial-specific and inducible expression of an atrial natriuretic factor transgene in an in vivo murine model of cardiac hypertrophy. *Proc Natl Acad Sci U S A*. 1991;88:8277-8281. doi: 10.1073/pnas.88.18.8277
129. Bell RM, Mocanu MM, Yellon DM. Retrograde heart perfusion: the Langendorff technique of isolated heart perfusion. *J Mol Cell Cardiol*. 2011;50:940-950. doi: 10.1016/j.yjmcc.2011.02.018
130. Prendergast EN, de Souza Fonseca MA, Dezem FS, Lester J, Karlan BY, Noushmehr H, Lin X, Lawrenson K. Optimizing exosomal RNA isolation for RNA-Seq analyses of archival sera specimens. *PLoS One*. 2018;13:e0196913. doi: 10.1371/journal.pone.0196913
131. Tetzlaff F, Fischer A. Human Endothelial Cell Spheroid-based Sprouting Angiogenesis Assay in Collagen. *Bio Protoc*. 2018;8:e2995. doi: 10.21769/BioProtoc.2995
132. McHugh CA, Guttman M. RAP-MS: A Method to Identify Proteins that Interact Directly with a Specific RNA Molecule in Cells. *Methods Mol Biol*. 2018;1649:473-488. doi: 10.1007/978-1-4939-7213-5_31
133. Gagliardi M, Matarazzo MR. RIP: RNA Immunoprecipitation. *Methods Mol Biol*. 2016;1480:73-86. doi: 10.1007/978-1-4939-6380-5_7
134. Wang L, Park HJ, Dasari S, Wang S, Kocher JP, Li W. CPAT: Coding-Potential Assessment Tool using an alignment-free logistic regression model. *Nucleic Acids Res*. 2013;41:e74. doi: 10.1093/nar/gkt006
135. Witwer KW, Buzas EI, Bemis LT, Bora A, Lasser C, Lotvall J, Nolte-'t Hoen EN, Piper MG, Sivaraman S, Skog J, et al. Standardization of sample collection, isolation and analysis methods in extracellular vesicle research. *J Extracell Vesicles*. 2013;2. doi: 10.3402/jev.v2i0.20360
136. Froese N, Cordero J, Abouissa A, Trogisch FA, Grein S, Szaroszyk M, Wang Y, Gigina A, Korf-Klingebiel M, Bosnjak B, et al. Analysis of myocardial cellular gene expression during pressure overload reveals matrix based functional intercellular communication. *iScience*. 2022;25:103965. doi: 10.1016/j.isci.2022.103965

137. Gerdes J, Lemke H, Baisch H, Wacker HH, Schwab U, Stein H. Cell cycle analysis of a cell proliferation-associated human nuclear antigen defined by the monoclonal antibody Ki-67. *J Immunol*. 1984;133:1710-1715.
138. Statello L, Guo CJ, Chen LL, Huarte M. Gene regulation by long non-coding RNAs and its biological functions. *Nat Rev Mol Cell Biol*. 2021;22:96-118. doi: 10.1038/s41580-020-00315-9
139. Viereck J, Buhrke A, Foinquinos A, Chatterjee S, Kleeberger JA, Xiao K, Janssen-Peters H, Batkai S, Ramanujam D, Kraft T, et al. Targeting muscle-enriched long non-coding RNA H19 reverses pathological cardiac hypertrophy. *Eur Heart J*. 2020;41:3462-3474. doi: 10.1093/eurheartj/ehaa519
140. Waldenstrom A, Genneback N, Hellman U, Ronquist G. Cardiomyocyte microvesicles contain DNA/RNA and convey biological messages to target cells. *PLoS One*. 2012;7:e34653. doi: 10.1371/journal.pone.0034653
141. Wagner KT, Nash TR, Liu B, Vunjak-Novakovic G, Radisic M. Extracellular Vesicles in Cardiac Regeneration: Potential Applications for Tissues-on-a-Chip. *Trends Biotechnol*. 2021;39:755-773. doi: 10.1016/j.tibtech.2020.08.005
142. Nolte-'t Hoen EN, van der Vlist EJ, Aalberts M, Mertens HC, Bosch BJ, Bartelink W, Mastrobattista E, van Gaal EV, Stoorvogel W, Arkesteijn GJ, et al. Quantitative and qualitative flow cytometric analysis of nanosized cell-derived membrane vesicles. *Nanomedicine*. 2012;8:712-720. doi: 10.1016/j.nano.2011.09.006
143. Houser SR, Margulies KB, Murphy AM, Spinale FG, Francis GS, Prabhu SD, Rockman HA, Kass DA, Molkentin JD, Sussman MA, et al. Animal models of heart failure: a scientific statement from the American Heart Association. *Circ Res*. 2012;111:131-150. doi: 10.1161/RES.0b013e3182582523
144. Burchfield JS, Xie M, Hill JA. Pathological ventricular remodeling: mechanisms: part 1 of 2. *Circulation*. 2013;128:388-400. doi: 10.1161/CIRCULATIONAHA.113.001878
145. Spinale FG. Myocardial matrix remodeling and the matrix metalloproteinases: influence on cardiac form and function. *Physiol Rev*. 2007;87:1285-1342. doi: 10.1152/physrev.00012.2007
146. Glasenapp A, Derlin K, Gutberlet M, Hess A, Ross TL, Wester HJ, Bengel FM, Thackeray JT. Molecular Imaging of Inflammation and Fibrosis in Pressure Overload Heart Failure. *Circ Res*. 2021;129:369-382. doi: 10.1161/CIRCRESAHA.120.318539
147. Liu X, Shi GP, Guo J. Innate Immune Cells in Pressure Overload-Induced Cardiac Hypertrophy and Remodeling. *Front Cell Dev Biol*. 2021;9:659666. doi: 10.3389/fcell.2021.659666
148. Chen B, Frangogiannis NG. The Role of Macrophages in Nonischemic Heart Failure. *JACC Basic Transl Sci*. 2018;3:245-248. doi: 10.1016/j.jacbts.2018.03.001
149. Hinderer S, Schenke-Layland K. Cardiac fibrosis - A short review of causes and therapeutic strategies. *Adv Drug Deliv Rev*. 2019;146:77-82. doi: 10.1016/j.addr.2019.05.011
150. Fan D, Takawale A, Lee J, Kassiri Z. Cardiac fibroblasts, fibrosis and extracellular matrix remodeling in heart disease. *Fibrogenesis Tissue Repair*. 2012;5:15. doi: 10.1186/1755-1536-5-15
151. Kong P, Christia P, Frangogiannis NG. The pathogenesis of cardiac fibrosis. *Cell Mol Life Sci*. 2014;71:549-574. doi: 10.1007/s00018-013-1349-6
152. Luther DJ, Thodeti CK, Shamhart PE, Adapala RK, Hodnichak C, Weihrauch D, Bonaldo P, Chilian WM, Meszaros JG. Absence of type VI collagen paradoxically improves cardiac function, structure, and remodeling after myocardial infarction. *Circ Res*. 2012;110:851-856. doi: 10.1161/CIRCRESAHA.111.252734
153. Naugle JE, Olson ER, Zhang X, Mase SE, Pilati CF, Maron MB, Folkesson HG, Horne WI, Doane KJ, Meszaros JG. Type VI collagen induces cardiac myofibroblast differentiation: implications for postinfarction remodeling. *Am J Physiol Heart Circ Physiol*. 2006;290:H323-330. doi: 10.1152/ajpheart.00321.2005
154. deAlmeida AC, van Oort RJ, Wehrens XH. Transverse aortic constriction in mice. *J Vis Exp*. 2010. doi: 10.3791/1729

155. Kim KM, Abdelmohsen K, Mustapic M, Kapogiannis D, Gorospe M. RNA in extracellular vesicles. *Wiley Interdiscip Rev RNA*. 2017;8. doi: 10.1002/wrna.1413
156. Pironti G, Strachan RT, Abraham D, Mon-Wei Yu S, Chen M, Chen W, Hanada K, Mao L, Watson LJ, Rockman HA. Circulating Exosomes Induced by Cardiac Pressure Overload Contain Functional Angiotensin II Type 1 Receptors. *Circulation*. 2015;131:2120-2130. doi: 10.1161/CIRCULATIONAHA.115.015687
157. Chu C, Qu K, Zhong FL, Artandi SE, Chang HY. Genomic maps of long noncoding RNA occupancy reveal principles of RNA-chromatin interactions. *Mol Cell*. 2011;44:667-678. doi: 10.1016/j.molcel.2011.08.027
158. Bell JC, Jukam D, Teran NA, Risca VI, Smith OK, Johnson WL, Skotheim JM, Greenleaf WJ, Straight AF. Chromatin-associated RNA sequencing (ChAR-seq) maps genome-wide RNA-to-DNA contacts. *Elife*. 2018;7. doi: 10.7554/eLife.27024
159. Isoda T, Moore AJ, He Z, Chandra V, Aida M, Denholtz M, Piet van Hamburg J, Fisch KM, Chang AN, Fahl SP, et al. Non-coding Transcription Instructs Chromatin Folding and Compartmentalization to Dictate Enhancer-Promoter Communication and T Cell Fate. *Cell*. 2017;171:103-119 e118. doi: 10.1016/j.cell.2017.09.001
160. Beckedorff FC, Ayupe AC, Crocci-Souza R, Amaral MS, Nakaya HI, Soltys DT, Menck CF, Reis EM, Verjovski-Almeida S. The intronic long noncoding RNA ANRASSF1 recruits PRC2 to the RASSF1A promoter, reducing the expression of RASSF1A and increasing cell proliferation. *PLoS Genet*. 2013;9:e1003705. doi: 10.1371/journal.pgen.1003705
161. Fei J, Ishii H, Hoeksema MA, Meitinger F, Kassavetis GA, Glass CK, Ren B, Kadonaga JT. NDF, a nucleosome-destabilizing factor that facilitates transcription through nucleosomes. *Genes Dev*. 2018;32:682-694. doi: 10.1101/gad.313973.118
162. Mattiazzi A, Bassani RA, Escobar AL, Palomeque J, Valverde CA, Vila Petroff M, Bers DM. Chasing cardiac physiology and pathology down the CaMKII cascade. *Am J Physiol Heart Circ Physiol*. 2015;308:H1177-1191. doi: 10.1152/ajpheart.00007.2015
163. Kirchhefer U, Schmitz W, Scholz H, Neumann J. Activity of cAMP-dependent protein kinase and Ca2+/calmodulin-dependent protein kinase in failing and nonfailing human hearts. *Cardiovasc Res*. 1999;42:254-261. doi: 10.1016/s0008-6363(98)00296-x
164. Li C, Cai X, Sun H, Bai T, Zheng X, Zhou XW, Chen X, Gill DL, Li J, Tang XD. The deltaA isoform of calmodulin kinase II mediates pathological cardiac hypertrophy by interfering with the HDAC4-MEF2 signaling pathway. *Biochem Biophys Res Commun*. 2011;409:125-130. doi: 10.1016/j.bbrc.2011.04.128
165. Backs J, Backs T, Neef S, Kreusser MM, Lehmann LH, Patrick DM, Grueter CE, Qi X, Richardson JA, Hill JA, et al. The delta isoform of CaM kinase II is required for pathological cardiac hypertrophy and remodeling after pressure overload. *Proc Natl Acad Sci U S A*. 2009;106:2342-2347. doi: 10.1073/pnas.0813013106
166. Backs J, Olson EN. Control of cardiac growth by histone acetylation/deacetylation. *Circ Res*. 2006;98:15-24. doi: 10.1161/01.RES.0000197782.21444.8f
167. Passier R, Zeng H, Frey N, Naya FJ, Nicol RL, McKinsey TA, Overbeek P, Richardson JA, Grant SR, Olson EN. CaM kinase signaling induces cardiac hypertrophy and activates the MEF2 transcription factor in vivo. *J Clin Invest*. 2000;105:1395-1406. doi: 10.1172/JCI8551
168. McKinsey TA, Zhang CL, Olson EN. MEF2: a calcium-dependent regulator of cell division, differentiation and death. *Trends Biochem Sci*. 2002;27:40-47. doi: 10.1016/s0968-0004(01)02031-x
169. Said M, Becerra R, Palomeque J, Rinaldi G, Kaetzel MA, Diaz-Sylvester PL, Copello JA, Dedman JR, Mundina-Weilenmann C, Vittone L, et al. Increased intracellular Ca2+ and SR Ca2+ load contribute to arrhythmias after acidosis in rat heart. Role of Ca2+/calmodulin-dependent protein

kinase II. *Am J Physiol Heart Circ Physiol*. 2008;295:H1669-1683. doi: 10.1152/ajpheart.00010.2008
170. MacLennan DH, Kranias EG. Phospholamban: a crucial regulator of cardiac contractility. *Nat Rev Mol Cell Biol*. 2003;4:566-577. doi: 10.1038/nrm1151
171. Gonzalez-Teran B, Pittman M, Felix F, Thomas R, Richmond-Buccola D, Huttenhain R, Choudhary K, Moroni E, Costa MW, Huang Y, et al. Transcription factor protein interactomes reveal genetic determinants in heart disease. *Cell*. 2022;185:794-814 e730. doi: 10.1016/j.cell.2022.01.021
172. Schram K, De Girolamo S, Madani S, Munoz D, Thong F, Sweeney G. Leptin regulates MMP-2, TIMP-1 and collagen synthesis via p38 MAPK in HL-1 murine cardiomyocytes. *Cell Mol Biol Lett*. 2010;15:551-563. doi: 10.2478/s11658-010-0027-z
173. Pathak M, Sarkar S, Vellaichamy E, Sen S. Role of myocytes in myocardial collagen production. *Hypertension*. 2001;37:833-840. doi: 10.1161/01.hyp.37.3.833
174. Gibbs CL. Cardiac energetics. *Physiol Rev*. 1978;58:174-254. doi: 10.1152/physrev.1978.58.1.174
175. Gertz EW, Wisneski JA, Stanley WC, Neese RA. Myocardial substrate utilization during exercise in humans. Dual carbon-labeled carbohydrate isotope experiments. *J Clin Invest*. 1988;82:2017-2025. doi: 10.1172/JCI113822
176. Doenst T, Pytel G, Schrepper A, Amorim P, Farber G, Shingu Y, Mohr FW, Schwarzer M. Decreased rates of substrate oxidation ex vivo predict the onset of heart failure and contractile dysfunction in rats with pressure overload. *Cardiovasc Res*. 2010;86:461-470. doi: 10.1093/cvr/cvp414
177. Zhabyeyev P, Gandhi M, Mori J, Basu R, Kassiri Z, Clanachan A, Lopaschuk GD, Oudit GY. Pressure-overload-induced heart failure induces a selective reduction in glucose oxidation at physiological afterload. *Cardiovasc Res*. 2013;97:676-685. doi: 10.1093/cvr/cvs424
178. Rabinowitz JD, White E. Autophagy and metabolism. *Science*. 2010;330:1344-1348. doi: 10.1126/science.1193497
179. Bugger H, Schwarzer M, Chen D, Schrepper A, Amorim PA, Schoepe M, Nguyen TD, Mohr FW, Khalimonchuk O, Weimer BC, et al. Proteomic remodelling of mitochondrial oxidative pathways in pressure overload-induced heart failure. *Cardiovasc Res*. 2010;85:376-384. doi: 10.1093/cvr/cvp344
180. Wysoczynski M, Khan A, Bolli R. New Paradigms in Cell Therapy: Repeated Dosing, Intravenous Delivery, Immunomodulatory Actions, and New Cell Types. *Circ Res*. 2018;123:138-158. doi: 10.1161/CIRCRESAHA.118.313251
181. Vagnozzi RJ, Sargent MA, Molkentin JD. Cardiac Cell Therapy Rejuvenates the Infarcted Rodent Heart via Direct Injection but Not by Vascular Infusion. *Circulation*. 2020;141:1037-1039. doi: 10.1161/CIRCULATIONAHA.119.044686